Effectiveness of sensors in flood defences

November 2012

T.N. Spaargaren

MSc thesis

Delft University of Technology
LIJN IN WATER

Effectiveness of sensors in flood defences

A study with emphasis on macro instability

Master of Science thesis

November 2012

This thesis is submitted in partial fulfillment of the requirements for the Master of Science degree in Civil Engineering at Delft University of Technology.

Author	T.N. Spaargaren
Address	Sjoukje Dijkstralaan 21 2134 CN Hoofddorp The Netherlands
Telephone	(+31) 0625015051
E-mail	tomspaargaren@gmail.com
Student number	1364987

Graduation Committee	Prof. drs. ir. J.K. Vrijling	(Delft University of Technology)
	Prof. dr. ir. M. Kok	(Delft University of Technology/HKV$_{\text{Lijn in water}}$)
	Ir. M.T. van der Meer	(Delft University of Technology/Fugro BV)
	Ir. K.A. Wojciechowska	(HKV$_{\text{Lijn in water}}$)

*"Although our intellect always longs for clarity and certainty,
our nature often finds uncertainty fascinating. "*

- Karl von Clausewitz

Cover picture: Military attempt to reinforce the dike near Tolbert with sand bags on January 6th 2012 (article in *Dagblad van het Noorden* on April 14th 2012 by Bas van Sluis).

Preface

This report is the result of the thesis research performed to complete the Master of Science in Civil Engineering at the faculty of Civil Engineering and Geosciences of the Delft University of Technology. HKV$_{\text{Lijn in water}}$ gave me the opportunity to carry out this research. The last nine months were not only a technical challenge to overcome, but turned out to be a mental challenge as well. Beside the technical experiences learned, I will also benefit from the increased self-knowledge gained during this period.

I would like to thank the members of my graduation committee Han Vrijling, Matthijs Kok, Martin van der Meer and Karolina Wojciechowska for their supervision and criticisms. Continuous remarks and discussions are in my opinion essential for projects like these. Also, I thank Hoogheemraadschap Hollands Noorderkwartier for providing information on the canal of Nauerna and Fugro BV for the accessibility to the D-Geo Stability software.

Furthermore, I'd like to add a personal note to the value of a statistical life as has been used for the cost-benefit analysis in this thesis. In my opinion, the value of real life, especially that of a human life, is impossible to express in any single number, word nor figure. I consider life as an evolutionary miracle, experienced by the individual on its own. And thereby the value of life remains an ethical and complicated question.

Finally, I would like to thank my colleagues from HKV for the pleasant conversations during the lunch, my friends for the necessary distraction from this thesis and my parents for the support during my whole educational career. But most of all, I owe my gratitude to Sanne for her endless faith and love.

Delft, November 2012

Tom Nicolaas Spaargaren

Summary

The popularity of monitoring dikes with sensor techniques is rising in the Netherlands. It is claimed that sensor techniques lead to significant cost savings and are capable of predicting an upcoming dike collapse, such that emergency measures to mitigate a flood can be taken based on this prediction. But a technical foundation to use the sensor monitoring information in flood safety assessment is lacking. This research investigates the contribution of sensor monitoring information to flood safety and the cost-effectiveness of sensor monitoring in the context of flood risk. This has been done by considering water pressure monitoring for the failure mechanism macro instability in a probabilistic approach, for the two implementation perspectives of permanent dike reinforcements and temporary measures based on early warning.

Sensor techniques have been tested in full-scale dike failure experiments at the IJkdijk, trying to predict an upcoming dike collapse. The sensor techniques are capable of continuously monitoring observable variables as deformation, temperature, water pressure, vibrations and moisture by either measuring from a distance (ex situ) or directly at the dike (in situ). The installation of in situ sensor techniques in existing dikes is an extensive undertaking. The state of the sensor techniques for monitoring flood defences is doubtful as the claimed prediction time for a dike collapse from experiments varies widely: the claimed failure prediction for macro instability ranges from 1,5 to 42 hours and for piping from 4 to 102 hours. Moreover, these results are obtained in a controlled testing environment and the analysis by sensor suppliers might be subjective.

Water pressure is the only variable that constitutes an input for dike safety assessment models, as water pressures form the loading condition for macro instability assessment. Monitoring water pressures affects the epistemic uncertainty of the water pressure schematization which is caused by the translation from the hydraulic load (e.g. water level, precipitation) to water pressures. One must be aware that sensor monitoring either leads to an increased assessment of flood safety if the prior schematization turns out to be done conservatively or leads to a decrease in flood safety if the prior schematization turns out too optimistic. Because of the conservative approach on flood safety assessment in the Netherlands, one would expect an increased assessed flood safety due to sensor monitoring. But prior schematization mistakes imply a decreased assessed flood safety due to sensor monitoring. Moreover, monitoring water pressures has minimum impact on the flood safety assessment if other uncertainty aspects (e.g. soil strength, soil layer composition) dominate the stability assessment. However, sensor monitoring on itself does not affect the real flood safety: only physical measures affect the real risk of flooding. Real-time monitoring of the water pressure gives insight into the water pressure development prior to a loading event, such as precipitation or internal storage processes. This information can be used to specify the short-term macro instability and gives an early warning, such that mitigating measures can be taken timely. Important information is obtained from monitoring high water events such that water pressure models can be calibrated to determine design loading conditions for the periodic safety assessment. For the proven strength method, water pressure monitoring can be used to determine the correlation between the historic and design loading conditions. Also, an additional application is to identify unforeseen risks following the next steps: an unforeseen risk must be present, then the monitoring system must be capable of identifying the risk, a correct interpretation of the unforeseen risk reveals schematization mistakes and then mitigating measures have to be executed.

The case study on the canal of Nauerna denotes that the monitoring of water pressures as performed by the water board has resulted in a higher assessed flood safety. However, the uncertainties regarding the soil strength and soil layer composition dominate the stability assessment. Therefore, additional investments to investigate these uncertainty aspects would have been recommended over the investment in water pressure monitoring.

Conceptual cost-benefit models have been set up to determine the cost-effectiveness of sensor monitoring over the long-term in two situations: permanent dike reinforcements of the periodic safety assessment and temporary measures based on early warning. The costs consist of sensor monitoring costs for purchase and installation of the system, annual maintenance costs to keep the system running and operational costs due to power supply and data storage. The benefit from permanent dike reinforcements is gained from specifying the long-term optimal investment strategy based on the minimum sum of flood risk and reinforcements costs. The monitoring information from relevant high water events affects the assessed flooding probability, such that the magnitude and time of dike reinforcement is adapted. If the sensor monitoring reduces the assessed flooding probability, this induces to a lower assessed flood risk and savings on permanent dike reinforcements. On the other hand, the monitoring can reveal a higher flooding probability than anticipated, such that additional investments must be done to reduce the higher flood risk. This financially leads to additional costs and negative benefits. But the value of knowing this higher flood risk is rationally beneficial: one must incorporate this value of information. The suggested cost-benefit model has been worked out in case studies for monitoring stretches of dike-ring 48 and 14. Under taken assumptions, applying the sensor monitoring system for dike-ring 48 is more cost-effective, than for dike-ring 14.

The benefit from temporary measures is gained from timely execution of an emergency flood protection measure based on the early warning of the sensor system. This benefit depends on the performance of the sensor monitoring system regarding the availability of the sensor monitoring system during a high water event, the reliability of the prediction time for an upcoming dike collapse and the reaction time to execute the emergency flood protection measure. This required time to execute the emergency flood protection measure depends on the time needed for decision making, transport to the dike and deployment. Therefore, the required reaction is dynamic as it depends on local circumstances and the extent of preparedness. Next to the costs for sensor monitoring, costs for executing the emergency flood protection measure must be incorporated. The suggested cost-benefit model has been worked out in case studies for monitoring stretches of dike-ring 48 and 14. Applying the sensor monitoring system for dike-ring 48 turned out to be more cost-effective than for dike-ring 14, under the taken assumptions.

The conclusion of this research is that sensor monitoring can be implemented in the flood safety, by specifying dike reinforcements in both the periodic safety assessment, as well as the operational situation. However, the investments in sensor monitoring have to be made while a long waiting time is expected before benefits turn out. Then these benefits can financially be disappointing, but have a value of information. The cost-effectiveness depends on numerous restrictions and conditions which are case specific. Further research is recommended on implementing the value of information in the cost-benefit model and to combine the models for both the permanent dike reinforcements and the temporary flood risk reduction measures.

List of symbols

Symbol	Unit	Description
b	[M€]	Variable costs for dike reinforcement
c	[kN/m^2]	Cohesion (drained)
C	[M€]	Fixed costs for dike reinforcement
C_D	[€/m]	Costs of deployment and removal of the flood protection measure per m
$C_{deployment}$	[€]	Costs for the deployment of the flood protection measure
$C_{installation}$	[€]	Installation costs
$C_{maintenance}$	[€]	Maintenance costs
$C_{operational}$	[€]	Operational costs
C_p	[€/m]	Purchase costs of the flood protection measure per m
$C_{purchase}$	[€]	Purchase costs for the flood protection measure materials
$C_{preparing}$	[€]	Yearly preparing costs
C_{sensor}	[€]	Discounted expected costs for the sensor system
d_{10}	[cm]	Decimation height
D_h	[m]	Horizontal correlation length
D_r	[m/hour]	Rate of deployment for the flood protection measure
D_v	[m]	Vertical correlation length
e	[€]	Execution costs per sensor
$E(costs)$	[€]	Expected costs
$E(costs)_{measure}$	[€]	Expected costs made for the execution of a flood protection measure
$E(damage)$	[€]	Discounted expected flood damage
$f(s)$	[-]	Probability density function of S
f_b	[-]	Factor for the base installation costs
f_m	[-]	Factor for the yearly maintenance costs
f_o	[-]	Factor for the yearly operational costs
f_p	[-]	Factor for the yearly preparing costs
F	[-]	Stochastic safety factor
h	[m]	Water level
h_{pr}	[m]	Short-term prediction of the water level
H_{dike}	[m]	Height of the dike
H_{water}	[m]	Height of the local water level
$I(strengthening)$	[€]	Discounted investment costs made for dike strengthenings
l_c	[m]	Distance between cross-sections
l_d	[m]	Length of the monitored dike

L	[m]	Length of the dike section
M_d	[kNm]	Stochastic driving moment
M_r	[kNm]	Stochastic resisting moment
n	[-]	Number of sensors installed per cross-section
N_φ	[-]	Number of tests for friction angle
N_c	[-]	Number of tests for cohesion
N_w	[-]	Number of work forces
p	[€]	Purchase costs per sensor
$P(t)$	[1/year]	Probability of flooding in year t
P_{d0}	[-]	Probability that no anomaly is detected, given a high water event
P_{d1}	[-]	Probability that an anomaly is detected, given a high water event
P_f	[-]	Probability of failure
P_f'	[-]	A-priori failure probability
P_f''	[-]	A-posteriori failure probability
$P_{f,d0}$	[-]	Probability that the dike fails, given no anomaly is detected and a high water event is present
$P_{f,m0}$	[-]	Probability that the dike fails, given the measure is not applied and an anomaly is detected and a high water event is present
$P_{f,m1}$	[-]	Probability that the dike fails, given the measure is applied and an anomaly is detected and a high water event is present
$P_H(t)$	[1/year]	Probability of occurrence on a high water event in year t
P_{m0}	[-]	Probability that the measure is not applied successfully, given that an anomaly is detected and a high water event is present
P_{m1}	[-]	Probability that the measure is applied successfully, given that an anomaly is detected and a high water event is present
q	[-]	Stochastic required limit value
R		Stochastic strength
R	[-]	Reduction rate, due to sensor monitoring
$R_{\%}$	[-]	Relative spread
S		Stochastic load
SF	[-]	Safety factor
t	[year]	Moment in time
$T_{available}$	[hour]	Available time due to the early warning potential of the monitoring system
$T_{decision}$	[hour]	Time needed for decision making upon start mobilizing for execution of the flood protection measure
$T_{deployment}$	[hour]	Time needed for complete deployment of the flood protection measure
$T_{required}$	[hour]	Required time to execute the flood protection measure
$T_{transportation}$	[hour]	Transportation time needed upon starting the deployment of the flood protection measure
u		Water pressure field
$V(t)$	[€]	Potential damage due to a flood in year t
Z		Limit state function

α_c	[-]	Variance factor cohesion
α_d	[1/cm]	Scale parameter for the exponential distribution
α_φ	[-]	Variance factor friction angle
β	[-]	Reliability index
γ	[%/year]	Economic growth
γ_d	[kN/m3]	Dry volumetric weight
γ_w	[kN/m3]	Wet volumetric weight
δ	[%/year]	Discount rate
Δ	[-]	Difference in either P_f or β
ε_p	[-]	Benefit-cost ratio for the periodic safety assessment
ε_o	[-]	Benefit-cost ratio for the operational situation
φ	[°]	Internal friction angle (drained)
ζ	[1/cm]	Impact parameter for additional damage due to increased dike height
η	[cm/year]	Relative water level rise, including subsidence
λ	[1/year]	Frequency of occurrence of a valuable loading event
μ		Expected value
ρ	[-]	Correlation coefficient cohesion-friction angle
σ		Standard deviation
ψ	[1/cm]	Impact parameter for additional damage due to the water level rise

Table of contents

Appendices

1 Introduction

This chapter gives an introduction to the research and general background information on the flood safety approach in the Netherlands.

1.1 Origin of the thesis subject

At the very beginning of 2012, a near dike breach at Tolbert (Groningen) was national news in the Netherlands. Due to heavy rainfall in the northern part of the country, the Eemskanaal reached a high water level. A small dike section next to the canal impended to breach. A crisis situation arose, because limited information was available about the physical processes occurring inside the dike section. All available means were conducted: water boards from across the country asked volunteers to inspect the dikes in Groningen and also the Royal Dutch Air Force provided a helping hand by performing reconnaissance flights, tracking the dike with an infrared camera.

Meanwhile, many projects for flood defence monitoring systems are initiated by various parties. Projects like IJkdijk, Livedijk, FloodControl2015, Digidijk and UrbanFlood are all busy with monitoring flood defences with innovative sensor techniques. New insights, expertise and data have been gathered within these projects, which might be of value for the assessment of flood risk. These sensors techniques might have been useful in the Tolbert crisis situation by providing real-time dike information to get a grip on the situation. However, the technical relevance of these monitoring techniques has not been evaluated yet: sceptisisms about the innovative techniques are heard because of the relatively high investment costs for yet to be determined benefits. This research elaborates the technical implementation of sensor techniques in the Dutch flood safety approach.

1.2 Short introduction to flood safety in the Netherlands

The Netherlands has a long history with floods and flood protection, because the Netherlands is located in the delta of the rivers Rhine and Meuse, and has a coast along the North Sea. In recent history, the major North Sea flood on February 1st 1953 took the lives of 1836 people, urged 100.000 evacuees, leaving flooded lands for up to 1 year and caused 1,5 million Gulden economic damage in the Netherlands only. As a reaction, the first Delta Committee was established and formulated a new approach on flood safety, which is based on an economic analysis. Nowadays, an estimated 65% of the gross national product is generated in flood-prone areas and these areas are also densely populated with almost 9 million inhabitants (Deltacommissie, 2008). A system of flood defences protects this valuable land, consisting of primary and secondary flood defences. The primary flood defences form (or connect) dike-rings: a dike-ring protects an area enclosed by primary water defences or high grounds (i.e. non flood-prone areas). The secondary flood defences consist of regional dikes situated within a dike-ring and they protect the dike-ring area from the threat of regional waters. A flood defence is divided into smaller dike sections: a dike section is defined as a part of a flood defence which has uniform strength and load characteristics.

The current safety standards for flood defences are based on the probability of exceedance of a certain water level. Flood defences have to withstand a water level and waves with a certain probability of occurrence per year: the design loading condition. The probability of occurrence is based on the protected economic value, such that these design loading conditions vary per area.

A more integrated approach for flood safety is the probabilistic flood risk approach, which is evaluated in the project *Veiligheid Nederland in Kaart* (English: Flood Risk in the Netherlands), see (VNK2, 2011). The flood risk is defined as the probability of flooding multiplied by the impact of a flood. The probability of flooding is derived from an analysis of different dike sections for different dike failure mechanisms, as described in the next paragraph. The failure probability of a flood defence is determined for various loading conditions and combined with the occurrence probability of the loading condition, which eventually results in the probability of flooding per year. On the other hand, the impact of such a flood is related to the flood risk. After all, why bother investing in an area with a high probability of flooding, while the flooding of the area does not cause any harm? The impact of a flood consists of numerous aspects, which are generally divided in material and immaterial consequences. The material consequences consist of direct damage to properties and indirect economic damage due to business closures. The immaterial consequences consist of fatal casualties, wounded and evacuees. The flood consequences not only depend on the presence of these values in the flooded area, but also on the impact and quickness of the flood. Thus, the flood risk is affected by either changing the probability of flooding or the consequences of a flood.

1.3 Dike failure mechanisms

The failure of a dike is defined as the condition that the dike function is not fulfilled. The dike function is to prevent a water volume from flooding a particular land section. A dike collapse induces the failure of a dike. The collapse of a dike is defined as a significant deformation of soil masses. In the Netherlands, the failure of a dike has been schematized with the help of failure mechanisms. Significant failure mechanisms for dikes are distinguished for the periodic safety assessment (Ministerie van Verkeer en Waterstaat, 2007a), i.e. overflow and overtopping, overtopping instability due to infiltration and erosion, macro instability, micro instability, piping, heave, revetment instability, foreland instability, horizontal sliding and instability due to non-water retaining objects. The failure mechanisms are discussed in Appendix A.

In the situation of high water levels, the mechanisms overflow and overtopping, macro instability of the inner slope, piping and damage of the revetment are considered as critical (VNK2, 2011). Recent research developments and reports on sensor techniques focus mainly on the mechanisms of piping and macro instability. The following paragraphs describe these mechanisms in more detail.

1.3.1 Piping

Independently, piping is especially considered as a problem for dike safety in the Netherlands (Vrijling et al, 2010). There are many factors that determine the actual occurrence of failure due to piping, which is a locally occurring phenomenon. In general, the piping process can be divided into four stages (TAW, 1999), see Figure 1-1.

The loading situation consists of a water level at the outer slope of the dike which is higher than the water level at the inner side. Seepage of (outer) water through the dike will occur due to the difference in hydraulic head between the two sides of the dike. This seepage occurs in aquifers i.e. sand layers with a high permeability. A typical setting for a dike is a (permeable) sandy foundation with an (impermeable) clay dike on top. The seepage will concentrate through the sand layer. When the external water level becomes significantly high, the water pressures at the inner side of the dike will increase. Eventually, a present impermeable top (clay) layer will start uplifting as soon as this water pressure exceeds the weight of the layer (Figure 1-1a). This uplifting can cause cracks in the impermeable layer. The seepage water will flow through these cracks and forms seepage wells (Figure 1-1b). This phenomenon has no direct consequences on the functioning of the dike (i.e. the amount of seepage water is limited). However, the seepage flow velocity induces a hydraulic load on the soil particles. As soon as this load becomes significant, soil particles start to move with the seepage flow. Sand boils are formed at the inner side of the dike (Figure 1-1c). The soil starts eroding near the well and this erosion process draws back under the dike. Pipes are being formed. The pipes grow backwards due to the head difference over the dike. They also become wider and meander. These growing processes reduce the seepage flow velocity in the pipe and thereby the erosion process. A fully developed pipe forms when the head difference is significant enough to create a pipe over the full seepage length (Figure 1-1d). The erosion under the dike body causes settlement. This settlement can induce the collapse of the dike and thereby failure.

The various stages demonstrate the complexity of this mechanism. The occurrence of seepage wells does not form a threat on its own. Exceeding the critical head can cause erosion along the seepage line. However, the critical head must remain for a certain time period. Finally, the deformations due to the pipes induce a dike collapse. However, the remaining dike part can be resistant enough to prevent a flood. This principle is known as residual strength. Thus, the occurrence of a collapse (due to piping) does not have to lead directly to the failure of the dike.

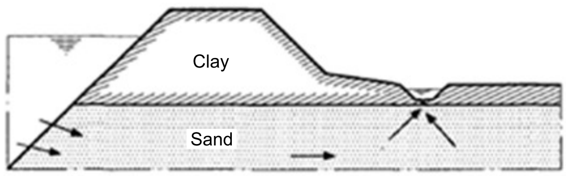

(a) Uplift of the top layer

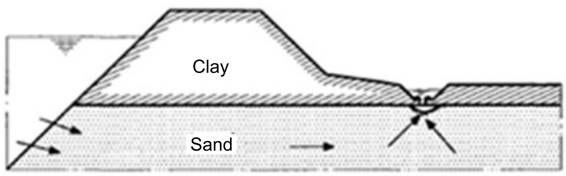

(b) Forming of seepage well, start of erosion

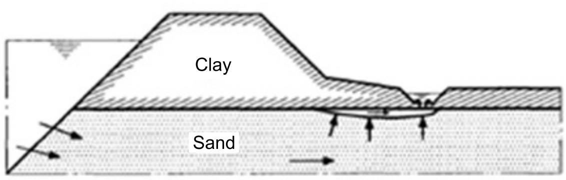

(c) Forming of pipes due to continuous erosion

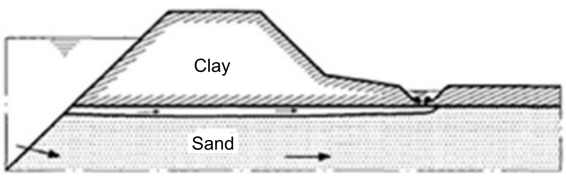

(d) Fully developed pipe (=piping mechanism)

Figure 1-1: Divided stages for piping (TAW, 1999)

1.3.2 Macro instability

Macro instability of the inner dike slope is considered as an important failure mechanism in the Netherlands. Other failure mechanisms, like overflowing and micro instability, might "trigger" macro instability (TAW, 1990). Macro instability is defined as insufficient resistance to loads such that significant deformations occur (collapse) and leads to dike failure. The deformations can occur due to sliding along straight or curved sliding surfaces or due to plastic zones. Plastic zones occur due to local overloading i.e. there is no equilibrium of forces. The balance between load and strength properties determines the safety referring to macro instability. For example, deformations due to macro instability along a curved slip surface are presented in Figure 1-2. The analysis of macro instability depends on the following dike properties (TAW, 2001):

- Geometry: outer dimensions of the dike shape
- Soil layers: layer structure of the subsoil and dike body
- Layer properties: the distinguished soil layers have their specific properties like volumetric weight (both dry and wet) and strength parameters
- Loading parameters: governing phreatic surface and water pressure distribution in the dike

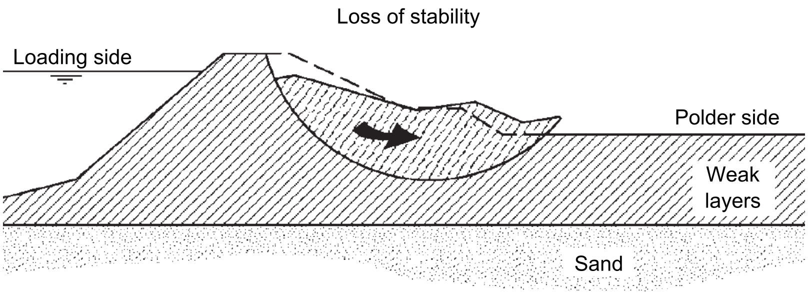

Figure 1-2: Macro instability with a curved slip surface (TAW, 2001)

The equilibrium of forces determines the macro instability of the dike. Dead weight of the soil can either act as active or passive. Active dead weight soil arises as a driving force which contributes to the macro instability. The passive dead weight soil acts as a resisting force. Macro instability occurs as soon as the balance of these forces is not in equilibrium. The dead weight of the soil is partly dependent on the water content. Therefore, the phreatic surface is an important property. The significant deformations due to macro instability induce a collapse of the dike. Yet, this partial collapse does not necessarily lead to direct failure of the dike when the crest level is not reduced. This phenomenon is known as residual strength.

1.4 Research framework

1.4.1 Problem definition

Worldwide, the constant threat of flooding triggers the need for a reliable flood risk assessment. In the Netherlands, this is even obligated by law. Guidelines are set up to guarantee a structural assessment of the flood risk. A lot of information input is needed from the flood defence system to implement these guidelines. Water boards gather this information by inspection. Both visual inspection and measurement techniques are used. However, not all required data is available in practice and assumptions need to be made regularly. For the sake of overall safety, these assumptions are often conservative. In this way, there is always a form of uncertainty of the safety margin. This safety margin can lead to unnecessary costs due to the conservative assumptions. The possible solution lies in the reduction of the safety margin uncertainty. With the application of sensor monitoring, this uncertainty might be reduced such that the risk assessment is more certain.

Another problem arises in a more critical situation when a flood defence is pushed to its limits. In this operational situation, decisions must be made within a short period of time. These decisions involve lots of responsibilities as public health and economic value are at stake. Often, not much is known about the actual state of the flood defence during operational times. This is not beneficial for the decision making processes. It is claimed that the use of sensor monitoring in flood defences leads to significant savings and provides additional warning time for operational situations, which contributes to the effectiveness of decision making during crisis situations.

The problem for this research can be defined as:

The popularity for the use of sensor techniques in flood defences is rising, but a technical foundation for the effect on the flood safety is lacking.

1.4.2 Research objective

The objective of this study is to investigate how the application of sensor techniques can be effective and cost-effective in the context of flood risk. This objective is split-up into sub-questions:

1. **What sensor techniques are available for flood defence monitoring? (chapter 2)**
   Many conventional techniques are used for the flood defence safety assessment. Also, more innovative techniques are being developed by commercial companies involved in sensor monitoring projects. In this whole field of sensors every technique would have its benefits and drawbacks.
2. **How can sensor monitoring contribute to the flood safety in the Netherlands? (chapter 3)**
   Different implementation opportunities are considered for the application of sensor monitoring; can they be applied for a more accurate flood defence failure assessment or as an early warning predictor? The implementation possibilities are discussed.
3. **What results can be attained with the help of sensor monitoring? (chapter 4)**
   The impact of sensor monitoring for the flood safety assessment is illustrated with a case study. What beneficial effects could be attained with the help of sensors?
4. **How can sensor techniques be applied in a cost-effective manner? (chapter 5 & 6)**
   From an economic point of view, an investment must turn out profitable in order to be cost-effective. The possible increase of the benefits due to the use of sensors needs to be substantial referring to the investment. Cost-benefit models are set up to give insight into the cost-effectiveness of sensor monitoring for the flood safety.

This research focusses on the application of sensor techniques in dikes consisting of soft soils (e.g. sand, clay and peat), for the failure mechanism of macro instability in the context of a probabilistic flood risk approach. The research further considers two distinct implementation perspectives, as described in the next paragraph.

1.4.3 Implementation perspectives

This research focusses on the application of sensor monitoring for two implementation perspectives. These implementation perspectives have the same purpose of increasing the flood safety, but in another perspective:

- Periodic safety assessment
- Operational situation

Periodic safety assessment

There is a legal base in the Netherlands that obligates the responsible institutes to have a 6 yearly review of the primary flood defences (article 2.12 Waterwet, 2009). This safety assessment is done with the help of a guideline (Ministerie van Verkeer en Waterstaat, 2007a). The secondary flood defences are assessed by provincial requirements. The principle of these two assessments is the same and is based on failure mechanisms (see paragraph 1.3). The hydraulic design loads are determined and presented in a legal document "*Hydraulische Randvoorwaarden*" (English: hydraulic boundary conditions). The safety assessment is elaborated for these loading conditions and the strength conditions from the flood defence information. This is done for distinguished sections of the dike-ring. A section is defined as a dike length which for both the load and strength is comparable along the length. The safety standard is met when all distinguished sections are able to resist the hydraulic design loads for different failure mechanisms. Failure mechanisms are assessed for a dike section with qualitative output parameters: Good (g), Sufficient (s) or Insufficient (i). A dike section does not satisfy the legal standard when at least one of the failure mechanisms are assessed as insufficient (i). The assessment can be made on three different levels:

- **Simple**: deterministic assessment based on geometrics and the applied design method.
- **Detailed**: deterministic assessment with the help data collection (interpretation of available information or additional field measurements) or models as described in technical guidelines and reports.
- **Advanced**: assessment by state-of-the-art knowledge, advanced calculation models, actual strength (e.g. proven strength or residual strength) or a probabilistic approach.

A top-down approach is valid; meaning that first a simple assessment is made. If the legal requirements are met, the assessment is done. If the requirements are not met, a detailed assessment follows. Eventually, an advanced assessment is the last method to assess the dike section as safe. The complexity of the assessment increases with each step.

Operational situation

The operational situation refers to the situation, in which the dike experiences an extreme load, e.g. a high water level at the outer slope. Dikes are designed and assessed to resist such design conditions. But the situation always remains when a high load is imposed on the dike and decisions must be made to secure overall safety. The definition of the operational situation is vague. Primary flood defences are frequently imposed to loads. The considered operational situation is when the hydraulic load is such that the community protected by the dike feels threatened. This is a political and social definition, which is influenced by technical aspects. When this definition of an operational situation is present, measures are often taken in order to control the situation.

1.4.4 Relevance of the operational situation

It should be emphasized that the Dutch flood safety approach is based on prevention norms and the use of repressive measures in the operational situation is considered as an additional mitigating effect (Ministerie van Verkeer en Waterstaat, 2007b). Historically, flood defences have been constructed to protect valuable land from flooding over the long-term and in times of operational situations, additional measures are instinctively taken to prevent a flood on the short-term. The high flood safety standards in the Netherlands have the consequence that operational situations occur less frequently, than would be the case with lower safety standards. Investing and improving this situation has less impact, because the operational situation is rare. Recent developments of the flood safety approach introduce Multilayered Safety to attain an integral flood safety approach (Hoss, 2010). According to the principle of Multilayered Safety (Dutch: *Meerlaagsveiligheid*), prevention of a flood is the first layer of defence, spatial solutions are considered as the second layer (e.g. elevating valuable structures) and lastly the operational situation is considered in Crisis Management (e.g. evacuation, training, flood warning and emergency measures). In (Vrijling et al, 2010), it is recommended not to rely on emergency flood protection measures as an integral discipline of the flood protection. Conditions to implement emergency flood protection measures in the flood safety approach are: first, to determine the minimal reliability of procedures for human interference during operational situations and to observe and train these procedures. And secondly to determine the structural reliability of the physical emergency measures in operational situations (Vrijling et al, 2010).

1.4.5 Outline of the report

The introduction to this study and the flood safety in the Netherlands are given in this chapter. The first phase of this research is the elaboration of relevant dike sensor techniques with the help of a literature study. An overview of the considered dike sensor techniques and their characteristics are given in chapter 2. The information obtained with these sensor techniques need to be implemented in the flood safety assessment. Chapter 3 elaborates the implementation opportunities of the sensor techniques for the failure mechanism macro instability of the inner slope, with emphasis on monitoring water pressures. After this theoretical framework, a more practical case study has been worked out in chapter 4 for an existing dike. This case study illustrates the different uncertainty aspects in a macro stability assessment and the impact of water pressure measurements on this assessment. The next two chapters present cost-benefit models to elaborate the cost-effectiveness of sensor monitoring for the two distinct implementation perspectives: chapter 5 considers the cost-benefit model for the periodic safety assessment and chapter 6 considers the operational situation. Both cost-benefit models are provided with case studies. Finally, the research conclusions and recommendations are given in chapter 7.

2 Dike sensor techniques

Different dike sensor techniques are discussed in this chapter, which can be used to monitor a dike. First, an introduction of the sensor techniques is given in paragraph 2.1. This is followed by relevant definitions in paragraphs 2.2, 2.3 and 2.4. The actual sensor techniques are elaborated in paragraph 2.5. Last, the sensor technique characteristics and conclusions are given in paragraph 2.6.

2.1 Introduction

The assessment of dike safety requires up-to-date information from the dike. This dike information can be divided into four structural elements (STOWA, 2006):

- Geometry of the dike body
- Geohydrological response on the hydraulic boundary conditions
- Soil layer composition of the dike body
- State of the revetments

This information is gathered by dike inspection. A traditional technique is visual inspection done with the 'human eye', but also other techniques (e.g. photographs, land surveying) contribute to the information supply. Nowadays, attention is paid to more advanced techniques which monitor the dike conditions over time. The initiative for the IJkdijk (English: *Calibration Dike*) projects conducted new insights and attention to innovative dike inspection techniques. Multiple full-scale dike tests are performed to validate numerous innovative sensor techniques and get insight into the failure mechanisms.

IJkdijk experiments

The IJkdijk consortium performs projects to increase the knowledge about the dike behavior during high loading conditions and to test sensor techniques for flood early warning systems (Rijkswaterstaat, 2009b and Stichting IJkdijk, 2010). The underlying motivation is as follows: if you can predict a dike collapse before it actually occurs with significant reliability, measures can perhaps be taken to reduce the effects of such am upcoming collapse. The tests are performed under controlled conditions at full-scale and with the purpose to enforce a dike collapse. The dike has been monitored with multiple sensor techniques. The controlled conditions include the loading forces on the dike and the exact positioning of the sensors. The controlled loading conditions attempt to imitate the behavior of a real hydraulic load. The soil composition and positioning of the sensors was exactly known, since the dike has been built from scratch and therefore the soil composition was known as well. Other full-scale test projects with sensors have been performed in existing dikes.

Based on the IJkdijk project results, numerous sensor techniques are discussed in this chapter. The considered sensor techniques monitor the change in geometry over time and/or the development of geohydrological processes over time. By monitoring this dynamic behavior of the processes, more information is gained on failure indicators to predict a dike collapse. The known failure indicator for macro instability is deformation: a change in geometry. The geometry can change due to consolidation processes in the dike, settlement of the subsoil or loading conditions (displacements due to e.g. piping, building activities). The known failure indicator for piping is excessive groundwater flow on a local scale: geohydrological information. The development of groundwater flow under a dike body exhibits a dynamic behavior, in the order of hours/days, and is influenced by the hydraulic boundary conditions (e.g. external water level, precipitation) and the soil layer composition. The soil layer composition is considered as static information and remains constant for decades. Heterogeneity of the soil causes uncertainties in the dike safety assessment, due to the lack of information regarding the soil layer composition. Completing, the state of the revetment is considered as static information, which can change due to loading events (e.g. storms, building activities) and can be notified by visual inspection.

2.2 Definition of a sensor technique

A sensor technique is defined as a system that monitors a physical process by transducing this process into a usable output signal. The principle of a sensor technique is schematized in Figure 2-1.

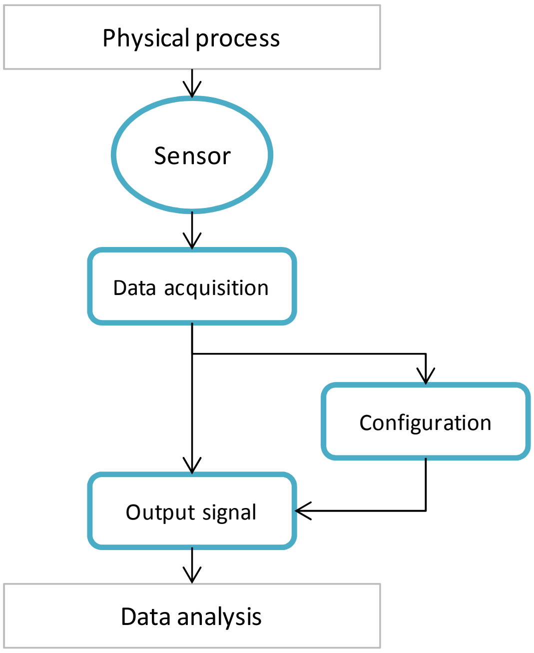

Figure 2-1: Schematic view of a sensor technique

The sensor is a transducer which converts one energy form into another. The energy of the physical process is transduced in electric energy. The sensor forms the link between the actual physical process and an analogue, electrical signal. The analogue signal from the sensor forms the input for the data acquisition system. The data acquisition system converts the analogue signal from the sensor into a digital signal. This digital signal is needed for further interpretation of the data with the help of computers. A monitoring system will consist of multiple sensors. The data acquisition system needs to cope with the different sensor inputs and acts as a gateway. The data acquisition can result in a direct output signal, which gives information about the observable variable (see paragraph 2.5.1). However, some dike sensor techniques measure other variables than the intended observable variable to be monitored. A configuration of the sensor data has to be made in order to give information referring the intended observable variable.

2.3 Definition of in situ/ex situ

Sensor monitoring can be divided by the place from which the sensor technique monitors the dike: in situ or ex situ. In situ means that the installed sensors are physically attached to the dike. Ex situ means that the sensor monitors the dike from a distance, also known as remote sensing. The distinction between in situ and ex situ is important for the influence of the sensor technique on the dike strength. If in situ sensors are placed deep in the dike core or on top of the crest, the presence of the in situ sensors can influence the physical behavior of the dike. The installation of the sensors requires equipment such as excavators or boring machines, which can damage the dike revetment or cause local settlements. Moreover, the presence of sensor strains in the dike are comparable to cables or pipelines and thus can be classified as non-water retaining objects. These objects can form a threat to the dike safety and are given special attention in the Dutch safety assessment (Ministerie van Verkeer en Waterstaat, 2007a).

2.4 Definition of early warning potential

The early warning potential (EWP) is defined as the time span between failure prediction and actual dike collapse that a sensor technique, in the current state of development, can give by continuous dike monitoring. The function of this time period is the ability to give time to execute mitigating measures before the dike fails. The presented early warning potentials are derived from literature study on IJkdijk experiments. The macro stability and piping experiments at the IJkdijk test facility granted sensor suppliers to analyze the monitoring data and determine a time span prior to collapse, at which the monitoring data indicates the upcoming collapse due to data anomalies. These early warning potential times are derived afterwards (i.e. after collapse) by geotechnical experts. Hence, that these early warning potentials can be subjective due to this work method and must be treated with care.

2.5 Overview of dike sensor techniques

The considered sensor techniques are derived from macro stability and piping IJkdijk experiments (Rijkswaterstaat, 2009b and Stichting IJkdijk, 2010) and the STOWA inspection techniques overview (STOWA, 2006):

- Water pressure meters
- Radar interferometry
- Passive microwave radiometry (PMR)
- Micro electromechanical system (MEMS)
- Thermal infrared cameras
- Fiber optics
- Laser scanning
- Mechanical sensors
- Seismic/acoustic instruments
- Self-Potential measurements

Paragraph 2.5.1 holds the observable variables that are measured by the sensor techniques. Whereas paragraphs 2.5.2 to 2.5.11 describe the considered sensor techniques in detail. The principle of the sensor technique is treated, together with the measured variables and whether an in situ or ex situ installation is concerned. Also, characteristics of the sensor technique are mentioned, together with the early warning potential as derived from IJkdijk experiments. Last, applications of the sensor technique during IJkdijk experiments are presented in text boxes.

2.5.1 Observable variables

The observable variables that are monitored tempt to give information about the failure mechanism of a dike. The considered observable variables are related with the considered sensor techniques. More traditional variables have already been measured on larger scales like water level, wave height and wind speed. However, these variables are not within the scope of this research. The following five observable variables are distinguished regarding the sensor techniques:

- **Water pressure**
  The water pressure in the dike determines the soil strength. As water pressure increases, the effective soil stress decreases according to Terzaghi's law (Verruijt, 2001). The water pressure is influenced by the effect of groundwater flow and impermeable soil layers. Heterogeneity of the soil and a water level difference over dike body cause local varieties of water pressure in the soil. Therefore, a hydrostatical distribution of the water pressure over the depth is not representative.
- **Temperature**
  Temperature is a physical property of a material. The temperature is used as an indicator for water flow through the dike. Within the context of dike monitoring, the temperature difference induces water flow. This principle is based on the groundwater temperature which differs over de depth. In general, deep laying groundwater will be colder as the influence of the air temperature is less. A concentrated groundwater flow (e.g. through a pipe) water will attract surrounding water particles from different depths. Thereby, this water mixture can induce a difference in temperature compared to the reference situation. However, this principle only holds for significant groundwater temperature gradient over the depth. Another possibility is to detect groundwater flow by temperature measurements as the surface water penetrates through the dike as a concentrated flow. In general, the surface water has a different temperature as the groundwater. This situation occurs for instance when a fully developed pipe has formed.
- **Deformation**
  Deformation is defined as a change in geometry over time. The occurrence of a deformation is the result of insufficient strength of the dike compared to the acting load. A deformation indicates that the load exceeds the strength. Thereby, the deformation parameter has an indirect relation to the strength and load on the dike. A distinction must be made for the three dimensional character of this parameter. The information of a horizontal (i.e. in two directions) or vertical deformation is different. Vertical deformation can be an indicator for both piping and macro instability. Horizontal deformation can be an indication for macro instability when the toe of the dike is pushed out due to sliding along a slip circle.
- **Vibration**
  A vibration is the oscillating deformation around an equilibrium state. Such a deformation causes pressure waves that travel through a continuum. The continuum can either be solid (e.g. soil), liquid (e.g. water) or gas (e.g. air). Deformations of the soil can induce seismic vibrations that travel through the soil. Also, groundwater flow can induce vibrations that travel through the groundwater.
- **Moisture**
  The moisture content of the soil indicates its saturation. Saturated soil has a larger volumetric weight than dry soil. This is important as heavy soil masses are more likely to slide down for sliding.

From above mentioned observable variables, the following conclusion must be emphasized:

Water pressure is the only observable variable, from the considered variables, that constitutes an input for existing (Dutch) dike safety assessment (Flood Control 2015, 2009).

2.5.2 Water pressure meters

Conventional techniques to measure water pressures inside the dike can be divided into three methods, which are all installed in situ:

- Piezometer
- Bourdon tube
- Electric pressure meter

The piezometer consists of an open tube placed in the dike with a filter at the bottom. The tube sticks out of the dike. The height of the water level in the tube determines the water pressure at filter depth relative to the atmospheric pressure. The height of the water level in the tube can be measured either by hand or automatically. However, the water needs to pass the filter. The filter separates the soil particles from the water. The filter induces a delay and damping of the water level height in the tube compared to the actual water pressure in the soil. This measurement delay is limited in the order of minutes for permeable sand layers, but it can take days for impermeable clay layers. A piezometer placed in a clay layer can therefore not measure the dynamic behavior of the water pressure (STOWA, 2006).

The Bourdon tube also consists of a filter and tube. The tube acts as a closed system and it is fully filled with water. As the water pressure in the soil changes, the pressure in the tube changes as well. This pressure change is measured with a conventional manometer at the top. The system is fragile for temperature changes and airtightness. Also the delay of the measure is significant ranging from hours (for sand) to days (for clay).

The third type is an electric water pressure meter. The difference with the previously mentioned systems is that the pressure is measured directly behind the filter. This means that a filter is placed in the soil and the pressure meter is placed directly behind this filter. The amount of water that needs to pass the filter is significantly reduced. Thereby, the adaptation time is significantly shorter and dynamic behavior of the water pressure can be monitored. Compared to the piezometer and Bourdon tube, the costs are significantly larger. The BAT water pressure meter is an example of an electric pressure meter.

The advantage using of water pressure meters is the simple installation with conventional CPT[1] push-in techniques. Also, water pressure meters have been used in dike management for decades and can therefore be considered as a proven technique. On the other hand, the sensors provide a low spatial density due to the point measurements. Information about the composition of the soil in front of the filter is essential for the interpretation of the results, due to possible damping and delay effects. Also, constipation of the filter over long monitoring periods could demand additional maintenance.

Reference monitoring (Deltares)

During the IJkdijk experiments, the reference monitoring consisted of various water pressure meters. The water pressure monitoring turned out to be a reliable reference monitoring, to which the test could be controlled and followed.

[1] CPT is the abbreviation of Cone Penetration Test. A CPT is used to determine geotechnical soil properties of soft soils by penetrating the soil with a steel cone at a constant rate. The push-in technique is referred to as the mechanical instrument used to penetrate the cone in the soil.

2.5.3 Radar interferometry

The technique refers to the Interferometric Synthetic Aperture Radar (INSAR) method and measures the geometry of the dike ex situ. The principle consists of a transponder which transmits radio waves (wave length in the order of centimeters), the waves reflect on the dike surface and the reflected waves are received again. The transponder can be mounted on an airplane or satellite. The time between transmitting and receiving indicates the distance of the surface to the transponder. The vertical resolution is in the order of decimeters and the horizontal resolution is half a meter. With a special technique analyzing the phase difference of two distinct measurements from the same measurement point, the (vertical) deformation can be computed more accurately in the order of millimeters to centimeters. This method is known as interfering. However, the positioning of the transponder is important. Positioning an airplane or satellite at the exact same location is difficult, but the problem can be partially solved by geometric correction. This method of interfering is an intense interpretation step. Besides, accuracy of the location still requires 10 m for airborne INSAR and 100 m for satellite based INSAR. This requires a tight flight schedule which is not possible in a busy airspace. Also, fixed reflecting points on the ground are required to calibrate the measurements. The positioning of these points needs to be very accurate and is subject to physical disturbances (e.g. vandalism, farmers).

The advantage of dike monitoring with INSAR is the large operation scale of the technique, such that long dike lengths can be monitored for long term settlements. Also, meteorological aspects like fog or clouds do not influence the performance of the sensor technique. On the other hand, the measurement resolution in the order of centimeters is limited for airborne INSAR. But a resolution in the order of millimeters for satellite based monitoring is obtained due to technological development. Yet, the measurement frequency is restricted by the passing frequency of a satellite, which is in the order of days. Future satellite programs might cope with this problem by launching new satellites. The measured data requires excessive interpretation by experts in order to grant dike deformation, which makes the technique less accessible for civil engineering practice. Moreover, the acquired monitoring data consists of superficial measurements (on a large scale) and does not provide local deformation inside the dike body.

2.5.4 Passive microwave radiometry (PMR)

This technique measures the microwave radiation, which is naturally transmitted by the earth with wave lengths ranging from millimeters to decimeters, to determine the moisture content of the top soil layers. PMR makes use of a limited wave spectrum (wireless communication techniques make use of the longer wave lengths whereas clouds and fog influence the shorter wave lengths). The transmitted radiation mainly depends on the water content at the earth’s surface, but also on the groundwater level, salinity and the presence of biomass (e.g. trees). The analyses of multiple radiation frequencies can give information on the water content in the top soil layers. The measurements are gathered ex situ and can be done either from an airplane or satellite. Figure 2-2 gives an example for an airborne measurement.

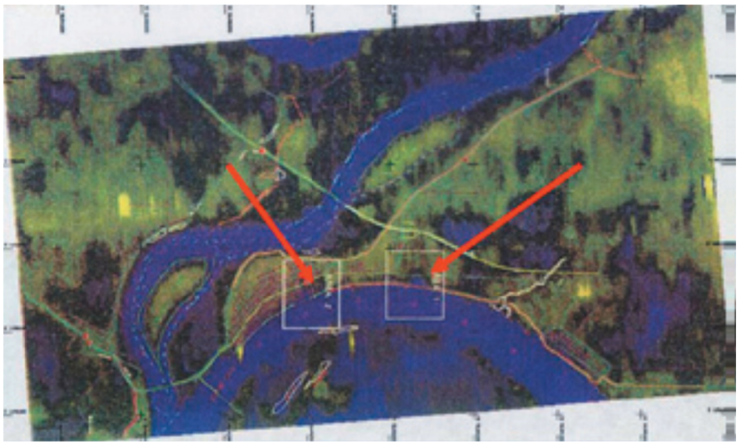
Figure 2-2: Airborne image of the water content at 1 m soil depth (STOWA, 2006)

The advantage of the PMR is the ability to monitor soil moisture on a large scale, independently of weather conditions (clouds or fog do not influence the data for specified frequencies). The disadvantage is the very course monitoring resolution and the frequency of data gathering. The latest satellite measurement instruments have a resolution of 35 to 50 km and retrieves data at a specified location every 3 days (Kerr, 2006). These specifications will need to be upgraded for the use of dike monitoring. The airborne variant can reach resolution of hundreds of meters, which is still insufficient for dike monitoring. The monitoring frequency is limited to the availability of the airspace. Another disadvantage is the signal quality near areas with a high communication density, i.e. airports and cities. The wireless communication systems in those areas disrupt PMR measurements. This disruption is known as Radio Frequency Interference (RFI). Whereas these disrupted areas have a higher priority for reliable flood protection systems due to the high economic value.

2.5.5 Micro electromechanical system (MEMS)

This technique originates from the chip building industry. Electrical and mechanical components on a micro scale are fabricated on a chip (with a micro scale from 0,001 mm to 0,1 mm). A direct conversion to a digital signal is made. The chip is installed in a protective steel module and installed in situ inside the dike body. Different variables can be monitored like water pressure, temperature, inclination and moisture. Most common MEMS-sensors are accelerometers, which are also used to trigger car air-bags, thus a proven technique in other industries.

The advantage of using MEMS sensor monitoring is the high monitoring accuracy and the ability of measuring multiple variables with a single sensor module: multisensor. The installation with CPT push-ins is a common used and simple technique in civil engineering. On the other hand, the sensor module retrieves point data measurements resulting in a low spatial density. For the interpretation of the data, the position of the module must be known. Also, monitoring of the groundwater flow requires exact positioning of the sensor module in the seepage well. Last, the sensor modules turn out to be vulnerable during experiments and cope with operational malfunctions.

Geobeads (AlertSolutions)

GeoBeads are sensor modules installed inside the dike with the ability to measure multiple parameters. The measured parameters are water pressure, temperature and deformation. The innovative, compact technology of MEMS is used. In fact, not the deformation is measured, but the change of inclination. Inclinometers measure the change in angle of the sensor module. Deformation of the surrounding soil causes this inclination. Other sensor types can be installed in a module, but the three mentioned parameters are installed in a standard module. The sensors are placed in a single steel cone. This steel cone forms the sensor module (Figure 2-3). Multiple modules are loosely connected to each other with a cable and form a chain of point sensors. The chains can either be installed vertically in a pre-drilled hole or horizontally. The horizontal installation close to the surface (in an existing dike) is done by digging a trench and filling it after with the original material. Installation in deeper parts of the dike body has not been performed in an existing dike. The data acquisition system is placed on board and a digital signal is sent through the communication cable. Power supply is granted through this same cable.

Figure 2-3: GeoBeads sensor module (Rijkswaterstaat, 2009b)

The water pressure sensor measures absolute values, which need to be compensated with the atmospheric pressure to obtain the actual water pressure value. The atmospheric pressure needs to be measured with a separate sensor outside the dike body. This correction step is not automated and needs to be done during the data configuration. The GeoBeads monitoring system had several malfunctions of 30 to 40 minutes during the macro stability IJkdijk experiment within a total monitoring period of several days. Also, longer term measurements in LiveDijk Eemshaven revealed eight malfunctions lasting 1 to 7 days (in total 36 days) during a monitoring period of half a year (Deltares, 2011a). The average downtime of the monitoring system was 20% in this case.

Smart Dike Probes (Koenders Instruments)

The MEMS technology is used in this system to measure the inclination and water pressure. A module can be expanded with a temperature sensor. Figure 2-4 illustrates the sensor modules. Different sensor modules are connected to each other and can be placed vertically or horizontally. The connecting points form hinges. The connected modules can be equipped with different sensors. The casing can be made of steel or plastic. Installation can be done with the use of CPT push-in techniques.

Figure 2-4: SDP sensor modules with rigid connections (Rijkswaterstaat, 2009b)

The power supply for the sensor modules is guaranteed by cable from the power network, with a battery on board for backup. The power supply from the cable failed during the IJkdijk experiment and the backup battery also ran down. This implied no data gathering during at least a day.

Multiple inclinometers can be placed vertically in different modules. Because of the hinged connections between the modules, an inclination pattern over the depth can be made. This can be translated into a deformation pattern, if a fixed point can be obtained for the deepest point of the module chain. By multiplying the module length with the measured inclination, the deformation over de total length of a single module can be obtained.

2.5.6 Thermal infrared cameras

Specialized thermal infrared cameras are used to detect differences in temperature at the surface of the dike from a distance. Either an airborne or terrestrial variant can be used for this ex situ technique. The terrestrial version is suitable for local monitoring and the airborne version can monitor large areas. The principle relies on measuring radiated infrared heat, which is measured with the thermographic cameras. Absolute measurements are not used. The relative temperature differences in time and space give contextual information. The cameras can either monitor a whole dike or particular sections of the dike (e.g. the dike toe). The radiated infrared waves from the dike are influenced by environmental factors like the air temperature, fog and radiation heat from the sun. Also, the presence of rain is expected to influence the measured radiation from the dike.

The advantage of thermal infrared cameras is the high monitoring resolution and the high spatial density. A distinction must be made based on the monitored area: the airborne variant can monitor a large area, whereas the terrestrial variant covers a relatively small monitoring area (per pylon). Also, the sensitivity for environmental circumstances influences the reliability of the monitoring data. Moreover, a clear sight on the dike surface is needed to guarantee reliable monitoring data. Last, thermal infrared cameras are applicable for piping detection only. Macro stability monitoring can be done by installing optical cameras (see text box *IDS System*). The early warning potential of the IDS System gives indications for collapse varying from 45 hours to 102 hours prior to collapse during the piping experiments. The extension with optical cameras granted deformation indicators some 4 hours prior to collapse.

IDS System (Intech)

The Intech Dike Security system makes use of a mobile sensor system installed in a car. The autonomous power supply can be delivered by batteries for a period of 8 hours. The cameras are mounted on a stabilized pylon, see Figure 2-5. Different types of thermographic cameras have been used and the system can be extended with optical cameras. During the piping experiment at the IJkdijk, a major malfunction occurred in the thermographic monitoring system due to a cable crack and software failure.

Figure 2-5: IDS system stabilized installation pylon (Stichting IJkdijk, 2010)

2.5.7 Fiber optics

Fiber optic cables are used to measure the temperature and/or deformation by in situ measuring. The initiative for this technique is the information density that is provided along the length of the fiber (often applied for monitoring along the dike length). This technique has been used in other civil engineering structures, like concrete dams, to detect leakage. The basic principle consists of a glass fiber cable, through which concentrated laser light is send. The signal is distorted due to environmental processes around the glass fiber cable, such as deformations and temperature changes. The spectrum of the laser light needs to be analyzed in order to detect these distortions; two methods are distinguished:

- Distributed, reflecting method
- Non-reflecting method

The distributed, reflecting method uses interpretation methods such that strain and temperature differences can be detected for several points along the (glass) fiber cable. The optical signal is thereby reflected at several points along the cable. In this way, information can be gathered for multiple points along the length of the cable. As the soil around the cable is distorted (soil deformation), the cable will be stretched. This cable strain induces a spectral change of the light signal. The temperature around the cable affects the mechanical properties of the cable. Thereby, the spectrum is also changed. Temperature differences are computed by data configuration using the Raman scattering principle. Strain differences in the cable are computed by data configuration using the Brillouin scattering principle. Specific frequency shifts in the reflected signal indicate the occurrence of either strain of temperature differences. Thus, this technique gives information for multiple points along the cable after data configuration. The non-reflecting method sends a signal through the optic cable and a read-out unit analyzes the output signal which has travelled through the cable. A difference in frequency or amplitude of the signal indicates a phenomenon along the cable. Thus, the configuration of one signal gives information over the whole length of the cable.

The advantage of fibers optics is the high monitoring density along the length of the cable, with a high resolution. The technique is new for applications in dikes, but is considered as a proven technique in the concrete dam industry for leakage detection. On the other hand, the fiber optic cable is thin and thereby measures only local physical processes. To detect seepage wells through the dike, the cable must be installed exactly in the permeable layer, which requires detailed knowledge about the soil layer composition. Last, the installation of the fiber optic cables in existing dike bodies requires excavation upon the installation depth, which influences the dike strength. Early warning potentials in the order of 24 hours are attained with the GeoDetect system for both the piping and macro stability experiments. The GTC system could detect data anomalies 1,5-2,5 hours prior to collapse during the macro stability experiment.

Dike Survey

The Dike Survey system consists of plastic fiber optic cables, through which laser light is sent through. The non-reflecting method has been applied. Spectral analysis shows distortions along the length of the cable. These distortions follow from strain differences in the cable, which identify soil deformations in the surrounding of the cable. During the IJkdijk piping experiment, the system worked well but the influence of other monitoring systems disrupted the data.

Geodetect (TenCate)

Glass fiber cables are implemented in a geotextile of 0,40 m width. Both cable strain (soil deformation) and temperature can be measured with a single geotextile. The reflecting method is applied whereas measurements can be made every 0,5 to 1 m along the cable. The beneficial effect of the geotextile is the increased sensitivity for to be detected phenomena compared to a single cable. The width of the geotextile increases the physical sensitivity. The system worked continuously during the macro stability experiment at IJkdijk without malfunctions.

GTC Kappelmeyer

This glass fiber optic cable uses the reflecting method to measure temperature differences every 0,5 m along the length of the cable. No strain measurements are done. The fiber optic cable is protected with a metal coating. This metal coating forms a protection to rodents. The unique property of this system lies in the so-called heat-pulse method, which is an active measuring technique. The metal cable coating is heated up with the use of an electric current. The generated heat is conducted by the surrounding groundwater. The rate of heat conduction increases if there is an increased groundwater flow (e.g. due to the formation of pipes). The sensitivity for the temperature differences is increased, compared to the passive measuring of the temperature change. Also the difference in water temperature is no longer required.

The system delivered continuous data during the IJkdijk experiments. However, during the LiveDijk Eemshaven project, a number of nine malfunctions occurred lasting 2 to 20 days (62 days in total) over a period of half a year (Deltares, 2011a). The downtime thereby is 33% in this project.

2.5.8 Laser scanning

Laser scanning is used for the inspection of flood defences for altimetry measurements to retrieve geometry information. This ex situ technique is used for deformation monitoring by comparing two altimetry measurements performed at different times. The automated system is known as LIDAR (Light Detection and Ranging). Two different execution methods are: airborne (plane or helicopter) and terrestrial. The airborne variant has the capabilities to measure large areas. The method is an active remote sensing technique based on sending laser pulses on a regular frequency and measure the reflected signal. The technique delivers superficial measurements. The laser signal is not visible for the human eye as the frequency is near-infrared (around 1000nm). The travelled distance of the optic signal can be derived from the reflection time. The intensity of the reflected signal gives an indication of the reflected surface. Fixed points are needed to determine the position of the scans with the help of Kinematic GPS. These fixed points are essential for the performance of the system.
A substantial difference between the terrestrial and airborne variant is the measuring angle with respect to the dike. The airborne variant has a top view of the dike and thereby the vertical deformation can be measured. The terrestrial variant has a horizontal viewpoint and thereby suits horizontal deformation detection. This distinction is important for the detection of different failure mechanisms. Performed airborne laser scanning in the Netherlands has a bias in the order of 0,03 m and a standard deviation is 0,04 m.

The advantage of laser scanning is the high monitoring density and the high resolution. On the other hand, a clear sight on the dike surface is required to attain reliable monitoring data. Also, sensitivity for fog, clouds and rain have a negative effect on the reliability. Moreover, the measurements only apply to the surface in the dike. The early warning potential of the Hansje Brinker laser scanning system detected anomalies 26 to 42 hours prior to collapse, that could indicate the fatal collapse.

> **Hansje Brinker**
> Terrestrial laser scans are performed as an ex situ sensor system to monitor local horizontal deformations. The used scanner (Leica ScanStation 2) is able to produce 250,000 measurement points per scan. The acquisition of one scan lasts 8 minutes. The maximum measurement distance is restricted. This restriction is caused by the absorption property of the measured material. The maximum distance for clay soil holds 130 m. A clear view from the measurement point is needed during the measurements. Fixed reference points need to be installed on the dike to calibrate the measurements by eliminating displacements of the axis. The measurement bias is 15 mm and the standard deviation is 5 mm. The system worked continuously during the IJkdijk macro stability experiment.

2.5.9 Mechanical sensors

Conventional mechanical sensors are used in other civil engineering industries to monitor deformations. All sensors need to be installed in situ. These sensor techniques are:
- Inverted Pendulum (inclinometer)
- In-place Inclinometer
- Liquid Level Settlement sensor
- Absolute water level sensor

The Inverted Pendulum measures horizontal deformation in two main directions. The sensor consists of a vertically placed (stiff) tube, in which a string is installed from bottom to top. This string is connected to a float at the top of the tube, which floats in water and remains in a vertical position due to gravitational forces. If the dike body deforms over the length of the vertical tube, this tube will deform as well. The deformation is measured as a position movement of the tube relative to the float: a single deformation is measured at the top of the tube and this deformation is caused by the inclination of the whole tube (see Figure 2-6). The bottom of the tube needs to be installed in a fixed layer. When this is not the case, the deformation at the bottom of the tube will disturb the measurements. This technique is a point sensor, however the total length of the tube influences one measurement.

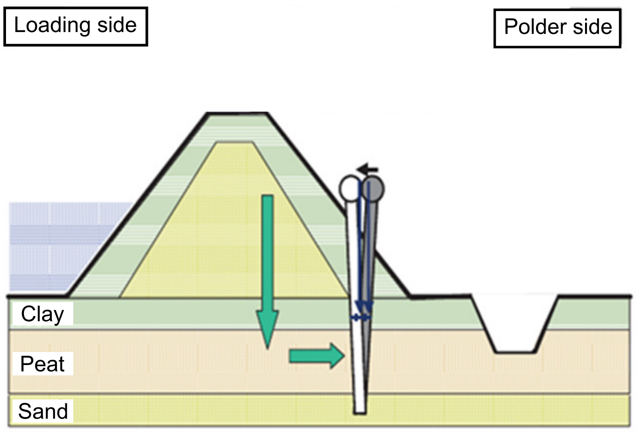

Figure 2-6: Cross-sectional view of the Inverted Pendulum measurement principle (Rijkswaterstaat, 2009b)

The In-place Inclinometer sensor consists of multiple stiff modules, in which inclinometers are installed. The modules are connected with hinges. An inclinometer sensor measures the inclination of the sensor relative to a starting position. The connected modules are installed vertically in a fixed layer, see Figure 2-7. As deformations occur in the dike body, the modules deform as well. By multiplying the inclination values with the length of the sensor module, a deformation profile over the depth of the dike body can be generated.

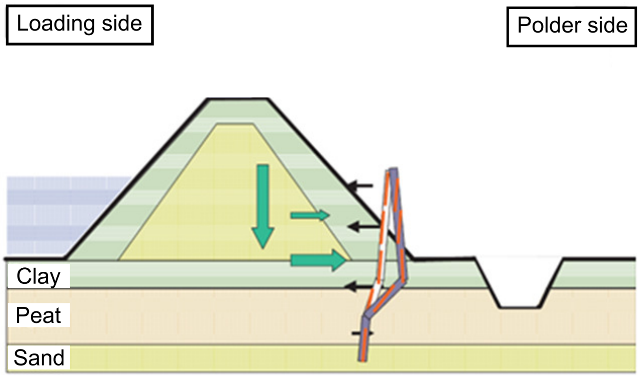

Figure 2-7: Cross-sectional view of the Inplace Inclinometer measurement principle (Rijkswaterstaat, 2009b)

The Liquid Level Settlement sensor measures the deformation differences. The system consists of several pressure meters, connected to each other with a closed, flexible hose system filled with water. A water pressure difference in the closed system is induced when deformation occurs around the sensors. So the relative deformation is measured by water pressure differences. The sensors are corrected for changes in temperature (by measuring the temperature in each sensor module) and air pressure changes (by measuring the atmospheric pressure). Absolute deformation data can be derived by installing a sensor at a fixed reference point. Horizontal installation of the sensor module, along the dike crest, can indicate vertical settlements.

The Absolute Pressure meter consists of pressure meters, which have been installed in a flexible hose. This hose is filled with water and forms a closed system. The principle is comparable with the LLS sensor, yet the AP sensor has a simpler design. The measurements are corrected for changes in temperature. The absolute pressure measurements are converted to absolute deformation with the help of a fixed point.

The advantage of the mechanical sensor techniques is the high monitoring density along the length of the module and the techniques are already applied in the geo-engineering industry. On the other hand, the monitoring density is restricted due to the single measurement over the length of the sensor. And the sensors require an extensive installation, which can be a problem for installation in existing dikes. Last, the sensors turned out to be vulnerable during the IJkdijk experiments. The IS-system detected deformation anomalies during the macro stability experiment 24 hours to 36 hours prior to collapse.

IS-system (RPS, IFCO)

A combined system of above mentioned sensors has been installed during the macro stability experiment at the IJkdijk location. Also, a BAT water pressure meter has been added to the monitoring system. Each sensor has been connected to a data logger, to save the data intern at an adjustable frequency. The system worked continuously during the macro stability IJkdijk experiment. Yet, installation problems caused disruptions in the data gathering.

2.5.10 Seismic/acoustic instruments

Seismic/acoustic instruments tempt to measure pressure waves caused by vibrations that travel through a continuum. Seismic instruments refer to the sensor technique which measures pressure waves travelling through a soil continuum. Acoustic instruments measure pressure waves traveling through a liquid or gas. A distinction must be made between passive and active seismic acoustic sensor techniques.

The passive sensor technique measures vibrations in the soil, which are pressure waves travelling though the soil. Geophones are used to measure seismic behavior of the subsoil due to earthquakes and are highly sensitive. A hydrophone is an acoustic instrument which can be used to detect vibrations of the pore water, when the soil is saturated. These vibrations can be caused by either groundwater flow or soil deformation. Microphones measure pressure waves travelling through air and can detect pressure waves traveling through the soil pores of unsaturated soils.

Active seismic measurements are used to get more information about the soil layer structure. Mechanical surface waves are generated and travel through the subsoil as Rayleigh waves. These surface waves are detected with seismic sensors. The traveling speed of different wave lengths is dependent on the (mechanical) properties of the soil layers (dispersion). By analyzing this dispersion of the surface waves on different positions along the dike, the soil structure can be specified. Local variations in the soil layers can be identified such as weak peat layers or compact sand layers. The seismic waves reach to approximately 30 m depth. By placing the seismic sensors inside the dike, groundwater flows can be detected. The reliability of this technique can be significantly increased with the availability of CPT push-ins.

The advantage of seismic/acoustic instruments is the high monitoring density that can be obtained with a network of multiple sensors and the high resolution of the sensors. On the other hand, the sensors are highly sensitive to surrounding activities that have no relevance to the dike strength (e.g. traffic, airplanes, talking), which reduces the reliability. Also, an extensive installation method is required to place the sensors inside existing dike bodies.

Luisterbuis (TNO, Landustrie, VolkerWessel Telecom)

The Luisterbuis system is a combination of sensors and an actuator (i.e. an instrument which influences the physical process). Hydrophones and microphones are installed in the dike body to measure vibrations. The microphones are placed above the expected phreatic groundwater level, thus in dry soil. The hydrophones are placed deeper in the dike body and can measure below the phreatic surface. Besides these pressure wave sensors, an actuator system is installed. This actuator consists of a drainage tube installed in a permeable soil layer along the length of the dike. When the drainage tube is activated, water will be drained from the aquifer and the hydraulic loads in the dike are reduced.

2.5.11 Self-potential measurements

Self-potential measurements refer to the geophysical sensor technique which measures the electric potential differences of the dike. The electric potential is generated as self-potential by water moving through the porous soil. The interaction of the water particles with the soil particles generates electric potential. Also objects in the dike, e.g. pipes, generate an electric potential. The measurement principle is based on measuring the presence of the naturally present electric potential and hereby is a passive sensor technique. The difference in electric potential is measured between a non-polarized measurement electrode and a reference electrode. The distance between the measurement and reference electrode needs to be incorporated in the electric potential difference. Spatial coverage is provided by installing multiple measurement electrodes. The technique originates from the mining exploration industry (minerals and fossil fuels).

Advantage of self-potential measurements is the high spatial density and the high measurement resolution. Besides, the technique is widely applied in other civil engineering industries. On the other hand, the high sensitivity of the sensors is vulnerable to surrounding activities and influences the monitoring data. The IJkdijk piping experiments resulted in an early warning potential time of 8 hours for the ITC system and 4 hours for the Fugro system.

ITC Enschede

ITC Enschede placed multiple electrodes at the surface of the dike. The reference electrode position was changed in order to create a reliable reference measurement. The measurement noise is relatively high due to activities around the dike. This has been filtered with a band pass filter.

SP monitoring (Fugro)

Fugro applied a self-potential sensor system on a dike section with a reference electrode on top of the dike and the measurement electrodes at the dike toe, see Figure 2-8. The raw measurement data was filtered with high-pass and low-pass filters to reduce measurement noise.

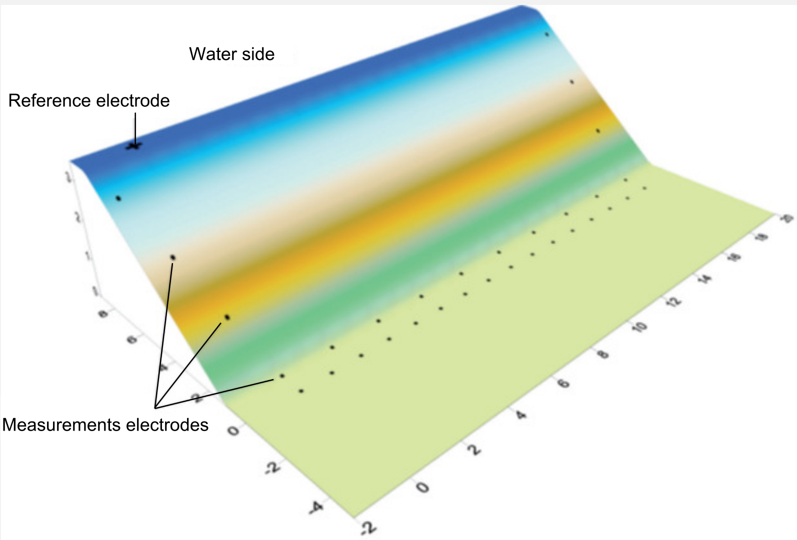

Figure 2-8: Electrode locations along a dike section (Stichting IJkdijk, 2010)

2.6 Conclusions

A sensor technique is defined as a transducer which monitors a physical process in a dike by transducing the physical process in a digital signal. Innovative sensor techniques are in development for dike monitoring within the IJkdijk project. The characteristics of the sensor techniques are summarized in Table 2-1.

The sensor techniques differ with respect to the monitored observable variable (e.g. water pressure, temperature, deformation, vibration, moisture), technical performance (e.g. resolution, measurement frequency), monitoring density (e.g. point measurement, full dike coverage), place of installation (in situ or ex situ). Thereby, the choice for a sensor technique (or a combination) differs per situation and critical failure mechanism.

The time span for potential early warning of a dike collapse, the early warning potential, varies widely from 1,5 hours to 42 hours for macro instability and from 4 hours to 102 hours for piping (attained from analysis of IJkdijk experiments). The wide spread depends on the applied sensor technique and corresponding interpretation. The reliability of these preliminary early warning potentials is doubtful at the current state of research, because the testing circumstances are controlled and the analyses are not done independently (i.e. possible subjectivity). Also the behavior of dike failures in existing dikes is expected to be different due to both strength and loading heterogeneities. Whereas the time to prediction is unreliable, all discussed sensor techniques are able to locate potential weak spots in the monitored dike section, if installed with a sufficient monitoring density.

The measurement interpretation of in situ sensor techniques (especially water pressure sensors, MEMS and fiber optics) is dependent on the surrounding soil in which the sensor has been installed. Therefore, information about the soil composition is required. Also, the installation of an in situ monitoring system can be extensive as the sensors might need to be installed in deep layers.

It must be emphasized that from the discussed observable variables, water pressure is the only variable that constitutes an input for the existing dike safety assessment models used in the Netherlands. Thereby, monitoring of water pressures is concerned the smallest step to a permanent dike monitoring system.

Table 2-1: Sensor technique characteristics (EWP= Early Warning Potential time from IJkdijk experiments ** no EWP obtained during this study)*

Sensor technique	Observable variable	In situ/ex situ	Advantages	Disadvantages	EWP* macro instability	EWP* piping
Water pressure meters	Water pressure	In situ	Installation with CPT push-in Proven technique in dikes	Possible damping and delay Point measurements Constipation of the filter	-**	-
Radar interferometry	Deformation	Ex situ	Large scale monitoring Long term settlement monitoring No meteorological influences	Low resolution Low monitoring frequency Superficial monitoring Intense interpretation	-	-
Passive microwave radiometry	Moisture	Ex situ	Large scale monitoring No metrological influences	Low resolution Low monitoring frequency	-	-
Micro electromechanical system	Deformation, water pressure, temperature, moisture	In situ	High resolution Multiple parameters Installation by CPT push-ins	Point measurements Vulnerable sensor modules Measurement position is important	-	-
Thermal infrared cameras	Temperature	Ex situ	High resolution High spatial density Large monitoring area (airborne)	Sensitive for fog, rain, clouds Small monitoring area (terrestrial) Clear horizontal sight required (terrestrial) Piping detection only	4 hours	45-102 hours
Fiber optics	Temperature, deformation	In situ	High spatial density over length High resolution Proven technique in civil engineering practice	Local detection only Intensive installation Installation in permeable layer required	1,5-24 hours	24 hours
Laser scanning	Deformation	Ex situ	High spatial density High resolution	Clear horizontal sight required (terrestrial) Superficial measurements Sensitive to fog and rain	26-42 hours	-
Mechanical sensors	Deformation	In situ	High vertical spatial density Partly proven techniques in geo-engineering	Extensive installation Vulnerable sensors Point measurements over length	24-36 hours	-
Seismic/acoustic instruments	Vibration	In situ	High spatial density High resolution	Highly sensitive to surrounding activities Extensive installation	-	-
Self-potential measurements	Electric potential (due to groundwater flow)	In situ	High spatial density High resolution Proven technique in civil engineering practice	Highly sensitive to surrounding activities	-	4-8 hours

3 Implementation of sensor information

This chapter holds implementation possibilities for the application of sensor techniques in the flood safety assessment. This has been worked out in a probabilistic approach, with emphasis on monitoring water pressures for macro instability. First, a general introduction to the probabilistic dike safety approach is given in paragraph 3.1, whereas paragraph 3.2 gives more details on the probabilistic approach for macro stability. Paragraph 3.3 holds the extrapolation of water pressure measurements. Next, paragraph 3.4 evaluates the implementation in early warning situations and paragraph 3.5 the implementation for unforeseen risks. Then the implementation in the proven strength method is evaluated in paragraph 3.6. Finally, paragraph 3.7 gives the conclusions.

3.1 Introduction

3.1.1 Dike failure probability

The dike failure probability P_f is elaborated from distinct failure mechanisms, each with a specified limit state function with the general form (TAW, 1990):

$$Z = R - S$$

Z	Limit state function
R	Stochastic strength
S	Stochastic load

The strength of the dike (dike characteristics) and the load affecting the dike (hydraulic boundary conditions) are specified by random variables to incorporate uncertainties. The strength and load can be described by an expected value μ and standard deviation σ. The probability of dike failure P_f is defined as:

$$P_f = P(Z < 0) = P(R < S)$$

As the load S exceeds the strength R, the strength R is unable to resist the load S and the dike fails. Determination of the strength and load characteristics is based on the available information. An example relation between the load S, strength R and the failure probability P_f is illustrated in Figure 3-1 (for normally distributed variables).

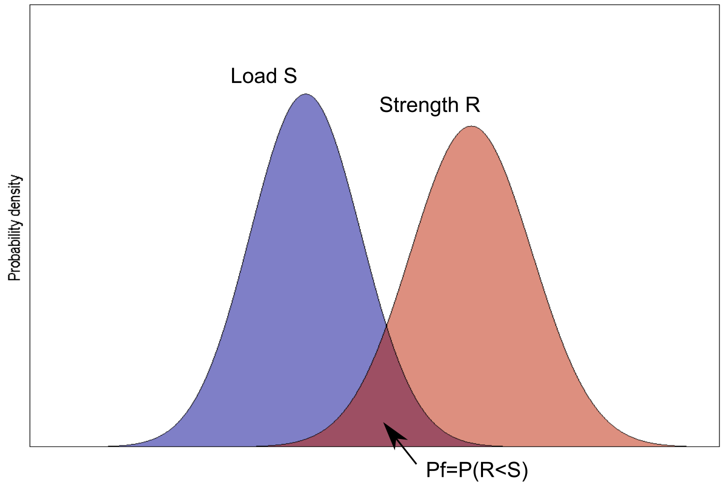

Figure 3-1: Example relation between load S, strength R and failure probability P_f

The fragility of a dike is defined as the dike failure probability, given a specific load. The development of the dike failure probability P_f can be elaborated by considering multiple loading conditions. Taking into account the probability distribution of these loading conditions, the dike failure probability P_f can be written as (assuming R and S are independent):

$$P_f = \int_{s=0}^{s=\infty} P(R < s \mid S = s) f(s) ds$$

s	Realization of variable load S
P(R<s|S=s)	Dike failure probability given load s
f(s)	Probability density function of S

The conditional dike failure probability P(R<s|S=s) increases as the loading condition increases (i.e. for a given dike strength). The relation between the conditional dike failure probability P(R<s|S=s) and the loading condition is presented in a fragility curve, see Figure 3-2.

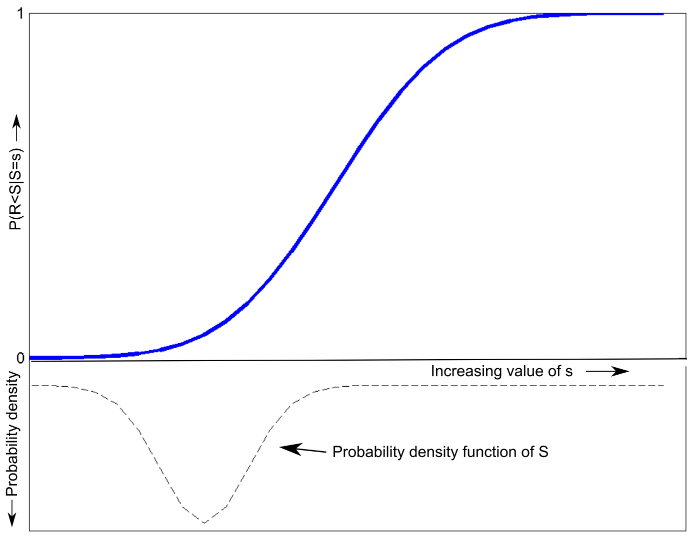

Figure 3-2: Fragility curve of a dike and the probability density function of S

The interpretation of the limit state function Z is dependent on the principle of each failure mechanism (see Appendix A). For example, the dike geometry is an important strength characteristic for overtopping, but not for revetment instability. The permeability of a sand layer does not affect the limit state function of overtopping, but is crucial for piping assessments. A simple example for the failure mechanism of overflow has been elaborated to illustrate the principle of a limit state function. The limit state function for overflow is defined as:

$$Z_{\text{overflow}} = H_{\text{dike}} - H_{\text{water}}$$

$Z_{overflow}$	Limit state function overflow
H_{dike}	Height of the dike
H_{water}	Height of the local water level (i.e. water level at the dike)

The load consists of the water height H_{water} and the resistance consists of the strength H_{dike}. The failure of the dike due to overflow is defined as the local water level H_{water} exceeding the dike height H_{dike} (i.e. the water will flow over the dike, harming the land protected by the dike):

$$P(Z_{\text{overflow}} < 0) = P(H_{\text{dike}} < H_{\text{water}}) = \int_{h=0}^{h=\infty} P(H_{\text{dike}} < h \mid H_{\text{water}} = h) f(h) dh$$

Here, f(h) is the probability density function of water levels H. Let's assume normal distributions for both H_{dike} and H_{water} with: $\mu(H_{dike})$=11 m, $\sigma(H_{dike})$=1 m, $\mu(H_{water})$=6 m and $\sigma(H_{water})$=1,8 m. The dike failure probability equals 7,5E-3. The corresponding probability density function is given in Figure 3-3.

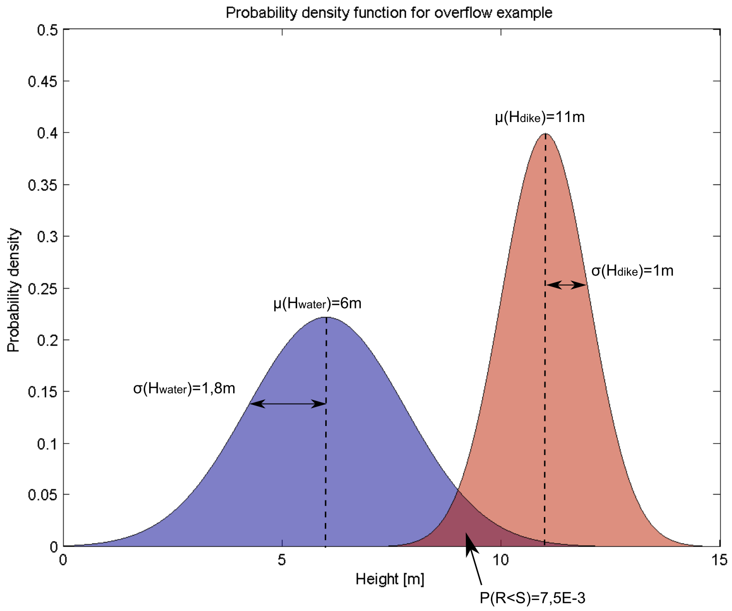

Figure 3-3: Probability density function for the failure mechanism overflow

3.1.2 A-priori and a-posteriori dike failure probability

A distinction is made between the dike failure probability without additional information (a-priori) and with additional information (a-posteriori). The a-priori dike failure probability consists of the assessment in a reference situation, as described in paragraph 3.1.1. The a-posteriori dike failure probability consists of the updated reference assessment by additional information. The relation between the a-priori failure probability and a-posteriori failure probability is given by (according to Bayes' theorem):

$$P(Z < 0 \mid \text{data}) = \frac{P(Z < 0 \cap \text{data})}{P(\text{data})} = \frac{P(\text{data} \mid Z < 0) \cdot P(Z < 0)}{P(\text{data})}$$

P(Z<0|data)	A-posteriori dike failure probability (conditional on the additional information
P(data|Z<0)	Likelihood function; probability on additional information given Z<0
P(Z<0)	A-priori dike failure probability
P(data)	A-priori probability on additional information

The a-priori dike failure probability has been updated with the extra information to the a-posteriori dike failure probability. Additional information might consist of traditional local investigation (e.g. CPT push-ins, borings, geophysical measurements), but especially sensor monitoring for this research. Applying additional investigation on the dike will influence the dike failure probability P_f. This induces an update for the strength characteristics, often leading to uncertainty reduction regarding the strength. To illustrate this effect, the overflow example from paragraph 3.1.1 is considered. The dike height H_{dike} has a standard deviation $\sigma(H_{dike})$=1 m. In practice, the dike height can be measured rather easily with altimetry measurements. The uncertainty regarding the dike height H_{dike} is reduced, due to the altimetry measurements: the dike height is measured with high spatial density. Assume that the mean value remains constant at $\mu(H_{dike})$=11 m and the standard deviation is reduced to $\sigma(H_{dike})$=0,1 m due to the altimetry measurements. Figure 3-4 shows the a-posteriori limit state function, due to a reduction of the dike strength uncertainty. The resulting a-posteriori dike failure probability P_f is equals 3,8E-3 (from the a-priori failure probability 7,5E-3). Monitoring of the water levels will affect the characteristics of the load S (instead of the strength R) in the a-posteriori assessment. The same holds for sensor monitoring of the water pressures.

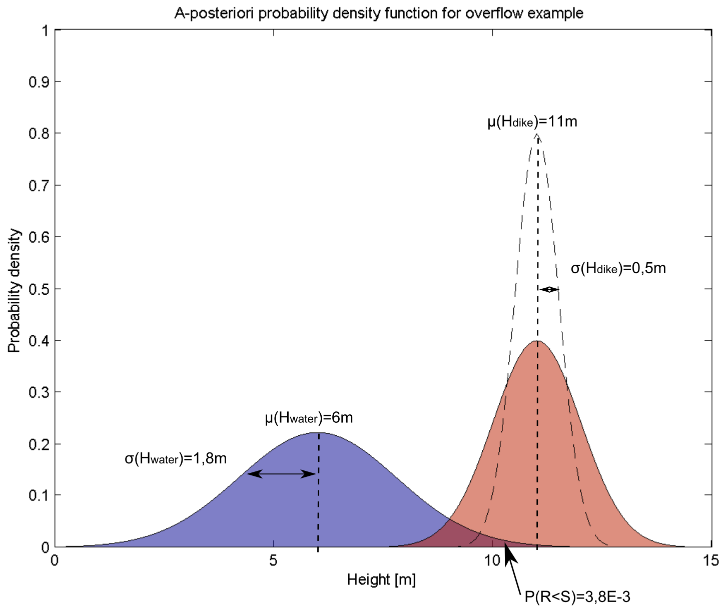

Figure 3-4: A-posteriori dike failure probability due a reduction of strength uncertainty by altimetry measurements

3.2 Probabilistic assessment of macro instability

3.2.1 Limit state definition

The assessment of macro instability is done by evaluating the resistance to soil sliding in relation with the loads causing the sliding. In the Netherlands, a safety evaluation is made with a physical model, for a determined loading condition: the water pressure field[2]. The critical slip surface is determined, for which the ratio F between the resistance and load is the smallest. The cross-sectional limit state function for a slip surface Z_{macro} can be defined as:

$$Z_{\text{macro}} = \frac{R}{S} - q = \frac{M_r}{M_d} - q = F - q$$

Z_{macro}	Limit state function for macro instability
M_r	Stochastic resisting moment of the critical slip surface (stochastic strength R)
M_d	Stochastic driving moment of the critical slip surface (stochastic load S)
F	Stochastic safety factor
q	Stochastic required limit value

[2] Loading conditions induced by earthquakes, traffic and wind are not considered in this research.

Here, the stochastic variable F is determined by the stochastic characteristics of the strength R and load S. The limit value q is a random variable representing the uncertainty of the model approach. Solving the limit state function Z_{macro} results in a failure probability P_f:

$$P_f = P(Z_{\mathrm{macro}} < 0) = P(F < q)$$

As the safety factor F exceeds the required limit value q, the determined safety factor F is considered insufficient and the dike is considered to fail. Determination of the F and q characteristics are based on the model input characteristics and schematizations. The failure probability P_f depends on the joint probability density of these input characteristics and schematizations, see 3.2.2. The relation between the safety factor F, limit value q and the failure probability P_f is illustrated in Figure 3-5. A perfect model, approaching reality, has an expected value of q=1 with a standard deviation 0. Higher probabilities of failure are attained by a higher value of q or a lower value of F.

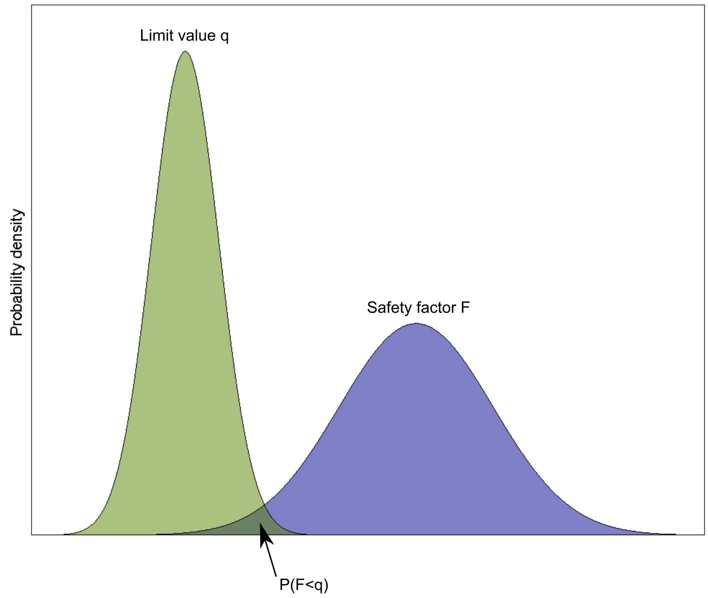

Figure 3-5: Probability density function for macro stability

The fragility of a dike regarding macro instability can be defined as the failure probability for macro instability, conditional on a specific loading condition. In the Netherlands, flood safety standards are based on the exceedance probability of a water level h. It should be emphasized that the water level h, on itself, does not act as a loading characteristic for the macro instability failure mechanism. The water pressure field u forms the loading condition for macro instability. However, the corresponding water pressure field u remains uncertain for given water level h. The development of the water pressure field u depends on numerous aspects, e.g. precipitation, water level, overtopping, soil permeability and time. The water level h is considered as a governing aspect, on which the hydraulic boundary conditions are based for primary water defences. Therefore, macro instability is assessed for the water pressure field u, related to the water level h: u(h). Taking into account the probability distribution of u(h), for given value of h, P_f can be defined as:

$$P_f(h) = \int_{u(h)=-\infty}^{u(h)=\infty} P\{Z_{\text{macro}} < 0 \mid u(h)\} f(u(h))du$$

h	Water level
$P_f(h)$	Macro instability failure probability, for given water level h
u(h)	Water pressure loading condition for corresponding water level h
$P\{Z_{macro}<0\|u(h)\}$	Failure probability for macro instability, conditional on the water pressure field for the corresponding water level h
f(u(h))	Probability density function of u(h)

The limit state function Z_{macro} is defined as a function of u(h), but Z_{macro} is a function of many aspects, see 3.2.2. $P_f(h)$ can be elaborated for numerous loading conditions consisting of the water pressure field u(h), given the water level h. But a different water pressure field u(h) is obtained for a different water level h. The total failure probability P_f can be elaborated by taking into account various water levels h, the probability density function of these water levels and the corresponding water pressure fields:

$$P_f = \int_{h=-\infty}^{h=\infty} \int_{u(h)=-\infty}^{u(h)=\infty} P\{Z_{\text{macro}} < 0 \mid u(h)\} f(u(h))du \cdot f(h)dh$$

h	Water level
u(h)	Water pressure field for corresponding water level h
$P\{Z_{macro}<0\|u(h)\}$	Total failure probability, conditional on the water pressure field for the corresponding water level h
f(u(h))	Probability density function of the water pressure field
f(h)	Probability density function of the water level

The total dike failure probability P_f due to macro instability is elaborated by taking into account the length effect of the dike. First, a cross-sectional macro instability analysis is made. Then, the length of the dike can be modeled as a chain of cross-sections, with equal cross-sectional analysis and varying strength. The macro instability of the dike increases as the dike length increases (GeoDelft, 1990). The length effect is not further discussed in this research.

3.2.2 Schematization uncertainties for macro stability assessment

The stochastic evaluation of the safety factor F requires schematization choices to be made referring the dike characteristics, due to limited availability of information. The schematizations are subject to uncertainties, due to interpretation differences of the available information. This uncertainty is known as epistemic uncertainty; see text box *Types of uncertainty*. A different interpretation leads to a different schematization, which eventually leads to a different safety factor F.

Types of uncertainty

Uncertainty in hydraulic engineering models can be divided in two categories (Slijkhuis et al, 1999): inherent and epistemic uncertainty. Inherent uncertainties represent the randomness and variety of nature in space and time, and can therefore not be reduced. Epistemic uncertainties are caused by the lack of knowledge on reality. Epistemic uncertainty can be subdivided in statistical uncertainty due to a limited number of observations (i.e. in space and in time) and model uncertainty due to schematizations in physical models. Epistemic uncertainties may change as the knowledge increases (e.g. increasing number of observations or new insight into physical processes).

Five aspects of uncertainty are distinguished for the assessment of macro instability, namely the geometry, soil layer composition, soil properties, water pressures and the stability model (Feitsma, 2002). These uncertainty aspects require an integral schematization approach, as the schematization choice of one aspect (e.g. soil layer composition) might influence another aspect (e.g. water pressures). The propagation of these uncertainty aspects is illustrated in Figure 3-6. Figure 3-6 is another presentation of to the probability density function of the stability factor F in Figure 3-5.

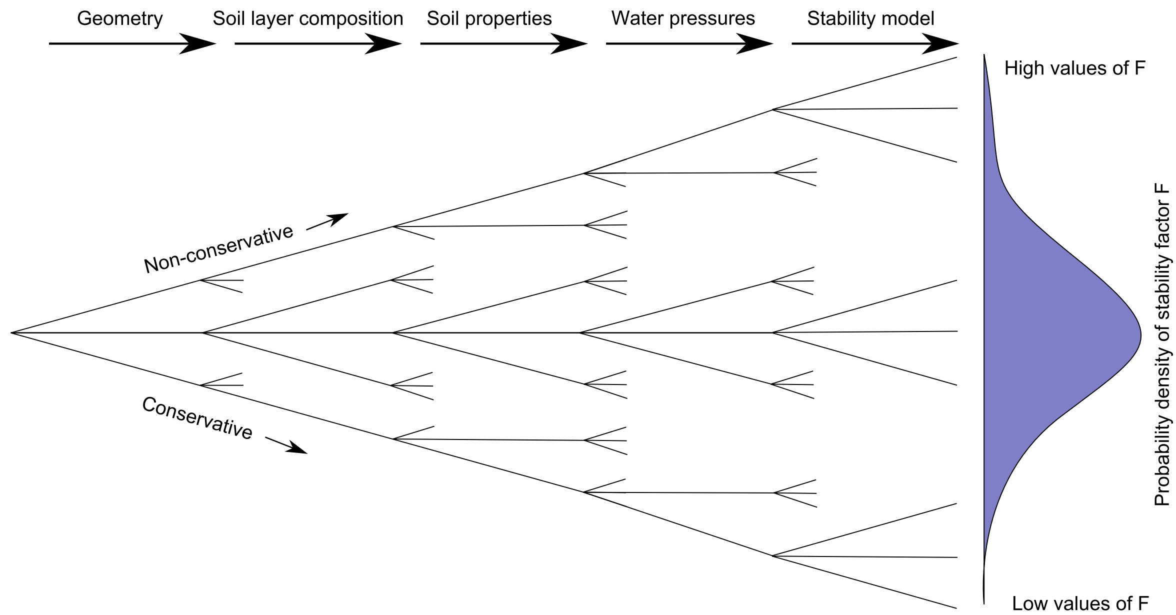

Figure 3-6: Uncertainty aspects in schematization choices for the stability factor F

The probability density of the stability factor F depends on the joint probability density of the uncertainty aspects in Figure 3-6. The classical engineering approach is to make conservative schematization choices, leading to relatively low and underestimated results of F. Reducing the schematization uncertainty of one aspect, affects the uncertainty of the stability factor F. The impact on the probability density of F by reducing the uncertainty of one aspect, depends on the relative uncertainty of the reduced uncertainty aspect compared to the other uncertainty aspects. The proportion of the uncertainty aspects differ per situation. The uncertainty aspects are described below in more detail:

- **Geometry**
  The geometry of the dike is the starting point of the stability assessment. The geometry is the basis for the determination of the distinct dike sections, as comparable dike parts are visible in the field. Steep slopes will result in higher failure probabilities. Local bumps, when situated close to the dike crest, increase the risk on slope failure due to the extra weight acting as active soil volume. On the other hand, the local absence of a stability berm can cause slope instabilities. Detection of these local geometry disturbances can be done either by regular visual inspection or laser altimetry measurements. Uncertainties are caused by a lack of geometry information in time and/or space. Out-of-date measurements are subject to changes over time. Incomplete measurements of only parts of the dike leave uncertainty about the geometry of the rest of the dike.
- **Soil layer composition**
  The composition of the soil, of both the dike and the subsoil, forms the core for the dike strength. A deviation in the soil composition might induce a different critical slip surface. The spatial variability of the soil profile can be significant due to heterogeneity. This variability is in both cross-sectional and longitudinal direction. The longitudinal variability is

important as the stability assessment is made for a single cross-section, which needs to be representative for the section length (e.g., what is the thickness of the weak peat layer over the section length?). The cross-sectional direction is important, as the stability assessment for the whole section length depends on the schematized cross-section (e.g., is the weak peat layer present along the whole section length?). The schematization of the soil layer composition is commonly based on limited information from CPT push-ins and borings. The soil layer composition between two CPT/boring points is deduced from the CPT/boring data. The lack of spatial information causes epistemic uncertainties. Increasing the density of CPT/boring points or executing geophysical measurements decreases the epistemic uncertainty of the soil layer composition. Moreover, additional CPT/borings or geophysical measurements increases the probability on detecting a sand trench, see (Feitsma, 2002). The presence of sand trenches is especially important for piping assessments.

- **Soil properties**
  The soil properties consist of the soil strength, permeability and volumetric weight of the distinct soil layers. The shear strength is defined by the cohesion c and internal friction angle φ. The determination of these shear strength parameters is done by performing laboratory tests (e.g. triaxial or cel tests) on soil samples, gathered at different sample locations. These tests induce uncertainties due to the used model tests and interpretation of test results. Additional test samples grant new information and thereby may result in a different (epistemic) soil strength uncertainty. This difference in uncertainty may be unfortunate for the stability assessment: increasing number of soil samples will increase the probability on detecting a soil strength anomaly, possibly resulting in weaker soil, but will give a better insight into the actual state of the dike. The benefit thereby lies in the better insight and not in the negative effect on the dike strength. The permeability of the soil layers is uncertain due to soil heterogeneity, which is also schematized with the help of soil samples. The soil permeability has an indirect effect on the assessment of macro instability: soil permeability determines the groundwater flow, which influences the development of water pressures. Lastly, the (dry and wet) volumetric weight of the soil determines the critical balance between resisting and driving forces for macro instability. Generally, variations in volumetric weight are limited.
- **Water pressures**
  The loading condition for macro instability is determined by the water pressure, which holds numerous sources of uncertainty in both time and space. Often, three different (cross-sectional) spatial information aspects can be distinguished in the Netherlands (TAW, 2004): phreatic surface, water pressures in semi-permeable layers (clay, peat) and water pressures in the aquifer. The development of water pressures over time is mainly dependent on water pressures due to groundwater flow, induced by fluctuations of the outer water level, precipitation and overtopping (TAW, 2004). Water pressure measurements due to sensor monitoring affect the uncertainty in the water pressure schematization, see paragraph 3.2.4.
- **Stability model**
  Assessing the probability on macro instability requires a physical model that approaches reality. Assumptions, schematizations and simplifications are made to approximate the complexity of dike failure reality. This model approximation induces epistemic uncertainties, which differ when another model would be used. Epistemic model uncertainties can be reduced by refining a model with new insights (i.e. model improvement). It should be emphasized that other models (i.e. approximations of reality) may be used to define input characteristics for a stability model (e.g. water pressure model in macro instability model).

3.2.3 Example calculations for the impact of uncertainty aspects

This paragraph elaborates a calculation example for the macro instability of the inner slope considering a fictitious dike in which the uncertainty aspects as presented in Figure 3-6. The objective of this paragraph is to get insight into the consequences of schematization choices on the stability assessment. Therefore, two different schematizations are computed for each uncertainty aspect of geometry, soil layer composition, soil properties and the water pressures: a conservative and a non-conservative schematization choice. The deterministic safety factor is calculated for each chain of schematization choices, in total 2^4=16 safety factors. The safety factors are determined with D-Geo Stability with the Bishop c-phi model, such that the uncertainty aspect stability model is not considered in this example. Uplifting of impervious layers is not considered. The fictitious dike has a clay core with a crest height at NAP +5 m, the dike toe at NAP +0 m and an outer slope of 1:3. The dike core is located on a subsoil of a peat layer, a clay layer and Pleistoceen sand. The impervious peat and clay layers have a total thickness of 3 m. The design water level is determined at NAP +4 m and the groundwater level in the hinterland is determined at NAP +0 m. The water pressures are assumed to be hydrostatically distributed over the depth from the phreatic surface. Further dike characteristics are specified by either the conservative of non-conservative schematization choices:

- **Geometry**
  The uncertainty in geometry consists of the inner dike slope. Where a steeper slope results in lower macro stability and safety factors. The conservative schematization consists of an inner slope of 1:2 and the non-conservative schematization consists of an inner slope of 1:2,5.
- **Soil layer composition**
  The uncertainty in soil layer composition consists of the transition from peat to clay and the thickness of the peat layer. Peat is a relatively weak soil type and this peat layer is located at a crucial depth. A thicker peat layer results in lower macro stability. The conservative peat layer thickness equals 1 m, with a clay layer thickness of 2 m. Whereas the non-conservative peat layer has a thickness of 2 m and a clay layer of 1 m.
- **Soil properties**
  The uncertainty in soil properties consists of the uncertainty in (drained) cohesion c and (drained) internal friction angle φ. Lower values of c and φ leads to less shear strength result in lower macro stability. The uncertainty in volumetric weight (dry γ_d and wet γ_w) is not considered. The conservative and non-conservative schematization choices are derived from (NEN6740, 2006) and summarized for each soil type in Table 3-1 (where "Con" is the abbreviation of conservative schematization choice and "Non-con" the abbreviation of non-conservative schematization choice).

Table 3-1: Conservative and non-conservative schematizations for the soil properties

Variable [unit]	Clay		Peat		Sand	
	Con*	Non-con**	Con	Non-con	Con	Non-con
c [kN/m^2]	7	13	5	10	0	0
φ [°]	15	20	12,5	17,5	25	30
γ_d [kN/m^3]	14	14	12	12	19	19
γ_w [kN/m^3]	15	15	13	13	20	20

** Con = conservative schematization choice ** Non-con = non-conservative schematization choice*

- **Water pressures**
  The uncertainty in water pressures consist of the position of the phreatic surface due to the design water level. The conservative approach is to schematize the phreatic surface from

the outer slope at design water level NAP +4 m and to the dike toe at the inner slope. The non-conservative approach is that the phreatic surface at the outer slope is positioned 1 m under design water level, at NAP +3 m.

The critical slip circles for both conservative and non-conservative schematization choices are given in Figure 3-7. The stability results in terms of safety factor F are given in Table 3-2. The value of the safety factor F varies from 0,97 to 1,97 depending on the schematization choices made. The wide range of the determined safety factors indicates the importance of thorough schematization choices in the stability assessment. An analysis of schematization uncertainties is elaborated for a probabilistic approach in the case study of chapter 4.

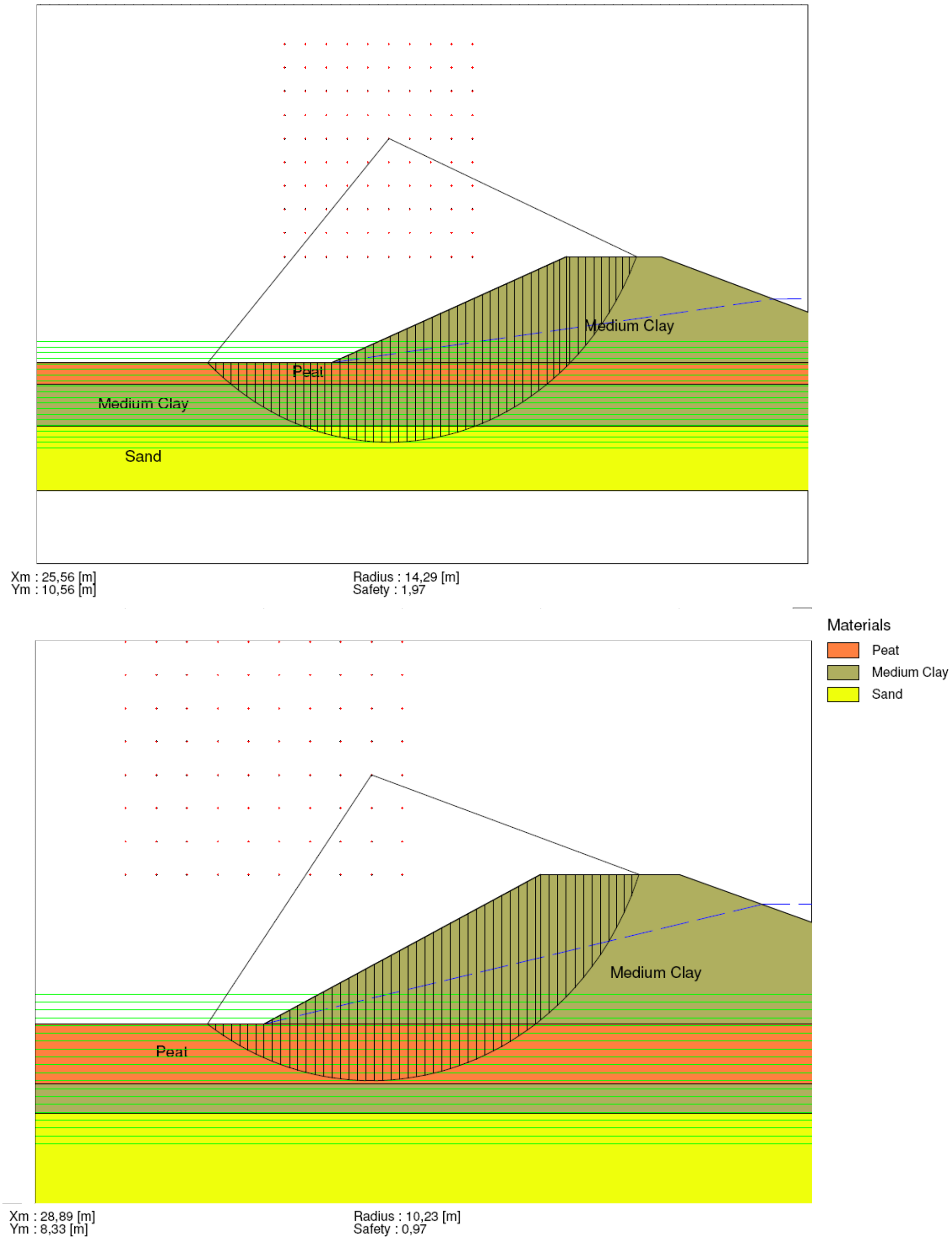

Figure 3-7: Critical slip circles for non-conservative (upper) and conservative (lower) schematization choices

Table 3-2: Stability results for the 16 different chains of schematization choices

Geometry	Soil layer composition	Soil properties	Water pressures	Safety factor F
Non-conservative	Non-conservative	Non-conservative	Non-conservative	1,97
			Conservative	1,83
		Conservative	Non-conservative	1,29
			Conservative	1,20
	Conservative	Non-conservative	Non-conservative	1,85
			Conservative	1,72
		Conservative	Non-conservative	1,13
			Conservative	1,05
Conservative	Non-conservative	Non-conservative	Non-conservative	1,87
			Conservative	1,75
		Conservative	Non-conservative	1,17
			Conservative	1,09
	Conservative	Non-conservative	Non-conservative	1,76
			Conservative	1,64
		Conservative	Non-conservative	1,05
			Conservative	0,97

3.2.4 Influence of water pressure measurements

The monitoring of water pressure measurements influences the epistemic uncertainty caused by the conversion of the water level h to the water pressure field u, represented by the probability density f(u(h)): the probability density function for random variables of the water pressure field. It should be emphasized that u(h) is not a single variable, but a multidimensional water pressure field as present in the dike. The a-priori probability density f(u(h)) (i.e. without sensor monitoring) is updated with the sensor monitoring data, leading to the a-posteriori probability density of u(h). As the probability density of u(h) is affected, the probability density of the stability factor F is also affected (see Figure 3-6). The impact of the sensor monitoring on the a-posteriori probability density of F is however dependent on the actual collected monitoring data, the contribution of the uncertainty in water pressures compared to other uncertainty aspects and the a-priori probability density of u(h). Because of these aspects, the impact of sensor monitoring data can have different forms, which will also change as time passes by and more data is collected. The expected benefit from sensor monitoring is a reduction of the uncertainty regarding u(h) and thus the uncertainty in F. If the contribution of the water pressure uncertainty has a large contribution to the total uncertainty, the uncertainty reduction of F is relatively large. This impact is illustrated in Figure 3-8 with an example calculation, in which the parameter values of F have been adapted.

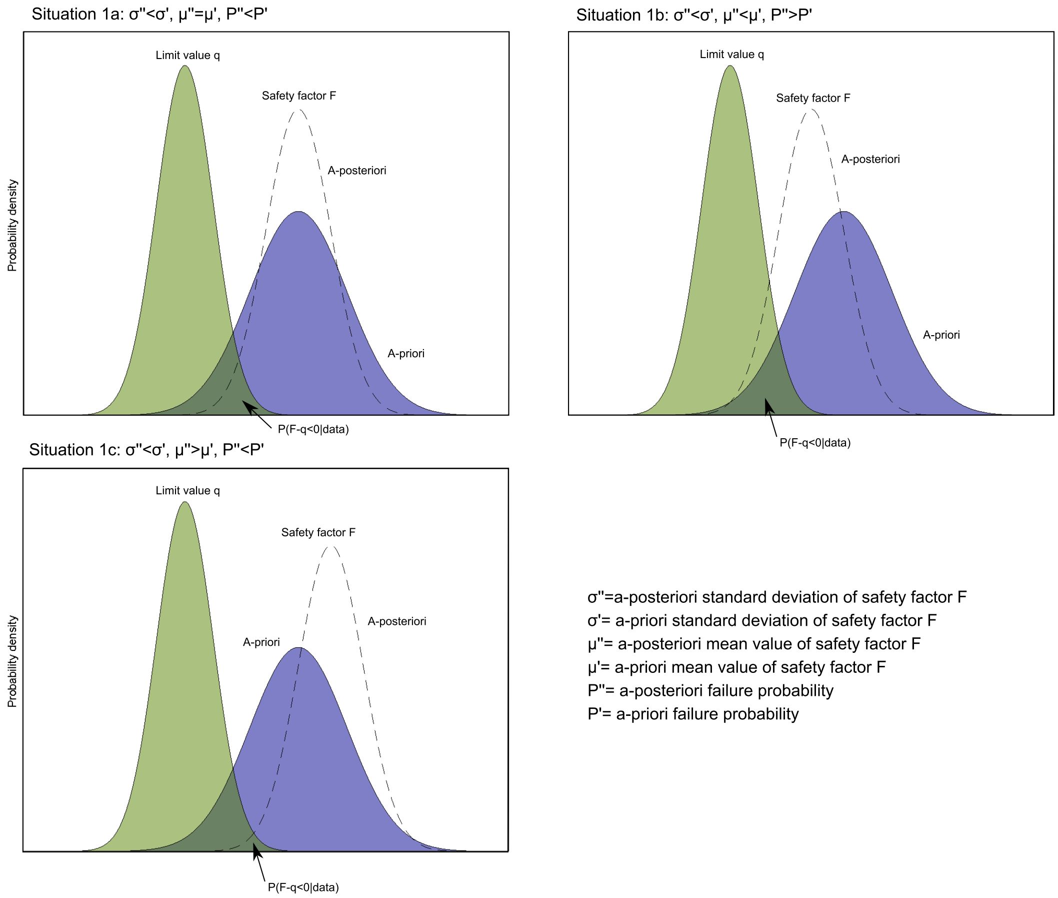

Figure 3-8: Relatively large impact of uncertainty reduction in u(h) on F

Figure 3-8 shows that an uncertainty reduction of u(h) reduces the uncertainty of F, but can eventually lead to either an increase or decrease of the failure probability. This depends on the mean value of the monitoring data, relative to the a-priori mean value: if the a-priori failure assessment has been done conservatively, the a-posteriori failure assessment is expected to decrease compared to the a-priori failure assessment and vice versa. The Dutch engineering practice on flood safety is to schematize according to a conservative approach, such that sensor monitoring would lead to a reduction of the failure probability. The impact of this expected reduction is not known on beforehand: this depends on the monitoring data. However, the impact of water pressure monitoring on the assessed failure probability is based on the of other uncertainty aspects. In the situation that the water pressure uncertainty is relatively small compared to other uncertainties, for instance the soil strength uncertainty, the impact will be less significant. After all, the reduced water pressure uncertainty is relatively small compared to the other uncertainty aspects. This impact is illustrated in Figure 3-9.

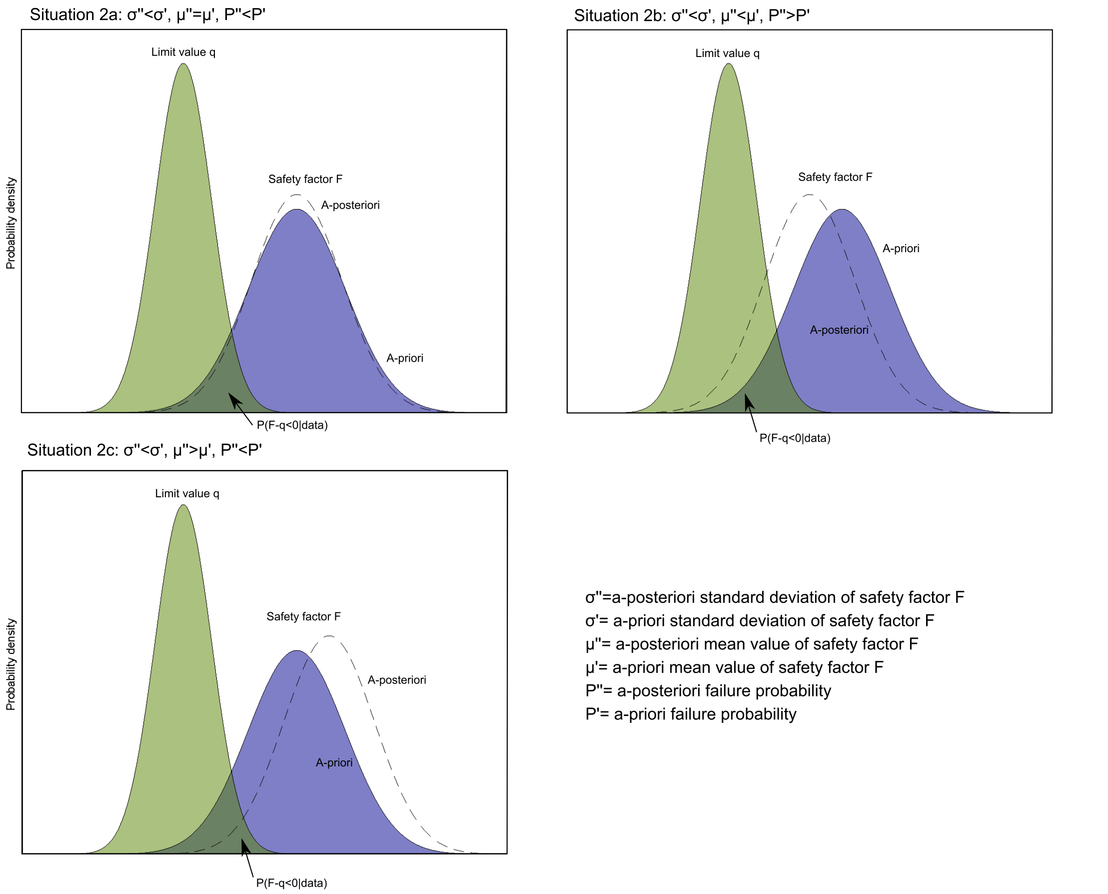

Figure 3-9: Relatively small impact of uncertainty reduction in u(h) on F

Figure 3-9 shows a similar impact on F as in Figure 3-6, yet the difference between the a-priori safety factor and the a-posteriori safety factor is marginal, because other uncertainty aspects dominate the probability density of F. This points out the importance of a complete picture of the macro stability assessment, before considering water pressure monitoring: if other uncertainties dominate the uncertainty of the assessment, revision of other possibilities to reduce those risks can be more effective. The distribution of uncertainty aspects is case specific. A case study has been worked out in chapter 4 to illustrate the identification of the relative contribution of different uncertainty aspects. The influence of water pressure sensor monitoring on the stability assessment is compared with uncertainty in soil strength and soil layer composition.

To complete the picture, the result of increased uncertainty of u(h) due to sensor monitoring is presented in Figure 3-10. The unwanted (and therefore possibly unforeseen), but plausible, situation occurs that the uncertainty in F is expected to increase. The chance on this situation is inversely proportional with the expertise and competence of the engineer.

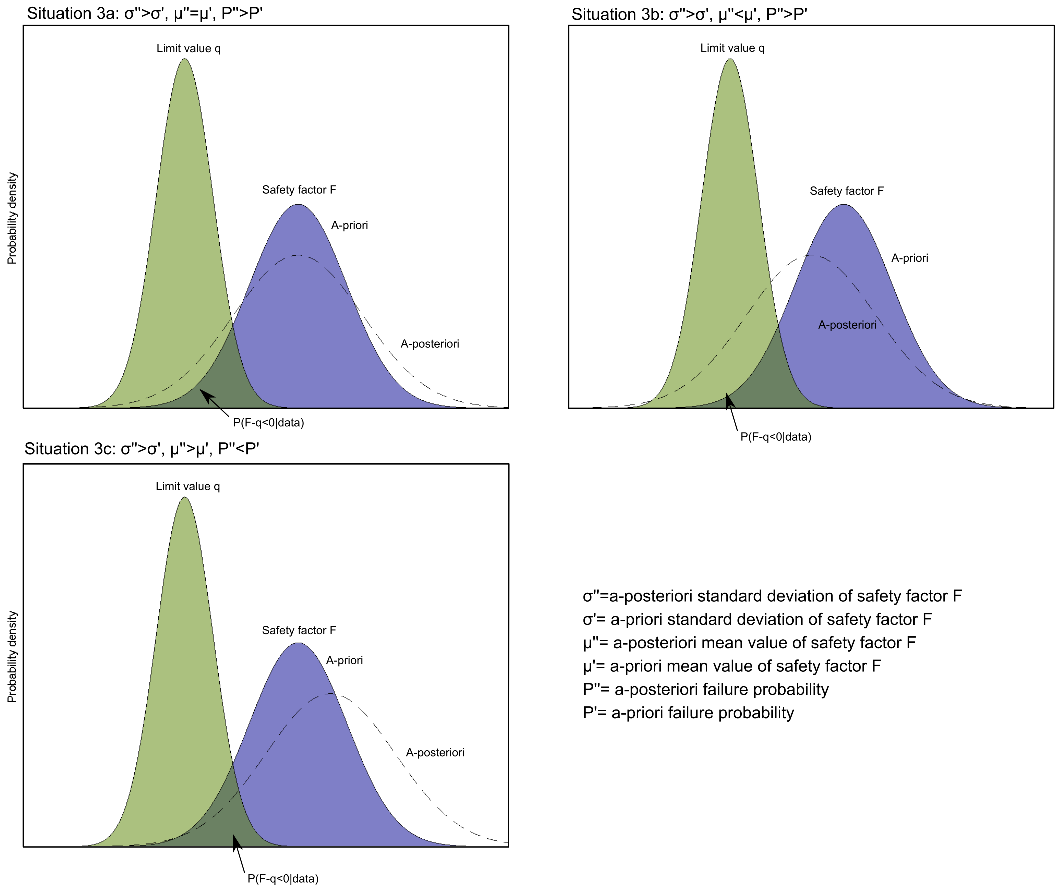

Figure 3-10: Impact on F of sensor monitoring for increased uncertainty in u(h)

Before investing in sensor monitoring, one should be aware of the possible effects on the flood safety assessment. Pre-posterior assessments can give insight into these possible effects. Also, it must be emphasized that similar impacts (as presented in Figure 3-8, Figure 3-9 and Figure 3-10) occur when other uncertainty aspects in the macro stability assessment are affected (e.g. additional laboratory tests to determine soil strength parameters can possible lead to more uncertainty regarding the soil strength). A consideration for the most cost-effective action must be made to determine

3.2.5 Sensor monitoring characteristics and residual uncertainty

Sensor monitoring of water pressures affects the uncertainty regarding u(h), of which the exact effect is not predictable on beforehand. However, the extent of the sensor monitoring determines a lower-boundary for the epistemic water pressure uncertainty, namely the residual uncertainty (i.e. excluding the inherent uncertainty): water pressure uncertainty will always be maintained, even for measuring with the most sophisticated sensors and for the longest periods. The following sensor monitoring characteristics are of importance for the residual uncertainty:

- **The technical reliability of the sensor system**:
  The technical reliability of a sensor system is defined as the capability of the sensor technique to monitor the actual physical phenomenon. This is done with a certain accuracy and precision (see text box *Accuracy and precision),* and a measurement resolution. When sensor monitoring is used for a stability assessment, the technical reliability forms the basis for further schematizations: this basis uncertainty propagates through the schematizations, which increases the uncertainty regarding F. Low sensor accuracy implies uncertainty among the gathered data, as the actual physical phenomenon might be different from the monitoring data. Also, the sensor resolution is a source of uncertainty. The measurement

resolution is the smallest deviation of the physical phenomenon that can be detected. The required resolution depends on the physical phenomenon to be measured and the application, e.g. measuring the air temperature with a resolution of 0,001 °C can be important in laboratory tests, but is needless for daily weather forecasts. Technically sophisticated sensors (i.e. high accuracy, precision and resolution) increase the technical reliability, thus reduce the residual uncertainty. Yet, these systems are more expensive as well. Also, redundant sensor systems contribute to the reliability (i.e. installing critical system elements in serial, to create a backup). A balance between the costs and technical reliability of the sensor system is required.

Accuracy and precision

The capability of the sensor to monitor the true physical phenomenon can be defined by accuracy and precision. Accuracy is defined as the extent of offset of the sensor output from the true value. The sensor measures the phenomenon with a certain measurement bias. Precision is defined as the extent of the spreading of the sensor outputs compared to the true value. This precision is also known as measurement noise. Figure 3-11 points out the difference.

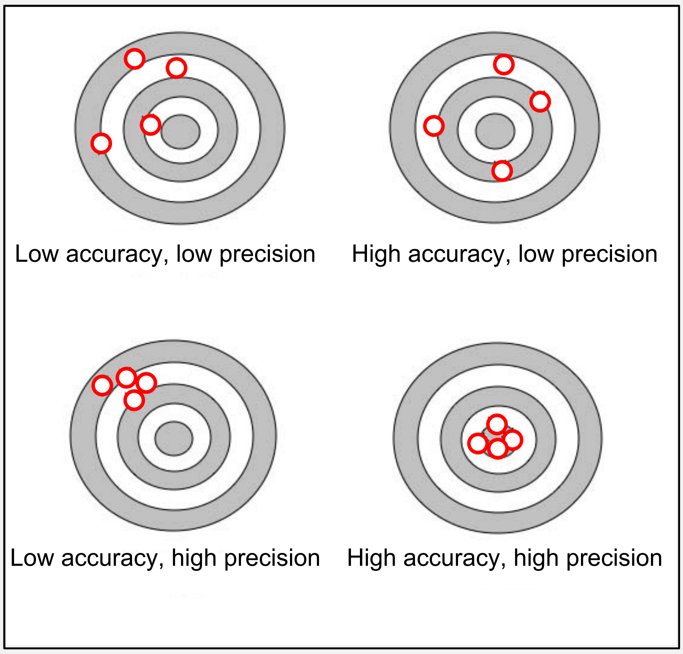

Figure 3-11: Visualization of accuracy and precision for hitting a bull's-eye

- **Sensor density**:
  The density of the sensor locations affects the epistemic uncertainty due to variations in space, because the monitoring is done at a limited number of locations. The physical behavior in the space between the measurement points remains unknown due to a lack of information. Especially the density along the length of the considered dike section is of importance, due to the relatively long dike length compared to the width and height. A dense sensor network decreases the spatial epistemic uncertainty and thus the residual uncertainty, see Figure 3-12. The probability of missing a peak value is reduced by increased sensor density. But the extra sensors are more expensive in purchase, maintenance and operation (due to more data storage). To give insight into the required spatial density over the length of a Dutch dike, a monitoring case in a sea dike is considered in (Deltares, 2011a). The data from sensor monitoring in cross-sections at 200 m distance from each other (placed in man-made sea dike) shows limited similarity due to inhomogeneity of the soil.

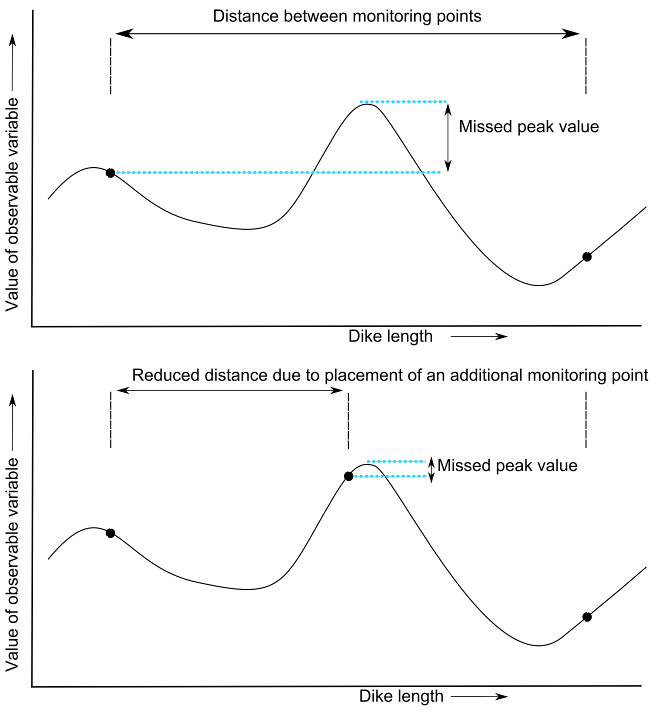

Figure 3-12: The effect of sensor density on epistemic uncertainty due to variations in space

- **Measurement frequency**:
  The frequency of the sensor measurements affects the epistemic uncertainty due to variations in time. The required measurement frequency depends on the physical phenomenon to be measured and the application of the monitoring data. Considering water pressure measurements, a measurement frequency of once a week (e.g. manual registration) leaves too much uncertainty about the physical behavior during the frequency interval. The frequency interval is the time between two measurements, in which no measurement is done. A higher measurement frequency reduces this uncertainty, see Figure 3-13. The probability of missing a peak value is reduced by increased measurement frequency. However, increasing the measurement frequency requires extra data storage and thus increased operational costs.

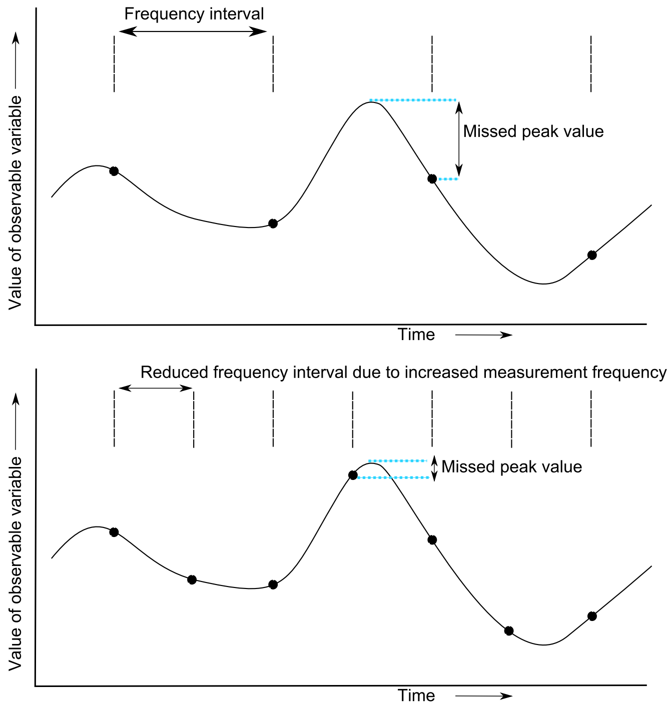

Figure 3-13: The effect of measurement frequency on epistemic uncertainty due to variations in time

- **Monitoring time**:
  The monitoring time is defined as the total time span in which the sensor monitoring is applied. The epistemic uncertainty decreases as the monitoring time increases, because the number of measurements increases over time. However, these measurements are attained during serviceability limit state (SLS)[3]. At a certain point additional data from SLS does not contribute to the uncertainty reduction, because sufficient data has already been gathered from this loading condition (e.g. the effects of the tide on a sea dike). The SLS data can be used to specify loading conditions leading to the ultimate limit state (ULS) (see paragraph 3.3). However, the behavior of the dike during loading conditions close to ULS is not yet monitored, leaving epistemic uncertainty for the ULS. As the monitoring time increases, the chance that a loading event is monitored increases as well. However, long-term monitoring results in increased maintenance and operational costs for the monitoring system.
- **Monitored loading events**:
  The occurrence of high water levels or precipitation during the monitoring period gives valuable information about the dike behavior under conditions inducing ULS. Both the magnitude and quantity of the loading events are important. The larger the magnitude, the closer ULS is approached and the more information on extreme loading conditions is attained: the epistemic uncertainty regarding extreme conditions is reduced. Besides, the more loading events are being monitored, the more information is acquired on possible side effects that affect the water pressure field during extreme conditions. The number of monitored loading events will increase as the monitoring time increases. The problem is however the randomness of occurrence: a loading event with an occurrence of 1/Y per year occurs once every Y years on average. But the occurrence stays random, which can lead to significant waiting times for a significant loading event.

[3] Serviceability Limit State (SLS) refers to the handling of daily loading conditions by the structure. Exceedance of the SLS leads to temporary and/or partial disfunctioning of the structure. The Ultimate Limit State (ULS) is related to extreme loading events and exceedance of the ULS leads to failure of the structure (e.g. dike breach causing a flood).

The residual uncertainty consists of the epistemic uncertainty that remains after the application of sensor monitoring data, due to limitations of the technical reliability, sensor density, measurement frequency, monitoring time and monitored loading events.

The quality of the monitoring system is defined by the technical reliability, sensor density and measurement frequency and forms the base of the monitoring. A poor monitoring system has a larger residual uncertainty and is relatively cheap: the monitoring data is thereby of lower quality. Also the method of installation and the quality of the executed installation are important to result in a qualitatively good sensor monitoring system. However, if the monitoring data generated with such a system is too poor, the data can cause unnecessary alarms and unrest among the responsible dike managers. This unrest is then caused by abnormal monitoring data due to sensor failure or false alarms on an upcoming dike failure. These facets of a poor quality monitoring system lead to unnecessary costs. To prevent unnecessary costs due to a poor sensor monitoring system, minimal requirements must be specified to guarantee a minimal sensor monitoring quality.

Also, the monitored loading events are a crucial aspect to affect the uncertainty in the stability assessment, which is elaborated in paragraph 3.3. A longer monitoring time will increase the probability on the occurrence of a loading event, but the actual appearance remains random and unsure. Therefore, the monitoring data will be extrapolated to extreme conditions (i.e. hydraulic design loads). The statistical extrapolation causes statistical uncertainty, because of lacking observations regarding the extrapolated situation. Different techniques can be used for the extrapolation, which are considered in the next paragraph.

3.3 Extrapolation of sensor monitoring data

3.3.1 Extrapolation distance

The water pressures under ULS loading conditions are of importance to assess the total flood risk, as the dike failure probability is high. The extrapolation is defined as the magnitude of the statistical extrapolation from monitored SLS loading conditions to uncertain ULS loading conditions. From a statistical point of view, the standard deviation rises as the extrapolation distance increases. Hence, the information gap between known (i.e. measured conditions) and unknown (i.e. design loading conditions) increases. A linear relation between the water level and the water pressure is expected from groundwater physics (TAW, 2004). This is illustrated in Figure 3-14.

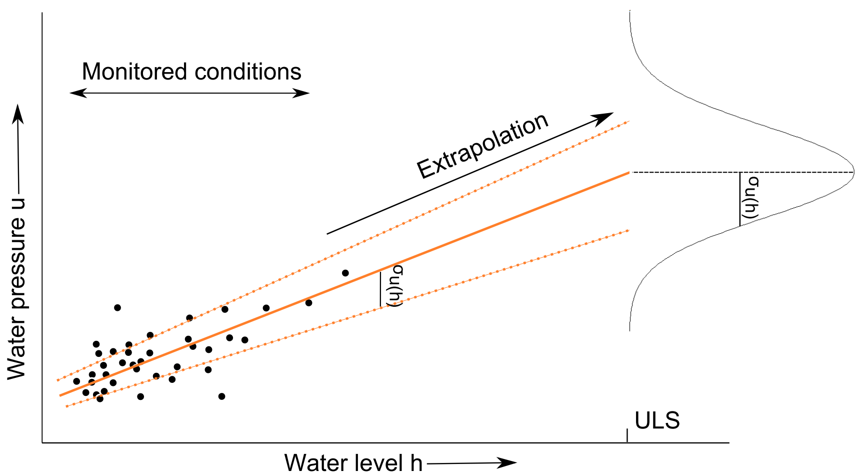

Figure 3-14: Increasing standard deviation due to extrapolation (example linear regression)

If the ULS loading condition is determined as a higher water level h, the uncertainty is increased due to the increased extrapolation distance. The extrapolation of the measured water pressure behavior from sensor measurements during SLS to design loading conditions can be done with regression analyses, supported with physical models. An increasing amount of data points, i.e. longer monitoring period and possibly more monitored significant loading events, affects the extrapolation. Figure 3-15 shows the effect on the extrapolation, when more sensor monitoring data has been gathered compared to the available data in Figure 3-14.

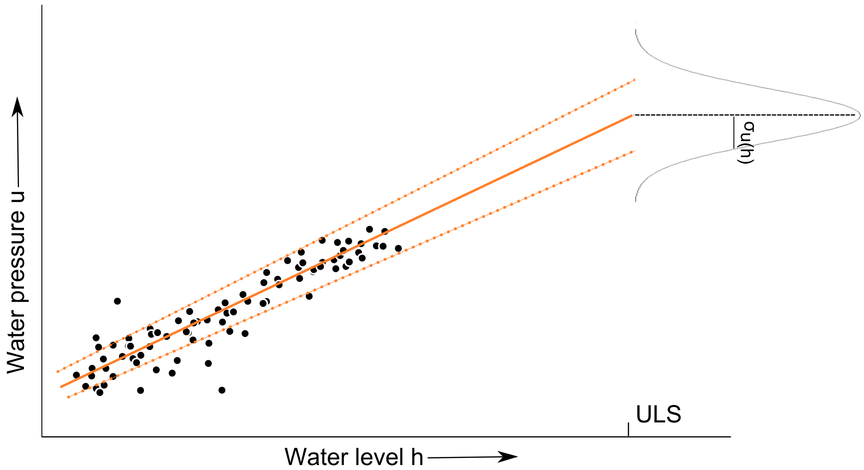

Figure 3-15: Example for the effect of additional data points on the extrapolation

Hence, the epistemic uncertainty due to the extrapolation is reduced by collecting additional monitoring data (and supported with physics), not the inherent uncertainty of the water pressure uncertainty at ULS loading conditions. The effect on the total uncertainty is unknown on beforehand, see paragraph 3.2.3. The basis of an extrapolation is formed by the physical relation between variables, of which (monitored) water pressures u and water level h is of importance for macro instability. Extrapolation models are primary used to specify the water pressures during ULS for the periodic safety assessment. Three different extrapolation models are distinguished, based on different physical relations (TAW, 2004):

- Extrapolation of multiple maximum values
- Extrapolation of continuous measurements during a high water
- Extrapolation by calibrating groundwater flow models

3.3.2 Multiple maximum values

Extrapolation of multiple maximum values is a direct extrapolation technique, assuming stationary (Dutch: *stationair*) flow conditions. During a high water event, both the external water level and the water pressure in the dike are monitored. Water pressure sensors provide the information about the corresponding water pressure in the dike. A peak level h_{max} is derived from the water level data. The corresponding maximum value of the water pressure u_{max} will occur with a certain delay, see Figure 3-16. A sufficient measurement frequency of the water pressure sensor is required, such that the water pressure peak is not missed.

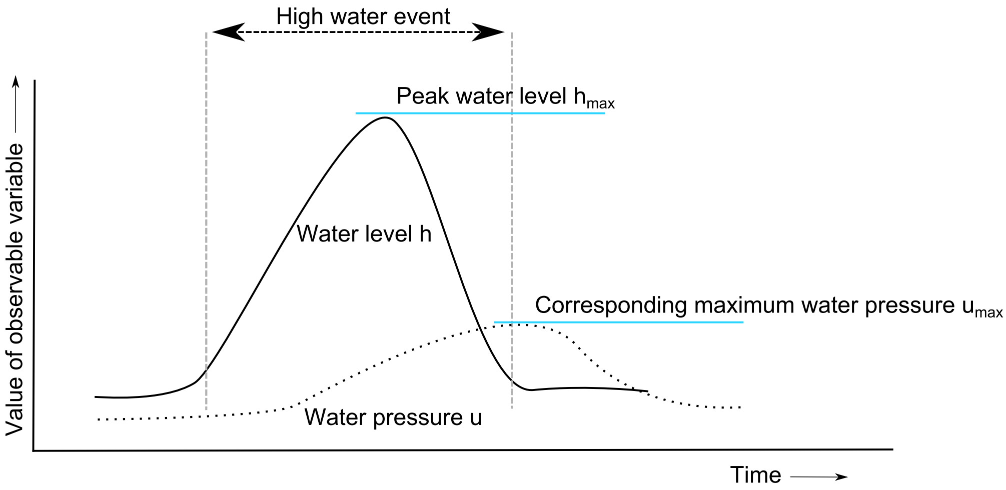

Figure 3-16: Relation between the water level h and the corresponding water pressure u

This extrapolation model requires measurements from multiple high water events, such that a relation can be plotted between a water level h and the corresponding maximum water pressure for the occurred water level. This can require a long monitoring time, depending on the occurrence of the events. Stationary flow conditions must be plausible, since the influence of time dependent water pressure development is not included. The statistical extrapolation to ULS loading conditions is expected to be a linear relation from the groundwater flow theory (i.e. for stationary flow conditions); see indicator I in Figure 3-17. However, non-linear behavior on site can be induced by the following physical phenomena (TAW, 2004):

- **Flooding of a dry foreland**
  Dikes are meant to retain water. In some cases the dike does not directly retain the water during SLS, i.e. when a dry foreland is present. This is typical for Dutch rivers having floodplains (Dutch: *uiterwaarden*) and sea dikes having beaches in front. However, the water can flood the foreland during loading events such that the water stands at the dike. This induces a non-linear behavior, indicated with II in Figure 3-17. This non-linear behavior can be revealed when relevant high water events are monitored, where relevant refers to the water level at which the foreland is inundated. The relevant high water is indicated with $h_{foreland}$ in Figure 3-17 and Figure 3-18.
- **Limit potential**
  The limit potential (Dutch: *grenspotentiaal*) is the hydraulic head in the aquifer at which the semi-permeable top soil layers are pushed upwards. I.e., the water pressure force in the aquifer has become larger than the dead weight force of the top soil layer. The water pressure reaches a physical limit $u_{limit\ potential}$ at water level h_{uplift} with uplifting of the top soil layer as a result, see Figure 3-17 and Figure 3-18. The extrapolation is indicated with III in Figure 3-17.
- **Internal storage processes in the dike**
  Storage processes in the dike can be induced by precipitation and wave overtopping (phreatic storage) and consolidation processes (elastic storage). The development of water pressures in the dike body due to high water is dependent on precipitation and wave overtopping: soil pores are saturated due to precipitation and/or overtopping water which leading to the development of higher water pressures. On the other hand, consolidation of clay layers increases the elastic storage which can lead to smaller water pressures when high water occurs.

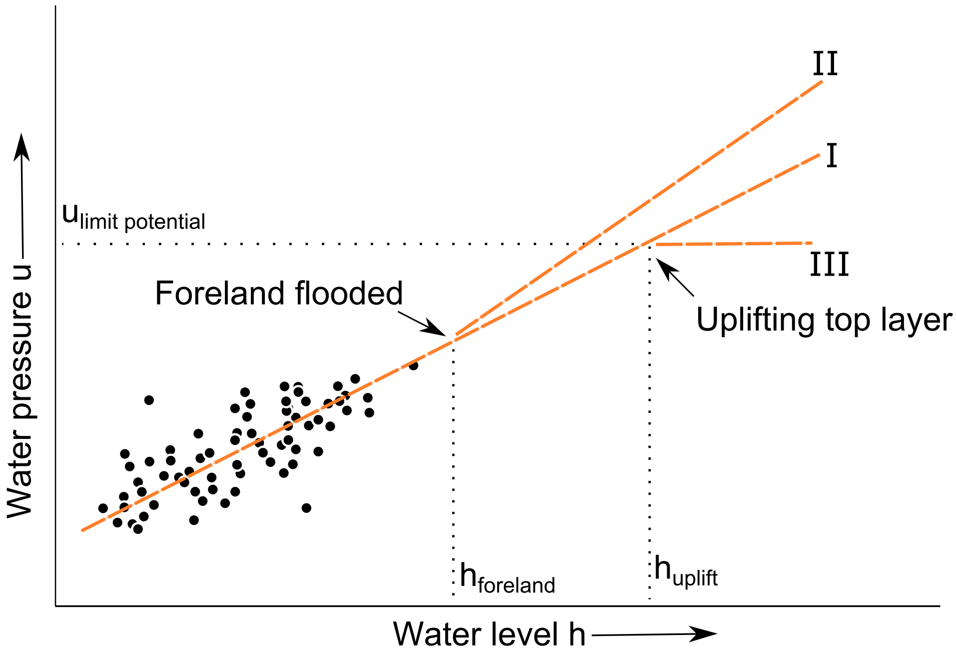

Figure 3-17: Non-linear effects in the extrapolation with multiple maximum values

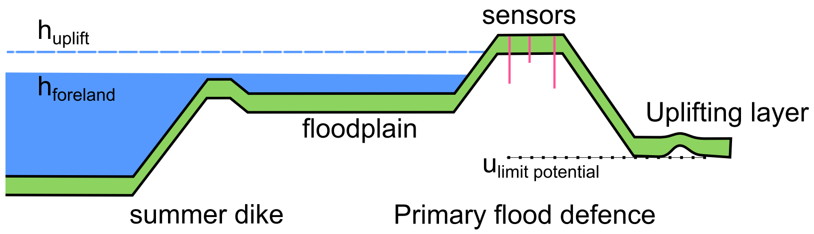

Figure 3-18: Physical effects causing non-linear extrapolation of water pressures

The actual effects of physical phenomena of a foreland, limit potential and internal storage are revealed with sensor monitoring, if relevant high water events for which these phenomena might occur are monitored. Monitoring less relevant high water events also has less impact. A limited monitoring time gives information about the SLS behavior and reduces this uncertainty. Essential schematization choices are only revealed if the monitoring period is extended such that relevant high water events are monitored. If the prior schematization deviates from the obtained data, the schematization is reviewed by a second opinion to analyze the deviation with the new monitoring information. The corrected interpretation due to the sensor monitoring is the base for further actions by the dike manager. This emphasizes the importance of monitoring these high water events, to be able to reduce the uncertainty caused by statistical extrapolation. The importance and relevance of a monitored high water event has been implemented in the cost-benefit model, see paragraph 5.2.2.

3.3.3 Continuous measurements during high water

Extrapolation from continuous measurements during a single high water event can be used when multiple high water events are not at hand. In the case of a long lasting high water event (e.g. a high river discharge wave or increased polder water level), sensor measurements from this single event can be used for extrapolation. Again, both water level data and water pressure data is required. By plotting the development of the external water level as a function of the water pressures, effects can be derived referring damping and delay. The delay of the water pressure reaction on the high water causes a hysteresis loop, see Situation A in Figure 3-19. The parameter t_0 indicates the time delay between the water level and the measured water pressure. Adaptation of t_0 will change the shape of the hysteresis loop; see Situation B in Figure 3-19. By adapting t_0 such that the water pressure data corresponds with the water level measurements (by assuming stationary flow conditions), extrapolation to design loading conditions can be done (as in Figure 3-17).

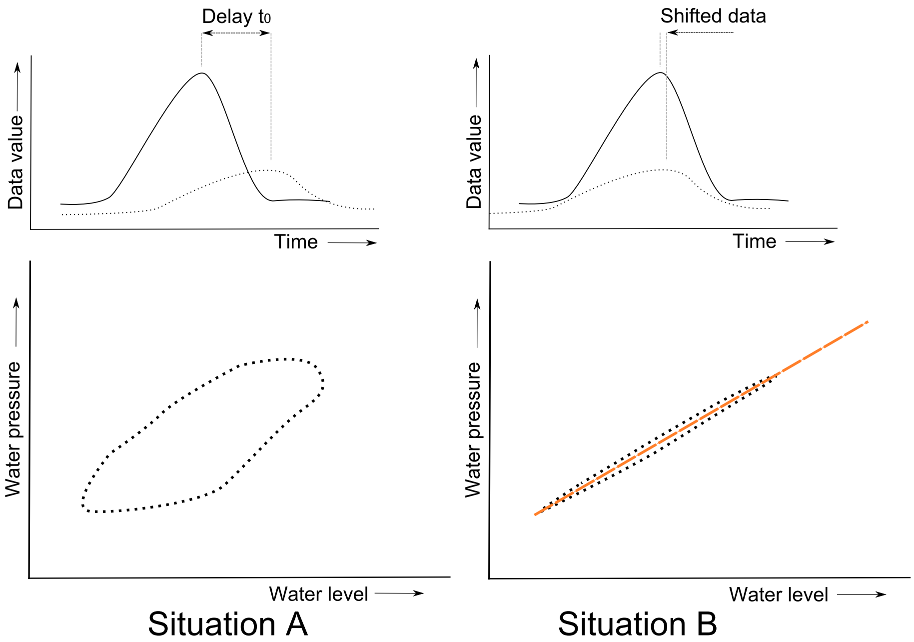

Figure 3-19: Measurement plots for different water pressure delays

This model assumes stationary flow conditions during the whole loading event. The required monitoring time is limited, as data from a single high water event is required instead of from multiple events (see paragraph 3.3.2). On the other hand, a single high water event provides information for that specific physical condition. Besides, the sensor technique monitoring the water pressures is required to have small measurement delay, because the model is based on actual occurring physical delay (i.e. t_0).

3.3.4 Calibration of groundwater flow models

Calibrating groundwater flow models with monitored water pressures, relates the water pressure field to the occurring high water event, combined with the characteristics of the soil composition. Groundwater flow models are in general used to calculate the water pressures in more complex situations such as around sheet piles and heterogonous soil compositions. Commonly used groundwater flow models calculate the water pressures in a 2D cross-section. The analysis of the total water pressure field is then based on the loading condition and soil specifications. However, attention is needed for the implementation of these measurements, as they need to be measured for the corresponding assumed flow conditions in the groundwater flow model. The heterogeneity of a soil layer can be incorporated by the calibration of the soil permeability with the help of water pressure data. In general, the calibration is integrated in the schematization process as indicated in Figure 3-20. The groundwater flow model is set up with the information from soil investigation, which is essential information for this extrapolation technique. The model is computed for the monitored loading condition (i.e. the hydraulic load for which water pressure measurements have been monitored). The computed water pressures are compared with the monitored data. The soil characteristics are adapted such that the computed water pressures correspond to the measured water pressures. The last step is to compute the groundwater flow model for ULS loading conditions and attain the computed water pressures (i.e. in ULS). The calibration method is described in more detail for the software WATEX and MSeep in the corresponding text boxes.

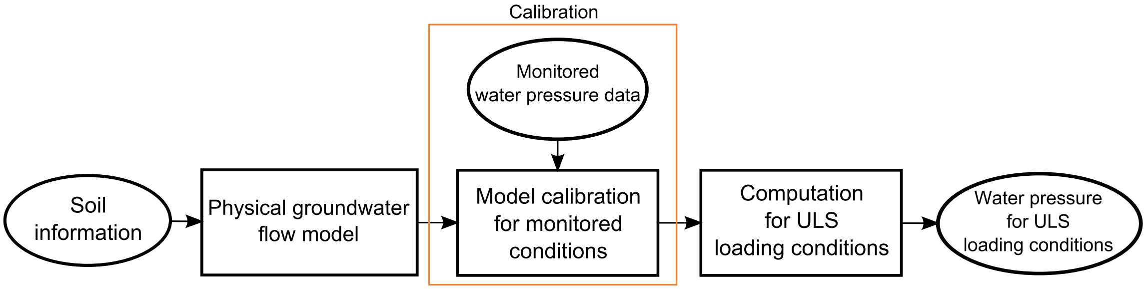

Figure 3-20: Extrapolation of water pressures using calibration of a groundwater flow model

WATEX

WATEX is used to calculate the hydraulic head in an aquifer (i.e. a permeable layer through which water flows) with a semi-impermeable layer on top. The soil properties for the two distinct layers can be specified for four different cross-sectional domains, see Figure 3-21. The analytical model calculates the water pressures in the aquifer based on the defined water level at both sides of the dike. The water pressures are calculated for non-stationary conditions (i.e. time dependent), for a specified loading condition.

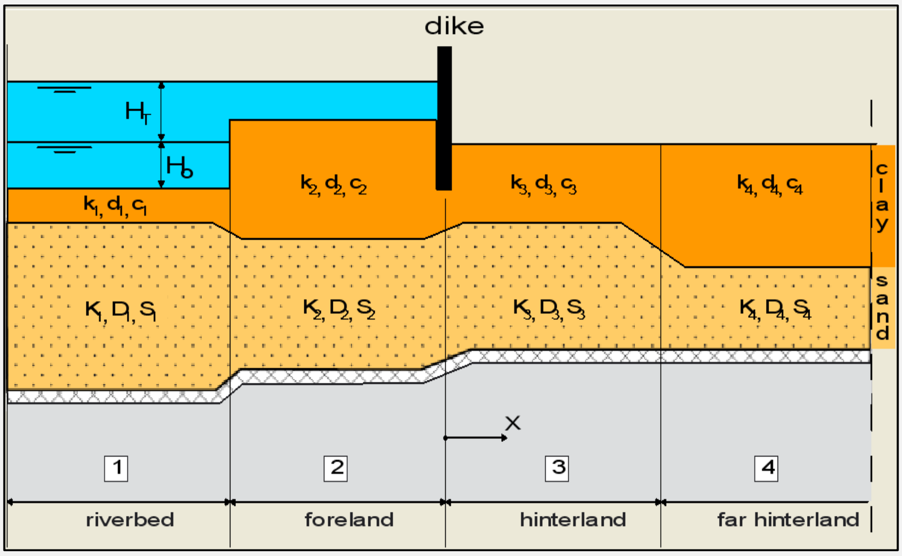

Figure 3-21: Cross-sectional schematization in WATEX

The calibration procedure consists of the iterative calibration of the soil input variables, such that the calculated water pressures correspond with the monitoring data:

1. Top layer: vertical permeability, layer height, consolidation coefficient
2. Aquifer: horizontal permeability, layer height, storage coefficient

The model is calibrated for the monitored (i.e. SLS) loading conditions. Then the soil input variables are set constant and the loading conditions are increased to ULS loading conditions. The calibrated model now returns the extrapolated water pressures in the aquifer, based on monitoring data and soil variables. The application of the WATEX program is limited for macro stability assessments due to the rough schematizations for the geometry and the twofold soil composition. The water pressures in the semi-permeable top layer are not computed. The non-stationary water pressures in the aquifer can be used to assess the piping stability.

MSeep

MSeep is a numerical groundwater flow model based on the Finite Element Method. An extensive description of MSeep can be found in (GeoDelft, 2002). The groundwater flow is modeled in a 2D cross-section for stationary conditions. The dike geometry must be defined and multiple soil layers can be determined, each with a specific horizontal and vertical permeability (see Figure 3-22).

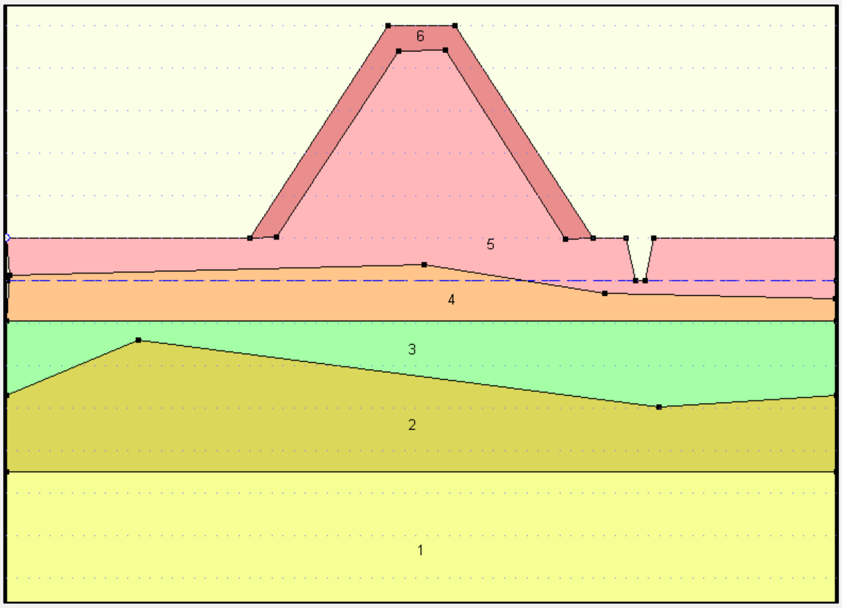

Figure 3-22: Cross-sectional schematization of soil layers in MSeep

The (stationary) water pressure field for a given boundary condition (i.e. often an external water level). The phreatic surface is calculated with an iterative process. The calibration of soil variables is done with sensor measurements, possibly including measurements on the phreatic surface. The soil variables consist of a vertical and horizontal permeability for each distinct soil layer. Also, the soil layer composition can be adapted. The required sensor data for the model calibration must be measured for stationary flow conditions. Due to the definition of the soil layer composition, the layer thicknesses form additional calibration parameters. Once the model is calibrated with the monitoring data, the soil input variables are set constant and the loading conditions can be increased. The detailed water pressure field from MSeep can be used for macro stability assessments, assuming stationary flow conditions.

3.4 Early warning

3.4.1 Implementation of water pressure monitoring for early warning

The early warning principle relies on the timely notification of an upcoming threat during operational situations, such that repressive measures can be executed in order to reduce the upcoming threat. Real-time sensor monitoring is claimed to be beneficial for the timely detection of an upcoming threat: the information provided with sensor monitoring indicates physical behavior which should lead to a dike failure. Based in this information, decision makers start the process to execute emergency measures in order to mitigate the short-term risk. Chapter 6 elaborates the cost-effectiveness of sensor monitoring for early warning situations.

Currently, real-time prediction models are used, e.g. FLIWAS (De Gooijer et al, 2007) and Delft-FEWS (Deltares, 2010), that combine different sources of information (e.g. water level predictions, calamity plans) to determine the real-time and short-term flood safety. The real-time monitoring might demand additional requirements on the sensor monitoring system to process the data for direct usage (the monitoring system for periodic safety assessment does not necessarily require this). The predictions are faced with uncertainties regarding the loading conditions for all relevant failure mechanisms and their development over time. The short-term failure probability of a dike for a predicted high water has been elaborated in (Ter Horst, 2005). The short-term failure probability due to macro instability is conditional on the a-priori expected water pressure u for short-term predicted high water h_{pr}:

$$P_{\text{macro,pr}} = \int_{h=a}^{h=b} \int_{u(h)=-\infty}^{u(h)=\infty} P\left\{Z_{\text{macro}} < 0 \mid u_{\text{a-priori}}(h)\right\} f(u_{\text{a-priori}}(h))du \cdot f(h;h_{pr},\sigma)dh$$

$P_{macro,pr}$	Short-term failure probability due to macro instability
$P\{Z_{macro}<0 \mid u_{a\text{-}priori}(h)\}$	Total failure probability due to macro instability, conditional on the a-priori water pressure
h_{pr}	Short-term prediction of the water level
$u_{a\text{-}priori}(h)$	A-priori water pressure loading condition for corresponding water level prediction
$f(u_{a\text{-}priori}(h))$	A-priori probability density function of water pressure u for corresponding water level prediction
$f(h;h_{pr},\sigma)$	Short-term probability density function of water level h, with mean h_{pr} and standard deviation σ

The long-term a-priori probability density of the water level h is affected, because a loading event is predicted with expected value h_{pr} and uncertainty σ: $f(h;h_{pr},\sigma)$. More certainty is gained about the actual occurring high water level. The macro instability is assessed by computing the water pressures for the upcoming water level. Thus, the probability density function of the water pressure is the a-priori expected value for the predicted water level h_{pr} and corresponding standard deviation σ: $f(u_{a\text{-}priori}(h))$. The actual occurring water pressure still remains uncertain, see Figure 3-23.

Operational situation for short-term water level prediction; no early warning monitoring

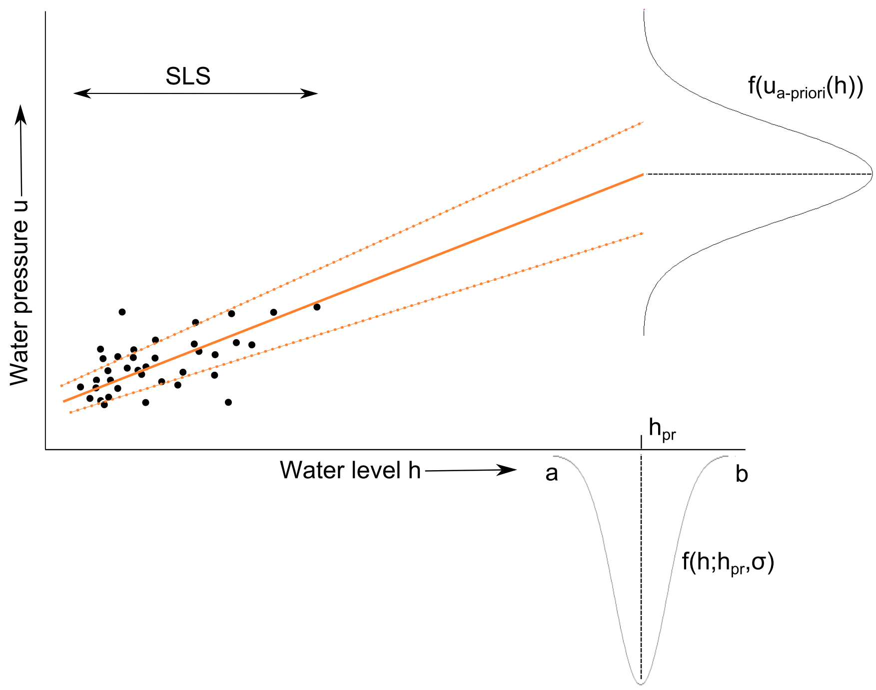

Figure 3-23: Early warning situation for short-term predicted water level h_{pr} without water pressure monitoring

Real-time water pressure monitoring can be used as an additional information source to determine the short-term failure probability for macro instability, by specifying the water pressure loading. The a-posteriori water pressure loading condition is dependent on the real-time monitored water pressures and the water level prediction. Now, this additional information is used to determine the short-term failure probability:

$$P_{\text{macro,pr}} = \int_{h=a}^{h=b} \int_{u=-\infty}^{u=\infty} P\left\{Z_{\text{macro}} < 0 \mid u_{\text{a-posteriori}}(h)\right\} f(u_{\text{a-posteriori}}(h))du \cdot f(h;h_{\text{pr}},\sigma)dh$$

$P\{Z_{macro}<0 \mid h_{pr}\}$	Total failure probability due to macro instability, conditional on the predicted water level h_{pr} and measured water pressure u_r
$u_{a\text{-}posteriori}(h)$	A-posteriori water pressure loading condition for corresponding water level prediction
$f(u_{a\text{-}posteriori}(h))$	A-posteriori probability density function of water pressure u for corresponding water level prediction
h_{pr}	Short-term prediction of the water level

The real-time water pressure before a predicted loading event is of special importance for the short-term failure probability, because of additional effects of other hydraulic loads on the water pressures during an operational situation (TAW, 2004). For instance, if the real-time water pressures are already increased due to precipitation or overtopping, then the impact of the predicted water level h_{pr} can be higher than was anticipated a-priori. The predicted short-term high water level h_{pr} and the monitored actual water pressures results in a short-term probability density function $f(u_{a\text{-}posteriori}(h))$, see Figure 3-25.

Operational situation for short-term water level prediction; with early warning monitoring

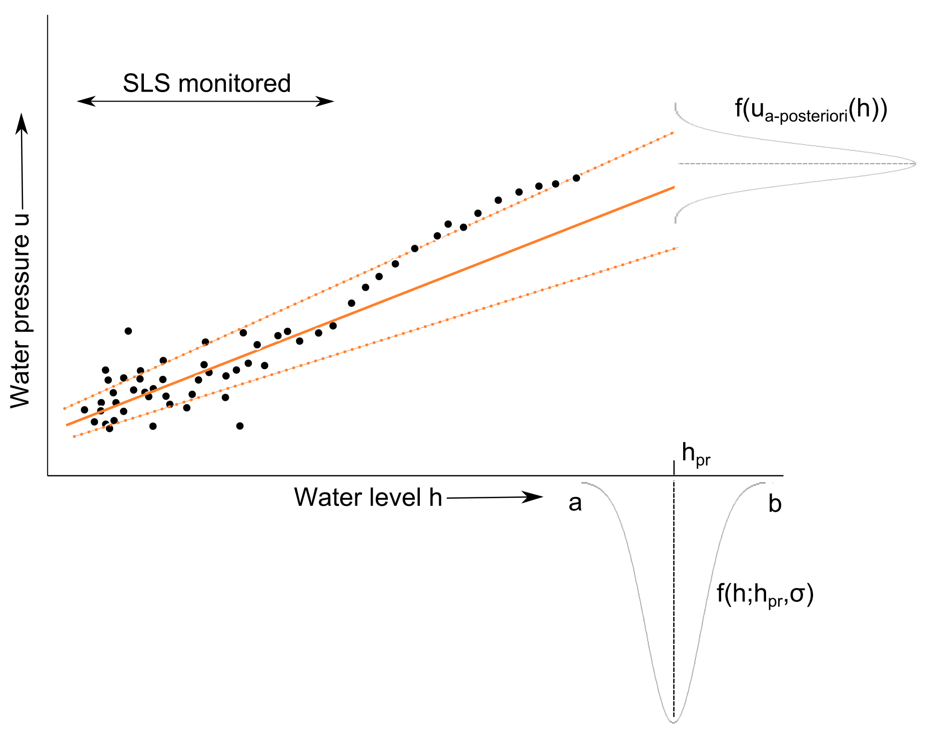

Figure 3-24: The effect of water pressure monitoring on for early warning application

The determination of the short-term failure probability is used to support decision making for taking repressive measures. The real flood risk is only affected by physical measures. Different types of temporary flood protection measures are discussed in the text box *Flood protection* *measures.* The short-term threat of the predictions makes the application of repressive measures dependent on the available reaction time. The use of water pressure monitoring for early warning purposes can contribute to the available reaction time, by reducing the short-term uncertainty in the stability assessment. More rational decision can be made due to the reduction of water pressure uncertainties. However, the application of sensor monitoring for early warning requires a high operational reliability during loading events, because the risk is short-term based. The reliability consists of the technical reliability of the sensor technique, but also the availability and accessibility of real-time sensor data. Besides, the data interpretation must be able to be executed real-time. Sensor monitoring for early warning applications is only effective if a flood protection measure can be executed, before the predicted threat occurs.

Emergency flood protection measures

In order to reduce the flood risk on a short-term basis, emergency flood protection measures are performed that temporary reduce the flood risk. The success of an emergency flood protection measure depends on the time frame of execution. The measure must be executed in time: that is before the dike fails. The measure tempts to reduce the flood risk, before it is too late. If the measure takes too long to execute, the flood risk has not been reduced and the measure is unsuccessful. Two types of measures can be distinguished:

- Measures that reduce the consequences of a flood
- Measures that reduce the probability on flooding: reducing the loads or increasing the strength

Emergency measures that reduce the consequences of a flood are commonly evacuation of inhabitants and cattle. A preventive evacuation requires time and is thereby dependent on the prediction time of the flood. Also preparedness plays a role, as an evacuation can be executed more efficiently (i.e. faster) when inhabitants are prepared, than would be the case if the evacuation is unplanned (e.g. inhabitants are still asleep). Moreover, a successful evacuation in densely populated areas requires more time, due to logistic congestions of the road network (Frieser, 2004).

An alternative is to reduce the probability of a flood; thus reducing the dike failure probability. Reducing the loads that cause the flood can be done by inundation of assigned polders (i.e. "controlled" flooding of less valuable land) or, for example, by regulating the river discharge at bifurcations. Yet, possibilities to reduce the load are not always available. The flooding probability can also be reduced by (temporary) increasing the strength of the dike. Sand bags are often placed to reduce the amount of water flowing over the dike, stability berms are placed to increase the sliding stability and piping boils are ringed with sand bags (Dutch: *opkisten*). More innovative initiatives can be found in (Boon, 2007).

3.4.2 Early warning by monitoring other observable variables

Other types of observable variables than water pressures can be monitored for flood safety matters like temperature, deformation, vibrations and moisture (see paragraph 2.5.1). The relevance of these observable variables for early warning purposes is currently investigated in IJkdijk experiments, see text box *Early warning during IJkdijk experiments*. The early warning potential is derived from failure indicators that consist of anomalies in the monitored data. Such an anomaly tempts to give a direct relation between the observable variable and an upcoming dike failure. The However, the current experiments reveal much uncertainty referring the relevance of the observable variable for the failure mechanism. Besides, the derived early warning potentials have a wide variety in this stage of research. The variety in early warning potential needs to be reduced in order to use early warning monitoring of other observable variables, because of the time dependency of the effectiveness of repressive measures.

Early warning during IJkdijk experiments

Multiple tests are performed by the IJkdijk consortium, with the purpose to find early warning indicators for weaknesses in the dike (Rijkswaterstaat, 2009b). After these tests, the gathered data has been analyzed by the sensor manufacturers. Data anomalies (i.e. data deviating from normal behavior) were coupled with the loading conditions and other activities around the dike. These analyses resulted in collapse indicators that claim to predict the dike collapse in an early stage. The time frame between the data anomaly and the dike collapse, i.e. the early warning potential, is the key factor during operational situations. The IJkdijk experiments resulted in a wide spread of early warning potentials (see Table 2-1). Yet, the circumstances in which these results are claimed are restricted due to the controlled circumstances. The fact that the claimed early warning potentials are widely spread, even for the controlled test setting, induces the need for further testing. The behavior during a real operational situation will be significantly different due to the heterogeneity of the dike material, the actual behavior of the occurring loading condition and the uncertainty in the prediction of upcoming loading conditions. The derivation of an empirical early warning relation requires significant numbers of tests, performed under representative circumstances referring both the loading conditions as the dike properties.

3.4.3 Social order

Water pressure monitoring can act as a political instrument to inform the public about the current state of the dikes during operational situations. Recent experiences in the northern part of the country indicate that uncertainty about the flood risk can cause more chaos than anticipated. The information supply towards the public is not to be underestimated (Flikkema, 2012). The fact that little to no information was on hand about the real-time status of the dikes, raised questions among the public. A difference in risk perception between the public and dike experts can disrupt the social order (Van Staveren, 2006). The perception of the expert on the real-time risk is formed by knowledge and expertise. But the risk perception of the public is driven by social factors, such as fear and the influence of the media. For example, the actual flood risk can be considered in control for experts, but the perception of the public can be that the risk is high because they see overtopping of dikes. In this way, the public becomes suspicious and indirect damage due to chaos might be the consequence. By supplying sufficient and effective information about the actual status of the flood risk, the public's risk perception can be (temporarily) influenced. Reliable and up to date water pressure data can give this information. However, this potentially beneficial aspect can hardly be quantified and therefore considered as an addition to other implementations of the sensor techniques during operational situations.

3.5 Risk awareness

3.5.1 Unforeseen risks

The application of sensor monitoring can help identify unforeseen risks by continuous monitoring. The assessment of macro instability (or any other civil engineering problem), requires interpretation and schematization choices to be made by an engineer. Apart from any technical uncertainties regarding the dike strength, hydraulic load or monitoring system, the final assessment thereby depends on the knowledge, expertise and subjectivity of the engineer. Misunderstandings of the engineer can lead to serious schematization errors, which are only to be revealed when the design loading condition occurs and may lead to a flood. This subconscious “engineering sloppiness” induces unforeseen risks, because the design is not made for these risks. A relation between uncertainty, foreseen risks and unforeseen risks is given in Figure 3-25, according to (Van Staveren, 2006).

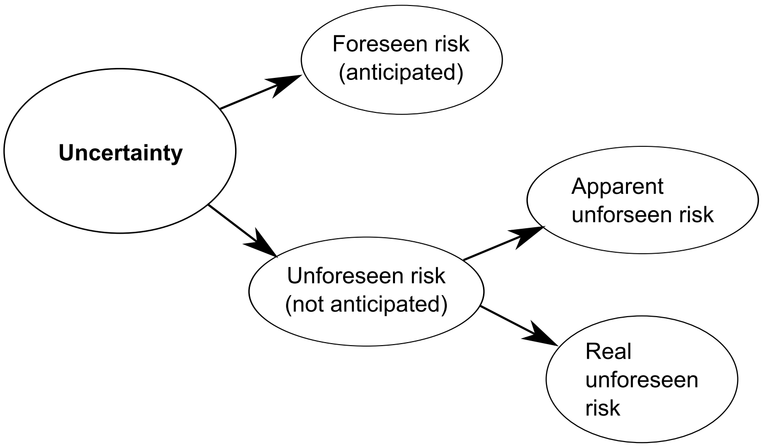

Figure 3-25: Relation between uncertainty, foreseen and unforeseen risk (Van Staveren, 2006)

Foreseen risks are risks that are identified a-priori and taken into consideration. For example during the design phase of a dike, the design loading condition for the life time is defined. An overview of events that might influence the design conditions are made to get insight into the circumstances (e.g. future building activities nearby, climate change). The listed events are thereby foreseen, as they are actively dealt with in the design. The uncertainty in the assessment is based on these foreseen risks. Unforeseen risks are caused by unwanted events with a negative impact, which was not anticipated on beforehand and are thereby unexpected. Apparent unforeseen risks are the risks that were not identified on beforehand, but eventually occur and have a negative effect. Real unforeseen risks remain unknown, as they are not noticed. An example of an unforeseen risk with a dike and dry foreland is given in Figure 3-26.

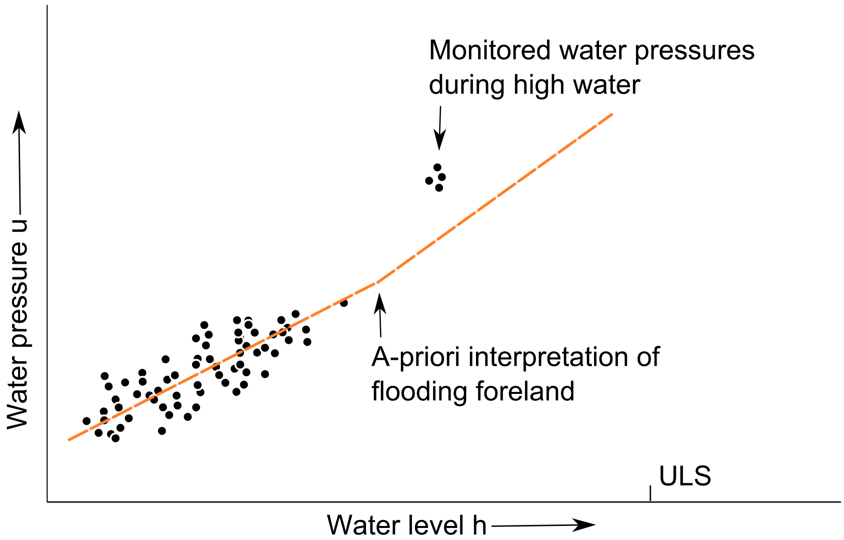

Figure 3-26: An unforeseen risk for a dike with foreland

During the a-priori assessment of macro instability, the effect of the dry foreland on the development of the water pressures is foreseen and the extrapolation is adapted. However, monitoring of the water pressures during a high water event, in which the foreland is flooded, revealed that the corresponding water pressures turned out to be higher than expected. This risk remained unforeseen by monitoring the water pressures under daily conditions (i.e. when the foreland remains dry), but the high water event revealed the unexpected behavior (i.e. when the foreland is inundated).

It should be emphasized that the actual presence of an unforeseen risk may be possible (i.e. due to the a-priori interpretation and schematization mistakes), but the presence is not always the case. The first requirement for identifying an unforeseen risk is the actual presence of the unforeseen risk. However, this remains per definition unknown until the risk has been identified.

3.5.2 Sensor monitoring and unforeseen risks

The implementation for sensor monitoring is to help identifying a real unforeseen risk by making them apparent in an early stage, i.e. before a flood occurs. Therefore, the monitoring system must be able to identify the unforeseen risk (if it is present in the first place), which depends on the relevance of the monitored observable variable for the unforeseen risk and the monitoring density. A monitoring system is not primarily designed to identify unforeseen risks in the first place, because the presence of the risk is per definition unknown. Consequently, the detection of an unforeseen risk must be considered as an additional effect when the monitoring system has been installed for other purposes.

Given the (prior unknown) presence of an unforeseen risk and the capability of the sensor system to monitor this risk, the theoretical implementation of sensor monitoring is given in Figure 3-27. The changes in the physical behavior can be identified with continuous monitoring. If these changes are not expected and revealed (i.e. real unforeseen), the cause of the changes can be investigated (i.e. apparent unforeseen risk). The awareness for unforeseen risks is dealt with by updating the assessment and taking measures to actually mitigate the unforeseen risk. This changes the apparent unforeseen risk into a foreseen risk. Again, the time required for the measure to be effective is crucial in the handling of unforeseen risks.

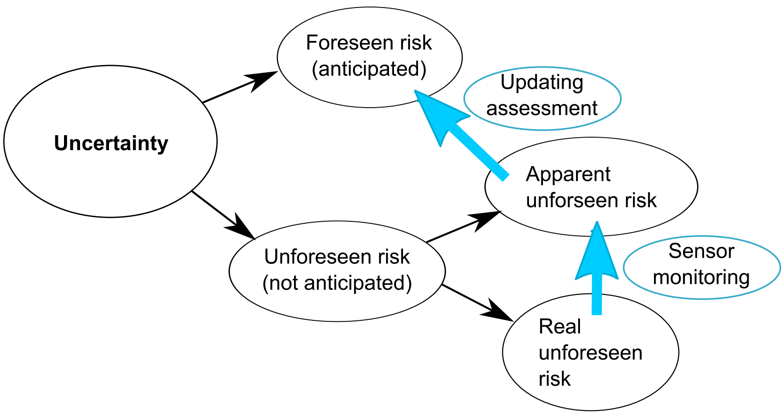

Figure 3-27: Theoretical implementation of sensor monitoring for risk awareness

However, the transition from an apparent unforeseen risk to a foreseen risk requires correct interpretation of the monitoring data by an engineer: the unforeseen monitoring data must be identified and explained. This leaves the a-posteriori “sensor sloppiness” instead of the a-priori “engineering sloppiness”. Thus, it should be emphasized that the interpretation of the monitoring data is crucial for identifying unforeseen risks with sensor monitoring. If the sensor data gives unexpected output, an explanation has to be found by the engineer. The interpretation of an unforeseen risk based on sensor monitoring is distinct for two types of lacking knowledge:

1. Lacking knowledge of the engineer, but knowledge is available in the engineering sector
2. Lacking knowledge of the engineer and in the engineering sector

In the first situation, the engineer is lacking knowledge about the monitored phenomena. This situation is plausible as the same engineer did not foresee the deviating behavior prior to the sensor monitoring in the first place. However, the knowledge about this phenomenon is available in the engineering sector at hand. Misinterpretation of the data is due to the lack of knowledge by the engineer, but the knowledge is available in the engineering sector and accessible by consulting a second opinion. If sensor monitoring reveals to deviating behavior, accessing the state of the art knowledge of the engineering sector leads to new insights into unforeseen risks. However, if the knowledge of the engineering sector is not accessed, premature conclusions due to a lack of knowledge by the engineer can lead to misinterpretations of the monitoring data. A premature conclusion is dangerous as it leads to pretended safety. Thus, the probability of detecting such an unforeseen risk with sensor monitoring is larger as the responsible engineer has no state of the art knowledge, because the probability that the engineer overlooked a potential risk in the prior assessment is larger. This is pointed out in the text box *Seepage wells in a building pit*.

Example of a premature conclusion: seepage wells in a building pit

The construction of a subway station is done in a building pit. As the execution progresses, the groundwater level has been raised because of precipitation in the last few days. Due to the higher groundwater level, seepage wells started to form in the building pit, creating sand boils. These sand boils are detected every morning by a diligent worker (in this case, the eyes of the worker functions as the "sensor" measuring with a frequency of once a day). The worker realizes that the sand boils form an obstacle for passing shovels (the data interpretation of the worker) and decides to remove the sand boils, every morning. In this case, the sensor has successfully detected the risk of stability loss (namely the formation of a sand boil). But due to misinterpretation of the sensor data, the wrong measure is taken to handle the observed risk. Any geotechnical engineer would make another data interpretation and decided for a different measure. Thus the human error is the dominant factor in this interpretation step.

The second situation refers to observed behavior of which knowledge is not incorporated in the engineering sector and thus neither by the responsible engineer. Another interpretation problem of the monitoring data occurs as data is inexplicable: unexpected monitoring data has been measured, but a thorough explanation for the unexpected behavior cannot be given within the available expertise. Thus appropriate measures to reduce the risk cannot be made, until the new expertise is gained on the observed phenomenon. Sensor monitoring can contribute to detecting these unforeseen risks by providing new insights for the engineering sector. The text box *Rijkswaterstaat vibrating office tower* is a recent example in the Netherlands of inexplicable detected behavior, which eventually resulted in a new insight.

Paragraph 3.5.6 gives examples of both types of unforeseen risks, i.e. lacking knowledge of the responsible engineer only and lacking knowledge of the engineering sector), in the context of flood safety in the Netherlands.

Rijkswaterstaat vibrating office tower

On June 28th 2012, employees working in the Westraven office tower of Rijkswaterstaat (the executive department of the Dutch Ministry of Infrastructure and Environment) are overwhelmed by sudden vibrations. Coffee cups clashed from the tables (in this case, the cups function as the "sensor") and the building was evacuated at the end of the day, bringing everybody in safety. However, what caused the vibrations? Different explanations were proposed: snapping of pre-stressed steel cables in the reinforced concrete, a too tight façade structure (the building originated from 1975, but has been renovated in 2007 by adding a new façade) or low frequency vibrations resonating with the buildings eigenfrequency. A definite interpretation of the incident was concluded after a thorough investigation lasting 2,5 months: vibrations due to the usage of the window-clean installation, which has been installed directly on the steel structure of the building, resonated with the structures eigenfrequency. The safety of the building has never been an issue according to the investigation conclusions. (Ministerie van Binnenlandse Zaken en Koninkrijkrelaties, 2012).

Finally, if the monitoring data was unexpected and given the data interpretation has revealed the cause of the risk, proper measures have to be taken in order to reduce the risk. After all, sensor monitoring alone does not affect the real flood risk, but just the assessment of flood risk. Executing physical measures influence the real flood risk, of which dike heightening is a common example. However, dealing with the detected risk *on time* is the key element. If the unforeseen risk is identified on time, a mitigating measure must be executed before the consequences of the risk take place for a successful application of sensor monitoring. Preparedness and willingness to mitigate unexpected risks increases the successfulness of sensor monitoring. Applying sensor monitoring in a broader context to optimize the costs and flood safety can be obtained by applying the observational method, see paragraphs 3.5.3 to 3.5.5.

3.5.3 Observational method with sensor monitoring for flood safety

The principle of the observational method grants opportunities to handle unforeseen risks in the flood safety assessment with sensor monitoring. The observational method is defined as an integral design, execution and risk-management method in which an optimal design is obtained, by adapting the original design based on observations during the execution (Van de Kamp, 2003). Sensor monitoring for flood safety updates the uncertainty regarding the flood safety assessment and by using the observational method, measures can be planned and executed based on the sensor monitoring data. Preparing measures for unforeseen flood risks can mitigate these risks. A list of conditions is given in (Jongejan, 2004) which can be used to determine the effectiveness of applying the observational method in geotechnics. Attention must be paid to specific conditions for applying the observational method with sensor monitoring for flood safety:

- **Relation of the observable variable with the failure mechanism**
  The monitored observable variable must give relevant information on the considered failure mechanism. Water pressures in the dike give relevant information about the loading conditions referring macro instability. Also the location of the monitored observable variable is important to relate the monitoring data with the failure mechanism (e.g. piping monitoring in permeable sand layers instead of a clay layer). Water pressure monitoring in a deep aquifer is not relevant for macro instability. Especially using the observational method for early warning purposes, the observable variable must have an unambiguous relation with the failure mechanism.

- **Value of SLS loading conditions for ULS loading conditions**
  Flood safety in the Netherlands is based on rare loading events (i.e. loading events inducing ULS) which form a threat for a potential flood. If the monitoring during SLS can provide sufficient information about the ULS loading conditions, the intervention time to mitigate the risk is increased.
- **Contribution of different failure mechanisms**
  Applying sensor monitoring for a critical failure mechanism can lead to underestimation of other failure mechanisms. When one failure mechanism is dealt with monitoring and by applying the observational method, another failure mechanism can become critical during extreme conditions. This causes unexpected risks from other failure mechanisms and must be considered before applying sensor monitoring.
- **Intervention time**
  The most critical requirement is the available time to mitigate an unforeseen risk after its detection. This is related to tenacious failure behavior of the failure mechanism: if an unforeseen risk has been detected, the system must fail tenaciously in order to grant time for intervention. Brittle failure behavior, especially during operational situations, is excluded. The required intervention time is dependent on the type of intervention and the preparedness of the intervention.
- **Guaranteed long-term monitoring**
  The observational method requires consisted monitoring and management of potential risks over the long-term, because valuable information is obtained from high water events. Future dike managers are thereby obligated to maintain the principles of the observational method and the corresponding costs, which can be problematic due to political and societal changes in the future (e.g. changing responsibilities for the dike maintenance).
- **Monitoring of a serial system**
  The serial working of dike sections forming a dike-ring requires cautious application of the observational method. Failure of any dike section causes a flood (i.e. assuming no sleeper dikes are present). A relatively high monitoring density is required, because the serial dike system is vulnerable for monitoring errors and discontinuities.
- **Continuous flood safety assessment**
  Flood safety must be guaranteed at any time. Therefore, applying the observational method for flood safety issues is more suitable for possible rationalizing of the a-priori design, than intervening in a lighter design. Because the safety standards must be met during the whole life time.

Applying sensor monitoring with the observational method for flood safety issues must be considered carefully per distinct situation for above mentioned conditions. But the principles of the observational method can be used to implement sensor monitoring by dealing with unforeseen risks in the periodic safety assessment and early warning.

3.5.4 Observational method for periodic safety assessment

The application of sensor monitoring for the periodic safety assessment of dikes can be implemented in the risk-based observational method. The risk-based observational method is proposed in (Van de Kamp, 2003), see text box *Observational method in geotechnical engineering.* This variant is based on a-priori determined scenarios; a positive, an expected and a negative scenario.

Risk-based observational method in geotechnical engineering

The observational method aims at achieving an optimal balance between safety and investment, and on the other hand at improving risk management. If the observed actual conditions are better than expected, the observations might be under the rationalization line. The planned investment is higher than required and the design can be rationalized, leading to savings. On the other hand, the actual conditions can also be worse than expected and the initial design does not meet the required safety. If the intervention line is crossed, investments must be made such that the design is adapted to meet the required safety, see Figure 3-28.

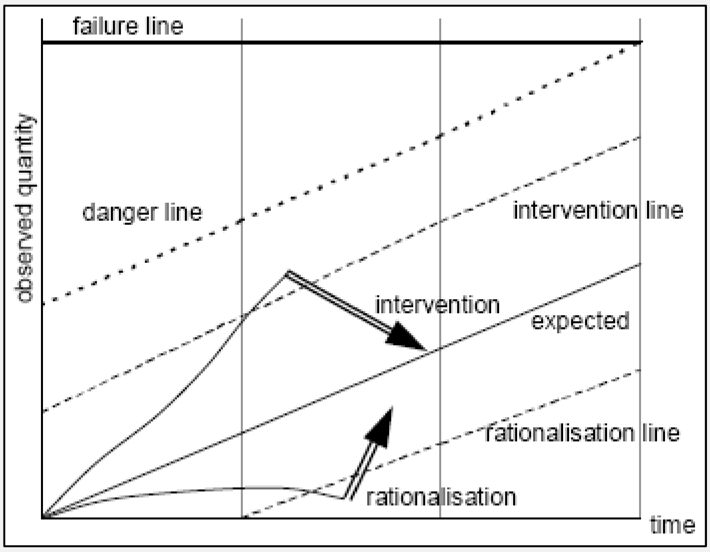

Figure 3-28: The observational method (Van de Kamp, 2003)

Here, the a-priori periodic safety assessment forms the expected situation (i.e. determined without sensor monitoring and based on inspection information), see Figure 3-29.

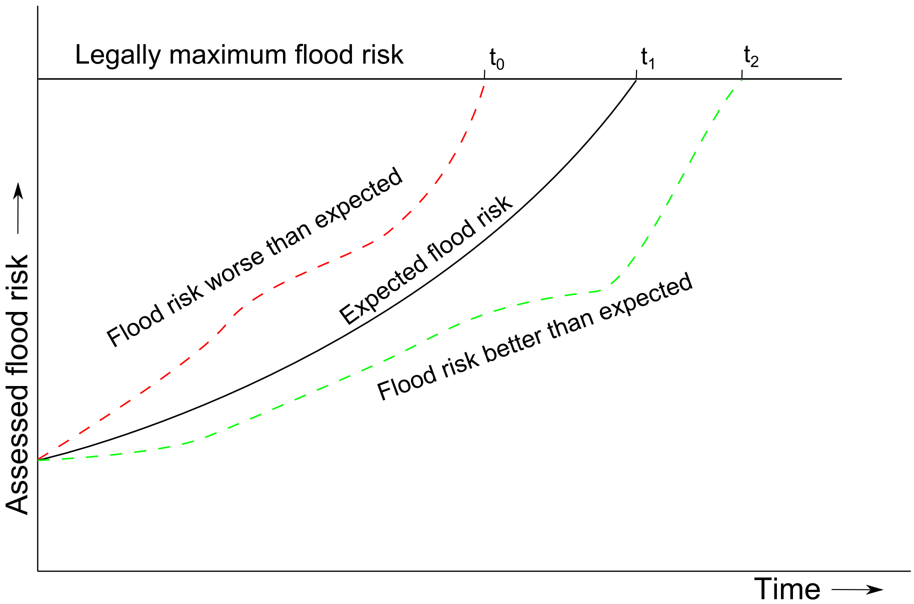

Figure 3-29: Risk-based observational method for periodic safety assessment

The flood risk is expected to rise over time due to climate change and economic growth. A dike reinforcement is expected at time t_1, when the critical value for the flood risk has been reached (i.e. legally required). The monitoring of the dike (e.g. water pressure monitoring for macro instability) affects the assessment of the flood risk: the actual flood risk is better than expected or the actual flood risk is worse than expected. It should be emphasized that the real flood risk is not affected, but just the assessment of the flood risk. If the sensor monitoring reveals a flood risk better than expected, the planned dike reinforcement can be rationalized: either postponing the reinforcement to time t_2 or lighten reinforcement at t_1, see Figure 3-30. Postponing a future investment grants economic benefit due to the net present value (discounted costs).

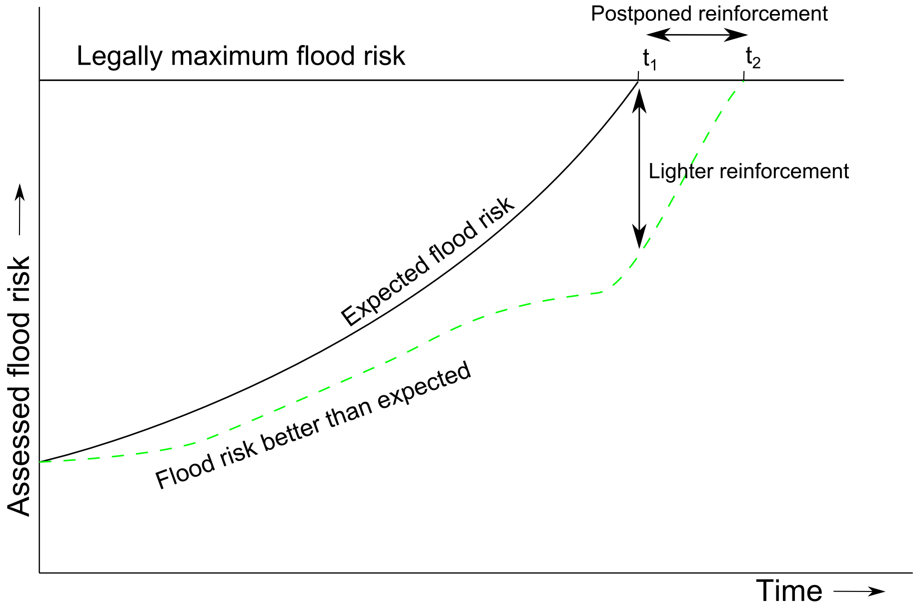

Figure 3-30: Rationalization with the observational method: postponed or lighter reinforcement

If the sensor monitoring reveals a worse than expected flood risk, the planned reinforcement at t_1 needs to be advanced to t_0 in order to meet the required flood risk level, see Figure 3-31.

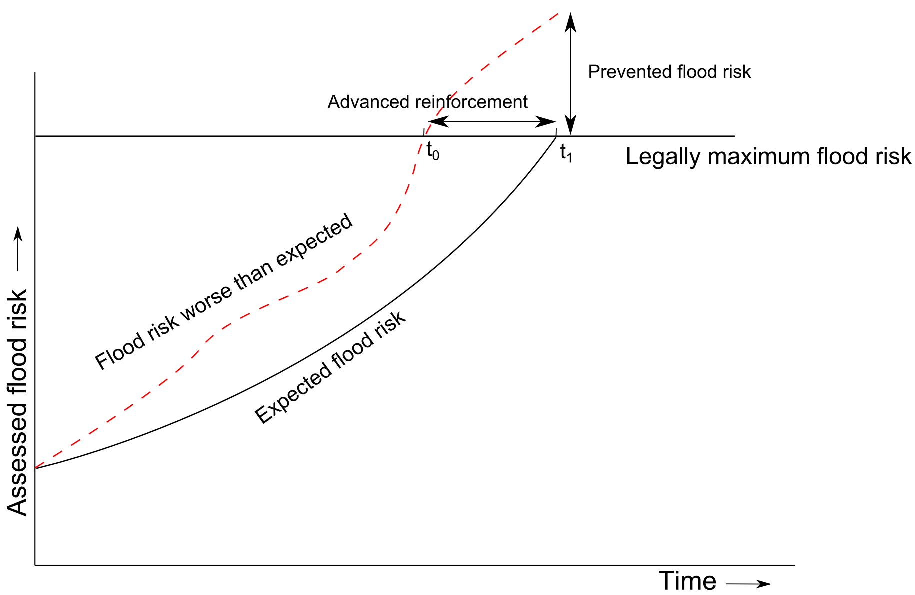

Figure 3-31: Intervention with the observational method: earlier reinforcement

Advancing the reinforcement to t_0 leads to a higher net present value of the investment. However, one must incorporate that due to the application of the sensor monitoring, legally unaccepted flood risk has been prevented: if the expected reinforcement has been executed as planned on t_1, unforeseen high flood risks were present over the time period from t_0 to t_1.

3.5.5 Observational method for early warning

The early warning application of sensor monitoring suits the best-way-out variant of the observational method. The best-way-out variant is applied when failure of the system is expected if no intervention is done (Van de Kamp, 2003). Short-term early warning predictions for flood safety implies an upcoming dike failure and decisions for risk mitigating measures are considered: this is an instinctual best-way-out application. Extending the early warning predictions with sensor monitoring provides a better insight into short-term uncertainties regarding a dike failure. The best-way-out variant requires preparation of measures for short-term interventions to be able to reduce the flood risk. In case of an unexpected threat elaborated from the monitoring data, a suitable measure must be on hand to be executed directly. The best-way-out observational method for early warning purpose is presented in an event tree in Figure 3-32.

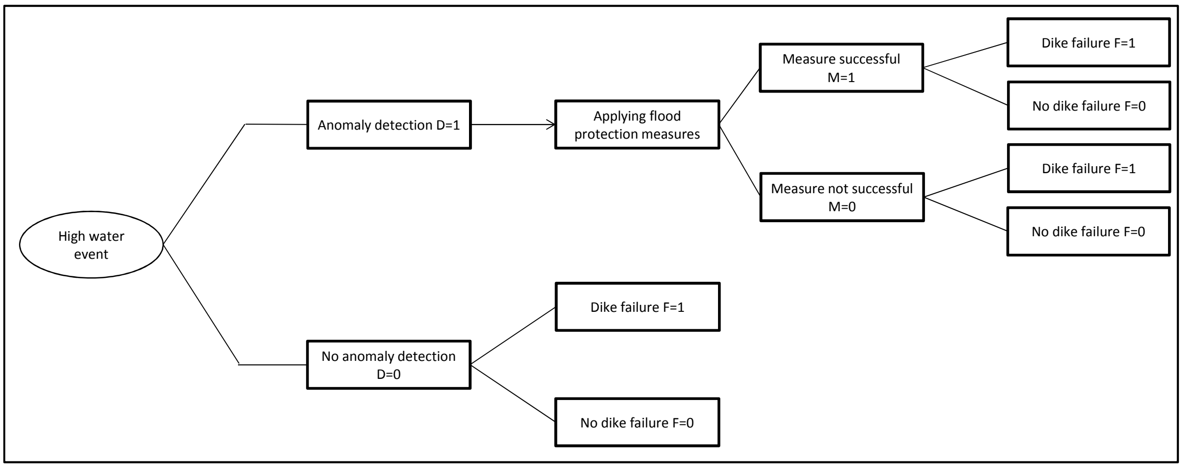

Figure 3-32: Event tree for the application of sensor monitoring in early warning situations

In case of a high water situation, a failure prediction is made based on the sensor monitoring data. The detection of an anomaly in the monitoring data is an indication for an upcoming dike failure. The definition of an anomaly must be determined beforehand by using e.g. threshold values and might be based on political decisions. The situation when no anomaly has been detected during an operational situation, D=0, gives no reason to execute a mitigating measure. When an anomaly has been detected, D=1, a dike failure is on hand and mitigating measures will be executed. The success of the best-way-out method depends on the *in time* execution of the mitigating measure, i.e. before the predicted failure would occur. The availability and feasibility of a mitigating measure varies per situation, but is dependent on the available prediction time and the required prediction time due to physical limitations of the mitigating measure (e.g. traffic congestions, availability of materials, buildings blocking the required space). The combination of the available prediction time and the required prediction time determines the successfulness of the mitigating measure. A successful mitigating measure, M=1, means that the intended measure has been executed on time: the flood risk has been reduced. Incomplete or delayed execution of the mitigating measure leaves the predicted risk unharmed: leading to a possible flood. The best-way-out method requires an extensively reliable monitoring system, prepared mitigating measures for different possible situations and enough time to execute these prepared measures.

3.5.6 Examples of unforeseen risks in practice

The common characteristic of unforeseen risks in the context of flood safety is that the direct influence is not noticed during SLS, because no flooding will occur. As long as everybody keeps dry feet, the unforeseen risk stays real unforeseen. Yet, during significant hydraulic loading conditions, the notification of the influence might be too late, because a dike has been breached and a flood is developing. Sensor monitoring can contribute to the awareness of the unforeseen risks in an early stage with the observational method. Example situations in which unforeseen risks can be present in the context of flood safety are elaborated. First, examples of unforeseen risks are given in the situation that the knowledge of the engineer is lacking, but the knowledge and expertise is available within the engineering sector:

- **Climate change**
  The climate change is a worldwide discussion point in which many uncertain aspects are involved. The Delta Committee has been assigned in the Netherlands to give insight into flood protection with respect to the expected climate change (Deltacommissie, 2008). The climate change is undisputedly considered to consist of sea level rise and weather changes due to global warning. But the magnitude and speed of the expected climate changes and corresponding consequences is governed by uncertainties. The recommendations of the Delta Committee are based on argued upper limit scenarios. Large scale and long term sensor monitoring can contribute to the awareness for the impact of climate change on flood safety. For example regular airborne LIDAR measuring can monitor the dike settlements. Increased long term settlement rates can be induced by climate changes. Also the influence of extreme precipitation over the long term can be noticed.
- **Hydraulic structures**
  The presence of hydraulic structures (e.g. storm surge barriers, bridges) in the waterway or other building activities can have a significant influence on the hydrological loading conditions. Large projects (e.g. Maeslant Barrier) contain impact assessment studies for the environmental changes. However, despite the rational approach, these impact studies are also exposed to unforeseen risks. Smaller building activities nearby a flood defence might cause local disturbances, which form a possible thread for the flood safety. As the life course of the flood defence passes by, the chance of being influenced by such unforeseen activities increases. Large scale sensor monitoring of deformations or water pressures can contribute to the awareness for the unforeseen consequences of building activities. Unexpected, long term anomalies in the data can be detected, whereas the cause for the anomaly can be retrieved.
- **Groundwater withdrawal**
  Groundwater withdrawal by industry plants or water treatment plants has a continuous influence on the regional geohydrological conditions. The withdrawal is done from an aquifer. If the aquifer continues under the dike, the groundwater withdrawal influences the water pressures in the dike. The number of permitted groundwater withdrawals decreases, because of the influence on the drought of nature. Yet, this can also have consequences on the local geohydrological behavior around dikes. Sensor monitoring of the geohydrological behavior in dikes can detect the influence of (temporary stopped) groundwater withdrawal.
- **Dredging activities influencing the silt layer**
  Dredging activities in rivers are performed to maintain the required water depth for both recreational and professional navigation. A poorly permeable slip layer is thereby removed. This slip layer forms an entrance resistance for the groundwater flow. The entrance resistance is the "effort" of the water particle to enter the soil. This effort results in a damping effect for the water pressures behind the dike. As soon as the silt layer is removed by dredging activities, the entrance resistance can be reduced as well. Frequent monitoring

of the water pressures behind the dike can identify the different behavior due to a changed entrance resistance.

- **Detection of a sand trench**
  Another known risk is the presence of a sand trench in a dike. A sand trench does not directly lead to slope instability, as sand is generally stronger than peat. But the permeable sand trench causes a high risk to piping failures. Also, higher local groundwater flow increases the risk for uplift of the impermeable top layer. Water pressure monitoring over the length of the dike, can result in deviating data if a sand trench is located at the monitoring position: the sand will cause concentrated groundwater flow. In this way, the presence of a sand trench could be detected during the monitoring period and measures can be taken.
- **Layer characteristics**
  Sensor monitoring could provide specific information on the characteristics of the layer in which the sensor has been installed. Layer characteristics are important for the geohydrological schematization of piping, macro and micro instability. Characteristics such as permeability, storage capacity and non-stationary flow conditions might be derived from monitoring the response on fluctuations of the hydraulic load. For instance, water pressure monitoring in an aquifer can be used to determine whether the aquifer is confined or unconfined. This specific information gives new insights into the geohydrological behavior of the soil. Information on layer characteristics does not require long-term sensor monitoring.

The examples above are caused by the lack of knowledge from a single engineer and might be solved by accessing the broader expertise of the engineering sector with the consult of a second opinion. Examples of unforeseen risks due to lack of expertise of the whole engineering sector are given below:

- **Instability due to pressure bar mechanism**
  The inner slope of a dike near Streefkerk unexpectedly slid down in October 1984. The deformations occurred due to the “pressure bar” principle (Dutch: *drukstaafmechanisme*) which was unknown at that time. The pressure bar mechanism occurs in the case when weak peat and/or clay layers are uplifted due to high water pressures in the aquifer. The horizontal shear resistance of these weak layers with the sandy aquifer vanishes due to this uplift, such that the weak layers act as a pressure bar. The horizontal forces induced by the inner dike slope need to be resisted by the pressure bar of weak layers. The weak layers generally have a low stiffness, such that the resistance is insufficient with deformations of the inner slope as a result. The mechanism was an unforeseen risk in the engineering sector until new insights were obtained due to the Streefkerk dike collapse.
- **Horizontal sliding of a peat dike due to drought**
  The danger for horizontal sliding of a peat dike body due to drought has been acquired by the Wilnis dike collapse in august 2003. The dike near Wilnis mainly consists of peat layers. In times of extreme drought, the water content in the peat lowers which results in low volumetric weight of this peat. The horizontal sliding occurred as the dead weight of the dike was drastically lowered due to the drought, such that the water in the canal pushed the lightweight dike aside. This danger of peat dikes in times of drought was an unforeseen risk, until new insights were obtained due to the Wilnis dike collapse.

3.6 Proven strength

3.6.1 Proven strength in a probabilistic analysis

A probabilistic analysis can be combined with the proven strength method. Proven strength is a part of the observational method, according to (Jongejan, 2004). The strength of the dike is specified by observed and survived loads. The total dike failure probability is a combination of the occurrence of a loading condition and the corresponding failure probability for each loading condition. If a certain loading condition has been observed in the past and the dike resisted this load, this acts as a proof of strength. Apparently, the real dike strength is at least the strength that is required to retain the survived load; otherwise the dike would have showed weaknesses. An example for the proven strength method is given for the failure mechanism overflow (see also paragraph 3.1.1), see Figure 3-33.

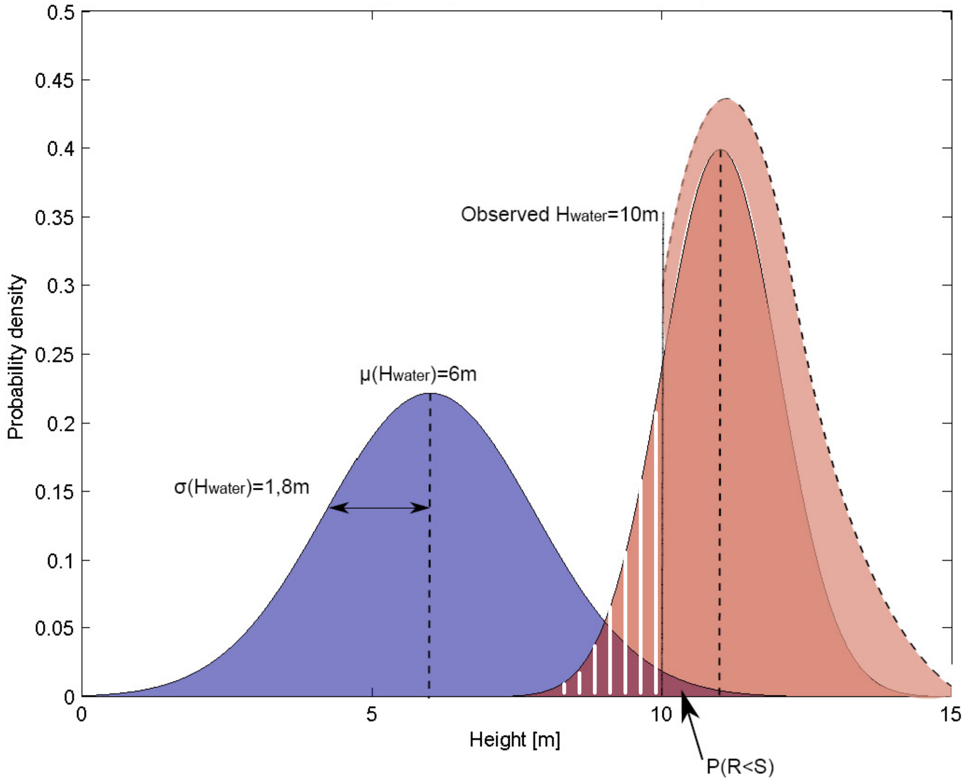

Figure 3-33: Proven strength principle for the failure mechanism overflow

A water level H* has been observed and during this load, no water flowed over the dike. These observations imply that the dike height H_{dike} (i.e. the dike strength) is at least the height of the observed load H*: otherwise water would have been flowing over the dike. The probability density of the dike height H_{dike} is updated with the proven strength. However, multi-dimensional analysis like macro instability, make the application of proven strength more complicated. The proven strength principle relies on two a-priori failure probabilities, which are used to determine the a-posteriori failure probability. The a-priori failure probabilities are the historical failure probability, which has been resisted by the dike. And the failure probability for design loading condition which is needed for the safety assessment. The a-priori failure probabilities are derived with available information on beforehand. The fact that the dike did not fail due to the historic load, while there was a significant a-priori probability that it did fail, is used to update the failure probability in the design loading condition: the a-posteriori failure probability. The a-posteriori failure probability for the design loading condition is derived according to (Calle, 2005):

$$P''\{fail_T \mid fail_H\} = \frac{P'[fail_T] - P'[fail_T \cap fail_H]}{1 - P'[fail_H]}$$

$P''\{fail_T \mid \overline{fail_H}\}$	A-posteriori failure probability for the design loading condition, given the survived historic loading condition
$P'[fail_T]$	A-priori failure probability for the design loading condition
$P'[fail_H]$	A-priori failure probability for the historic loading condition
$P'[fail_T \cap fail_H]$	Probability that failure occurs in both the historic and design loading conditions: dependent on the correlation between the failure mechanism for historic and design loading conditions

The probability that failure occurs in both the historic and design loading condition is dependent on the correlation between the two failure situations. The determination of this correlation is in practice difficult, due to a lack of information regarding the actual historic loading condition (Rijkswaterstaat, 2009a).

Starting point of the proven strength method is the survival of the historic load. Considering macro instability, any signs of deformations caused by the historic load imply weaknesses in the dike. The confirmation of the strength after the historic load, commonly by visual inspection, is important in order to apply the proven strength method.

3.6.2 Application of water pressure monitoring in proven strength

Water pressure monitoring can be used to determine the correlation between historic and design failure mode. This correlation is the result of the differences in schematizations and corresponding assumptions between the two loading conditions. The soil can be assumed to behave similar during the historic and design situation, if no executional works are carried out meanwhile. The soil strength and soil composition are thereby correlated for both loading conditions. The same holds for the model uncertainty, if the failure mechanisms are similar. The water pressures can however vary for each loading condition, due to the combined effects of the external water level, the duration of this water level and precipitation. Therefore, the correlation regarding water pressures is less obvious. Monitoring the water pressure prior, during and after the historic event, gives information regarding the actual occurred loading. The correlation with the design loading situation can hereby by specified by expert judgment, based on monitoring data.

However, the historic loading event needs to be of a minimum significance, such that the resisting of this load is valuable enough to give information about the dike strength. In practice, these loading conditions are comparable with the design loading conditions. The occurrence of such a load is unwanted as it forms a possible threat for the stability of the dike (per definition, assumed that the safety standard forms approximates the ULS). Thus, a possible threat is required to give insight into the actual strength based on proven strength. But exactly this threat is unwanted and measures might be taken, because the actual dike strength is to be determined. Due to this contradiction, the method of proven strength is only suitable for applying sensor monitoring. Thus, if sensors have been installed already and a significant load has been resisted, the sensor data can be used to apply the proven strength method afterwards. This is also applicable for exceptional conditions present during the construction phase, where situations might occur which act as a proof of minimum strength.

3.7 Conclusions

Monitoring of water pressures affects the epistemic uncertainty caused by the translation of hydraulic loads to water pressures, in which the water pressure forms the actual loading condition for macro stability assessments. Applying water pressure monitoring affects the assessment of the failure probability due to macro instability and thereby the assessment of the flood risk. Thus, the real flood risk is not affected, but the method to assess the real flood risk. The impact of the water pressure monitoring on the a-posteriori failure probability is however dependent on the actual collected monitoring data, the contribution of the uncertainty in water pressures compared to other uncertainty aspects and the a-priori failure probability. The impact can thereby either be a decrease or increase of the flood risk.

Applying sensor monitoring in a macro stability assessment leaves residual uncertainty, which forms the base of the water pressure uncertainty. The residual uncertainty is determined by the technical reliability of the sensor system, the sensor density, the measurement frequency, the monitoring time and the monitored loading events. The quality of the sensor monitoring system (i.e. technical reliability, density and measurement frequency) forms the base of the residual uncertainty and is required to be of a minimum quality in order to prevent unnecessary unrest and false alarms for the dike manager, leading to extra and unnecessary costs due to the sensor monitoring system. The number of monitored loading events is crucial for the extrapolation to ULS loading conditions, which is an important source of epistemic uncertainty. Monitoring the water pressures during multiple high water events reduces this epistemic extrapolation uncertainty. The extrapolation can be done by using multiple maximum values, continuous measurements during a high water or calibration of groundwater flow models.

The data is used to specify the extrapolation of water pressures to design loading conditions. Direct statistical extrapolation requires sensor data measured during multiple significant loading conditions. The analytical extrapolation method requires sensor measurements from daily conditions (e.g., tides). Also calibration of geohydrological models requires sensor data from at least daily conditions. More significant loading conditions benefit the reliability of the extrapolation. Overall, extrapolation of the water pressures to design loading conditions does not require continuous sensor monitoring. Sensor monitoring only during expected loading periods or quick sensor installation for predicted loads is sufficient.

Real-time water pressure monitoring can contribute to the flood safety during operational situations by specifying the early warning prediction for macro instability. The actual water pressures are monitored and the short-term macro stability failure probability is elaborated on the predicted high water event and the corresponding water pressures. The real flood risk can be reduced by timely execution of risk mitigating measures. An additional implementation is the use of real-time water pressure data to influence the social order during operational situations.

Long-term water pressure monitoring can also be used to identify unforeseen risks. Unexpected physical behavior of the water pressures in time and space benefits to the understanding of the local physical system and possible schematization mistakes that have been made a-priori. However, this implementation to identify unforeseen risks must be considered as an additional effect of sensor monitoring, because the presence of an unforeseen risk is per definition unknown on beforehand. Also, the monitoring system is not designed to identify an unforeseen risk and if so, the unexpected data must be interpreted correctly and the unforeseen risk must be mitigated by applying measures on time. The observational method can be applied to handle unforeseen risks with water pressure monitoring. First, the monitoring data must reveal unexpected system behavior, then the right interpretation of this data must be made in order to retrieve the cause. The appropriate mitigating measure should be chosen and this measure must be executed one time, before failure occurs.

Last, water pressure monitoring can also be implemented in the proven strength method. The correlation between the historic and design loading condition is specified with the help of water pressure monitoring prior, during and after an occurred high water event. However, this means in practice that the occurrence of a hydraulic design load has to be monitored. This requirement is contradictory with the purpose of sensor monitoring to be safely prepared for such an event. The implementation of sensor monitoring in the proven strength method is therefore considered as an additional implementation opportunity, when a sensor monitoring system was already present.

4 Case study: the canal of Nauerna

This chapter holds a case study for the canal of Nauerna, in which insight is given into the effect of water pressure monitoring on the macro instability assessment. First, an introduction to the case study is given in paragraph 4.1 and the technical characteristics are given in paragraph 4.2. A first insight into the macro stability is given in paragraph 4.3. Paragraph 4.4 explains a crucial model adaptation to avoid computation problems. Next, different cases are worked out in paragraphs 4.5, 4.6, 4.7 and 4.8. Finally, computations are made in paragraph 4.9 concerning all cases and the conclusions are summarized in paragraph 4.10.

4.1 Introduction

4.1.1 Background information

The water board *Hoogheemraadschap Hollands Noorderkwartie*r (HHNK) maintains the embankments along the canal of Nauerna in the Netherlands (located northeast of Amsterdam). The total length of the embankments is 9,7 km and the design water level in the canal is NAP +0 m. The embankments have been divided into nine sections that have different safety standards, see Table 4-1.

Table 4-1: Characteristics of the dike sections (Arcadis, 2011)

Section number	Section length [km]	Safety standard [1/year][4]
1	0,29	1/30
2	2,16	1/30
3	0,44	1/1000
4	1,40	1/1000
5	1,48	1/30
6	1,17	1/1000
7	1,59	1/1000
8	1,02	1/1000
9	0,18	1/1000

A deterministic safety assessment has been performed by HHNK for each of the nine sections. A local investigation program was carried out for this purpose: information was collected on the dike geometry (terrestrial laser altimetry), soil layer composition (CPT push-ins and borings), soil strength (borings and laboratory tests), phreatic surfaces and water pressure in the aquifer (piezometers); see (Arcadis, 2011).

The dike sections have been assessed for macro stability of the inner slope. A single representative cross-section has been determined per dike section. The simple assessment method assessed sections 3, 4, 5, 6 and 8 as. A detailed assessment was made for sections 1, 2, 7 and 9. The piezometer measurements were used for these sections to determine the position of the phreatic surface at design loading conditions. This detailed assessment resulted in sections 1 and 9 to be safe and sections 2 and 7 to be unsafe. A qualitative motivation whether to perform an advanced assessment for sections 2 and 7 resulted in no expected benefit from an advanced assessment. Thereby, the sections 2 and 7 were assessed as unsafe.

[4] Safety norms of regional dikes are based on the IPO-standards. The safety norm is assigned per dike section and is based on the potential damage caused by a section failure. A higher safety norm represents more potential flood damage.

4.1.2 Case study objectives

The aim of this case study is to analyse the effect of the piezometer measurements on the probabilistic slope stability assessment of an embankment. The macro instability dike failure mechanism is considered. Basically, the safety assessment is performed with and without the measurements and the resulting failure probabilities are compared. Also safety assessments are performed for adaptations of other uncertainty aspects to get insight into the effect of these aspects. These computations refer to the conclusions stated in paragraph 3.2.3, where the impact of sensor monitoring depends on the distribution of uncertainties in the stability assessment. The focus of this case study lies on the schematization of the water pressures under design loading conditions.

The main objectives of this case study are to obtain insight into:
1. Variety in the failure probability due to different water pressure schematization methods (i.e. with and without the piezometer measurements)
2. Relative influence of the water pressure schematizations on the failure probability with respect to other uncertainty aspects (e.g. soil strength and schematizations)

4.2 Case study setup

4.2.1 Characteristics of the considered dike section

Dike section number 2 was found to be the most suitable cross-section for this case study. The most important requirement was the amount of available piezometer measurements on the in the particular cross-section. Piezometer measurements in two different cross-sections were gathered over a period varying from 15 to 18 weeks.

The specifications for dike section 2 are:
- Dike section length of 2,16 km
- Soil layer composition consisting of clay core layer, peat layer and sand layer
- Piezometer phreatic surface measurements from 8 piezometers during 15-18 weeks (4 piezometers in two cross-sections)
- Determined design phreatic surface, elaborated from piezometer measurements
- Detailed, deterministic assessment for macro stability gave an unsafe result
- Safety standard of 1/30 per year and the design water level is NAP +0,0 m
- Polder water level is NAP -1,04 m
- Traffic loads are not taken into account
- Precipitation data from weather station Assendelft (at 2 km distance)

4.2.2 Description of the case study approach

In this case study, the safety assessment of dike section 2 is performed for the two main tracks:
1. Probabilistic macro stability assessment of dike section 2 using no measurements when deriving the phreatic surface in the dike (a-priori)
2. Probabilistic macro stability assessment of dike section 2 using the piezometer measurements for deriving the phreatic surface in the dike (a-posteriori)

The calculations are performed with the D-Geo Stability module Bishop Probabilistic Random Field. Appendix B contains the theoretical background on the Bishop Probabilistic Random Field model, in which assumptions and limitations are discussed. Five modelling aspects are faced when performing the calculations with the Bishop Probabilistic Random Field model. These modelling aspects correspond to the uncertainty aspects in Figure 3-6 and are sources of uncertainty:

- Geometry of the dike
- Soil layer composition of the dike and subsoil
- Phreatic surface and corresponding water pressures (the two main tracks, given the design water level)
- Shear strength
- Model factor

The model steps used in this case study are presented in Figure 4-1. The calculation starts with the input of the geometry. Then the schematization of the distinct soil layers is determined, followed by the shear strength characteristics of each soil layer; based on the available soil information. Also the model uncertainty is implemented with the determination of a random model factor. Then the water pressures for the two tracks are schematized by different phreatic surfaces: the a-priori phreatic surface when no sensor data is available and the a-posteriori phreatic surface based on the collected piezometer measurements. Finally, the probabilistic stability assessment is made for the design water level and the results are compared for the a-priori and a-posteriori tracks.

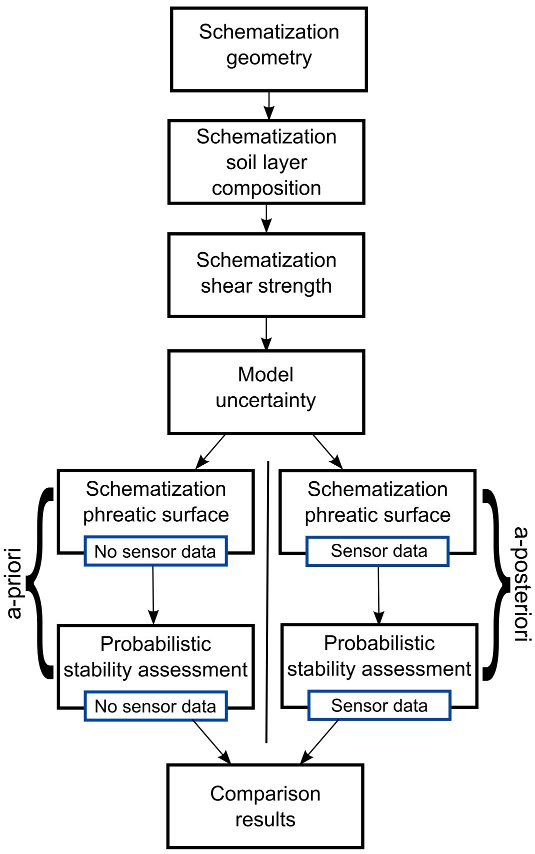

Figure 4-1: Model steps for the analysis of the effectiveness of piezometer measurements

The following cases are analysed in this study. The two types of the phreatic surface are considered in each case:

- Case 0: deterministic slope stability assessment of dike section 2 (paragraph 4.3)
- Case 1: probabilistic slope stability assessment of dike section 2 for different values of the horizontal correlation length (paragraph 4.5)
- Case 2: probabilistic slope stability assessment of dike section 2 for different values of the vertical correlation length (paragraph 4.6)
- Case 3: probabilistic slope stability assessment of dike section 2 for reduced soil strength deviation (paragraph 4.7)
- Case 4: probabilistic slope stability assessment of dike section 2 for variation in soil layer composition (paragraph 4.8)

Here, the cases 1 to 4 each represent a source of uncertainty in the schematization for macro stability, see Figure 3-6 in paragraph 3.2.2.

The calculations result in slope failure probabilities P_f (and the corresponding reliability indices β), which are consequently compared for the a-priori and a-posteriori track. The computed slope failure probability P_f is a conditional failure probability, i.e. the slope failure probability given the external design water level. Thus, the slope failure probability equals $P_f=P(Z<0|h)$, in which h is the design water level. Note that a high slope stability is associated with small values of the slope failure probability P_f and high values of the reliability index β. The used notation for the model input variables is given in Table 4-2.

Table 4-2: Notation of the model input variables per distinct soil type

Variable	Symbol	Unit
Dry volumetric weight	γ_d	[kN/m^3]
Wet volumetric weight	γ_w	[kN/m^3]
Mean value cohesion	$\mu(c)$	[kN/m^2]
Mean value friction angle	$\mu(\varphi)$	[°]
Standard deviation cohesion	$\sigma(c)$	[kN/m^2]
Standard deviation friction angle	$\sigma(\varphi)$	[°]
Correlation coefficient cohesion-friction angle	ρ	[-]
Standard deviation hydraulic pressure	$\sigma(p)$	[m]
Horizontal correlation cohesion	$D_h(c)$	[m]
Vertical correlation cohesion	$D_v(c)$	[m]
Number of tests for cohesion	N_c	[-]
Variance factor cohesion	α_c	[-]
Horizontal correlation friction angle	$D_h(\varphi)$	[m]
Vertical correlation friction angle	$D_v(\varphi)$	[m]
Number of tests for friction angle	N_φ	[-]
Variance factor friction angle	α_φ	[-]
Length of the dike section	L	[m]

4.2.3 Geometry of the dike

The geometry of dike section 2 is assumed to be deterministic in this case study (i.e. no differentiations of the geometry are considered). The exact shape of the geometry will differ along the dike and is measured with laser altimetry. However, the sections have per definition a comparable geometry and thus the variety in geometry must be limited. Figure 4-2 shows the used cross-sectional geometry. The water level difference to be retained is 1,04 m.

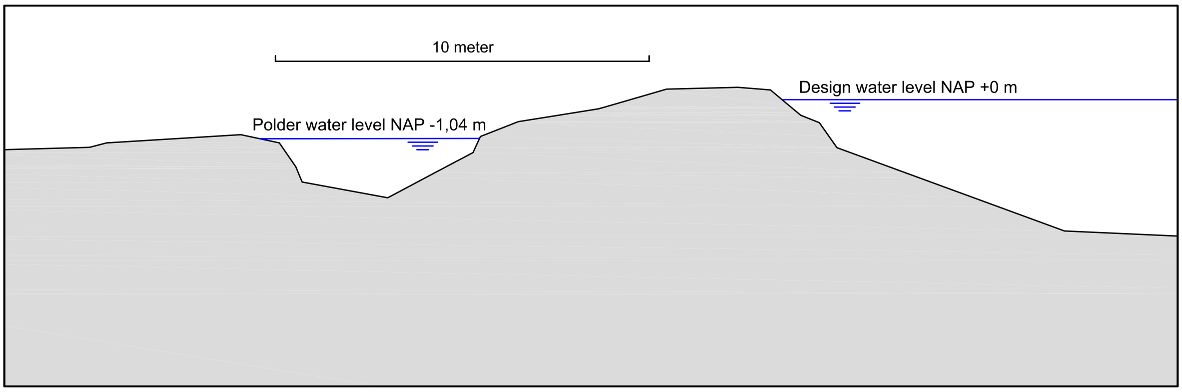

Figure 4-2: Representative geometry of dike section 2

4.2.4 Soil layer composition of the dike

The soil layer composition is assumed to be deterministic in this case study. The variety of the soil layers along the length of the dike section can be significant. The influence of this variety can be severe as the section is long (2,16 km). A representative layer composition for the considered cross-section has been determined in (Arcadis, 2011), based on the executed soil investigations. The soil layer composition consists of three clayey soils, two sandy soils and three peaty soils (see Figure 4-3).

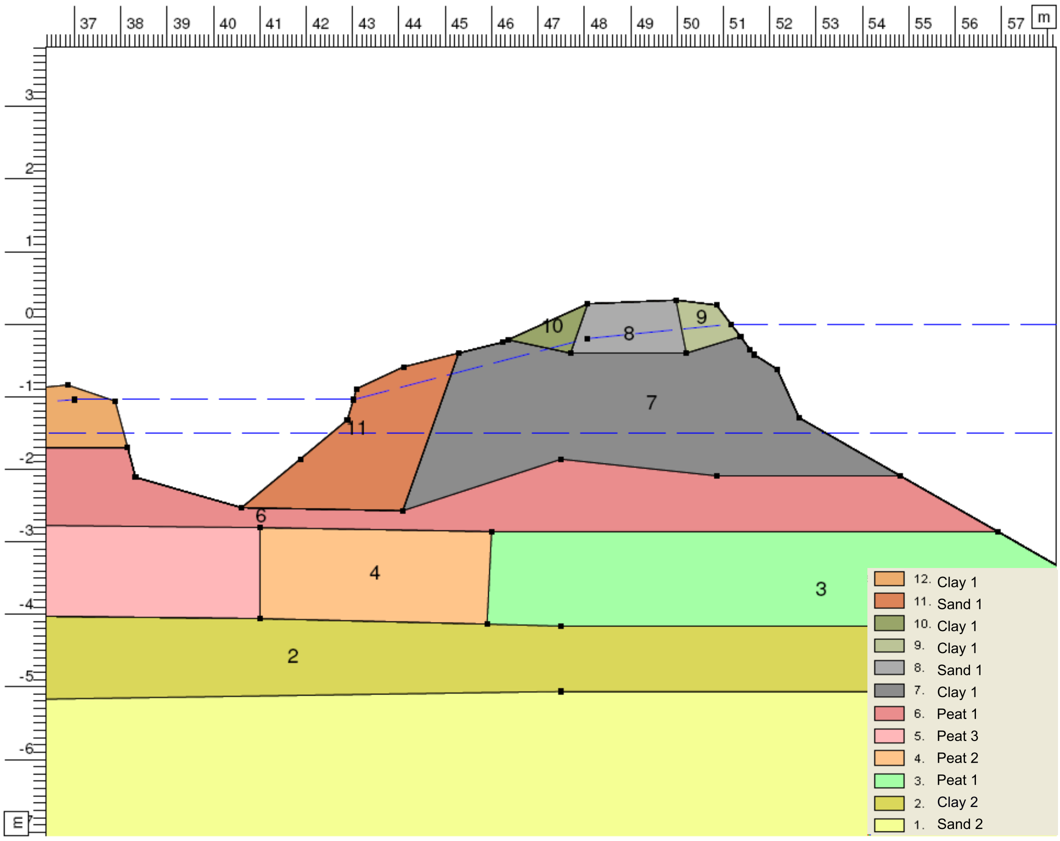

Figure 4-3: Representative soil layer composition of dike section 2 (Arcadis, 2011)

4.2.5 Phreatic surface and the water pressures

The phreatic surface under the design loading conditions is assumed to be random. The water pressures in the dike are modelled on the basis of two boundary conditions: the phreatic surface and the head in the aquifer, see Figure 4-4.

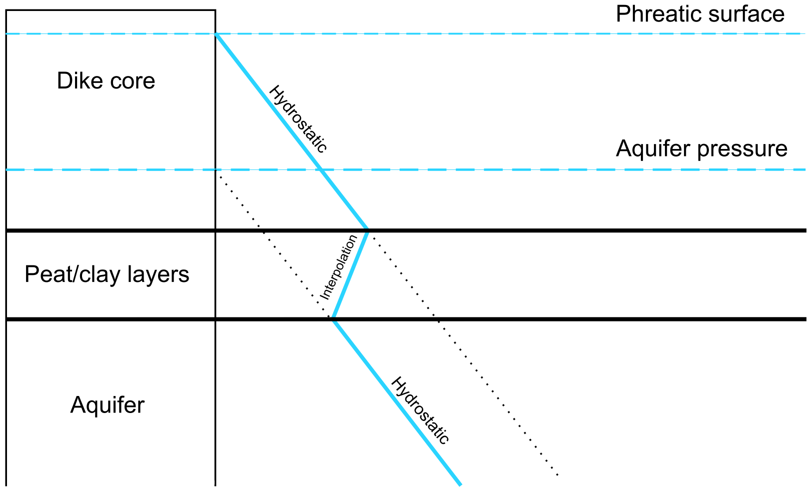

Figure 4-4: Modeled water pressure distribution through the soil layers

The position of the phreatic surface indicates the spatial upper boundary of the water pressure development in the dike body. A hydrostatic distribution is assumed over the depth of the dike body. The hydraulic head at the top of the aquifer is defined as well and assumed hydrostatically distributed over the depth. A linear interpolation is made between the water pressure at the bottom of the dike layer and the top of the aquifer. This modelling approach is analogue to the approach suggested in (TAW, 2004), see Appendix C. The random aspect of the phreatic surface requires specifications of the expected position of the surface and the corresponding standard deviation (both are inputs to the Bishop Probabilistic Random Field model).

The expected position of the phreatic surface under the external design water level is derived without the piezometer measurements and with the piezometer measurements. Respectively used for the a-priori and a-posteriori model computations.

Position of the phreatic surface without measurements (a-priori)

The expected position of the phreatic surface in dike section 2 without measurements is determined according to the technical guidelines, which are set up with past experience from engineering practice. The phreatic surface is derived in Appendix C. This derivation is conservative as it is meant for deterministic slope stability assessment.

Position of the phreatic surface with measurements (a-posteriori)

Piezometer measurements are used in the detailed deterministic macro stability assessment of dike section 2. A geotechnical expert determined the position of the phreatic surface in the dike under the design loading conditions by comparing the piezometer measurements with the corresponding measurements of the external water level and precipitation (Arcadis, 2011). The precipitation data were collected at a nearby weather station in Assendelft (2 km away). In the study, the response of the piezometer measurements on the external water level and precipitation is analysed. The expert concluded 80% response of the phreatic surface (in the middle of dike body) on the external water level and (almost) no response on the precipitation. This response relation was used to extrapolate the phreatic surface to the design water level of NAP +0 m; the data does not include measurements under the design loading conditions due to the limited monitoring time of 18 weeks. Furthermore, a linear interpolation has been made for the phreatic surface between the piezometer measuring points. An important aspect of this schematization is its conservative base. Although actual water pressure measurements are used for the schematization, the resulting phreatic surface is considered as a safe derivation including a certain safety margin (after all, a deterministic safety assessment of this dike has been performed). This schematization is affected by expert subjectivity, but this schematization is effective for the restricted monitoring data set (i.e. short monitoring period, few significant data points) when geohydrological expertise is available.

The results of these two schematization approaches are presented in Figure 4-5. The phreatic surface derived without the measurements, is situated higher than the phreatic surface derived with the measurements. The vertical difference between the levels varies from approximately 0,08 m at the polder side to 0,13 m at the canal side.

In this case study, the standard deviation of the phreatic surface σ(p) ranges from 0 to 0,5 m. From the engineering practice, the standard deviation of the phreatic surface is in the order of 0,5 m (Kanning, 2005). Another reference in (Kanning, 2005), considers a standard deviation of 0,12 m. This value has been obtained by an extensive amount of measurements.

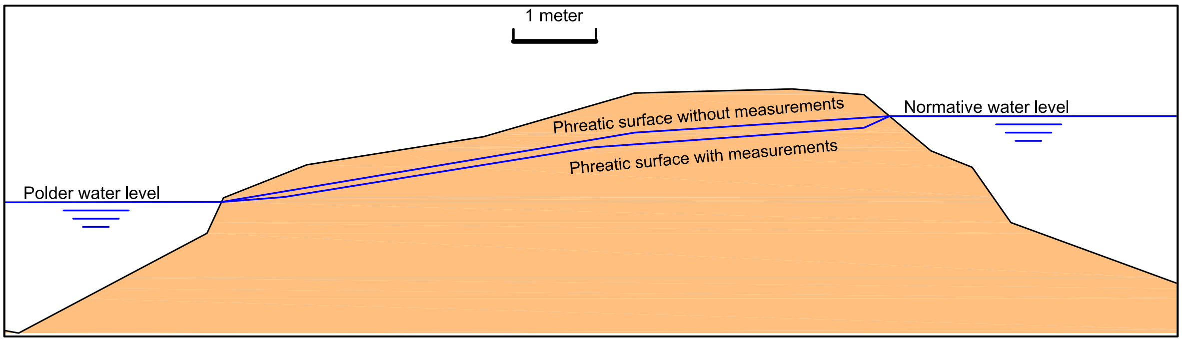

Figure 4-5: Expected position of phreatic surfaces with and without measurements in dike section 2

Furthermore, the position of the phreatic surface determines the type of volumetric weight of the soil; the soil below the phreatic surface has a wet volumetric weight γ_w and soil above the phreatic surface remains dry γ_d. This can be of special importance for the assessment of macro instability, as a wet soil has a higher weight and thereby influences the sliding forces. This effect is beneficial for the slope stability if the increased soil weight is on the passive side, but increased soil weight on the active side induces lower slope stability. This additional effect is elaborated in Appendix D for an elementary dike example. The volumetric weights are determined by laboratory tests and the average values have been used in this case study. The dry and wet volumetric weights (γ_d and γ_w) are schematized conservatively for cohesive soils (i.e. clay and peat), according to Dutch engineering practice. For macro instability of the inner slope, this holds that the dry volumetric weight is assumed equal to the wet volumetric weight. Sand layers are considered as permeable soils, in which water particles can drain instantaneously. Therefore, γ_d and γ_w are distinct for sand layers.

4.2.6 Shear strength

The shear strength varies from point to point within a soil layer, which is modelled. The shear strength is defined for each soil type by cohesion c and friction angle φ (μ(c), σ(c), μ(φ), σ(φ)). Laboratory tests on local soil samples are used to determine these parameters: trixial tests with 5% compression are used in this case. Increasing number of test samples (i.e. N_c and N_φ) reduces the epistemic uncertainty due to the increase in data samples. Yet, this can result in lower shear strength than was expected with fewer samples: the same principle applies to sensor monitoring. The number of performed test samples varies in this case study per soil type. A number of 10 to 15 tests are performed for the clay type, whereas no samples have been computed for sand. The strength of the sand is of minor importance, because the sand is located in the subsoil. Therefore, the sand characteristics are derived from (NEN6740, 2006) with a fictive number of test samples of 100. The strength of the peat in the dike has been determined with 18 test samples. But the peat in the hinterland is conducted from only 5 test samples.

The spatial variations of the shear strength within one soil layer are determined with a spatial correlation function which is specified by D_h, D_v, α_c and α_φ (see Appendix B). A conservative value of 0,75 is assumed for the variance factors α_c and α_φ, which represent overall weak and strong locations within the soil layers. Furthermore, a correlation coefficient ρ between the cohesion and friction angle of 0 is assumed; this value is conservative and common in Dutch engineering practice. The values of the horizontal and vertical correlation lengths depend on the extent of spatial shear strength fluctuations within a soil layer. A small correlation length represents fast fluctuations of the soil strength in space. The determination of the correlation lengths requires extensive amounts of soil information and analyses, which are not on hand in this case study. In the Netherlands, the horizontal correlation length ranges from 25 m to 150 m and the vertical correlation length from 0,1 m to 3 m (Rijkswaterstaat, 2009a). The horizontal correlation length is often ambiguous and should be taken conservatively (Rijkswaterstaat, 2009a). The uncertainty in correlation lengths is investigated in this case study in respect with the uncertainty in the water pressure schematization.

4.2.7 Model factor

The approximations of the stability model are included in a random model factor, with a mean μ(q) and standard deviation σ(q). The approximations include 3D sliding effects for slope failures and the interpretation method to determine soil strength parameters. In general, this model approximation has a significant effect on the failure probability. Suggested model factors to be used for the Bishop Probabilistic Random Field model are based on the type of laboratory test, see Table 4-3. The model factor for this case study is determined as mean μ(q)=1,0 and standard deviation σ(q)=0,075.

Table 4-3: Random model factors characteristics for the Bishop Probabilistic Random Field model (Rijkswaterstaat, 2009a)

Lab test	μ(q)	σ(q)
Triaxial-test 2% strain	0,91	0,075
Triaxial-test 5% strain	1,00	0,075
Cel-test	0,91	0,075

4.3 Case 0: Deterministic computations

A first insight into the case study model is gained by performing deterministic calculations. The safety factors for the two schematized phreatic surfaces are presented in Table 4-4. The reference situation with the a-posteriori phreatic surface, from engineering practice including sensor measurements, has a safety factor of 0,951. The conservative schematization of the phreatic surface results in a safety factor of 0,918. The piezometer measurements are therefore beneficial for the slope stability. The benefit due to the sensor monitoring for various situations is given in the last column in Table 4-4 and is derived following:

$$\text{Benefit} = \frac{SF_{\text{a-posteriori}} - SF_{\text{a-priori}}}{SF_{\text{a-priori}}}$$

Benefit	Relative benefit of the change in phreatic surface	[%]
$SF_{\text{a-posteriori}}$	Safety factor for the phreatic surface derived with sensor measurements	[-]
$SF_{\text{a-priori}}$	Safety factor for the phreatic surface without sensor measurements	[-]

The safety factor of the a-priori phreatic surface acts as the reference variable, as this represents the situation when no sensor monitoring has been applied yet.

Table 4-4: Deterministic slope stability safety results

Situation	$SF_{\text{a-posteriori}}$ [-]	$SF_{\text{a-priori}}$ [-]	Benefit [%]
Reference	0,951	0,918	3,6
Peat layer 6 is clay	0,996	0,962	3,5
Peat layer 5 is clay	1,039	1,000	3,9
Peat layer 4 is clay	1,167	1,127	3,5
Increased volumetric weight clay core	0,921	0,891	3,4
Clay layer 2 is sand	0,951	0,918	3,6

For all considered situations, the safety factor for the phreatic surface with the measurements is higher than the safety factor for the phreatic surface without the measurements. The average relative difference is 3,6%. The piezometer measurements are therefore beneficial for the slope stability.

The replacement of peat layer 4, 5, 6 with stronger clay layer leads in all cases to a stronger dike (with respect to the reference situation). This is expected, as the weak peat layers are placed in the critical slip circle zone (see Figure 4-6). Replacing the deeper clay layer 2 with sand does not influence the safety factors, as the critical slip circle does not cross this layer. If the volumetric weight of the dike clay soil is increased from 15,8 kN/m^3 to 17 kN/m^3 (derived from NEN6740, Table 1 (NEN6740, 2006) and it is plausible taken the laboratory tests into consideration), absolute safety decreases, as expected, since the active soil weight has increased.

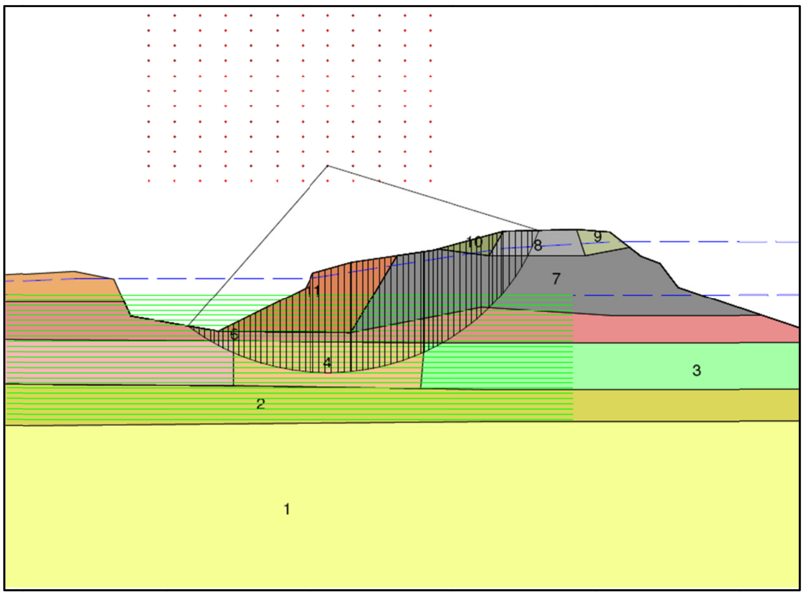

Figure 4-6: Computed critical slip circle for dike section 2

4.4 Original case study

The case study is performed for the original situation as described in section 4.2, with a section length of 2000 m. Computations have been made for the two distinct phreatic surfaces, varying the standard deviation of the phreatic surface σ(p) and assuming three values of the horizontal correlation length D_h: 50, 100 and 150 m. The input data and results can be found in Appendix E. The presented failure probability P_f and the corresponding reliability index β are representative for the whole dike section. These stability results are conditional failure probabilities, given the external design water level.

An erratic relation between σ(p) and the reliability index β is found for D_h=50 m (Figure E-1). Considering the phreatic surface derived with sensor measurements, in general, the β decreases as the σ(p) increases (as one would expect). An anomaly is observed for σ(p)=0,3 m, resulting in a higher β. The same anomaly is observed for the phreatic surface without the measurements. The cause of these anomalies lies in the value of the reliability index β: very low values are obtained approaching β=0. When D_h is 100 m or 150 m, the results are less erratic. Still anomalies are observed when the trend of β for increasing σ(p) reaches β=0. Apparently, the used model (the D-Geo Stability module Bishop Probabilistic Random Field, version 10.1) gives disturbed results for β=0 (i.e. slope failure probability P_f=0,5). When this limit is reached, the iterative process seeks to another minimum β, which is higher than 0. This is obtained by another critical slip circle with a different deterministic safety factor. The erratic relation diminishes as the horizontal correlation length D_h increases, see Figure 4-7.

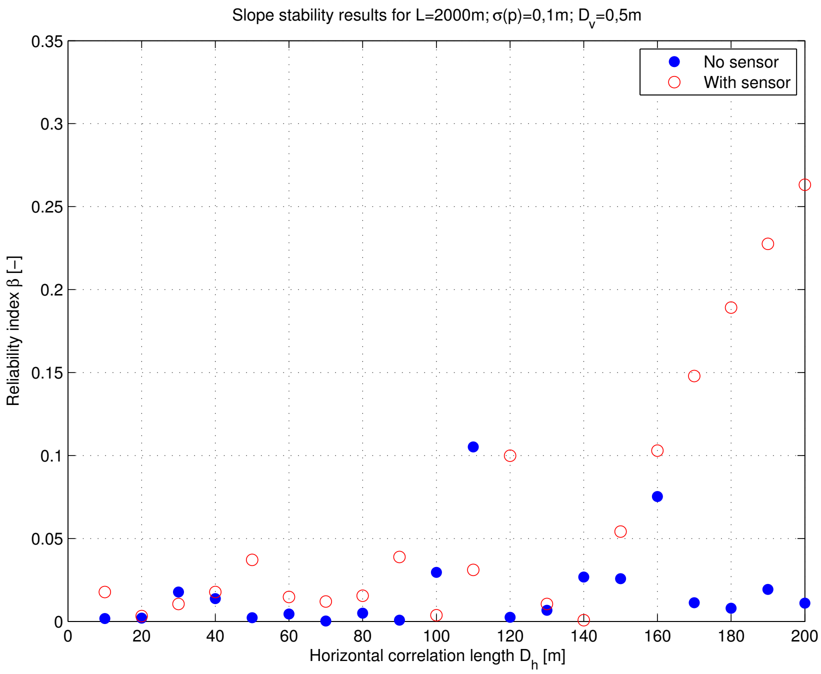

Figure 4-7: Influence of the horizontal correlation length D_h ranging from 10 to 200 m

In Figure 4-7, the phreatic surface without sensor measurements entails an erratic result for all D_h. The phreatic surface with the measurements yields an erratic behaviour for D_h<150 m. The reliability index β increases gradually for values of D_h≥150 m. The value of D_h compared to the section length of 2000 m is importance, which relates to the influence of D_h on the spatial variability. However, values of D_h larger than 150 m are not representative. Investigating multiple cases (Case 1, 2 and 3) with representative input parameters would result in reliability indices β of approximately 0 and failure probabilities P_f of approximately 0,5. The high slope failure probabilities are due to the relatively long section length compared to the relatively large soil strength variability (especially of the peat).

The results around $\beta=0$ are unexpected as the failure probability of the cross-section is affected when the probability of failure of the section (including length effect) approximates $\beta=0$. An explanation for the behavior is suggested to be found in (Deltares, 2012):

- Search routine for minimum β for the section failure probability
- Programmed simplification that $\beta>0$ in all cases; absolute values of β are taken (i.e. this simplification is valid for small failure probabilities as the program is designed for)
- Fault in the implementation of the length effect

Concluding, the stability assessment of dike section 2 (assuming the length of 2000 m) results in very low safety. With the current schematization and information regarding the soil strength and water pressures, this dike section is insufficiently safe for macro instability of the inner slope. Also, the objective to indicate the influence of sensor monitoring on the slope stability is affected. Therefore, the following measure is taken to avoid this problem:

> To be able to investigate the effectiveness of sensors in this case study, the encountered problems for a section length of 2000 m is not desired. Therefore, further computations are made for a section length of 500 m instead of 2000 m to avoid the problems.

4.5 Case 1: Variation of horizontal correlation length D_h

This case considers the probabilistic slope stability assessment of dike section 2 (with the length 500 m) if the horizontal correlation length D_h is uncertain. However in this case, there is no information on the horizontal correlation length D_h, meaning that the determination of D_h is considered ambiguous. Therefore, computations are made for three values of the horizontal correlation length D_h: 50, 100 and 150 m. These values cover the suggested range for D_h of 25-150 m (Rijkswaterstaat, 2009a). The information concerning the horizontal correlation length can be obtained with laboratory tests performed on borings or geophysical measurements. Two types of the phreatic surface are considered: a-posteriori schematization with the piezometer measurements and a-priori schematization without the piezometer measurements. The standard deviation of the phreatic surface $\sigma(p)$ is assumed to vary between 0 and 0,5 m. The vertical correlation length D_v is assumed equal to 0,5 m. Other inputs can be found in Appendix F, Table F-1. The results, in the form of reliability indices β, are presented in Figure 4-8, Figure 4-9 and Figure 4-10. Additionally, slope stabilities are derived for values of D_h ranging from 10 to 200 m and σ (p) equal to 0,1 m in Figure 4-11. The results are also summarized in Appendix F; Table F-2, Table F-3, Table F-4 and Table F-5.

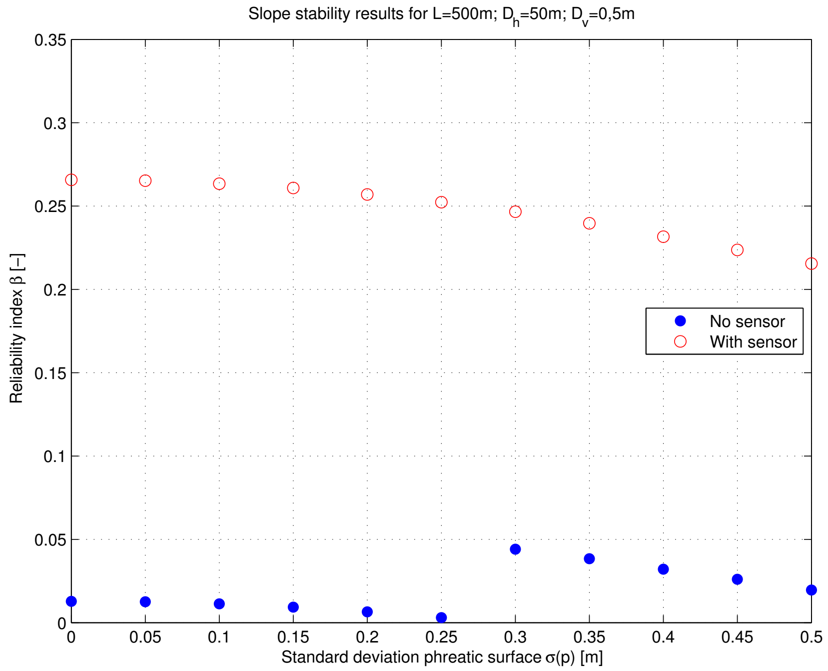

Figure 4-8: Comparison of the slope stability for varying σ(p) and D_h=50 m

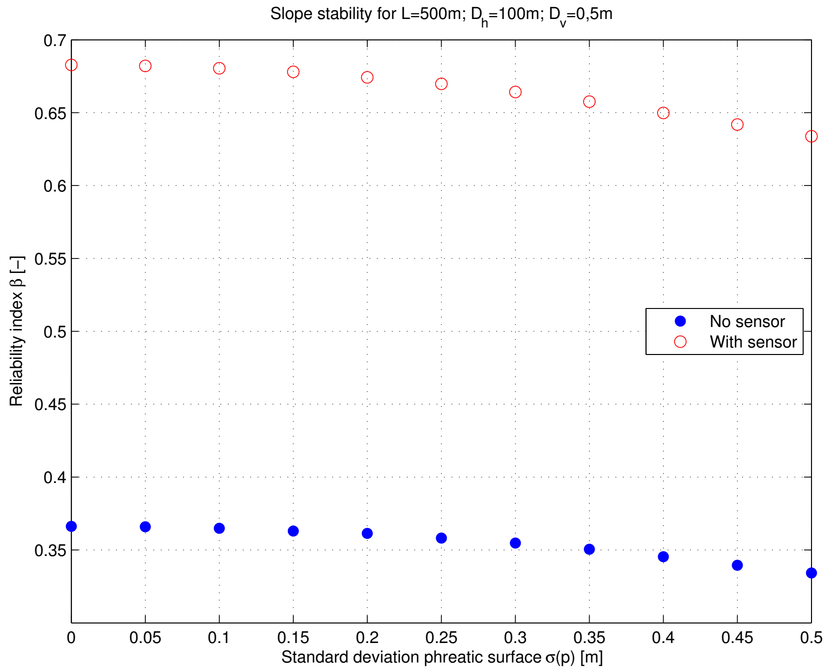

Figure 4-9: Comparison of the slope stability for varying σ(p) and D_h=100 m

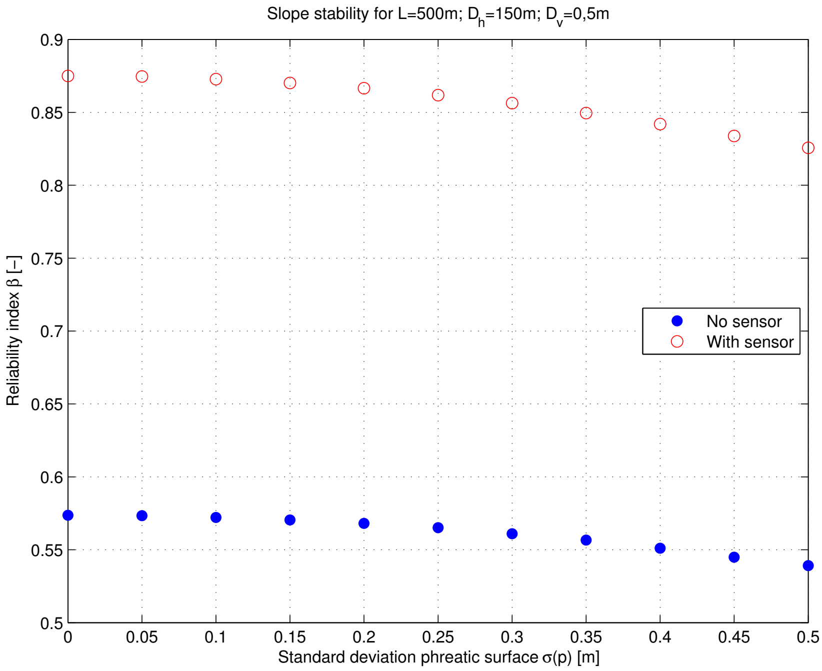

Figure 4-10: Comparison of the slope stability for varying σ(p) and D_h=150 m

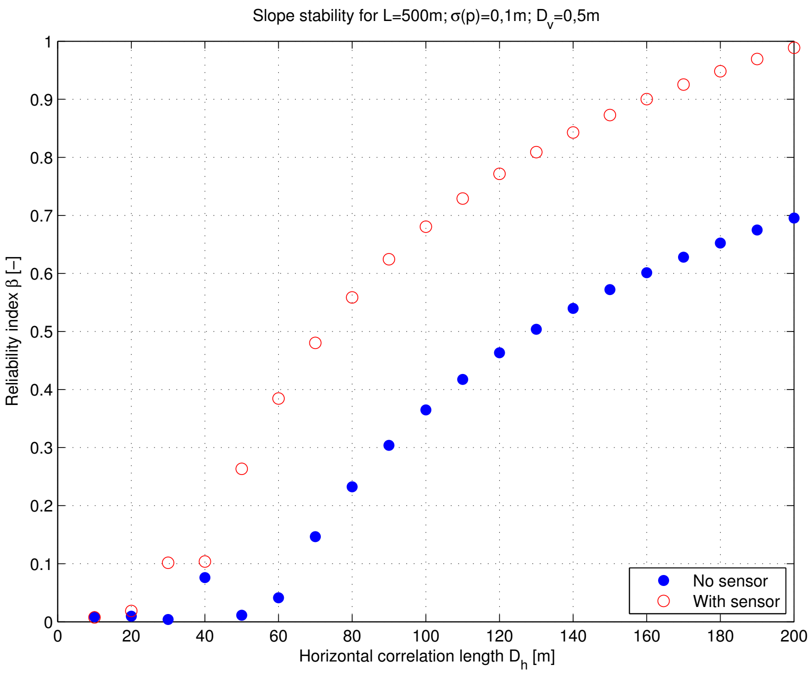

Figure 4-11: Slope stability results with horizontal correlation length D_h ranging from 10 to 200 m

The results for D_h<50 m in Figure 4-11 and the computations for the a-priori phreatic surface without measurements in Figure 4-8, still hold the model anomaly (i.e. β=0). Therefore, these results must be treated with care.

Under taken assumptions, the reliability index β decreases as the standard deviation of the phreatic surface increases. Contrary, the reliability index β increases as the horizontal correlation length D_h increases. In all computations, the reliability indices derived for the phreatic surface with the measurements are higher than the reliability indices derived for the phreatic surface without the measurements. Relative difference in the safety due to the piezometer measurements decreases in terms of reliability index β as the value of D_h increases.

These are mean relative differences between the reliability indices with and without the measurements (i.e. the increase due to the a-posteriori schematization compared to the a-priori schematization). This phenomenon is due to the increasing overall stability if D_h increases, whereas the mean relative difference between the a-priori and a-posteriori schematizations stays in the same order. It can also be observed that σ(p) does not have a significant influence on the relative differences. Furthermore, it can be observed that the position of the phreatic surface has a larger influence on the slope stability than the reduction of the standard deviation σ(p) from 0,5 m to 0 m. Changing D_h from 100 to 110 m, which is ambiguous in this case study, has a comparable influence on the stability as the change of σ(p) from 0,5 to 0 m, which might be obtained by water pressure monitoring (see Table 4-5). To obtain the same change in slope stability with adaptation of D_h, as it is achieved with the new position of the phreatic surface (i.e. with the measurements), D_h needs to increase from 100 to 160 m.

Table 4-5: Influence of uncertainty in D_h in β (and P_f) for D_v=0,5 m

Phreatic surface	Uncertainty in D_h	
	100→110 m	**150→160 m**
A-posteriori (with sensor)	0,049 (1,5E-2)	0,027 (7,4E-3)
A-priori (no sensor)	0,052 (1,9E-2)	0,029 (9,8E-3)

4.6 Case 2: Variation of the vertical correlation length D_v

In this case, the probabilistic slope stability assessment of dike section 2 is performed for uncertain vertical correlation length D_v. Therefore, two values of the vertical correlation length D_v are considered: 1,5 and 2,5 m. These values fall in the suggested range of D_v that is 0,1 to 3 m (Rijkswaterstaat, 2009a); the value of 0,5 m has been computed in Case 1. Two types of the phreatic surface are considered: a-posteriori schematization with the piezometer measurements and a-priori schematization without the piezometer measurements. The standard deviation of the phreatic surface σ(p) is assumed to vary between 0 and 0,5 m. The horizontal correlation length D_h is assumed equal to 100 m, such that the computed reliability indices β remain larger than 0. The input parameters are given in Appendix F; Table F-6. The results, in the form of reliability indices β, are presented in Figure 4-12 and Figure 4-13. Additionally, Figure 4-14 shows reliability indices derived for different values of D_v (from 0,2 to 3 m), σ(p) equal to 0,1 m and D_h equal to 150 m (the value of D_h=150 m is chosen to prevent erratic behaviour for large values of D_v). The results are also summarized in Appendix F; Table F-7, Table F-8 and Table F-9.

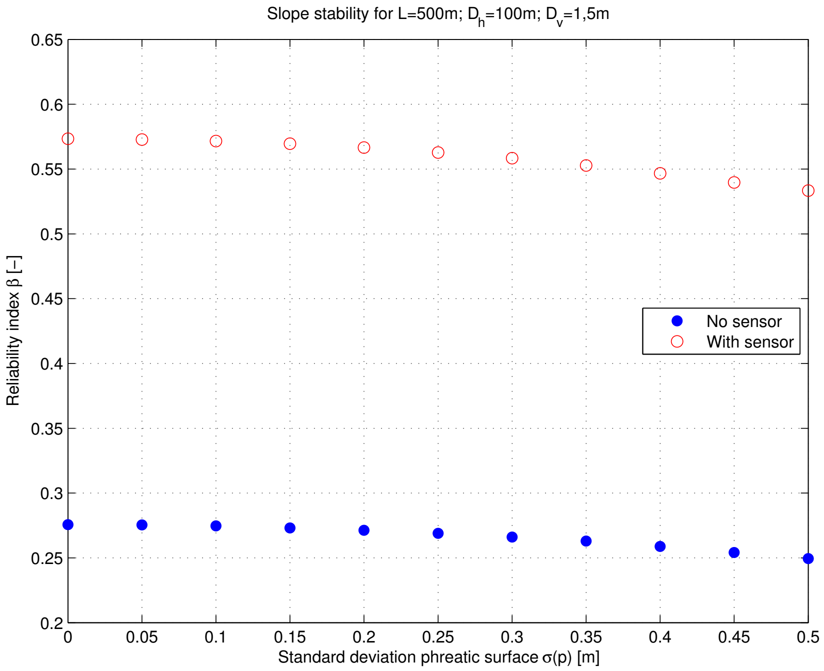

Figure 4-12: Comparison of the slope stability for D_v=1,5 m

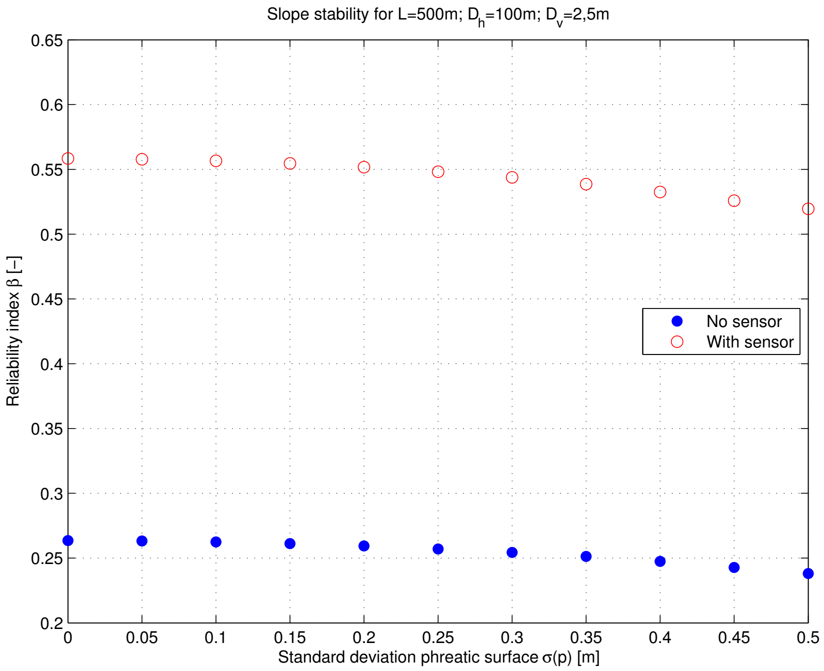

Figure 4-13: Comparison of the slope stability for D_v=2,5 m

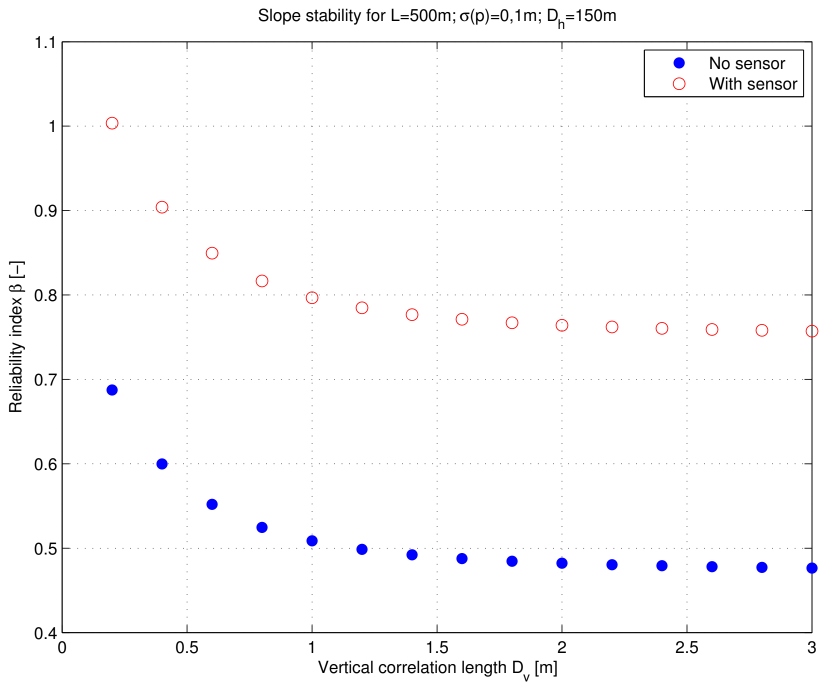

Figure 4-14: Slope stability with vertical correlation length D_v ranging from 0,2 to 3 m

The reliability index β decreases as the standard deviation of the phreatic surface or the vertical correlation length increases. In all computations, the reliability indices derived for the phreatic surface with the measurements are higher than the reliability indices derived for the phreatic surface without the measurements. Relative difference in the safety due to the piezometer measurements increases in terms of reliability index β as the value of D_v increases. These are mean relative differences between the reliability indices with and without the measurements. This phenomenon is due to the decreasing overall stability if D_v increases, whereas the mean relative difference between the a-priori and a-posteriori schematizations stays in the same order. It can also be observed that σ(p) does not have a significant influence on these differences. The behaviour in Figure 4-14 is opposite to one given in Figure 4-11. In general, the slope stability increases as D_v increases and the slope stability decreases as D_h increases. The influence of the vertical correlation length D_v is significant for small values, say D_v<1,5 m. Influence of the position of the phreatic surface on the slope stability is superior over the reduction of the standard deviation σ(p) from 0,5 m to 0 m. Adapting D_v from 1,4 m to 1,6 m or from 2,4 m to 2,6 m is ambiguous for the available information in this case and considered a plausible uncertainty aspect. It can be observed that this effect of uncertainty in D_v on the slope stability is negligible compared to the impact of sensor monitoring expressed in terms of the position of the phreatic surface and the standard deviation σ(p), see Table 4-6 However, the adaptation of D_v from 0,4 m to 0,6 m has significantly more influence. Thus, information regarding D_v is required, yet a detailed investigation of D_v has a limited influence if D_v is large compared to the relatively thin soil layers.

Table 4-6: Influence of uncertainty in D_v slope stability in β (and P_f) for D_h=100 m

Phreatic surface	**Uncertainty in D_v**		
	0,4→0,6 m	**1,4→1,6 m**	**2,4→2,6 m**
A-posteriori (with sensor)	0,055 (1,5E-2)	0,005 (1,6E-3)	0,001 (4,0E-4)
A-priori (no sensor)	0,048 (1,6E-2)	0,004 (1,6E-3)	0,001 (4,0E-4)

4.7 Case 3: Reduced soil strength deviation

In this section, the probabilistic slope stability assessment of dike section 2 is performed under the assumption of reduced soil strength deviation. The standard deviation of cohesion c and internal friction angle φ are reduced. This reduction could be attained by laboratory tests on additional test samples gathered from borings. Thus, an investment is made in order to reduce the epistemic uncertainty regarding the soil strength. Note that this additional research does not necessarily lead to increased soil strength. Analogue to the influence of water pressure monitoring, the influence of additional soil investigation can lead to a reduction of the assessed macro stability. However, the determined deviation in soil strength in this case study is relatively high. Therefore, it is assumed plausible that additional soil investigation leads to reduced soil strength deviation as considered in this case. The reduction of the soil strength deviation is done for those soil types with a large deviation and which are crossed by the critical slip circle (see Figure 4-6). Two types of the phreatic surface are considered: a-posteriori schematization with the piezometer measurements and a-priori schematization without the piezometer measurements. The standard deviation of the phreatic surface σ(p) is assumed to vary between 0 and 0,5 m. The vertical correlation length D_v is 0,5 m and the horizontal correlation length D_h is either 100 or 150 m. The input parameters for this case can be found in Appendix F: Table F-10. Additionally, Figure 4-17 shows reliability indices derived for different values of D_h (from 10 to 200 m), σ(p) equal to 0,1 m and D_v equal to 0,5 m. The results are also summarized in Appendix F: Table F-11, Table F-12 and Table F-13.

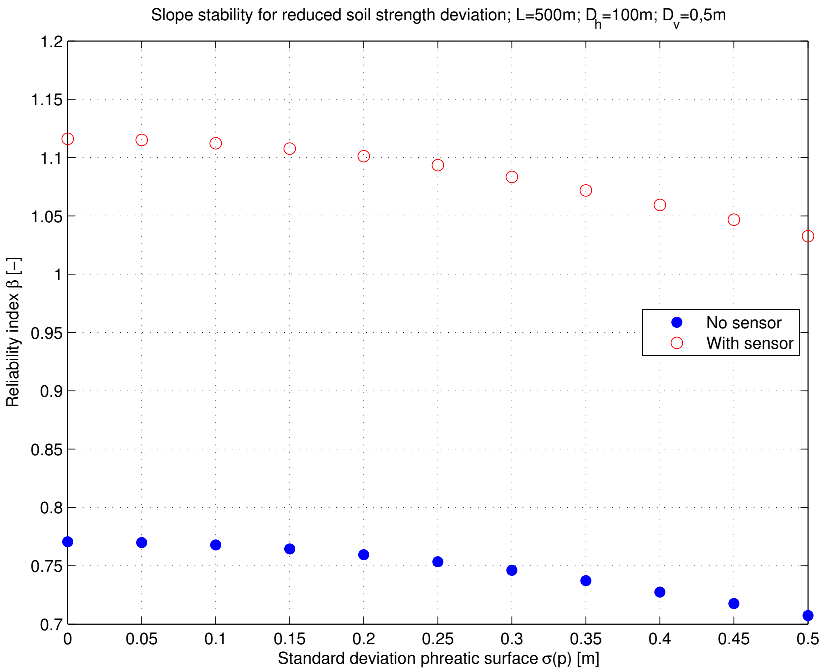

Figure 4-15: Comparison of the slope stability for reduced soil strength deviation and D_h=100 m

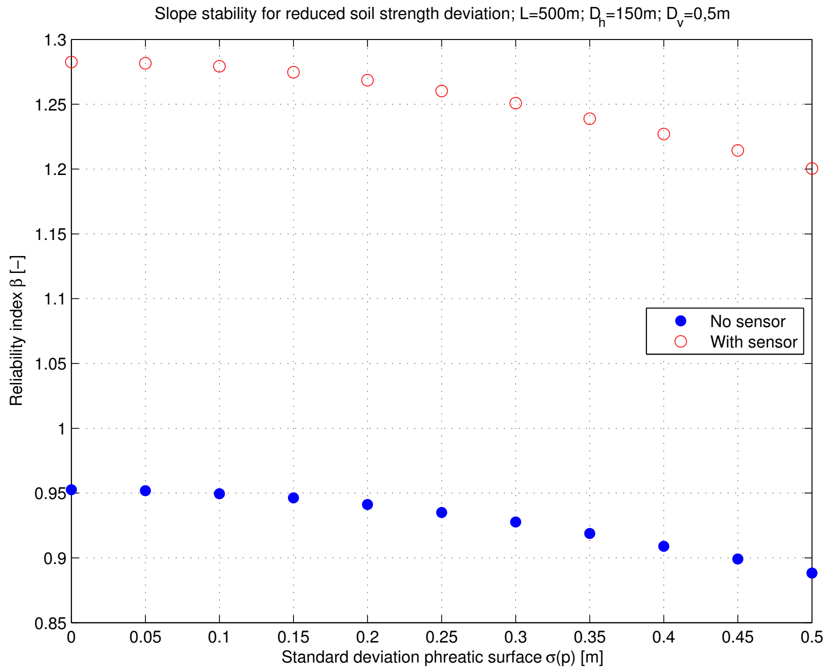

Figure 4-16: Comparison of the slope stability for reduced soil strength deviation and D_h=150 m

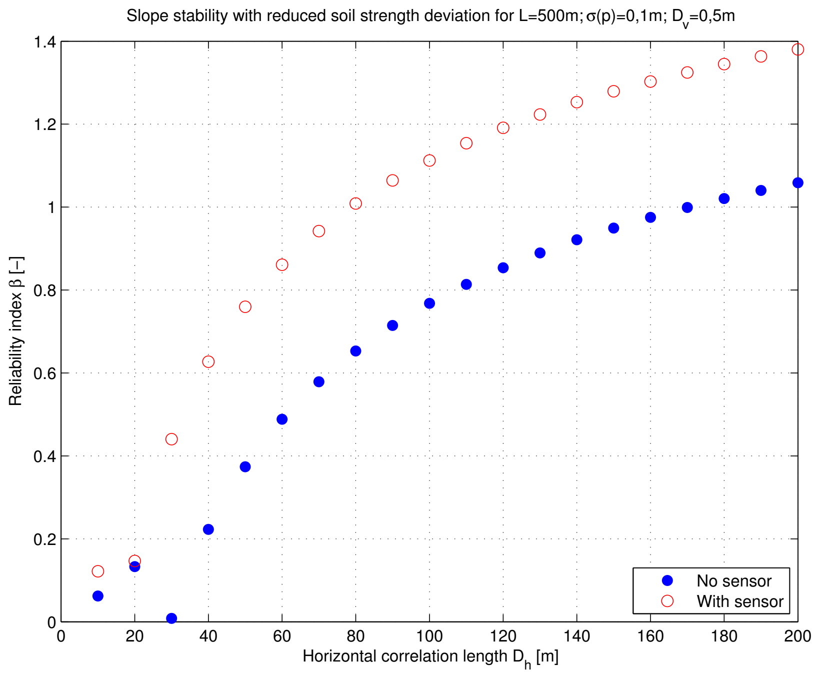

Figure 4-17: Slope stability with horizontal correlation length D_h ranging from 10 to 200 m for reduced soil strength deviation

The results for D_h<40 m still hold the anomaly (i.e. β=0). Therefore, these results must be treated with care.

Analogue to the results in case 1, the reliability index β decreases as the standard deviation of the phreatic surface increases and the reliability index β increases as the horizontal correlation length increases. In all computations, the reliability indices derived for the phreatic surface with the measurements are higher than the reliability indices derived for the phreatic surface without the measurements. Relative difference in the safety due to the piezometer measurements decreases in terms of reliability index β as the value of D_h increases. These are mean relative differences between the reliability indices with and without the measurements. This phenomenon is due to the increasing overall stability if D_h increases, whereas the mean relative difference between the a-priori and a-posteriori schematizations stays in the same order. However, these differences are lower than the differences for Case 1: hence, reduction of the soil strength deviation reduces the benefit of the piezometer measurements. Additionally, it can be observed that σ(p) does not have a significant influence on the differences. Influence of the position of the phreatic surface on the slope stability is superior over the influence of the standard deviation σ(p). The impact of the reduced soil strength deviation is superior over other uncertainties investigated. The impact reduces however as D_h increases, see Table 4-7.

Table 4-7: Influence of the reduction in soil strength deviation in β (and P_f) for different D_h

Phreatic surface	Stability difference due to reduced soil strength deviation		
	D_h=60 m	**D_h=100 m**	**D_h=150 m**
A-posteriori (with sensor)	0,48 (1,6E-1)	0,42 (1,1E-1)	0,40 (9,1E-2)
A-priori (no sensor)	0,45 (1,7E-1)	0,40 (1,3E-1)	0,37 (1,1E-1)

4.8 Case 4: Variation in soil layer composition

This case considers variations in the soil layer composition which are due to schematization uncertainties, because of information shortage regarding the soil. The reference soil layer composition has been schematized with the available information. Slope stability computations have been made for small adaptations in the soil layer, which cross the critical slip circle (see Figure 4-6). Three adaptations are distinguished: reduced width of peat layer 4 with 0,75 m, reduced thickness of peat layer 6 with 0,5 m and increased thickness of peat layer 6 with 0,5 m. The adaptations are visualized in Figure 4-18, Figure 4-19 and Figure 4-20. Peat layer 4 functions as a transitions layer between the compacted, stronger peat layer 3 under the dike and the weak peat layer 5 in the hinterland. Soil samples are available from peat layers 3 and 5, but not from peat layer 4. The width of peat layer 4 is thereby undefined and subject to uncertainty. The thickness of peat layer 6 is determined from boring analysis, yet the exact thickness can vary along the length of the dike. The thickness of peat layer 6 can have a significant influence on the slope stability, as the relatively weak peat crosses the critical slip circle.

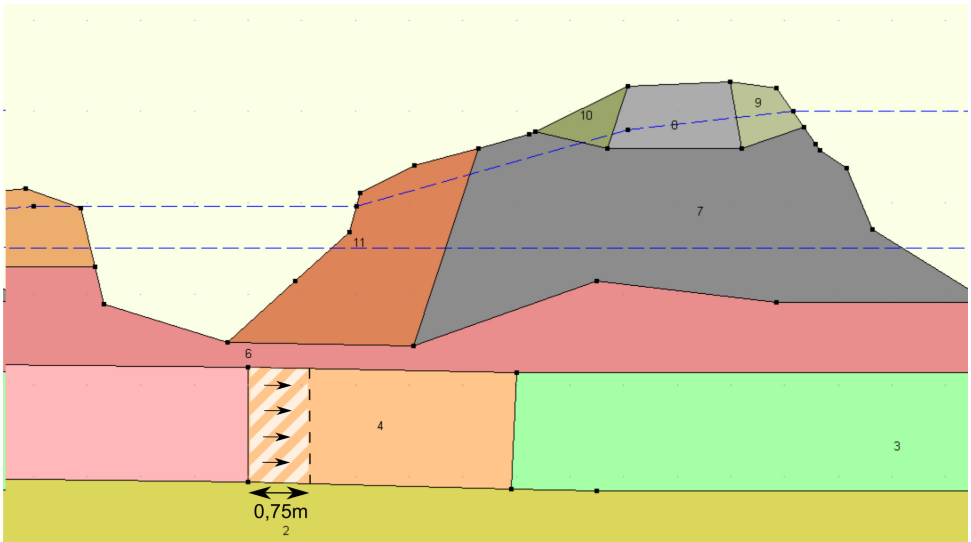

Figure 4-18: Adapted soil layer composition with reduced width peat layer 4 for case 4

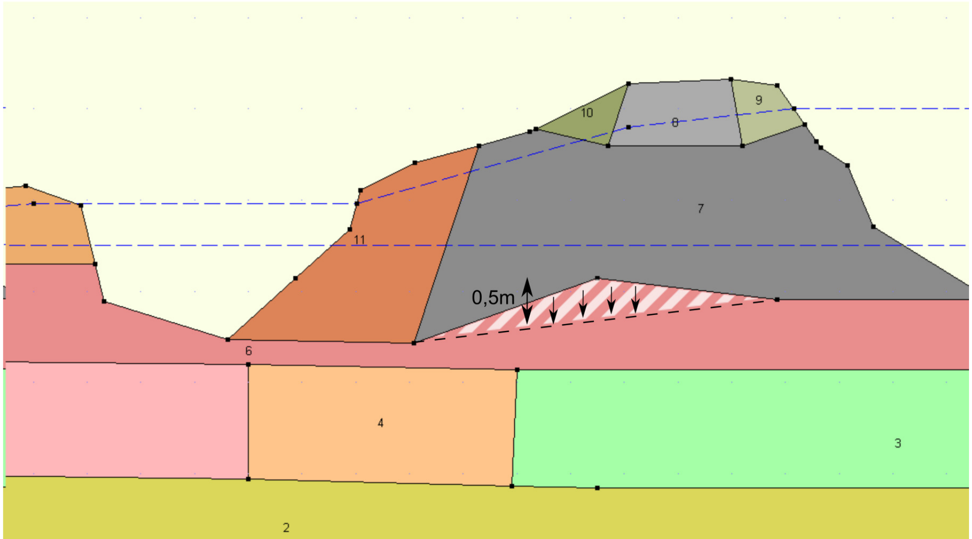

Figure 4-19: Adapted soil layer composition with reduced thickness of peat layer 6 for case 4

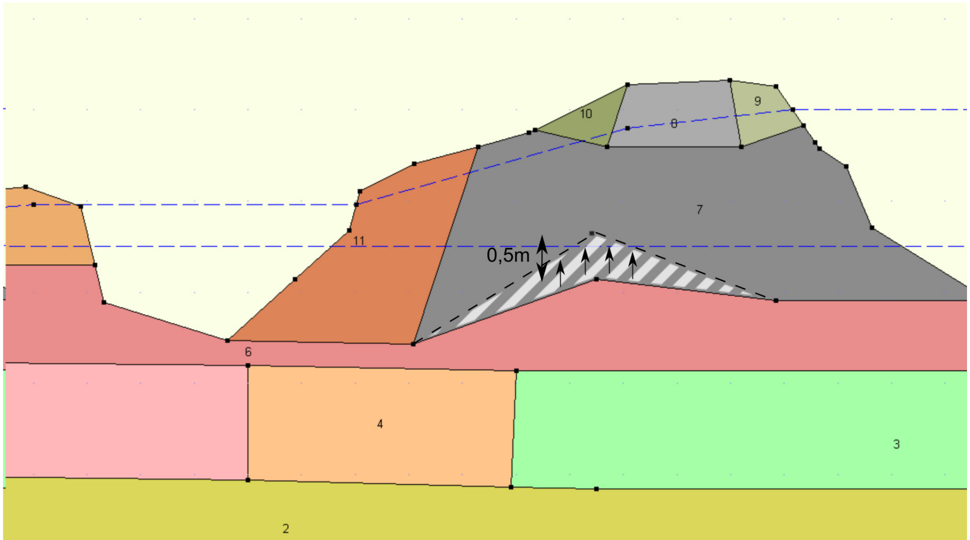

Figure 4-20: Adapted soil layer composition with increased thickness of peat layer 6 for case 4

The computations have been done for dike section 2 with D_h=100 m and D_v=0,5 m, see Table F-14 for all input parameters. The computation results for the variations in soil layer composition are presented in Table 4-8, besides the results for the reference composition. The difference in slope stability of the three computed soil layer composition adaptations referring the reference composition is given in Table 4-9. The results show that the reduced width of peat layer 4 significantly reduces the slope stability, forming a high risk. The thickness of peat layer 6 has demonstrably less influence on the slope stability. Increasing the thickness of peat layer 6 has a negligible impact and decreasing the thickness even increases the slope stability.

Table 4-8: Slope stability results for variation in soil layer composition with D_h=100 m and D_v=0,5 m

Phreatic surface	Reference composition	Reduced width layer 4	Reduced thickness layer 6	Increased thickness layer 6
	β (P_f)	**β (P_f)**	**β (P_f)**	**β (P_f)**
A-posteriori (with sensor)	0,66 (2,55E-01)	0,39 (3,47E-01)	0,73 (2,31E-01)	0,65 (2,57E-01)
A-priori (no sensor)	0,37 (3,57E-01)	0,12 (4,52E-01)	0,46 (3,21E-01)	0,35 (3,63E-01)

Table 4-9: Influence of the variation in soil layer composition in β (and P_f)

Phreatic surface	Reduced width layer 4	Reduced thickness layer 6	Increased thickness layer 6
	β (P_f)	**β (P_f)**	**β (P_f)**
A-posteriori (with sensor)	0,27 (9,2E-02)	-0,07 (-2,4E-02)	0,01 (2,0E-03)
A-priori (no sensor)	0,25 (9,5E-02)	-0,09 (-3,6E-02)	0,02 (3,0E-03)

4.9 Additional considerations

4.9.1 Evaluation measures

In this section, the results of Case 1, 2 and 3 are additionally considered using four evaluation measures:

- Spread: *Spread*
- Relative spread: $R_{\%}$
- Difference: Δ
- Relative difference: $\Delta R_{\%}$

Decreasing the value of σ(p) can theoretically be done by extensive water pressure monitoring. The considered situation is a hypothetical adaptation of σ(p)=0,5 m to σ(p)=0 m, due to sensor monitoring, for a given position of the phreatic surface μ(p). The difference in slope stability between σ(p)=0,5 m and σ(p)=0 m is determined as the spread: the spread in standard deviation of the phreatic surface. The spread of the slope stability under influence of σ(p) is thereby defined as:

$$\text{Spread} = \text{Stability}_{\sigma(p)=0,5} - \text{Stability}_{\sigma(p)=0}$$

Spread	Spread in terms of P_f or β due to varying σ(p)	[-]
$\text{Stability}_{\sigma(p)}$	Slope stability result for given standard deviation of the phreatic surface σ(p) in terms of P_f or β	[-]

To compare the results, the relative influence of the spread $R_{\%}$ is computed, both in terms of slope failure probability P and in terms of reliability index β. The relative influence of the spread $R_{\%}$ is defined as:

$$SR_{\%} = \frac{\text{Spread}}{\text{Stability}_{\text{reference}}}$$

$SR_{\%}$	Relative influence of the spread in terms of P_f or β	[-]
$\text{Stability}_{\text{reference}}$	Reference slope stability result for σ(p)=0,5 m in terms of P_f or β	[-]

The reference stability is taken for σ(p)=0,5 m because this considered is the starting point, i.e. large uncertainty referring the water pressure, before using water pressure monitoring to possibly reduce the uncertainty. The newly developed theoretical situation is the stability for σ(p)=0 m: maximum possible uncertainty reduction due to sensor monitoring.

One of the main interests of this chapter is to determine the effect of the piezometer measurements on the slope stability assessment of dike section 2. This effect is considered in terms of the reliability indices and slope failure probabilities, derived for the phreatic surface with and without the measurements (i.e. a-posteriori and a-priori). The standard deviation of interest for the phreatic surface without the measurements ranges from 0 to 0,1 m, because the safety margin is already accounted in the schematization of μ(p). The interesting standard deviations for the phreatic surface with the measurements range from 0,3 to 0,4 m. This is due to the subjective determination of the phreatic surface, leaving uncertainty. The effect of the measurements is computed as the difference Δ:

$$\Delta = \text{Stability}_{\text{a-priori}} - \text{Stability}_{\text{a-posteriori}}$$

Δ	Difference in terms of P_f or β due to adapted phreatic surface: respectively ΔP_f and $\Delta\beta$	[-]
$\text{Stability}_{\text{a-priori}}$	Slope stability result for the phreatic surface without the measurements and σ(p)=0,05 m in terms of P_f or β	[-]
$\text{Stability}_{\text{a-posteriori}}$	Slope stability result for the phreatic surface with the measurements and σ(p)=0,35 m in terms of P_f or β	[-]

The relative influence of the difference in phreatic surface, due to measurements, is derived as:

$$\Delta R_{\%} = \frac{\Delta}{\text{Stability}_{\text{a-priori}}}$$

$\Delta R_{\%}$	Relative influence of the difference Δ in terms of P_f or β	[-]
$\text{Stability}_{\text{a-priori}}$	Slope stability result for the a-priori phreatic surface without the measurements and σ(p)=0,05 m in terms of P_f or β	[-]

The reference situation consists of the stability result without the piezometer measurements, i.e. the a-priori situation.

4.9.2 Evaluation of cases 1, 2, 3

Values of the evaluation measures for the three case studies are summarized in the following tables and discussed in the next paragraphs.

Table 4-10: Spread of the slope stability in terms of β (and P_f) by adapting σ(p) from 0,5 m to 0 m

Case 1: variation of D_h				
D_h [m]	**A-posteriori (with sensors)**		**A-priori (without sensors)**	
	Spread β (P_f)	**SR% β (P_f)**	**Spread β (P_f)**	**SR% β (P_f)**
50	0,050 (2,0E-02)	23% (4,7%)	-[5]	-
100	0,049 (1,6E-02)	7,7% (6,0%)	0,032 (1,2E-02)	9,6% (3,3%)
150	0,049 (1,4E-02)	6,0% (6,7%)	0,035 (1,2E-02)	6,4% (4,0%)
Case 2: variation of D_v				
D_v [m]	**A-posteriori (with sensors)**		**A-priori (without sensors)**	
	Spread β (P_f)	**SR% β (P_f)**	**Spread β (P_f)**	**SR% β (P_f)**
0,5	0,049 (1,6E-02)	7,2% (6,4%)	0,032 (1,2E-02)	8,7% (3,4%)
1,5	0,040 (1,4E-02)	7,0% (4,8%)	0,026 (1,0E-02)	9,5% (2,6%)
2,5	0,039 (1,3E-02)	7,0% (4,6%)	0,025 (9,8E-03)	9,6% (2,5%)
Case 3: reduced soil strength deviation				
D_h [m]	**A-posteriori (with sensors)**		**A-priori (without sensors)**	
	Spread β (P_f)	**SR% β (P_f)**	**Spread β (P_f)**	**SR% β (P_f)**
100	0,083 (1,87E-2)	7,5% (14%)	0,063 (1,92E-2)	8,2% (8,7%)
150	0,082 (1,52E-2)	6,4% (15%)	0,064 (1,68E-2)	6,8% (9,9%)

[5] These values are affected by the boundary of β=0. Therefore, these results are not presented.

Table 4-11: Difference in slope stability in terms of β (and P_f) due to adapted phreatic surface

Case 1: variation of D_h				
D_h [m]	A-posteriori (with sensors)	A-priori (without sensors)	Difference Δβ (ΔP_f)	ΔR% β (P_f)
	β (P_f) for σ(p)=0,35	β (P_f) for σ(p)=0,05		
50	0,24 (4,1E-1)	-[6]	-	-
100	0,66 (2,6E-1)	0,37 (3,6E-1)	0,29 (1,0E-1)	80% (28%)
150	0,85 (2,0E-1)	0,57 (2,8E-1)	0,28 (8,6E-2)	48% (30%)
Case 2: variation of D_v				
D_v [m]	A-posteriori (with sensors)	A-priori (without sensors)	Difference Δβ (ΔP_f)	ΔR% β (P_f)
	β (P_f) for σ(p)=0,35	β (P_f) for σ(p)=0,05		
0,5	0,66 (2,6E-1)	0,37 (3,6E-1)	0,29 (1,0E-1)	80% (28%)
1,5	0,55 (2,9E-1)	0,28 (3,9E-1)	0,28 (1,0E-1)	101% (26%)
2,5	0,54 (3,0E-1)	0,26 (4,0E-1)	0,28 (1,0E-1)	105% (26%)
Case 3: reduced soil strength deviation				
D_h [m]	A-posteriori (with sensors)	A-priori (without sensors)	Difference Δβ (ΔP_f)	ΔR% β (P_f)
	β (P_f) for σ(p)=0,35	β (P_f) for σ(p)=0,05		
100	1,07 (1,4E-1)	0,77 (2,2E-1)	0,30 (7,9E-2)	39% (36%)
150	1,24 (1,1E-1)	0,95 (1,7E-1)	0,29 (6,3E-2)	30% (37%)

Case 1: variation of D_h

The spread of the slope stability in terms of failure probability P_f decreases as the horizontal correlation length D_h increases. The rate of decrease is lower for the a-priori phreatic surface without the measurements, than with measurements. In terms of reliability index β, the spread remains approximately the same for different D_h and phreatic surfaces. Furthermore, the relative spread $SR_{\%}$ increases as D_h increases in terms of P_f. However, $SR_{\%}$ decreases for increasing D_h in terms of β. This is due to the effect that the absolute slope stability in terms of P_f and β are opposite.

The difference Δ is positive for all three values of D_h, i.e. the measurements lead to a safer assessment of the dike. This benefit depends on the chosen value for D_h and the benefit decreases as D_h increases in terms of ΔP_f, but the relative influence $\Delta R_{\%}$ increases.

Case 2: variaton of D_v

The spread in terms of P_f and β decreases as D_v increases. The spread is smaller for the a-priori phreatic surface without the measurements than for the phreatic surface with the measurements. Furthermore, the relative spread $SR_{\%}$ decreases as D_v increases in terms of P_f. The relative spread $SR_{\%}$ in terms of β remains in the same order. Concluding, decreasing the standard deviation of the phreatic surface σ(p) leads to a reduction of the failure probability P_f (i.e. increase in β). The magnitude of this reduction decreases as the vertical correlation length D_v increases.

The application of the measurements leads to increased slope stability for all considered D_v. The difference Δ, in terms of P_f, remains approximately equal.

[6] These values are affected by the boundary of β=0. Therefore, these results are not presented.

Case 3: reduced soil strength deviation

The reduction of σ(p) from 0,5 to 0 m leads to a larger difference in slope stability, than in the case with a larger soil strength deviation (see Case 1). The relative spread $SR_{\%}$ in terms of P_f is also larger.

Comparing with Case 1, the gained benefit from using the measurements (ΔR%) is now reduced in terms of reliability index β. Performing successful soil investigation leads to increased slope stability. However, the impact of the sensor monitoring (i.e. the measurements) is thereby reduced.

4.10 Conclusions

The water pressure monitoring of the phreatic surface results in a beneficial adaptation of the slope failure assessment, for each considered situation in this case study. This benefit is gained by an adaptation of the position of the phreatic surface μ(p). Reducing the standard deviation σ(p) has a minor effect on the slope stability. The relative influence of the sensor monitoring depends on the other uncertainty aspects. The absolute slope failure probability reduces, as the uncertainty of other model aspects is reduced. Thereby, the relative effect of sensor monitoring increases as other uncertainties are reduced. The impact will differ for each case study. The relative influence of uncertainties in the considered case study is arranged as follows:

1. Reduced soil strength deviation
2. Mean value of phreatic surface μ(p) (obtained by a-posteriori interpretation of sensor data)
3. Horizontal correlation length D_h
4. Standard deviation of the phreatic surface σ(p) (reduction from 0,5 m to 0,0 m)
5. Vertical correlation length D_v

In which the reduction of the soil strength deviation has the largest impact and adapting the vertical correlation length D_v has the least impact. Moreover, schematization uncertainties regarding the soil layer composition have a significant effect on the safety assessment: the uncertainty referring to the width of peat layer 4 is in the same order of the uncertainty in D_h. Overall, the uncertainty regarding the soil strength and soil layer composition dominate in this case study. Therefore, performing additional soil investigation would have been recommended in this case over performing water pressure monitoring.

The following conclusions can be made about the adaptations which are influenced by additional information:

- The relative impact of reduced soil strength deviation increases as D_h rises, σ(p) lowers and μ(p) lowers
- The impact of lowered μ(p) increases as D_h rises and D_v lowers
- The impact of reducing σ(p) increases as D_h rises, D_v lowers and μ(p) lowers

In order to decide on applying water pressure monitoring, with the purpose of updating the period safety assessment, uncertainties concerning all modeling aspects needs to be taken into account. Other investigation options affecting these modeling aspects need to be considered. Feasible adaptations on the schematization due to these additional investigations are computed. A decision on performing which investigation can be made by estimating the cost-effectiveness of the investigations on beforehand.

Assumptions have been made in this case study regarding the following aspects:

- **Geometry**
  Uncertainty regarding the geometry is not considered. The starting point of any period safety assessment, in particular an advanced assessment as considered, must be an up to date and detailed information of the geometry.
- **Model approximation**
  The model approximation can affect the conclusions, as a single slope stability model has been used. The model factor is assumed to be a constant stochastic model variable. However, determining a less conservative model factor is possible when motivated. This principle is applied in the *Veiligheid Nederland in Kaart* studies (VNK2, 2011). Important condition is that all relevant stakeholders agree on the decision.
- **Volumetric weight**
  The volumetric weight has been taken as a conservative schematization aspect, according to Dutch engineering practice. The potential influence on the slope stability referring the uncertainty in volumetric weight is not considered exclusively.
- **Traffic loads**
  The traffic loads are not taken into account in this case study. But traffic loads can be of substantial influence at smaller, regional dikes for the dike stability. Especially during an operational situation, trucks are likely pass which transport sand bags to reinforce another dike. The additional weight can act as active and induce slope instability. Also horizontal forces, which cannot be implemented in the used stability model, may be present in corners. However, a regular measure during crisis situations is to close of critical dike roads to ensure minimum loading at the dike crests.

5 Cost-benefit analysis for the periodic safety assessment

A cost-benefit model is treated in this chapter to determine the cost-effectiveness of sensor monitoring in the context of the periodic safety assessment. Paragraph 5.1 starts with an introduction in which the status of the model is considered. The model fundamentals are presented in paragraph 5.2, ending with a simplified example to illustrate the model principle. To give further insight into the model, case studies have been elaborated for dike-ring 48 (paragraph 5.3) and dike-ring 14 (paragraph 5.4). Final conclusions are given in paragraph 5.5.

5.1 Introduction

This chapter considers a cost-benefit model which has been set up to get insight into the cost-effectiveness of sensor monitoring for the application in periodic safety assessment. The presented model is a suggested approach to elaborate the cost-effectiveness of sensor monitoring. The main objective of the model is to give insight on how to define benefits from sensor monitoring and which relevant aspects are involved to determine the benefits and costs. Solely the benefit in the context of flood risk and permanent dike reinforcements for the periodic safety assessment are considered. Benefits in the context of early warning in operational situations are evaluated separately in chapter 6. Therefore, the presented model only considers the benefit of permanent dike reinforcements and discards the use of information for short-term handling (i.e. early warning). The basic principles on how to implement sensor monitoring information in the flood safety assessment have been treated in paragraph 3.2. Where paragraph 3.3 and 3.6 amplify the use of significant hydraulic loads for the flood safety assessment, which is essential in the presented model. Also, the unforeseen risks as discussed in paragraph 3.5 are considered in the presented cost-benefit model, see paragraph 5.2.4.

This model has the objective to evaluate the cost-effectiveness of sensor monitoring prior to sensor installation. By giving insight into the costs and benefits, the model aims to support the decision on installing a sensor monitoring system by economic considerations. In a broader context, the presented cost-benefit model also contributes to the decision on investing in dike investigations other than sensor monitoring: for example additional borings, CPT's or geophysical measurements. The base cost-benefit approach is derived from the project *Waterveiligheid 21^{e} eeuw* (English: *Water Safety in 21st century*) to determine the economic optimal flooding probability, see textbox *Project Waterveiligheid 21^{e} eeuw (WV21)*. This chapter suggests an extension of the base WV21 model to model the effect of sensor monitoring. Calculations are performed with OptimaliseRing version 2.3.1 (Deltares, 2011d), which uses a time span of 300 years to determine the economic optimal flooding probability.

It should be emphasized that the calculated benefit-cost ratios have limited value in absolute terms, because the defined variables for defining the benefit have not been verified.

Project Waterveiligheid 21e eeuw (WV21)

The WV21 project conducts the updating of the Dutch safety standards for primary flood defences, based on the economic optimal flooding probability (Deltares, 2011c). The cost-benefit analysis considers the costs and benefits of preventing a large-scale flood. The WV21 project investigates whether the current flood safety standards fulfill the required protection for the economic value and potential casualties behind the flood defences. The first Delta Committee determined the current safety standards after the North Sea flood in 1953. The consequences of a flood have been increased over time due to social and economic developments. Measures can be taken to reduce the flood risk. The cost-benefit analysis relies on the general principle of investment costs in dike reinforcements (modeled by considering dike heightening), which reduces the flood risk as the flooding probability decreases. The optimal dike investment is the minimum total costs, consisting of the dike investment costs and expected flood damage: further dike investments costs exceed the reduction of the flood damage. Figure 5-1 illustrates the general cost-benefit principle of the first Delta Committee.

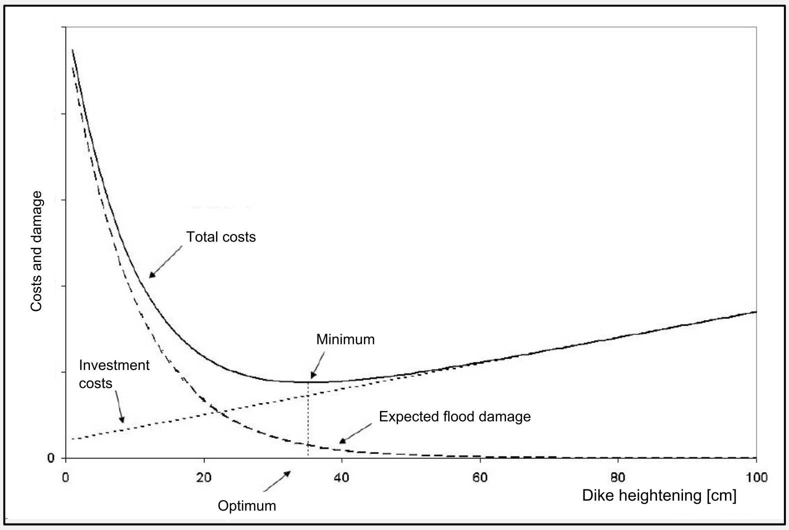

Figure 5-1: General principle of the cost-benefit analysis (Deltares, 2011c)

5.2 Model setup

5.2.1 Definition of the benefit-cost ratio

The application of sensor monitoring is considered in the cost-benefit model by a benefit-cost ratio. The benefit is formed by an updated safety assessment regarding water pressure uncertainties for macro stability. Costs are made due to the investment in water pressure monitoring. The expected benefit-cost ratio for applying sensor monitoring in the periodic safety assessment is defined as:

$$\varepsilon_p = \frac{\text{benefit}}{\text{cost}} = \frac{\mathrm{E(costs)}_{\text{a-priori}} - \mathrm{E(costs)}_{\text{a-posteriori}}}{\mathrm{C}_{\text{sensor}}}$$

ε_p	Benefit-cost ratio for the periodic safety assessment: ratio of benefits and costs	[-]
$\mathrm{E(costs)}_{\text{a-priori}}$	Expected costs for the initial situation, i.e. no sensors applied, over a given time period	[€]
$\mathrm{E(costs)}_{\text{a-posteriori}}$	Expected costs for the situation with sensors applied, over a given time period	[€]
$\mathrm{C}_{\text{sensor}}$	Costs made due to the application of sensor monitoring	[€]

The use of sensor monitoring is cost-effective if the benefit-cost ratio $\varepsilon_p>1$: the benefits exceed the costs. Additional costs are made by applying sensor monitoring, which is expected to return in a benefit over the given time period. The benefit consists of the difference between expected costs of the optimal investment strategy for dike reinforcements with and without sensor monitoring. The optimal investment strategies are determined with OptimaliseRing (Deltares, 2011d), by computing numerous investment strategies: the investment strategy with the minimum expected discounted costs over the considered period T is defined as the optimal investment strategy. The expected costs for the initial situation without sensor monitoring, is determined by:

$$\mathrm{E(costs)}_{\text{a-priori}} = \mathrm{E(damage)} + \mathrm{I_i(strengthening)} =$$

$$\sum_{t=0}^{T} \frac{P(t)\cdot V(t)}{(1+\delta)^t} + \sum_i \frac{I_i(\text{strengthening})}{(1+\delta)^{t_i}}$$

$\mathrm{E(costs)}_{\text{a-priori}}$	A-priori expected costs for optimal investment strategy, without sensor monitoring	[€]
E(damage)	Discounted expected flood damage	[€]
I_i(strengthening)	Discounted investment costs made for dike strengthenings in year i	[€]
P(t)	Probability of flooding in year t, without sensors	[1/year]
V(t)	Potential damage due to a flood in year t	[€]
δ	Discount rate	[%/year]
t_i	Year t in which investment I_i(strengthening) is made	[year]

The expected costs for the a-posteriori situation without sensor monitoring, is determined by:

$$\mathrm{E(costs)}_{\text{a-posteriori}} = \mathrm{E(damage)} + \mathrm{I_j(strengthening)} =$$

$$\sum_{t=0}^{T} \frac{P''(t)\cdot V(t)}{(1+\delta)^t} + \sum_j \frac{I_j(\text{strengthening})}{(1+\delta)^{t_j}}$$

$\mathrm{E(costs)}_{\text{a-posteriori}}$	A-posteriori expected costs for optimal investment strategy, with sensor monitoring	[€]
E(damage)	Discounted expected flood damage	[€]
I_j(strengthening)	Discounted investment costs made for dike strengthenings in year j	[€]
P''(t)	Probability of flooding in year t, with sensor monitoring	[1/year]
V(t)	Potential damage due to a flood in year t	[€]
δ	Discount rate	[%/year]
t_j	Year t in which investment I_j(strengthening) is made	[year]

The optimal investment strategy is determined in OptimaliseRing by the discounted minimum of the long-term expected flood damage (i.e. flood risk) and total costs of investments in dike reinforcements, over a period of T years: defined as E(costs). This is analogue to the economic approach in WV21 (Deltares, 2011c). The economic optimal investment strategy is determined with OptimaliseRing (Deltares, 2011d).

The discounted expected flood damage E(damage) is the net present value of the summed potential flood damage per year over the considered time period T. The discounted investment costs I(strengthening) is the net present value of the summed investments I over the time period T. The magnitude and timing of the reinforcements determine the net present value. The flooding probability P(t) changes over time due expected climate changes: future changes of the global climate are expected to cause water level rise and subsidence of the subsoil lowers the dikes. Therefore, the probability of flooding increases over time which is modeled in OptimaliseRing as an exponential function. Moreover, P(t) is affected by the investments in dike strengthening at the specific time i or j: a dike reinforcement decreases the flooding probability (i.e. the strength of the dike has increased for the same loading conditions). The application of sensor monitoring affects the assessment of P(t) over time, due to additional monitoring information. It should be emphasized that sensor monitoring only affects the determination of the probability of flooding P(t), due to increasing knowledge (see chapter 4) and the real flood risk remains equal in both situations. Nota bene, one could even argue whether the installation of in situ sensors reduces the real dike strength and thus increases the real flood risk. This model assumes that the sensors are installed such that the strength of the dike is not affected. Also, the potential flood damage V(t) changes over time: the economic consequences of a flood increase due to economic growth. Appendix G gives background information on the modeled development of P(t) and V(t) in the cost-benefit model.

5.2.2 Modeling the effect of sensor monitoring

Water pressure monitoring affects the assessment of the a-priori flooding probability. The a-posteriori flooding probability is modeled on the a-priori flooding probability, the impact of the additional information on the flooding probability assessment and the return rate of a certain loading event. The a-posteriori probability of flooding is modeled as:

$$P''(t) = P(t)(1-R)^{\lambda t}$$

P''(t)	A-posteriori probability of flooding in year t, with sensor monitoring	[1/year]
P(t)	A-priori probability of flooding in year t, without sensor monitoring	[1/year]
R	Reduction rate, due to sensor monitoring	[-]
λ	Frequency of occurrence of a valuable loading event	[1/year]

The a-posteriori flooding probability P''(t) is related to the a-priori flooding probability P(t) since the base information remains the same in both situations, just additional information has been added. P(t) is equal to the expected development of the flooding probability over time without sensor information. The reduction rate R represents the amount of reduction which is expected to be attained from a given loading event, with frequency of occurrence λ, due to the installed monitoring system. This formula is derived with a compound Poisson process, see the corresponding text box *Compound Poisson process*.

A value of R=0 represents no influence of the obtained monitoring information from a loading event: P''(t) equals P(t). The situation that the obtained monitoring information from a loading event reduces the flooding probability is represented for positive values of R: 0<R<1. Where R=1 represents the fictive situation that there is no probability of flooding. Contrary, negative values of R represent an increase in the flooding probability due to the monitoring information of a loading event or unforeseen risks: R<0.

Compound Poisson process

The effect of sensor monitoring on the flooding probability is determined with the a-priori probability of flooding and a compound Poisson process. A Poisson process is a stochastic process to count the number of events (i.e. relevant high water events) with average occurrence frequency λ (i.e. the time between events is described with the exponential distribution with parameter λ) and the increments ("jump sizes") of the events is also random (i.e. impact of the sensor information from the high water event on the flood safety). This process is illustrated in Figure 5-2.

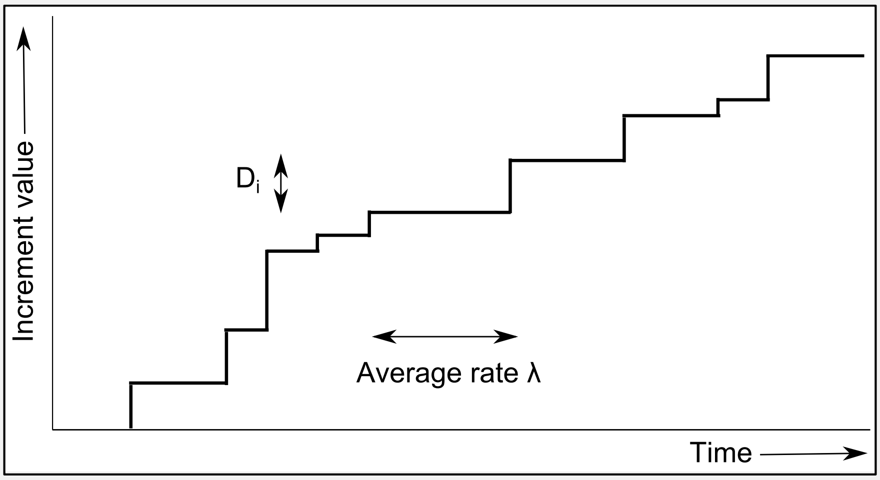

Figure 5-2: General principle of a compound Poisson process

Here, the a-posteriori annual flooding probability P''(t) is written as:

$$P''(t) = P(t) \cdot e^{X(t)}$$

For t=0,1,2,… and where P(t) is the a-priori annual flooding probability and X(t) a compound Poisson process, such that:

$$X(t) = \sum_{i=1}^{N(t)} D_i$$

For t≥0 and where N(t) is a Poisson process (i.e. the counting function) with the rate λ>0 and {D_i, i=1,2,…} are independent random variables. The Poisson process describes the random occurrence of a relevant high water event and D_i describes the random changes of the flood safety due to the sensor information obtained during a relevant high water event. Because the impact of the sensor information remains unknown until the sensor information is obtained, the expected value of this process is taken for the period of t years: $\lambda E(D_i)t$. In which $E(D_i)$ is the expected value of the random variables D_i. In this research, the a-posteriori annual flooding probability is approximated with the lower boundary of its expected value, following from the Jensen's inequality for a convex exponential function.

$$E(P''(t)) = E\left(P(t)e^{X(t)}\right) = P(t)E\left(e^{X(t)}\right) \geq P(t)e^{E(X(t))} = P(t)e^{\lambda E(D_i)t}$$

Now the reduction rate R is introduced, such that positive values of R represent a decrease of the a-posteriori annual flooding probability and negative values of R represent an increase:

$$(1-R) = e^{E(D_i)}$$

Substituting this definition of R, the a-posteriori annual flooding probability is written as:

$$P''(t) = P(t)(1-R)^{\lambda t}$$

The frequency of occurrence λ relates to the occurrence of a hydraulic loading event, of which the expected gained monitoring information from such an event gives relevant information for assessing the flooding probability. The monitoring of daily loading conditions gives new information. However, the occurrence of significant loading events gives additional information on the design loading conditions. Commonly in the Netherlands, this is a high water level event related to the safety standard. In general, a loading event with a higher frequency of occurrence λ gives less relevant information: the extrapolation to design loading conditions is larger. The physical circumstances of the considered local flood defence system further specify the relevance of the loading event. The starting point for this cost-benefit model is to determine the minimally required loading event, which is expected to yield relevant information, and the corresponding λ for this loading event. The text box *Summer dikes and inundated floodplains* illustrates the relevance of a water level for sensor monitoring and the corresponding frequency of occurrence λ. The larger the value of λ, the more benefit is obtained from the sensor monitoring: relevant information is expected to be obtained more frequent.

Summer dikes and inundated floodplains

Along Dutch rivers, summer dikes prevent the floodplain to be regularly flooded, such that the navigation channel is maintained and the floodplain can be used for grazing cattle. This example illustrates that a physical aspect determines the frequency of occurrence λ of a relevant high water event. Figure 5-3 holds a river with floodplains and a sensor monitoring system installed in the primary flood defence.

Usually, a small river discharge with water level h_1 flows through the navigation channel with frequency of occurrence λ_1. Now, the sensors in the primary flood defence measure irrelevant circumstances as the water is kept in the navigation channel. Only if the water level rises, the summer dikes overflow and the floodplains get inundated, the water is directly retained by the primary flood defence. This is a relevant loading condition to be monitored. The river discharge for water level h_2 with frequency of occurrence λ_2 causes the floodplain just to be flooded. If the water level rises again until h_3, more relevant information is obtained from the monitoring, with frequency of occurrence λ_3. Hence, that the water level are related as $h_1<h_2<h_3$ and because higher water levels (and thus river discharges) occur less frequent, the frequencies of occurrence are related as $\lambda_1>\lambda_2>\lambda_3$. Thus, the relevant high water in this example situation is h_2 and any higher water levels, with corresponding relevant frequency of occurrence λ_2.

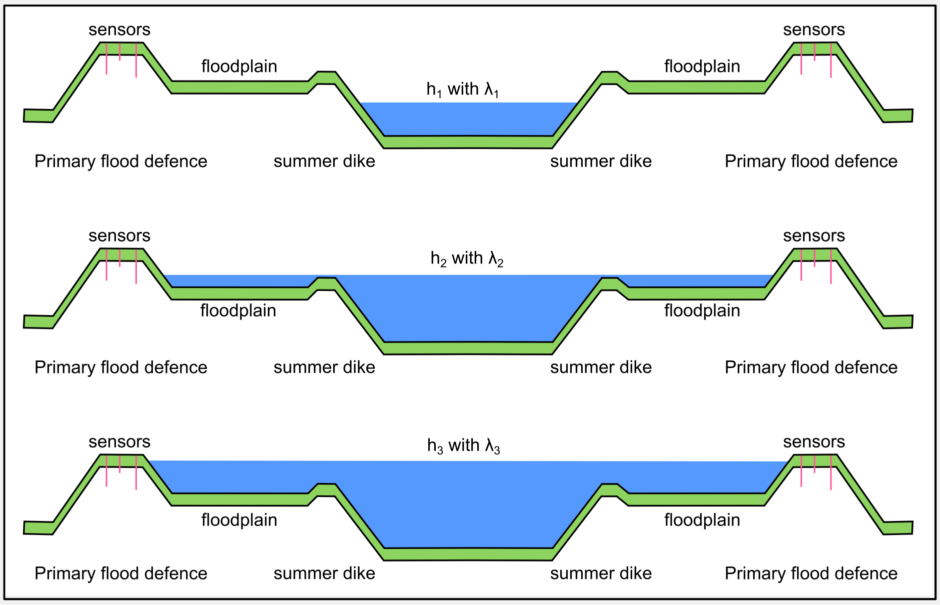

Figure 5-3: Schematic view of a summer dike preventing the floodplain to inundate

The value of R depends on the quality of the installed sensor system and the prior knowledge of the behavior of the dike. R is the expected effect of the monitored data (yet to be attained) on the flooding probability per monitored loading event with frequency of occurrence λ. This loading event is assumed not to cause a flood. The quality of the monitoring system influences the value of R: a qualitatively high monitoring system, with a low residual uncertainty, will result in higher absolute values of R. Because the potential uncertainty reduction is higher due to the low residual uncertainty. The quality of the monitoring system can be increased, thus increasing R, but this comes with higher sensor monitoring costs. Also the available knowledge on the behavior of the flood defence determines R: the more knowledge is already available, the less additional knowledge can be obtained from sensor monitoring (e.g. a value of R=0 is expected for the fictitious situation that everything is known from the flood defence). Thus if the prior relative uncertainty is small compared to other uncertainties, the impact of monitoring is smaller (i.e. small values of R). It should be emphasized that the reduction rate R affects the total flooding probability, incorporating all relevant failure mechanisms, but the monitoring data does not affect all failure mechanisms assessments. Therefore, the relevance of the monitored observable variable for the total flooding probability must be analyzed. The value of R remains ambiguous for constant quality of the monitoring system, because the reduction of the flooding probability depends on the real monitored data.

The a-posteriori expected costs $E(\text{costs})_{\text{a-posteriori}}$ are determined with OptimaliseRing by implementing P''(t). As the development of the flooding probability is affected, the optimal investment strategy in dike reinforcements is expected to change as well: the magnitude and timing of the reinforcements change, which results in a different shifted minimum for the E(costs) and thus for the optimal investment in reinforcement. It is assumed that the value of R and λ do not change over time.

5.2.3 Sensor monitoring costs

The sensor monitoring system influences the reduction rate R by the quality of the monitoring system. But a better quality generally leads to higher costs. The expected costs of a sensor system C_{sensor} depend on the installation costs, maintenance costs and operational costs and are discounted over the period T:

$$C_{\text{sensor}} = \sum_{t=0}^{T} \frac{C_{\text{installation}}}{(1+\delta)^{t_j}} + \sum_{t=0}^{T} \frac{C_{\text{maintenance}}}{(1+\delta)^{t}} + \sum_{t=0}^{T} \frac{C_{\text{operational}}}{(1+\delta)^{t}}$$

C_{sensor}	Discounted expected costs for the sensor system over time period T	[€]
$C_{\text{installation}}$	Installation costs in year t_j	[€]
$C_{\text{maintenance}}$	Yearly maintenance costs	[€]
$C_{\text{operational}}$	Yearly operational costs	[€]
δ	Discount rate	[%/year]
t_j	Year in which new sensors are installed	[year]

The expected costs of the sensor monitoring system C_{sensor} is the net present value of summed sensor costs discounted over the considered monitoring period. The costs aspects $C_{\text{installation}}$, $C_{\text{maintenance}}$ and $C_{\text{operational}}$ are assumed to remain constant over time. The discount rate δ consists of a real risk-free part of 2,5% and a risk averse part of 3%, according to (Ministerie van Financiën, 2007). The total discount rate equals 5,5 %/year in this research. This value is subject to changes over time due to economic developments, but is assumed constant over time.

The installation costs $C_{installation}$ are invested every t_j (e.g. purchase costs, installment costs), in which t_j is the expected lifetime of the sensors and assuming that after t_j years the system needs to be renewed. The installation costs can vary widely, depending on the scale of installation, the cover of the dike, accessibility of the dike and execution state (i.e. whether the dike is in execution phase or already finished). Assuming a monitoring system with sensors installed in cross-sections, the installation costs are defined as:

$$C_{\text{installation}}(t_j) = l_d \cdot (p+e)\frac{1000}{l_c} \cdot n \cdot (1+f_b)$$

$C_{installation}(t_j)$	Installation costs in year t_j	[€]
t_j	Year in which new sensors are installed	[year]
l_d	Length of the monitored dike	[km]
p	Purchase costs per sensor	[€]
e	Execution costs per sensor	[€]
l_c	Distance between cross-sections	[m]
n	Number of sensors installed per cross-section	[-]
f_b	Factor for base installation costs: $f_b>0$	[-]

The costs are calculated per km dike, such that the dike length l_d can be modified. The purchase costs p and the execution costs e are determined per installed sensor. The total number of installed sensors per monitored kilometer is defined by the number of sensors per cross-section n and the distance between two cross-sections l_c. The factor f_b incorporates the base installation costs, such as wiring, labor and data servers. These costs are assumed to be proportional to the dike length l_d, because additional sensors require extra base installation costs. A value of 0,2 is assumed for f_b.

The maintenance costs $C_{maintenance}$ are yearly costs, which keep the system working during the lifetime t_j (e.g. cleaning sensors). The maintenance costs can vary between sensor systems, e.g. as mechanical sensors suffer more from wear and tear than fiber optics will. The yearly maintenance costs are assumed to be a fraction of the installation costs:

$$C_{\text{maintenance}}(t) = f_m \cdot C_{\text{installation}}(t_j)$$

f_m	Factor for the yearly maintenance costs: $f_m>0$	[-]
$C_{installation}(t_j)$	Installation costs in year t_j	[€]
t_j	Year in which new sensors are installed	[year]

The value of f_m is assumed equal to 0,1. The operational costs $C_{operational}$ are yearly costs, which are made such that the sensor system keeps monitoring (e.g. power supply, data storage). This implies data storage costs and also engineering costs to interpret the collected data, in order to give value to the data referring the dike safety. The yearly operational costs are assumed to be a fraction of the installation costs:

$$C_{\text{operational}}(t) = f_o \cdot C_{\text{installation}}(t_j)$$

f_o	Factor for the yearly operational costs: $f_o>0$	[-]
$C_{installation}(t_j)$	Installation costs in year t_j	[€]
t_j	Year in which new sensors are installed	[year]

The value of f_o is assumed equal to 0,1. Apart from continuous monitoring over time, ideas exist for more purposeful monitoring by preparing the monitoring site on beforehand, and start monitoring when a loading event is at hand. This stand-by installation method tempts to reduce the overall monitoring costs, see text box *Stand-by installation method*. This method however is not discussed in this research, due to the highly uncertain unreliability aspects that occur due to the quick installation.

Stand-by installation method

Stand-by installation of sensor monitoring deals with the problem of the high costs for long-term monitoring with the randomness of occurring loading events. The monitoring system does not continuously gather data, but a sensor monitoring plan has been computed and is stand-by to be installed when a loading event is forecasted. The periodic costs are reduced, because maintenance and operational costs are replaced by preparation measures like storage of sensors and stand-by costs. Characteristics of the stand-by installation principle are:

- Structural schematization and assumption mistakes are not revealed over time (i.e. due to discontinuous monitoring)
- Additional unreliability aspects due to quick installation (e.g. human error, logistics, deployment)
- Prediction of the loading event must grant sufficient response time (e.g. river floods)
- Reduced maintenance and operational costs

5.2.4 Direct and indirect monitoring effects

This paragraph considers the difference in monitoring effects for the cost-benefit results: a direct and an indirect monitoring effect. As stated before, the effect of sensor monitoring on the flood safety assessment affects the epistemic uncertainty of the assessment, which results in either an increased or decreased assessed flood risk. Either one of these situations occurs because the assessed flood risk is based on limited information and the "real" flood risk remains unknown. Each situation has a different impact in the cost-benefit analysis, but which situation will occur is unknown until further information has been obtained from sensor monitoring. Therefore, this section describes the approaches based on different utility of both situations, assuming that the information provided by sensor monitoring gives true information, i.e. the a-posteriori flood risk with sensor monitoring information approaches the "real" flood risk closer than priory was assessed. The cost-benefit case studies performed in paragraphs 5.3 and 5.4 evaluate the direct and indirect monitoring effects separately.

Direct monitoring effect

The first situation is referred to as the direct monitoring effect and concerns sensor monitoring information which leads to a reduction of the flood risk, i.e. the a-priori flood risk was schematized conservatively and the "real" risk is lower than anticipated. This leads to direct savings in terms of dike reinforcements due to the lower flood risk. This situation is referred to as the direct monitoring effect, in which "direct" refers to the intuitively direct benefit for a dike manager. This monitoring effect corresponds to positive values of the reduction rate R in the cost-benefit analysis. Intuitively and financially, this is the preferred situation for a dike manager: one invests in a sensor monitoring system which obtains new information and the investment is returned by means of savings in the dike reinforcements. The comparison is made for the situation when nothing is done, i.e. no sensor monitoring. The simplest example is a time independent situation where the sensor monitoring always leads to a reduction of the reinforcements costs (i.e. the prior schematization turns out too conservative with probability P=1), thus the value of R has a positive value. The corresponding event tree is given in Figure 5-4.

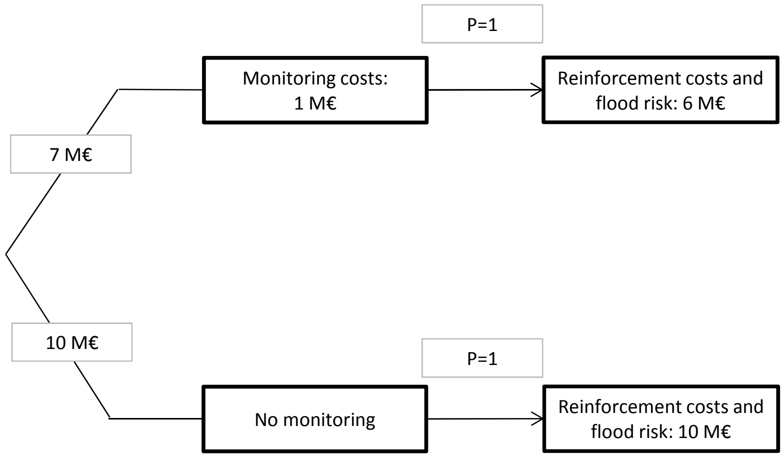

Figure 5-4: Event tree for the time independent example situation

The sensor monitoring system costs 1 M€ for monitoring for 1 year and the information obtained with this investment leads to a required dike reinforcement costing 6 M€ with probability P=1. The expected value thereby equals 7 M€. The initial situation has prior reinforcement costs of 10 M€ (also with probability P=1), such that every dike manager would decide on investing in sensor monitoring as this would lead to a saving of 3 M€. In this simple example, the sensor information is obtained instantaneously. However, the information obtained from sensor monitoring costs time as relevant high water events give important information, as has been stated in chapter 3. The cost-benefit model incorporates this time effect with the variable λ. Due to this time effect, the required monitoring costs to obtain the same information is higher: after all, it is expected to monitor for a longer time. The event tree incorporates a longer monitoring time, say 2 years, before the expected information is gained. The

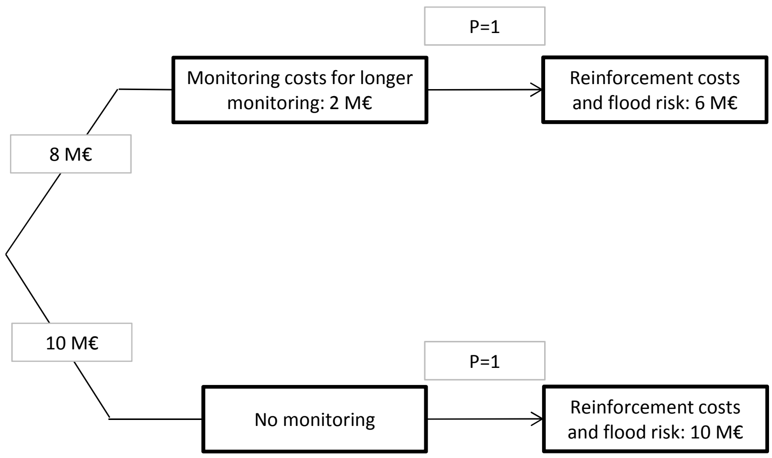

Figure 5-5: Event tree for a time dependent example situation

The expected monitoring costs are doubled to 2 M€, but the information gained results in a required dike reinforcement of 6 M€. Still, the dike manager would invest in the sensor monitoring as this leads to a reduction of the total expected costs of 2 M€. However, the saving from the dike reinforcement is ambiguous: maybe the saving is smaller because the uncertainty of the monitored variable is relatively small (see paragraph 3.2.4). This results in numerous new outcomes from the obtained sensor monitoring information leading to different required dike reinforcements. The event tree in Figure 5-6 gives the example for uncertain outcome: two different required reinforcement costs are expected evenly with P=0,5. The new situation for the required dike reinforcement of 8 M€ refers to a smaller value of the reduction rate R in the cost benefit model.

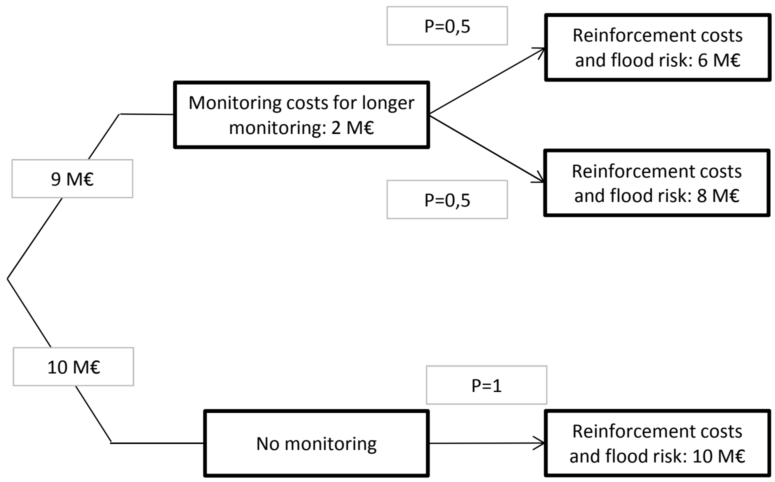

Figure 5-6: Event tree for the time dependent and uncertain outcome example situation

Incorporating the situation that the sensor monitoring leads to a smaller reduction (i.e. smaller value of the reduction rate R in the cost-benefit model), leads to total expected costs of 2+(0,5*6+0,5*8)=9 M€. Still, this example situation would make the dike manager decide on investing in the sensor monitoring system. The general remark for these examples is that when the investment for gaining additional information is relatively small and the information is gained fast, the benefit is higher. This is the situation for construction projects using the observational method (see paragraph 3.5.3), but not for monitoring long dike sections. Moreover, paragraph 3.2.4 refers to the situation that the schematization turns out to be too optimistic: the indirect monitoring effect.

Indirect monitoring effect

The second situation is referred to as the indirect monitoring effect and concerns an increase of the flood risk due to sensor monitoring information: the a-priori flood risk was schematized too optimistic and the "real" risk is higher than anticipated. Financially, this leads to higher costs for dike reinforcements in order to mitigate the increased flood risk. Expanding the event tree with a single situation for the indirect monitoring effect resulting in reinforcement costs of 12 M€ and each outcome has a probability of P=1/3, results in the event tree in Figure 5-7.

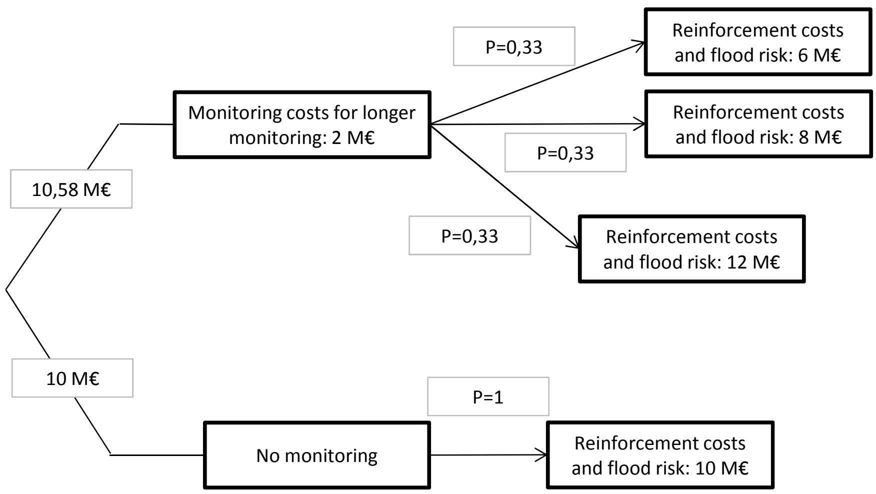

Figure 5-7: Event tree for the example situation with indirect monitoring effect

The monitoring system now results in an expected total costs of 2+(0,33*6+0,33*8+0,33*12)=10,58 M€. The decision on investing in the monitoring system is not cost effective, as doing nothing costs 10 M€. Intuitively, this situation is disappointing since an investment has been made (for the sensor monitoring) and the information gained from this investment leads to additional costs (for the dike reinforcements). Rationally, this situation is not disappointing since the information gained with the monitoring revealed a prior unforeseen risk (see also paragraph 3.5.2): the information from sensor monitoring reveals a higher flood risk than anticipated with prior information, which was unforeseen without sensor monitoring applied. After all, if the risk had been foreseen in advance, this risk would have been covered in the prior flood risk assessment. Identifying an unforeseen risk is desirable, because otherwise this unforeseen risk is to be observed due to system failure and leading to damage as a consequence. This situation is referred to as the indirect monitoring effect, in which "indirect" refers to the indirect benefit if the information is approached rationally (i.e. the direct monitoring effect is intuitively not beneficial due to higher costs). In the cost-benefit model, this monitoring effect corresponds to negative values of the reduction rate R: the assessed a-priori flood risk increases (i.e. negatively reduces).

Suggestion for combining both monitoring effects

The direct and indirect monitoring effects lead to two different benefits and benefit-cost ratios, which one wants to combine into a single benefit cost ratio. Here, a suggestion to combine both monitoring effects is made based on the theory on value of information. Concluding from the example event trees above, the information gained from sensor monitoring rationally has a certain value if the information is available: this is known as the value of information in decision theory (Hammitt & Shlyakhter, 1999). The value of information can be interpreted as the willingness to pay for gaining information prior to the decision (EuroGEOSS, 2012). In the context of this research, the value of information is the amount a dike manager is willing to pay for sensor monitoring information in order to decide on investing in sensor monitoring. To be able to make this decision, the expected value of information must be derived. Prior of making the decision of investing in monitoring, one has an expectation of the value of information to be gained: is it likely to gain a direct or indirect monitoring effect? This likelihood is subjective by the situation of the decision maker. Because of the conservative approach on flood safety assessment in the Netherlands, one can expect that the sensor monitoring leads to direct savings. But it should be emphasized that the benefit of sensor monitoring is only known afterwards, when the information has been gathered.

In fact however, the prior flooding probability constitutes the expected value of the posterior probabilities before the extra information has been obtained. This relationship can be derived by combining the Bayes theorem and the law of tot probability, where P(x) is the prior flooding probability and P(x|data) the posterior flooding probability given collected data i:

$$\text{Bayes theorem: } P(x \mid \text{data}_\text{i}) = \frac{P(\text{data}_\text{i} \mid x)P(x)}{P(\text{data}_\text{i})}$$

$$\text{Law of total probability: } P(x) = \sum_{i=1}^{n} P(x \mid \text{data}_\text{i})P(\text{data}_\text{i})$$

Substituting the Bayes theorem into the law of total probability denotes the fundamental relationship:

$$\text{Substitution: } P(x) = \sum_{i=1}^{n} \frac{P(\text{data}_\text{i} \mid x)P(x)}{P(\text{data}_\text{i})} P(\text{data}_\text{i}) =$$

$$P(x)\sum_{i=1}^{n} P(x \mid \text{data}_\text{i}) = P(x)$$

After all, if the expected values of the posterior probability differs from the prior probability, extra information is implicitly already been taken into account. One can expect to learn something from the yet to be collected data (i.e. either direct or indirect monitoring effect in this case), in the sense that the posterior distribution differs from the prior distribution, but one cannot know what to expect to learn (Hammitt & Shlyakhter, 1999). If one knew on beforehand what to learn from the data (i.e. how the prior distribution is expected to change, like the example event trees given above), the prior distribution inadequately represents the prior available information. This statement is used to combine both direct and indirect monitoring effects in the cost-benefit model.

Thus, the prior flooding probability constitutes the expected value of the posterior probabilities before the extra sensor monitoring information is obtained. Hence, the following must hold for the annual flooding probabilities, considering for simplicity two expected situations direct and indirect monitoring effect:

$$P(t) = P^{"}_{\text{direct}}(t) \cdot P_s(t) + P^{"}_{\text{indirect}}(t) \cdot (1 - P_s(t))$$

P(t)	A-priori probability of flooding in year t, without sensor monitoring	[1/year]
$P^{"}_{\text{direct}}(t)$	A-posteriori flooding probability in year t, for the sensor monitoring information reducing the a-prior flooding probability; P(t) > $P^{"}_{\text{direct}}(t)$ (the direct monitoring effect)	[-/year]
$P^{"}_{\text{indirect}}(t)$	A-posteriori flooding probability in year t, for the sensor monitoring information increasing the a-prior flooding probability; P(t) < $P^{"}_{\text{direct}}(t)$ (the indirect monitoring effect)	[-/year]
$P_s(t)$	Probability that the prior flooding probability is reduced due to sensor monitoring information in year t; occurrence of the direct monitoring effect (i.e. 0<R<1) in year t	[-]

The determination of $P_s(t)$ must therefore be done for every time step t, with a considered time span of 300 years. Also, the probability $P_s(t_j)$ at time step t_j depends on the previously collected data and probabilities $P_s(t)$ before time step t_j:

$$P(t) \approx P''_{\text{direct}}(t) \cdot P_s + P''_{\text{indirect}}(t) \cdot (1 - P_s)$$

P(t)	A-priori probability of flooding in year t, without sensor monitoring	[1/year]
$P''_{\text{direct}}(t)$	A-posteriori flooding probability in year t, for the sensor monitoring information reducing the a-prior flooding probability; P(t) > $P''_{\text{direct}}(t)$ (the direct monitoring effect)	[-/year]
$P''_{\text{indirect}}(t)$	A-posteriori flooding probability in year t, for the sensor monitoring information increasing the a-prior flooding probability; P(t) < $P''_{\text{direct}}(t)$ (the indirect monitoring effect)	[-/year]
P_s	Time independent probability that the prior flooding probability is reduced due to sensor monitoring information; occurrence of the direct monitoring effect (i.e. 0<R<1)	[-]

Using this time independent approximation P_s, the benefit-cost ratio for combined sensor monitoring effects can be defined as:

$$\varepsilon_{p,c} = \frac{\text{benefit}}{\text{cost}} = \frac{\text{E(costs)}_{\text{a-priori}} - \{P_s \cdot \text{E(costs)}_{\text{direct}} + (1 - P_s) \cdot \text{E(costs)}_{\text{indirect}}\}}{\text{C}_{\text{sensor}}}$$

$\varepsilon_{p,c}$	Benefit-cost ratio for the periodic safety assessment for combined sensor monitoring effects	[-]
$\text{E(costs)}_{\text{a-priori}}$	Expected costs for the initial situation, i.e. no sensors applied, over a given time period	[€]
P_s	Time independent probability that the prior flooding probability is reduced due to sensor monitoring information; occurrence of the direct monitoring effect (i.e. 0<R<1)	[-]
$\text{E(costs)}_{\text{direct}}$	Expected costs for the situation with direct monitoring effect from sensor monitoring, over a given time period	[€]
$\text{E(costs)}_{\text{indirect}}$	Expected costs for the situation with direct monitoring effect from sensor monitoring, over a given time period	
C_{sensor}	Costs made due to the application of sensor monitoring	[€]

However, the implementation of the combined sensor monitoring effects in the available calculation model OptimaliseRing (Deltares, 2011d) is not possible. Therefore, this implementation is recommended to be subject of further research.

5.2.5 Example calculation for first upcoming dike reinforcement

A simplified example has been worked out for a fictive dike-ring area to illustrate the principle of this cost-benefit model. Specifications of this example case are given in Appendix H. A dike manager considers the possible effect of sensor monitoring on the first dike reinforcement over the next 50 years. Reinforcement of the dike is required if the flooding probability exceeds 1/2000 per year, as this is the safety standard of the dike-ring. A dike reinforcement is expected to be carried out after 19 years, for a height of 30 cm. Thus, without any sensor monitoring considered. The net present value of this reinforcement is 6,1 M€. The dike manager first considers a relatively cheap monitoring system M_1, with R=0,1 and λ=0,01 per year. The monitoring data can result in an increased flood safety, modeled with R=0,1 or a decreased flood safety which is modeled with R=-0,1. The dike reinforcement is optimized due to the potential effect of sensor monitoring, see Figure 5-8.

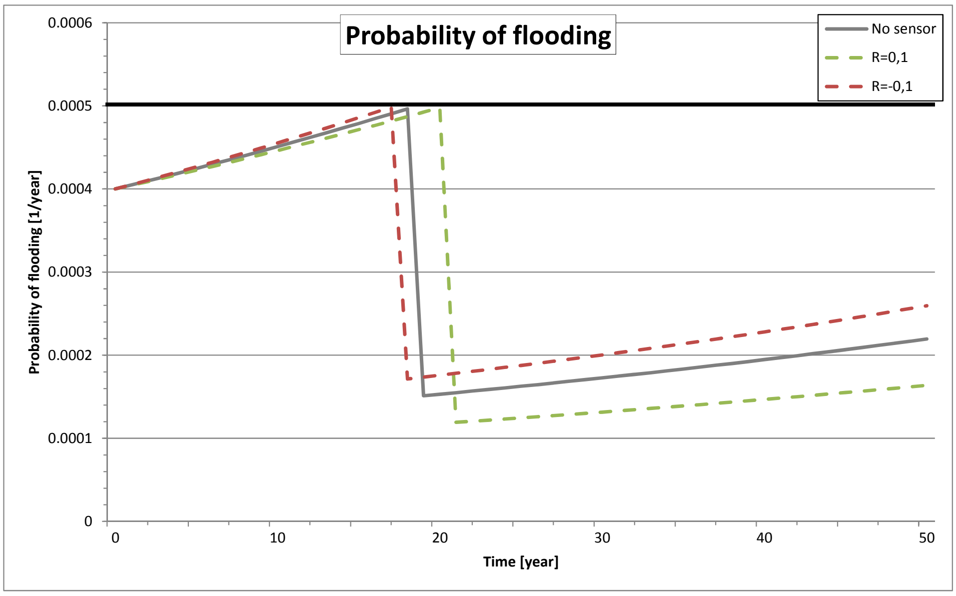

Figure 5-8: Dike reinforcements for expected situation (no sensor monitoring), monitoring effect of R=0,1 and monitoring effect of R=-0,1 for monitoring system M_1

The investment strategy is based on the available funds at t=0 (i.e. net present value of the reinforcement): the dike manager has a reserved funds at t=0 for future dike reinforcements. All three dike reinforcements have a net present value of 6,1 M€[7]. A direct monitoring effect on the safety assessment grants the opportunity to delay the dike reinforcement with 2 years, because then the minimum required safety standard will be exceeded. This delay grants the opportunity for the dike manager to execute a reinforcement of 36 cm, for the same net present value at t=0. On the other hand, the indirect monitoring effect of the sensor monitoring requires a reinforcement 1 year earlier than expected and then there is only money available for a heightening of 27 cm. The total discounted flood risk over the coming 50 years is influenced by the different reinforcement strategies. The monitoring system has a net present value of 0,763 M€ for continuous monitoring for the coming 50 years. The results of the cost-benefit analysis are presented in Table 5-1.

Table 5-1: Cost-benefit analysis for monitoring system M_1

	Discounted E(costs) [M€]	Difference in E(costs) [M€]	Sensor costs C_{sensor} [M€]	Benefit-cost ratio ε_p [-]
Expected (no sensor)	72,4	-	-	-
Direct monitoring effect R=0,1	71,6	0,8	0,763	1,05
Indirect monitoring effect R=-0,1	73,8	-1,4	0,763	-1,83*

**The negative benefit-cost ratio is caused by the unforeseen risk leading to higher costs than anticipated on beforehand. The value of information has not been taken into account (see paragraph 5.2.4).*

If the monitoring data, from the loading event occurring every 100 year, reveals a higher flood safety than expected, the benefit-cost ratio ε_p=1,05 and the sensor monitoring is cost-effective. However, if the flood safety is lower than expected, the benefit cost ratio equals ε_p=-1,83.

The dike manager also considers installing a more dense monitoring system M_2, which is expected to have a higher quality: R=0,2 and λ=0,01 per year. The discounted monitoring costs are increased to 2,036 M€. A direct monitoring effect with R=0,2 would grant a reinforcement of

[7] Note that this method differs from the optimization method as used in paragraphs 5.3 and 5.4.

43 cm with a delay of 4 years. The indirect monitoring effect with R=-0,2 requires a reinforcement of 24 cm executed 2 years earlier than expected, see Figure 5-9.

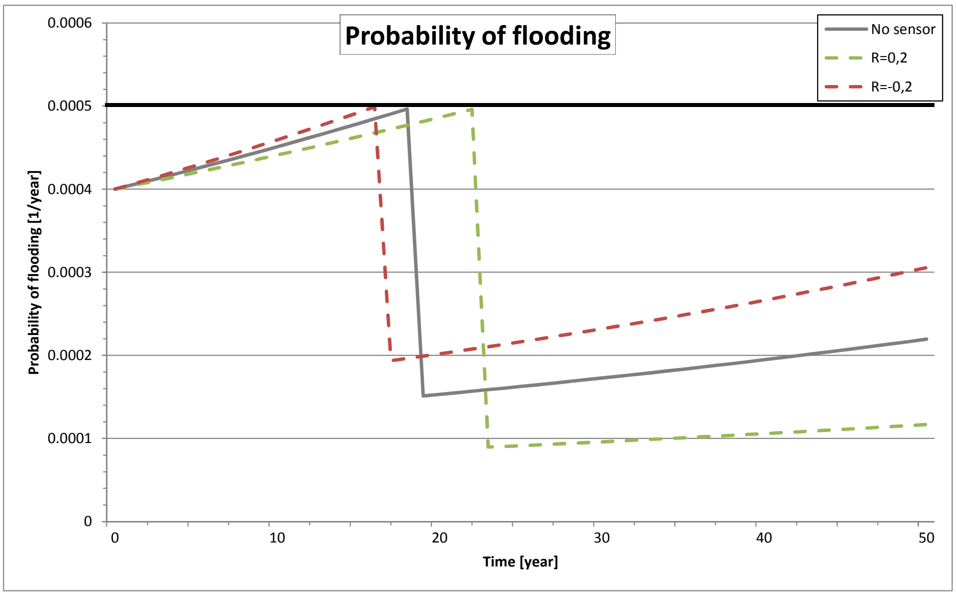

Figure 5-9: Dike reinforcements for expected situation (no sensor monitoring), monitoring effect of R=0,2 and monitoring effect of R=-0,2 for monitoring system M_2

The time and magnitude of the reinforcements is expected to be influenced by installing another monitoring system, because the epistemic spatial uncertainty is reduced. The benefit-cost ratio of the dense monitoring system is in this case smaller than the cheaper monitoring system M_1. Table 5-2 gives an overview of the cost-benefit analysis for the monitoring system M_2.

Table 5-2: Cost-benefit analysis for monitoring system M_2

	Discounted E(costs) [M€]	Difference in E(costs) [M€]	Sensor costs C_{sensor} [M€]	Effectiveness ε_p [-]
Expected (no sensor)	72,4	-	-	-
Direct monitoring effect R=0,2	71,3	1,1	2,036	0,54
Indirect monitoring effect R=-0,2	75,6	-3,2	2,036	-1,54*

**The negative benefit-cost ratio is caused by the unforeseen risk leading to higher costs than anticipated on beforehand. The value of information has not been taken into account (see paragraph 5.2.4).*

However, the approach in this example is based on the required safety standard and the available funds for dike reinforcement and not the complete optimal investment strategy based on minimum flood risk and investment costs. The feasibility depends on many case specific characteristics. The optimal investment strategy is determined per dike-ring stretch with the software OptimaliseRing (Deltares, 2011d) and corresponding database from 2011. The potential flood damage is determined per dike-ring stretch, assuming that any dike failure in one of the stretches leads to the same flood damage. The optimal investment strategy is determined with reference year 2015 and considers a life span of 300 years. In the next paragraphs, two dike-ring parts are evaluated for the application of sensor monitoring:

- Dike-ring 48, part Rhine and IJssel downstream (paragraph 5.3)
- Dike-ring 14, part Nieuwe Waterweg east (paragraph 5.4)

Each of these dike-ring parts has different characteristics regarding the safety standard, loading conditions, flood consequences and flood reduction costs.

5.3 Case study for dike-ring 48

5.3.1 Dike-ring characteristics

Dike-ring 48 is situated in the east of the Netherlands adjacent to Germany, where the Rhine enters the country. The considered dike-ring part Rhine and IJssel downstream protects urban areas like Zevenaar, Duiven, Didam and Westervoort and consists of three dike stretches:

- Stretch canal of Pannerden (6 km)
- Stretch IJssel (21 km)
- Stretch Old IJssel (12 km)

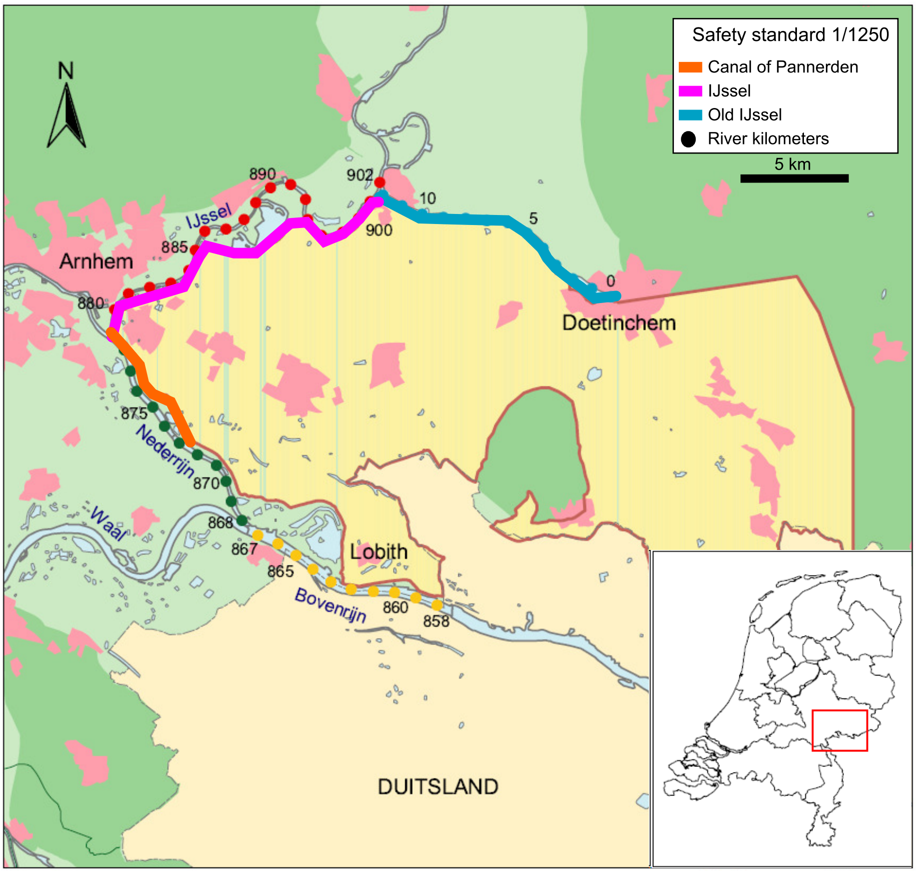

Figure 5-10: Dike-ring area 48 with the considered dike stretches

Dike-ring 48 is threatened by high discharges of the Rhine, the Waal and the canal of Pannerden. The water flows in the Lower Rhine (Dutch: *Nederrijn*) and the IJssel at the bifurcation point IJsselkop. The loading characteristics along the dike stretches are thereby highly correlated. The characteristics of each dike stretch are summarized in Table 5-3 and are deduced from the database in (Deltares, 2011d).

Table 5-3: Dike stretch characteristics for dike-ring 48 part Rhine and IJssel downstream

Parameter	Canal of Pannerden	IJssel	Old IJssel	
P(0)	0,000574	0,000605	0,000605	[1/year]
α_d	0,057	0,0635	0,0635	[1/cm]
η	0,294	0,494	0,494	[cm/year]
V(0)*	7092	7092	7092	[M€]
ψ	0	0	0	[1/cm]
ζ	0	0	0	[1/cm]
C	3	8,55	6,55	[M€]
b	0,15	0,34	0,32	[M€/cm]

**Including 21 potential casualties with VOSL[8]=6,7 M€ (Deltares, 2011c).*

Here, P(0) is the probability of flooding of the considered dike stretch in year t=0, α_d is a scale parameter related to the decimation height, η is the relative water level rise, V(0) is the potential flood damage in year t, ψ is an impact parameter for additional flood damage due to water level rise, ζ is an impact parameter for additional flood damage due to failure of increased dike height, C are the fixed investment costs for a dike reinforcement and b the variable dike reinforcement costs. The safety standard of dike-ring 48 equals 1/1250 per year, meaning that Rhine discharges occurring once every 1250 years on average must be withstood. Discharges occurring once every 100 years are assumed to give sufficient monitoring information: λ=0,01 per year.

Three monitoring cases are considered, with increased monitoring costs in each case:

- **Case 1: Monitoring of stretch canal of Pannerden**
  Monitoring with a simple monitoring system S_1 along 6 km of the stretch canal of Pannerden.
- **Case 2: Extensive monitoring of stretch canal of Pannerden**
  Monitoring with an advanced monitoring system S_2 along 6 km of the stretch canal of Pannerden.
- **Case 3: Extensive monitoring of stretches canal of Pannerden and IJssel**
  Monitoring with an advanced monitoring system S_2 along 27 km of the stretches canal of Pannerden and IJssel.

5.3.2 Case 1: Monitoring of stretch canal of Pannerden

The first case considers monitoring of the smallest stretch of 6 km with a simple monitoring system S_1. The monitoring system consists of MEMS sensor modules (e.g. GeoBeads) with a claimed life time of 10 years, which are installed with conventional CPT push-in techniques. Three sensors are installed per cross-section and a cross-section is installed every 100 m. The total installation costs of monitoring system S_1 are, with l_d=6 km, p=350 € per sensor module (Ng & Oswalt, 2010), e=200 € per CPT push-in (Feitsma, 2002), l_c=100 m, n=3, f_b=0,2:

$$C_{\text{installation}}(t_j) = 6 \cdot (350 + 200)\frac{1000}{100} \cdot 3 \cdot (1 + 0,2) = 118800 \text{ €}$$

These installation costs have to be invested every t_j=10 years. The yearly maintenance and operational costs sum up to:

[8] VOSL is the abbreviation of the Value of a Statistical Life and is a monetary value for the immaterial damage of a fatal casualty caused by a flood. In fact, it represents the value that people give to a reduction of the probability to prematurely die from a flood (Deltares, 2011c).

$$C(t) = 0{,}1 \cdot 118800 + 0{,}1 \cdot 118800 = 23760 \text{ €/year}$$

The total discounted costs over 300 years, with δ=5,5 %/year equal 0,74 M€. Monitoring system S_1 is assumed to obtain R=0,2 with λ=0,01 per year. The obtained optimal investment strategies as computed with OptimaliseRing influence the probability of flooding of the monitored dike stretch given in Figure 5-11.

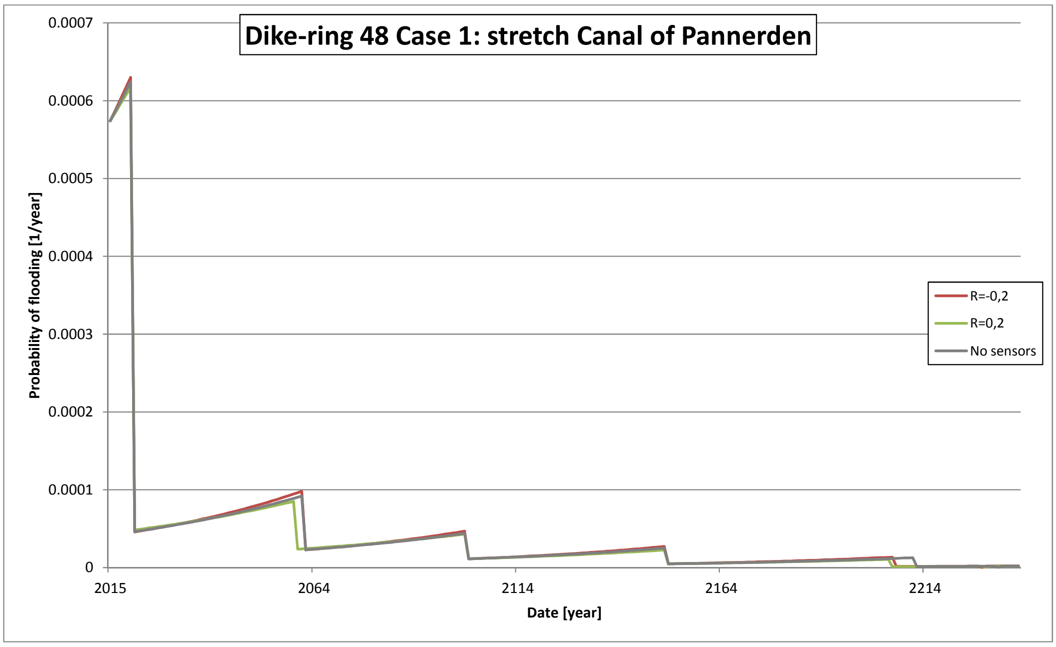

Figure 5-11: Optimal investment strategy for dike-ring 48 Case 1: stretch canal of Pannerden (considering λ=0,01, R=0,2 and R=-0,2)

The first, third and fourth planned reinforcements are not affected by the monitoring information. The second investment is advanced with 2 years for a direct monitoring effect and an indirect monitoring effect requires a heavier dike reinforcement. Whereas, the fifth reinforcement is advanced for both situations. The difference in expected discounted costs for all three investment strategies is small, thus the effect of this monitoring strategy is marginal. The cost-benefit analysis is given in Table 5-4.

Table 5-4: Cost-benefit analysis for case 1, considering λ=0,01, R=0,2 and R=-0,2

	Discounted E(costs) [M€]	Difference in E(costs) [M€]	Sensor costs C_{sensor} [M€]	Benefit-cost ratio ε_p [-]
Expected (no sensor)	106,5	-	-	-
Direct monitoring effect R=0,2	106,4	0,1	0,74	0,14
Indirect monitoring effect R=-0,2	106,6	-0,1	0,74	-0,14*

**The negative benefit-cost ratio is caused by the unforeseen risk leading to higher costs than anticipated on beforehand. The value of information has not been taken into account (see paragraph 5.2.4).*

The benefit-cost ratio ε_p for Case 1 equals 0,14 for R=0,2 and -0,14 for R=-0,2. Sensor monitoring is in this case not cost-effective, because the additional monitoring costs exceed the benefits. The monitoring costs have to be reduced with purchase costs p=50 €/sensor and e=25 €/CPT push-in to become cost-effective for R=0,2 (C_{sensor}=0,10 M€ and ε_p=1), which is not realistic.

5.3.3 Case 2: Extensive monitoring of stretch canal of Pannerden

The second case considers monitoring of the smallest stretch of 6 km with an advanced monitoring system S_2. The monitoring system consists of the same sensors as in Case 1, but has a denser sensor setup. Four sensors are installed per cross-section and a cross-section is installed every 50 m. The total installation costs of monitoring system S_2 are, with l_d=6 km, p=350 € per sensor module (Ng & Oswalt, 2010), e=200 € per CPT push-in (Feitsma, 2002), l_c=50 m, n=4, f_b=0,2:

$$C_{\text{installation}}(t_j) = 6 \cdot (350+200)\frac{1000}{50} \cdot 4 \cdot (1+0,2) = 316800 \text{ €}$$

These installation costs have to be invested every t_j=10years. The yearly maintenance and operational costs sum up to:

$$C(t) = 0,1 \cdot 316800 + 0,1 \cdot 316800 = 63360 \text{ €/year}$$

The total discounted costs C_{sensor} over 300 years, with δ=5,5 %/year equal 1,98 M€. Monitoring system S_2 is assumed to obtain R=0,5 with λ=0,01 per year. The obtained optimal investment strategies as computed with OptimaliseRing influence the probability of flooding of the monitored dike stretch as given in Figure 5-12.

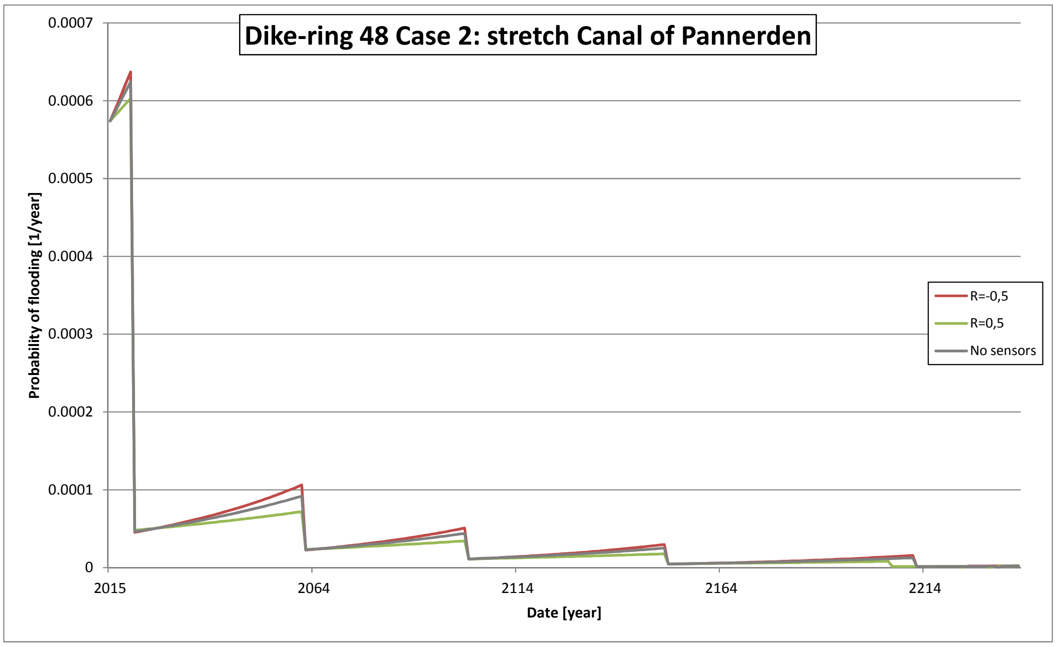

Figure 5-12: Optimal investment strategy for dike-ring 48 Case 2: stretch canal of Pannerden (considering λ=0,01, R=0,5 and R=-0,5)

The first, second, third and fourth planned reinforcements are not affected by means of the time of reinforcement, but the magnitude of reinforcement is larger for an indirect monitoring effect and smaller for a direct monitoring effect. The fifth reinforcement is advanced with 6 years for a direct monitoring effect. The effect of the monitoring on the expected discounted costs has been increased and the cost-benefit analysis is given in Table 5-5.

Table 5-5: Cost-benefit analysis for case 2, considering λ=0,01, R=0,5 and R=-0,5

	Discounted E(costs) [M€]	Difference in E(costs) [M€]	Sensor costs C_{sensor} [M€]	Benefit-cost ratio ε_p [-]
Expected (no sensor)	106,5	-	-	-
Direct monitoring effect R=0,5	106,2	0,3	1,98	0,15
Indirect monitoring effect R=-0,5	106,7	-0,2	1,98	-0,10*

**The negative benefit-cost ratio is caused by the unforeseen risk leading to higher costs than anticipated on beforehand. The value of information has not been taken into account (see paragraph 5.2.4).*

The benefit-cost ratio ε_p for Case 2 equals 0,15 for R=0,5 and -0,10 for R=-0,5. Sensor monitoring in this case is not cost-effective and comparable with the results of Case 1. The monitoring costs have to be reduced with purchase costs p=50 €/sensor and e=35 €/CPT push-in to become cost-effective for R=0,5 (C_{sensor}=0,30 M€ and ε_p=1), which is not realistic.

5.3.4 Case 3: Extensive monitoring of stretches Canal of Pannerden and IJssel

The third case considers monitoring of an additional dike stretch of 21 km with monitoring system S_2. The total installation costs of monitoring system S_2 are, with l_d=27 km:

$$C_{\text{installation}}(t_j) = 27 \cdot (350 + 200)\frac{1000}{50} \cdot 4 \cdot (1 + 0,2) = 1425600 \text{ €}$$

These installation costs have to be invested every t_j=10years. The yearly maintenance and operational costs sum up to:

$$C(t) = 0,1 \cdot 1425600 + 0,1 \cdot 1425600 = 285120 \text{ €/year}$$

The total discounted costs C_{sensor} over 300 years, with δ=5,5 %/year equal 8,91 M€. Monitoring system S_2 is assumed to obtain R=0,5 with λ=0,01 per year. The obtained optimal investment strategies as computed with OptimaliseRing influence the probability of flooding of the monitored dike stretch as given in Figure 5-13 and Figure 5-14.

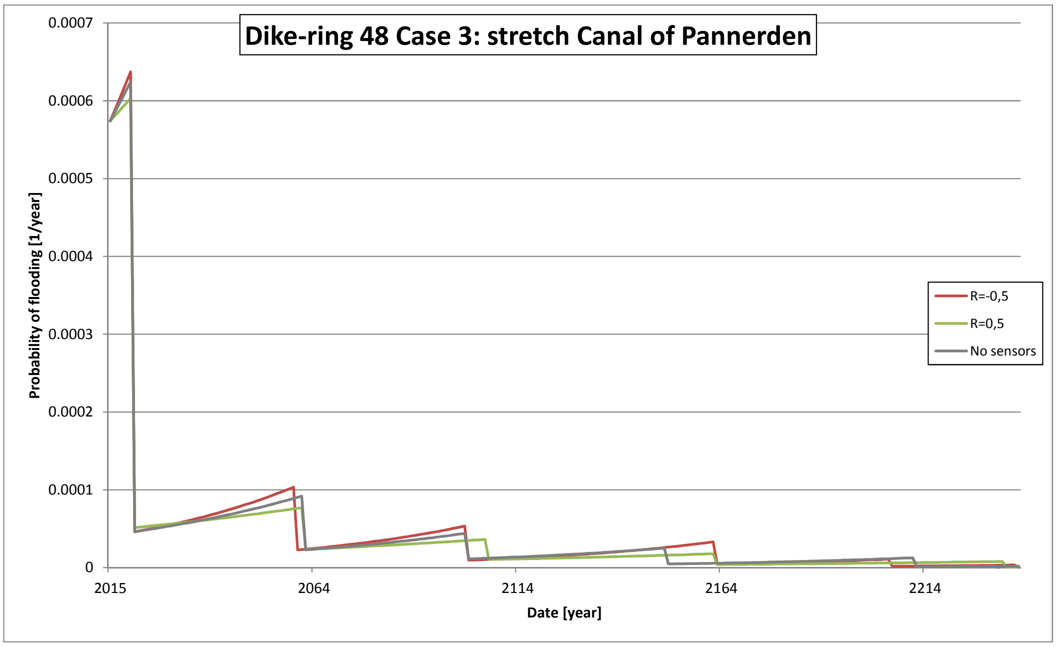

Figure 5-13: Optimal investment strategy for dike-ring 48 Case 3: stretch canal of Pannerden (considering λ=0,01, R=0,5 and R=-0,5)

Considering the direct monitoring effect for the stretch canal of Pannerden, the third, fourth and fifth reinforcements can be delayed with multiple years: the first two reinforcements have a reduced magnitude. Regarding the indirect monitoring effect, the first and third reinforcement have a smaller magnitude and the second reinforcement is advanced with 2 years. Then the fourth reinforcement is delayed with 15 years, whereas the fifth reinforcement is advanced again with 5 years.

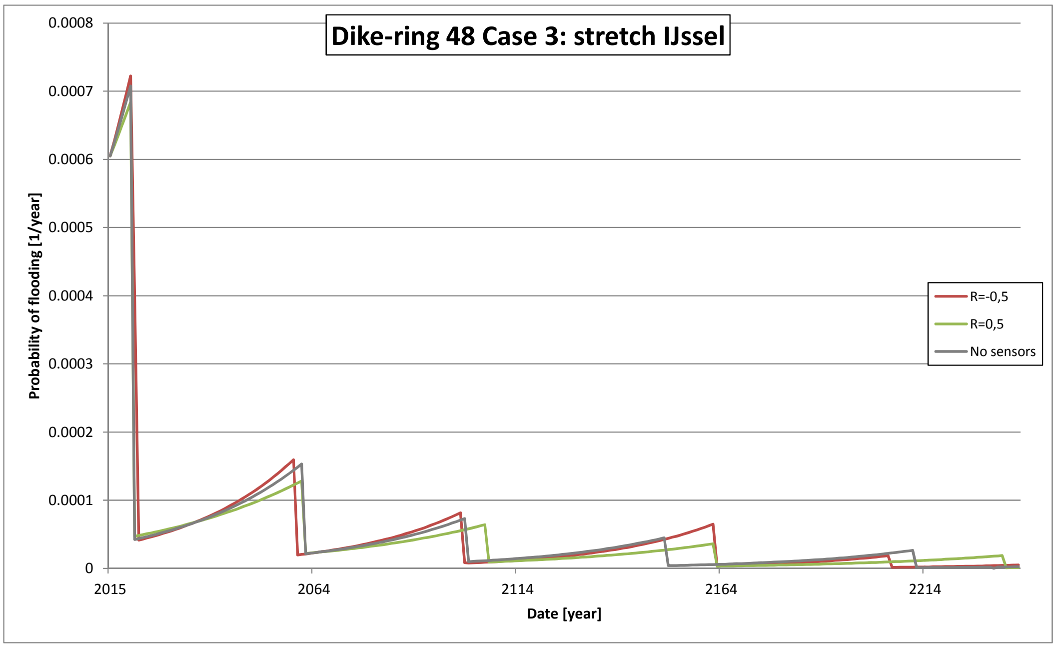

Figure 5-14: Optimal investment strategy for dike-ring 48 Case 3: stretch IJssel (considering λ=0,01, R=0,5 and R=-0,5)

Comparable monitoring effects on the optimal investment strategy are obtained for stretch IJssel, as was obtained for stretch canal of Pannerden. The effect of the monitoring on the expected discounted costs is severe, but the monitoring costs have increased significantly as well, see Table 5-6.

Table 5-6: Cost-benefit analysis for case 3, considering λ=0,01, R=0,5 and R=-0,5

	Discounted E(costs) [M€]	Difference in E(costs) [M€]	Sensor costs C_{sensor} [M€]	Benefit-cost ratio ε_p [-]
Expected (no sensor)	106,5	-	-	-
Direct monitoring effect R=0,5	103,9	2,6	8,91	0,29
Indirect monitoring effect R=-0,5	108,8	-2,3	8,91	-0,26*

**The negative benefit-cost ratio is caused by the unforeseen risk leading to higher costs than anticipated on beforehand. The value of information has not been taken into account (see paragraph 5.2.4).*

The benefit-cost ratio ε_p for Case 3 equals 0,29 for R=0,5 and -0,26 for R=-0,5. Sensor monitoring is in this case still not cost-effective. However, Case 3 is the most cost-effective of all considered cases for this dike-ring part. The monitoring costs have to be reduced with purchase costs p=85 €/sensor and e=75 €/CPT push-in to become cost-effective for R=0,5 (C_{sensor}=2,59 M€ and ε_p=1).

5.4 Case study for dike-ring 14

5.4.1 Dike-ring characteristics

Dike-ring 14 is situated at the west coast of the Netherlands and protects the economic heart of the country: the Randstad. The considered dike-ring part Nieuwe Waterweg east protects cities like Rotterdam, Schiedam, Vlaardingen and Delft with three dike stretches, see Figure 5-18:

- Stretch Nieuwe Waterweg 1010-1019 (9 km)
- Stretch Nieuwe Waterweg 1019-1026 (7 km)
- Stretch New Meuse (19 km)

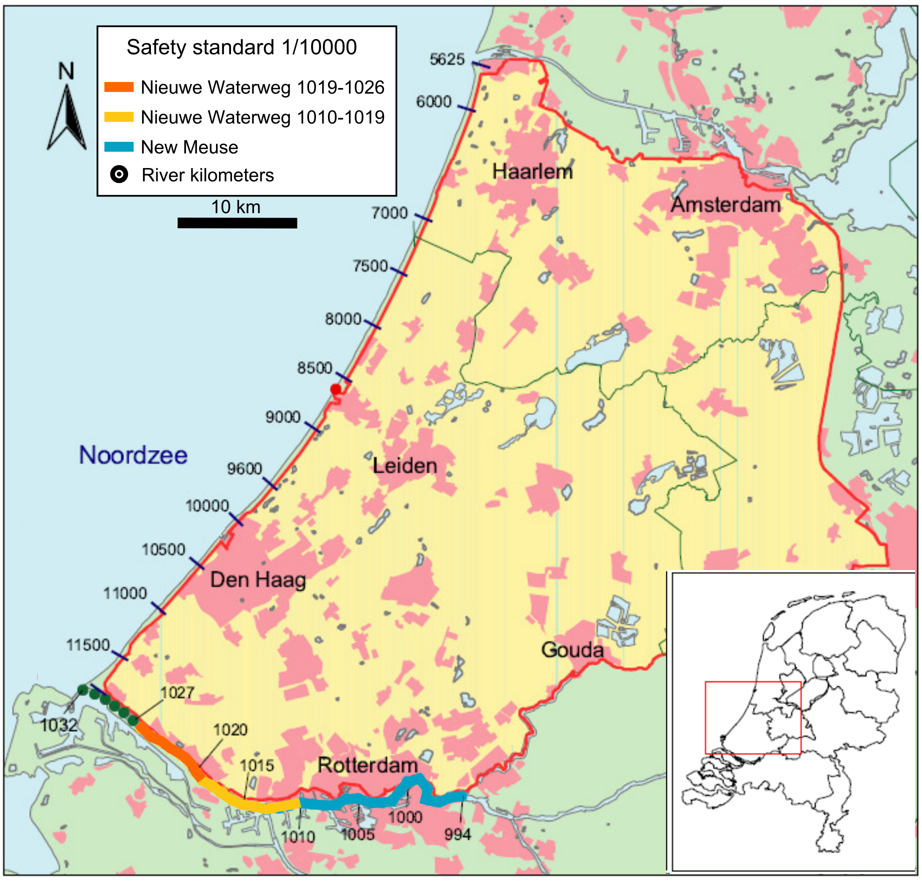

Figure 5-15: Dike-ring area 14 with the considered dike stretches

Dike-ring 14 part Nieuwe Waterweg east is mainly threatened by storm surges from the North Sea, which are handled by the Maeslantkering. However, the storm surge barrier can fail or be closed too late, such that the storm surges threat the dikes behind the barrier (Rijkswaterstaat, 2003). Peak discharges from the Rhine and less significant by the Meuse, have a smaller influence. Also tidal fluctuations are present, of which the influence decreases in the upstream direction. The loading characteristics along the dike stretches are highly correlated. The characteristics of each dike stretch are summarized in Table 5-7 and are deduced from the database in (Deltares, 2011d).

Table 5-7: Dike stretch characteristics for dike-ring 14 part Nieuwe Waterweg east

Parameter	Nieuwe Waterweg 1010-1019	Nieuwe Waterweg 1019-1026	New Meuse	
P(0)	0,0001	0,0001	0,0001	[1/year]
α_d	0,0363	0,0588	0,1143	[1/cm]
η	0,2	0,201	0,2	[cm/year]
V(0)*	9844	9844	9844	[M€]
ψ	0	0	0	[1/cm]
ζ	0	0	0	[1/cm]
C	9,9	9,9	45,4	[M€]
b	0,16	0,16	0,74	[M€/cm]

**Including 191 potential casualties with VOSL=6,7 M€ (Deltares, 2011c).*

Here, P(0) is the probability of flooding of the considered dike stretch in year t=0, α_d is a scale parameter related to the decimation height, η is the relative water level rise, V(0) is the potential flood damage in year t, ψ is an impact parameter for additional flood damage due to water level rise, ζ is an impact parameter for additional flood damage due to failure of increased dike height, C are the fixed investment costs for a dike reinforcement and b the variable dike reinforcement costs. The safety standard of dike-ring 48 equals 1/10000 per year, meaning that water levels occurring once every 10000 years on average must be withstood. Water levels occurring once every 1000 years are assumed to give sufficient monitoring information: λ=0,001 per year.

Three monitoring cases are considered:

- **Case 1: Extensive monitoring of stretch Nieuwe Waterweg 1010-1019**
  Monitoring with an advanced monitoring system S_2 along 9 km of the stretch Nieuwe Waterweg 1010-1019.
- **Case 2: Extensive monitoring of stretches Nieuwe Waterweg 1010-1019 and Nieuwe Waterweg 1019-1026**
  Monitoring with an advanced monitoring system S_2 along 16 km of the stretches Nieuwe Waterweg 1010-1019 and Nieuwe Waterweg 1019-1026.
- **Case 3: Extensive monitoring of stretches Nieuwe Waterweg 1010-1019 and Nieuwe Waterweg 1019-1026 with increased λ**
  Monitoring with an advanced monitoring system S_2 along 16 km of the stretches Nieuwe Waterweg 1010-1019 and Nieuwe Waterweg 1019-1026 and an increased value for the frequency of occurrence λ of a relevant loading event.

5.4.2 Case 1: Extensive monitoring of stretch Nieuwe Waterweg 1010-1019

This first case considers monitoring of the most downstream stretch of 9 km with an advanced monitoring system S_2. This stretch is directly located next to the canal Nieuwe Waterweg. The total installation costs of monitoring system S_2 are, with l_d=9 km:

$$C_{\text{installation}}(t_j) = 9 \cdot (350+200)\frac{1000}{50} \cdot 4 \cdot (1+0,2) = 475200 \text{ €}$$

These installation costs have to be invested every t_j=10 years. The yearly maintenance and operational costs sum up to:

$$C(t) = 0,1 \cdot 475200 + 0,1 \cdot 475200 = 95040 \text{ €/year}$$

The total discounted costs C_{sensor} over 300 years, with δ=5,5 %/year equal 2,97 M€. Monitoring system S_2 is assumed to obtain R=0,5 with λ=0,001 per year for this dike-ring. The obtained optimal investment strategies as computed with OptimaliseRing influence the probability of flooding of the monitored dike stretch as given in Figure 5-16.

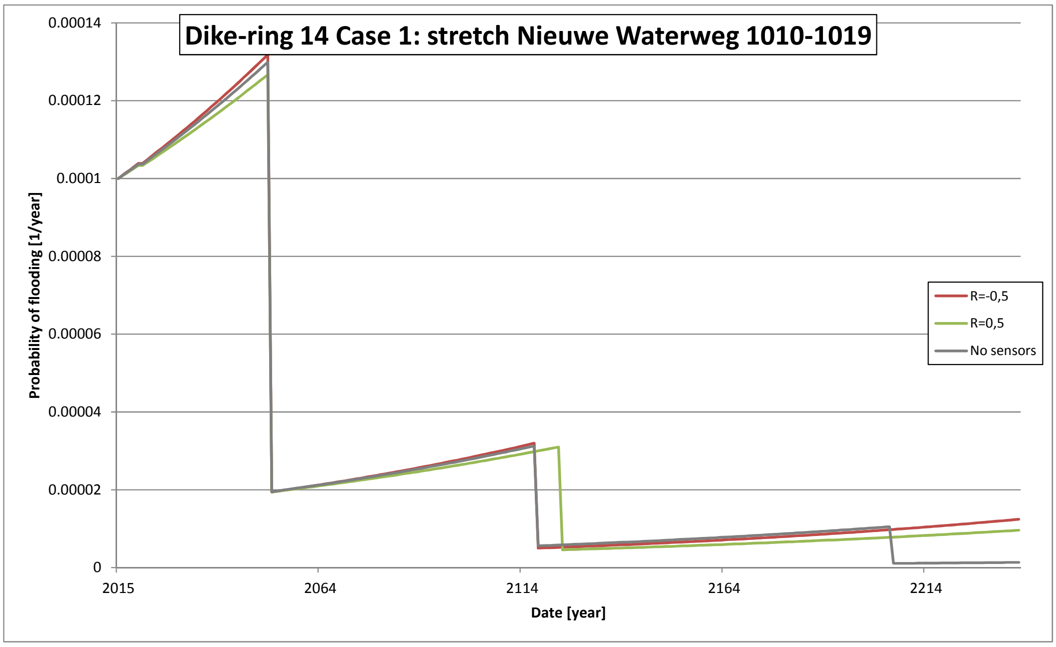

Figure 5-16: Optimal investment strategy for dike-ring 14 Case 1: stretch Nieuwe Waterweg 1010-1019 (considering λ=0,001, R=0,5 and R=-0,5)

The time of the first reinforcement is not affected by the monitoring information, but the magnitude of the reinforcement is increased for an indirect monitoring effect and decreased for a direct monitoring effect. The second reinforcement can be delayed with 6 years if a direct monitoring effect is obtained. A third reinforcement is not performed when the effect of monitoring is considered. The influence of the sensor monitoring is however negligible for monitoring effects, see Table 5-8.

Table 5-8: Cost-benefit analysis for case 1, considering λ=0,001, R=0,5 and R=-0,5

	Discounted E(costs) [M€]	Difference in E(costs) [M€]	Sensor costs C_{sensor} [M€]	Benefit-cost ratio ε_p [-]
Expected (no sensor)	75,9	-	-	-
Direct monitoring effect R=0,5	75,9	0	2,97	0
Indirect monitoring effect R=-0,5	75,9	0	2,97	0

The benefit-cost ratio ε_p for Case 1 equals 0 for both R=0,5 and R=-0,5. Sensor monitoring in this case is not cost-effective, because the additional costs does not lead to benefits. The monitoring system cannot be adapted in order to be cost-effective, as no benefits are obtained in this case.

5.4.3 Case 2: Extensive monitoring of stretches Nieuwe Waterweg 1010-1019 and Nieuwe Waterweg 1019-1026

This second case considers the monitoring of a stretch of 7 km with the advanced monitoring system S_2, additional to the initial stretch of 9 km in case 1. The total installation costs of monitoring system S_2 are, with l_d=16 km:

$$C_{\text{installation}}(t_j) = 16 \cdot (350 + 200)\frac{1000}{50} \cdot 4 \cdot (1 + 0,2) = 844800 \text{ €}$$

These installation costs have to be invested every t_j=10 years. The yearly maintenance and operational costs sum up to:

$$C(t) = 0,1 \cdot 844800 + 0,1 \cdot 844800 = 168960 \text{ €/year}$$

The total discounted costs C_{sensor} over 300 years, with δ=5,5 %/year equal 5,28 M€. Monitoring system S_2 is assumed to obtain R=0,5 with λ=0,001 per year for this dike-ring. The obtained optimal investment strategies as computed with OptimaliseRing influence the probability of flooding of the monitored dike stretch as given in Figure 5-17 and Figure 5-18.

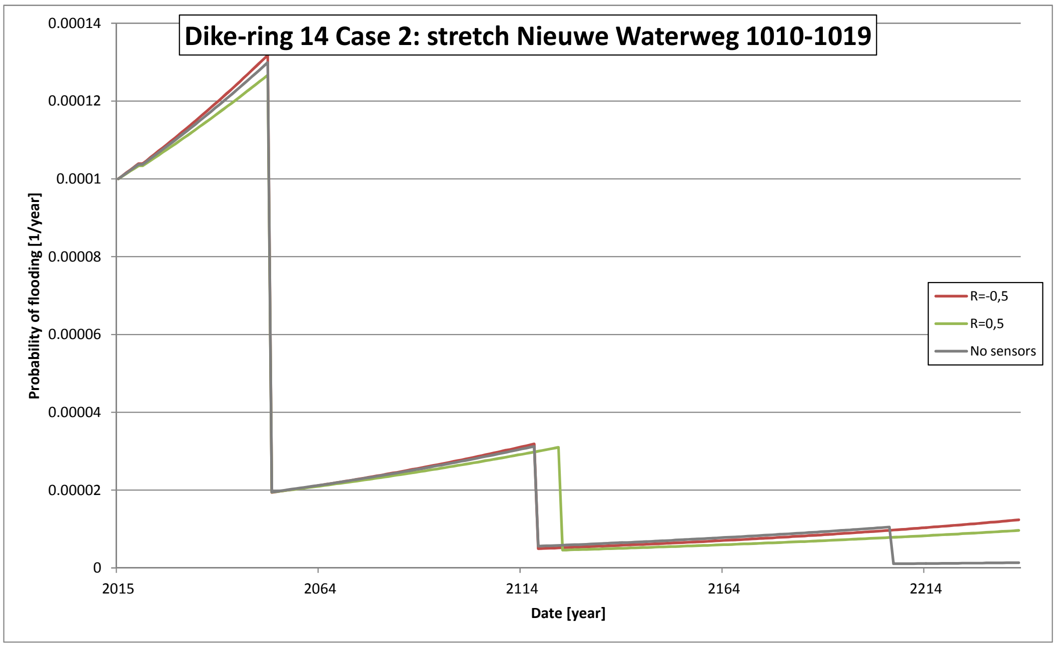

Figure 5-17: Optimal investment strategy for dike-ring 14 Case 2: stretch Nieuwe Waterweg 1010-1019 (considering λ=0,001, R=0,5 and R=-0,5)

The optimal investment strategy for stretch Nieuwe Waterweg 1010-1019 in Case 2 is similar to the strategy obtained in Case 1. After all, the same monitoring system has been applied in both cases.

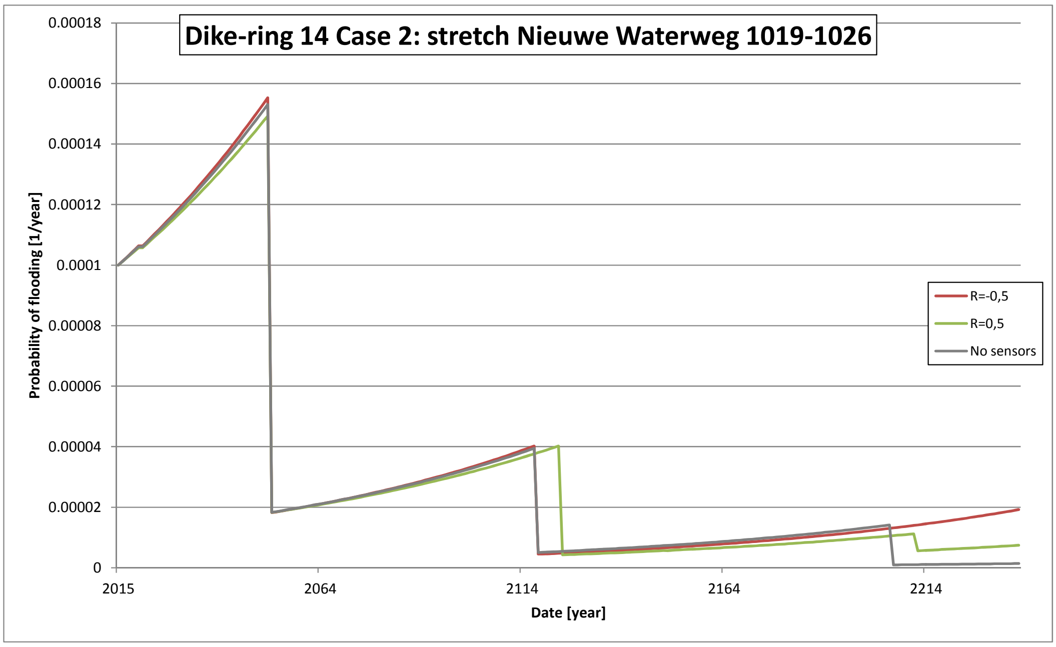

Figure 5-18: Optimal investment strategy for dike-ring 14 Case 2: stretch Nieuwe Waterweg 1019-1026 (considering λ=0,001, R=0,5 and R=-0,5)

The optimal investment strategy for stretch Nieuwe Waterweg 1019-1026 has been affected due to the installed monitoring system. The first reinforcement is only adapted in terms of the magnitude of the reinforcement. The second and third reinforcement is delayed with 6 years for a direct monitoring effect. Whereas, the second reinforcement is unaffected for an indirect monitoring effect and the third reinforcement is not executed at all. The effect of the monitoring on the expected discounted costs is still marginal and the results of the cost-benefit analysis are given in Table 5-9.

Table 5-9: Cost-benefit analysis for case 2, considering λ=0,001, R=0,5 and R=-0,5

	Discounted E(costs) [M€]	Difference in E(costs) [M€]	Sensor costs C_{sensor} [M€]	Benefit-cost ratio ε_p [-]
Expected (no sensor)	75,9	-	-	-
Direct monitoring effect R=0,5	75,8	0,1	5,28	0,02
Indirect monitoring effect R=-0,5	76,0	-0,1	5,28	-0,02*

**The negative benefit-cost ratio is caused by the unforeseen risk leading to higher costs than anticipated on beforehand. The value of information has not been taken into account (see paragraph 5.2.4).*

The benefit-cost ratio ε_o for Case 2 equals 0,02 for R=0,5 and -0,02 for R=-0,5. Sensor monitoring is in this case not cost-effective, because of the small obtained benefit. The monitoring costs have to be drastically reduced with purchase costs p=5 €/sensor and e=5 €/CPT push-in to become cost-effective for R=0,5 (C_{sensor}=0,1 M€ and ε_p=1).

5.4.4 Case 3: Extensive monitoring of stretches Nieuwe Waterweg 1010-1019 and Nieuwe Waterweg 1019-1026 with increased λ

This third case considers the same monitoring as in case 2. Monitoring of the last stretch New Meuse is not considered, because of physical complications with the dikes due to harbor activities. Further updating of the monitoring system is expected not to have much effect, as results from the previous two cases. Therefore, only increasing the frequency of occurrence λ can affect the effect of the sensor monitoring. It is assumed that loading conditions with λ=0,005 per year gives relevant information instead of the earlier determined value of λ=0,001 per year. Yet, a possible reason for increasing λ in this case might be the closure regime of the Maeslantkering storm surge barrier: accidental closure failures can lead to more frequent loading events than expected. The total discounted sensor costs C_{sensor} equal the costs of Case 2, namely 2,97 M€.

Monitoring system S_2 is assumed to obtain R=0,5 and adapted frequency of occurrence λ=0,005 per year. The obtained optimal investment strategies as computed with OptimaliseRing influence the probability of flooding of the monitored dike stretch as given in Figure 5-19 and Figure 5-20.

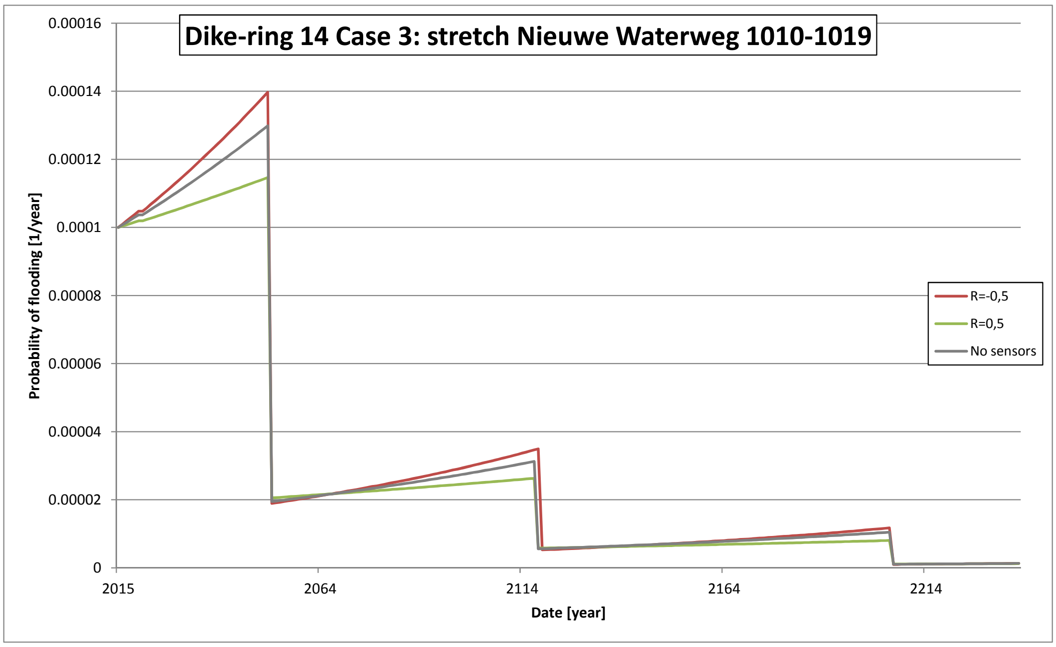

Figure 5-19: Optimal investment strategy for dike-ring 14 Case 3: stretch Nieuwe Waterweg 1010-1019 (considering λ=0,005, R=0,5 and R=-0,5)

The effect of the sensor monitoring is significantly increased compared to Case 1 and 2 for the stretch Nieuwe Waterweg 1010-1019. Yet, the first and third reinforcements are only adapted in terms of magnitude and not in time of reinforcement. The second reinforcement is delayed with 1 year for the indirect monitoring effect. A direct monitoring effect leads to a smaller second reinforcement.

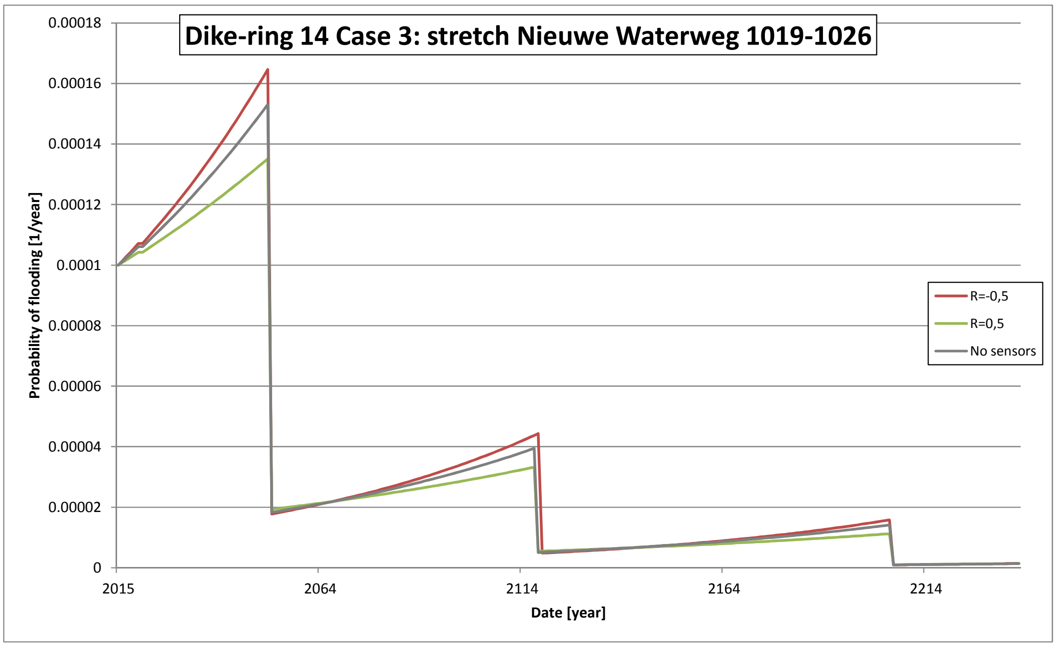

Figure 5-20: Optimal investment strategy for dike-ring 14 Case 3: stretch Nieuwe Waterweg 1019-1026 (considering λ=0,005, R=0,5 and R=-0,5)

Again, the impact of the sensor monitoring is increased for the stretch Nieuwe Waterweg 1019-1026. Similar dike reinforcement strategies are obtained for this stretch, as was obtained for stretch Nieuwe Waterweg 1010-1019: the magnitude of the reinforcements is adapted due to the sensor monitoring and the second reinforcement is delayed with 1 year for the indirect monitoring effect. The differences in the discounted expected costs have been increased compared to the previous cases, see Table 5-10.

Table 5-10: Cost-benefit analysis for case 3, considering λ=0,005, R=0,5 and R=-0,5

	Discounted E(costs) [M€]	**Difference in E(costs) [M€]**	**Sensor costs C_{sensor} [M€]**	**Benefit-cost ratio ε_p [-]**
Expected (no sensor)	75,9	-	-	-
Direct monitoring effect R=0,5	75,5	0,4	5,28	0,08
Indirect monitoring effect R=-0,5	76,1	-0,2	5,28	-0,04*

**The negative benefit-cost ratio is caused by the unforeseen risk leading to higher costs than anticipated on beforehand. The value of information has not been taken into account (see paragraph 5.2.4).*

The benefit-cost ratio ε_o for Case 3 equals 0,02 for R=0,5 and -0,02 for R=-0,5. Sensor monitoring is in this case not cost-effective. Yet, Case 3 is the most cost-effective regarding the previous cases, yet the possibility for the adaptation of λ must be analyzed cautiously. The monitoring costs have to be reduced with purchase costs p=20 €/sensor and e=20 €/CPT push-in to become cost-effective for R=0,5 (C_{sensor}=0,38 M€ and ε_p=1).

5.5 Conclusions

A cost-benefit method has been set up to determine the cost-effectiveness of sensor monitoring for the application in periodic flood safety assessment with a flood risk approach. Optimal investment strategies for dike reinforcements are determined for an expected situation without sensor monitoring, a potential direct monitoring effect (i.e. the prior flooding probability is larger than the posterior flooding probability) and a potential indirect monitoring effect (the prior flooding probability is smaller than the posterior flooding probability) of the monitoring data. The optimal investment strategy is determined by the minimum expected costs over a time period of 300 years, consisting of the discounted total flood risk and discounted reinforcement costs. The influence of sensor monitoring is determined with a reduction rate R and frequency of occurrence λ corresponding to a relevant loading condition.

Two case studies are performed to investigate the cost-effectiveness of monitoring systems consisting of MEMS. Dike-ring part 48 Rhine and IJssel downstream and dike-ring part 14 Nieuwe Waterweg east are considered, in which monitoring is in both cases not cost-effective under the taken assumptions (ε_p<1). The benefit-cost ratio considering the two case studies is the highest for dike-ring part 48 Rhine and IJssel downstream. The monitoring influence is marginal for dike-ring part 14, due to the low frequency of occurrence λ. Increasing the value of λ grants more monitoring influence on the optimal investment strategy and higher benefit-cost ratios. The determination of the reduction rate R and frequency of occurrence λ is ambiguous and requires further research. Moreover, the determination of negative benefit-cost ratios ε_p, i.e. due to negative values of R, does not incorporate the time and costs needed to mitigate the identified unforeseen risk. Due to the ambiguous value of R in the current state of knowledge, the absolute results of these case studies must be treated with care.

Combining the potential direct and indirect monitoring effects in the cost-benefit model is recommended to be subject for further research. Especially concerning the value of information if sensor monitoring leads to an increase of the assessed flooding probability.

6 Cost-benefit analysis for the operational situation

A cost-benefit model is treated in this chapter to determine the cost-effectiveness of sensor monitoring in the context of early warning during operational situations. However, the relevance of controlling this operational situation for the Dutch flood safety approach is disputable in the first place, see paragraph 1.4.4. First, an introduction is given in paragraph 6.1, followed by paragraph 6.2 in which the general model setup is elaborated. Case studies are worked out in paragraphs 6.3 and 6.4 for respectively dike-ring areas 48 and 14. Finally, the conclusions are summarized in paragraph 6.5.

6.1 Introduction

This chapter considers a cost-benefit model which has been set up to get insight into the cost-effectiveness of sensor monitoring for the use of early warning. The presented model is a suggested approach to elaborate the cost-effectiveness of sensor monitoring. Solely the benefit in the context of short-term reaction on early warning signs from sensor monitoring are considered. Benefits in the context of permanent dike reinforcements for the periodic safety assessment are evaluated separately in chapter 5. Therefore, the presented model only considers the benefit from temporary measures which reduce the flood risk and discards the influence of permanent reinforcements. It should be emphasized that the benefit is derived using an initial situation in which no emergency measures are executed at all times: emergency measures are assumed to be executed based on sensor monitoring only. This situation is not representative for the current crisis management approach, as emergency measure may be executed based on other information.

This model has the objective to evaluate the cost-effectiveness of sensor monitoring prior to sensor installation. By giving insight into the costs and benefits, the model aims to support the decision on installing a sensor monitoring system by economic considerations. The obtained benefits during the operational situation depends on local, dynamic circumstances. These circumstances vary per considered dike, sensor technique and emergency flood protection measure. The presented model has not the objective to evaluate the cost-effectiveness of sensor monitoring in these varying circumstances, by considering an exhaustive enumeration of examples. The basic principles on how to implement sensor monitoring information for early warning have been treated in paragraph 3.4. Requirement for benefits from early warning situations is the frequency of occurrence of such a situations: after all, no benefits can be obtained from the early situation if this situation is not present.

It should be emphasized that the calculated benefit-cost ratios have limited value in absolute terms, because the defined variables for the sensor technique characteristics (i.e. prediction time and operational reliability and availability) are not representative for the current state of sensor performance, according to the analysis in chapter 2.

6.2 Model setup

6.2.1 Definition of the benefit-cost ratio

The application of sensor monitoring for early warning purposes during the operational situation requires a cost-benefit consideration to determine the cost-effectiveness of the monitoring. The benefit is formed by the increased flood safety obtained by taking a flood protection measure, executed on the base of the early warning monitoring system. Costs are made due to the investment in the monitoring system and the execution of the flood protection measure. The benefit-cost ratio for applying sensor monitoring in the operational situation is defined as:

$$\varepsilon_o = \frac{\text{benefit}}{\text{cost}} = \frac{\text{E(damage)}_{\text{a-priori}} - \text{E(damage)}_{\text{a-posteriori}}}{C_{\text{sensor}} + \text{E(costs)}_{\text{measure}}}$$

ε_o	Benefit-cost ratio for the operational situation	[-]
$\text{E(damage)}_{\text{a-priori}}$	Discounted expected flood damage for the a-priori situation, i.e. no sensors applied, over a given time period	[€]
$\text{E(damage)}_{\text{a-posteriori}}$	Discounted expected flood damage for the a-posteriori situation, i.e. with sensors applied, over a given time period	[€]
C_{sensor}	Costs made due to the application of sensor monitoring	[€]
$\text{E(costs)}_{\text{measure}}$	Expected costs made due to the execution of a flood protection measure	[€]

The use of sensor monitoring is cost-effective if the benefit-cost ratio $\varepsilon_o>1$: the benefits exceed the costs. This benefit-cost ratio for the operational situation is difficult to compare with the benefit-cost ratio as defined for the periodic safety assessment. The principle definition of benefit-cost ratio in paragraph 5.2.1 is extended with the expected costs for the execution of a flood protection measure $\text{E(costs)}_{\text{measure}}$ and the investment costs for dike reinforcements I(strengthening) have been excluded. It should be emphasized that both cost-benefit models have a different approach and can therefore not be combined directly. The expected flood damage for the situation without sensor monitoring is defined as:

$$\text{E(damage)}_{\text{a-priori}} = \sum_{t=0}^{T} \frac{P_f'(t) \cdot V(t)}{(1+\delta)^t}$$

$\text{E(damage)}_{\text{a-priori}}$	A-priori discounted expected flood damage, without sensor monitoring	[€]
$P_f'(t)$	A-priori probability of flooding in year t, without the use of an early warning monitoring system	[1/year]
V(t)	Potential damage due to a flood in year t	[€]
δ	Discount rate	[%/year]

The a-posteriori expected costs for the situation with sensor monitoring is equal to the expected discounted flood damage over period T:

$$\text{E(damage)}_{\text{a-posteriori}} = \sum_{t=0}^{T} \frac{P_f''(t) \cdot V(t)}{(1+\delta)^t}$$

$\text{E(damage)}_{\text{a-posteriori}}$	A-posteriori discounted expected flood damage, with sensor monitoring	[€]
$P_f''(t)$	A-posteriori probability of flooding in year t, including the effect of an early warning monitoring system	[1/year]
V(t)	Potential damage due to a flood in year t	[€]
δ	Discount rate	[%/year]

The monitoring costs C_{sensor} are determined according to the definition stated in 5.2.3. Any additional costs for real-time processing of the monitoring data as required for the early warning implementation is not considered. The expected costs for the execution of the flood protection measure $\text{E(costs)}_{\text{measure}}$ is defined in 6.2.4. The potential flood damage V(t) equals the definition given in Appendix G and increases over time due to the expected economic growth γ.

6.2.2 Definition of the flooding probability

The determination of the flooding probability per year with and without a monitoring system (i.e. respectively $P_f''(t)$ and $P_f'(t)$) is done according to the event tree in paragraph 3.5.5, analogue to the implementation with the best-way-out observational method, see Figure 6-1.

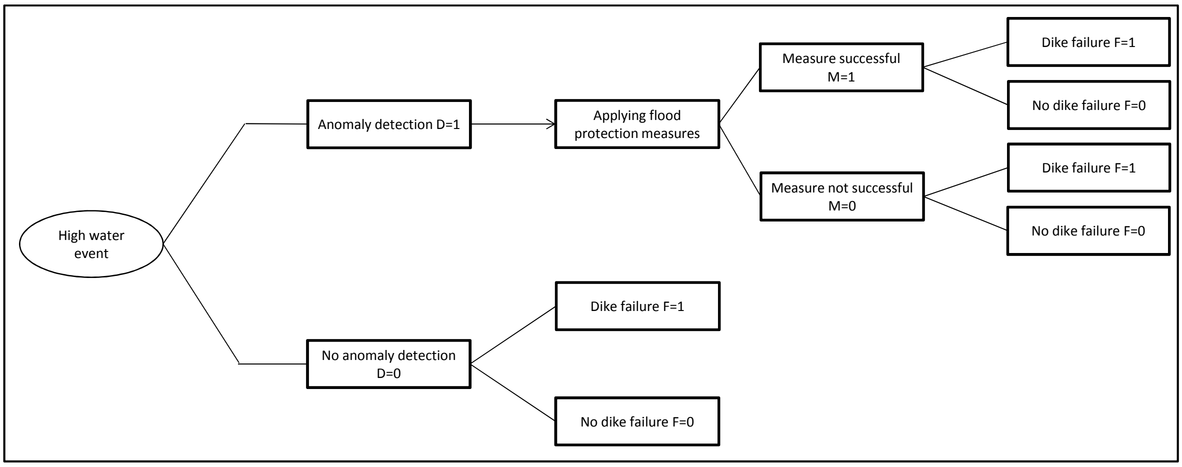

Figure 6-1: Event tree for the application of sensor monitoring in operational situations

The event tree considers the working of an early warning sensor system in the case of a high water event, on which the decision is based whether to execute a flood protection measure or not. This model implies the following assumptions:

- An anomaly detection by the monitoring system in case of no high water event does not cause a dike failure. Only anomalies detected during high water events are considered and anomalies detected under daily circumstances are assumed to be handled by the responsible engineer (e.g. as measurement error)
- The monitored observable variable must have a substantiated and demonstrated relation with the failure mechanism considered
- A flood protection measure is applied based on the early warning monitoring system: a measure is always executed for D=1 and never executed for D=0
- The flood protection measure reduces the probability of flooding and does not affect the consequences of the flood

The mathematical derivation of dike failure according to the event tree in Figure 6-1 is given in Appendix I. Using the derivation and notation from Appendix I, the a-posteriori probability of flooding per year, with an early warning monitoring system, is defined as:

$$P_f''(t) = P_{f,m1} \cdot P_{m1} \cdot P_{d1} \cdot P_H(t) + P_{f,m0} \cdot P_{m0} \cdot P_{d1} \cdot P_H(t) + P_{f,d0} \cdot P_{d0} \cdot P_H(t)$$

$P_f''(t)$	A-posteriori probability of dike failure in year t	[1/year]
$P_{f,m1}$	Probability that the dike fails, given the measure is applied and an anomaly is detected and a high water event is present	[-]
P_{m1}	Probability that the measure is applied successfully, given that an anomaly is detected and a high water event is present	[-]
P_{d1}	Probability that an anomaly is detected, given a high water event	[-]
$P_H(t)$	Probability of occurrence on a high water event in year t	[1/year]
$P_{f,m0}$	Probability that the dike fails, given the measure is not applied and an anomaly is detected and a high water event is present	[-]
P_{m0}	Probability that the measure is not applied successfully, given that an anomaly is detected and a high water event is present: $P_{m0}= 1-P_{m1}$	[-]
$P_{f,d0}$	Probability that the dike fails, given no anomaly is detected and a high water event is present	[-]
P_{d0}	Probability that no anomaly is detected, given a high water event: $P_{d0}=1- P_{d1}$	[-]

The a-priori probability of flooding per year, without the sensor monitoring system, is also derived from Figure 6-1, with the difference that a flood protection measure is not applied (i.e. the effect of the sensor monitoring system is only visible due to the emergency flood protection measure). The a-priori dike failure probability $P_f'(t)$ is elaborated from Figure 6-1 with $P_{m1}=0$ and $P_{m0}=1$. Hence, the influence of the dike sensors is modeled by the reduction factor and the probability that the flood protective measure can be applied on time. The a-priori dike failure probability per year is defined as:

$$P_f'(t) = P_{f,m0} \cdot P_{d1} \cdot P_H(t) + P_{f,d0} \cdot P_{d0} \cdot P_H(t)$$

$P_f'(t)$	A-priori probability of dike failure in year t	[1/year]
P_{d1}	Probability that an anomaly is detected, given a high water event	[-]
$P_H(t)$	Probability of occurrence on a high water event in year t	[1/year]
$P_{f,m0}$	Probability that the dike fails, given the measure is not applied and an anomaly is detected and a high water event is present	[-]
$P_{f,d0}$	Probability that the dike fails, given no anomaly is detected and a high water event is present	[-]
P_{d0}	Probability that no anomaly is detected, given a high water event: $P_{d0}=1- P_{d1}$	[-]

Here, the dike failure probabilities $P_{f,m1}$ and $P_{f,m0}$ are conditional dike failure probabilities respectively with and without emergency measure applied, given the detection of an anomaly and a high water event. A high value of $P_{f,m0}$ is obtained by an early warning system having a thorough relation with an upcoming failure: the relation of the monitored observable variable with the failure mechanism is important. Higher values of $P_{f,m0}$ grant more benefit than low values. $P_{f,m0}$ and $P_{f,m1}$ are assumed to be related according to:

$$P_{f,m1} = \frac{P_{f,m0}}{R_m}$$

In which R_m is defined as the reduction rate due to the executed measure, with $R_m \geq 1$. The initial situation has a dike failure probability $P_{f,m0}$ and the emergency flood protection measure reduces the initial dike failure probability $P_{f,m0}$ with a factor $1/R_m$. Consequently, a measure with a value of $R_m=1$ has no effect on the dike failure probability. The larger the value of R_m, the larger the effect on the failure probability. It should be emphasized that R_m represents a reduction of the total dike failure probability, consisting of all relevant failure mechanisms. Thus, applying the same flood protection measure on another dike stretch results in a different value of R_m.

The parameter $P_{f,d0}$ represents the probability that the dike fails, when no anomaly has been detected during a high water theat. The value of $P_{f,d0}$ indicates the amount of missed alarms: the conditional dike failure probability in case the monitoring system does not predict a dike failure. Also, the contribution of other failure mechanisms than considered with the sensor monitoring system to the failure probability are incorporated in $P_{f,d0}$. The determination of this probability by expert judgment can be complicated. An upper boundary can be computed, if the following assumption is made (see also Appendix I): the probability of a dike failure for a given high water event, is higher when an anomaly has been detected than as no anomaly has been detected. This assumption agrees with the principle of a well performing monitoring system. Despite the difficulties facing the determination of this parameter, $P_{f,d0}$ has no effect on the benefit-cost ratio, since both the a-priori and a-posteriori flooding probabilities are affected by $P_{f,d0}$ by the same order.

The probability that an anomaly is detected, given a high water event, P_{d1} depends on the reliability of the monitoring system during the high water event and the threshold value for an anomaly. A reliable monitoring system is required for continuous early warning monitoring: down-time of the system leads to no possibility for an anomaly detection and thereby forms a risk. Here, an anomaly is defined as the exceeding of a threshold value, for which the dike safety is considered insufficient. The variable consists of the real-time failure probability exceeding a threshold value (see paragraph 3.4.1) or the observable variable (as in the IJkdijk experiments, see paragraph 3.4.2). The threshold value represents the willingness to take the extent of risk: a low anomaly threshold suits a risk aversive flood policy, leading to relative frequently executed flood protection measures and the associated costs are high. The threshold value must be determined beforehand.

The probability of a high water event in year t $P_H(t)$ represents the occurrence frequency of a flooding threat. Thus the frequency of a flood being on hand. In case of macro stability, this is often related to a high outer water level. The benefit of an early warning monitoring system is lower as the occurrence frequency $P_H(t)$ is low. After all, the fictitious case with $P_H(t)=0$ leads to the situation that the early warning situation never occurs, mitigating measures are never taken and thus the flood risk is not reduced. In this case study, it is assumed that $P_H(t)$ equals the probability of flooding P(t) as used in chapter 5, which increases over time due to relative water level rise, see also Appendix G. The occurrence of one specific water level is considered.

The probability of a successful execution of the flood protection measure P_{m1} is elaborated in paragraph 6.2.3, with the assumption that partial completion of the execution has no influence on the dike failure probability $P_{f,m0}$. The probability of unsuccessful execution is defined as $P_{m0}=1- P_{m1}$.

6.2.3 Probability of successfully executing the measure P_{m1}

The probability of a successful execution of the flood protection measure P_{m1} is a complex, though important parameter. The value of P_{m1} depends on the available and required time to execute the intended measure and the constructional reliability of the measure. First, the emergency measure must be executed on time. The available time is given by the prediction of the monitoring system: the larger the available time to execute the measure, the larger the probability that the measure is executed on time. The required time is the reaction time needed to execute the emergency flood protection measure which depends on numerous aspects like the decision making, the required length of the emergency measure, the accessibility of the dike (e.g. traffic congestions), the transportation distance to the dike, the space available for deployment and extreme weather conditions. These aspects are very local and vary in time. The shorter the time required, the larger the probability that the measure is executed on time. The required execution time can be reduced by preparing for an upcoming operational situation. Training exercises are meant to improve the emergency process, after an anomaly has been detected by the monitoring system. The decision time can be reduced by creating and maintaining short lines to responsible authorities within the bureaucracy system. Also, the transportation time can be reduced by storing the required materials nearby and keeping access roads clear of traffic. The preparedness for an upcoming operational situation will however increase the costs to execute the emergency measure. Apart from these logistical problems, the flood protection measure has a probability of constructional failure, which reduces the probability P_{m1}. After all, if the emergency measure fails after completion, the dike failure probability is not reduced. It should be emphasized that the constructional failure of the flood protection measure is not considered in this research. In general, the success of emergency measures is considered to be low, because of the complexity and uncertainty of emergency measures (Vrijling et al, 2010). Yet, the application of sensor monitoring in the operational situation relies on the temporary reduction of the flooding probability on the short-term.

Theoretically, a monitoring system can give a perfect prediction of an upcoming dike failure (i.e. $P_{d1}=1$). But if the available time to execute the emergency measure is short, the probability of successfully executing the measure P_{m1} is small. On the other hand, an unreliable monitoring system (i.e. P_{d1} is small) might give a long prediction time, which will result in a higher probability P_{m1}.

Starting point for the execution is a tailor-made crisis plan containing: the availability of the required material nearby and available deployment space at the dike. Thus, P_{m1} is assumed as the probability that the time available (i.e. early warning potential of the monitoring system) exceeds the time required to execute the intended measure. The corresponding limit state function is defined as:

$$Z_{P_{m1}} = T_{\text{required}} - T_{\text{available}}$$

$Z_{P_{m1}}$	Limit state function for P_{m1}	
T_{required}	Required time to execute the flood protection measure	[hour]
$T_{\text{available}}$	Available time due to the early warning potential of the monitoring system	[hour]

The probability of a successful execution of the flood protection measure P_{m1} is the probability that T_{required} is smaller than $T_{\text{available}}$:

$$P_{m1} = P(Z_{P_{m1}} < 0) = P(T_{\text{required}} < T_{\text{available}})$$

P_{m1}	Probability of a successful execution of the flood protection measure	[-]
$P(Z_{P_{m1}} < 0)$	Probability that $Z_{P_{m1}}$ has a negative value	[-]

The mean available time $T_{\text{available}}$ is derived from the performance of the sensor monitoring system. Chapter 2 gives insight in the early warning potentials of multiple sensor techniques. As has been stated in paragraph 2.6, these results are disputable in the current state of investigation. The required time T_{required} depends on the preparedness, decision making time, transport time and deployment time of the flood protection measure, which are random variables. Thereby, the $T_{required}$ is defined as:

$$T_{\text{required}} = T_{\text{decision}} + T_{\text{transport}} + T_{\text{deployment}}$$

$T_{required}$	Time required to successfully execute an emergency flood protection measure	[hour]
$T_{decision}$	Time needed for decision making upon starting mobilizing for execution of the flood protection measure	[hour]
$T_{transportation}$	Transportation time needed upon starting the deployment of the flood protection measure	[hour]
$T_{deployment}$	Time needed for complete deployment of the flood protection measure	[hour]

The decision making time $T_{decision}$ involves the time needed to get the authorization to start the mobilization for execution of the flood protection measure. This decision time can be significant for complex hierarchic bureaucracies, in which many authorities are involved. An estimation for the required decision time is $T_{decision}$=4 hours, derived from decisions on preventive evacuation in (Frieser, 2004). The transportation time $T_{transportation}$ accounts for the arrival time at the dike after the decision has been made. A value of $T_{transportation}$=3 hours is assumed in this case study. A low preparedness results in higher values of $T_{decision}$ and $T_{transportation}$, and lower $E(costs)_{measure}$ and vice versa. The deployment time $T_{deployment}$ is defined as:

$$T_{\text{deployment}} = \frac{l_d}{D_r \cdot N_w \cdot 2}$$

$T_{deployment}$	Time needed for complete deployment of the flood protection measure	[hour]
D_r	Rate of deployment for the flood protection measure	[m/hour]
N_w	Number of work forces	[-]
l_d	Length of the monitored dike	[m]

The length of the flood protection measure determines $T_{deployment}$: the longer the required flood protection, the longer it takes to complete the execution. In case of an anomaly detection, the monitoring system will indicate the location of the critical spot. However, both hydraulic loading and dike strength conditions are correlated within a monitored dike section. Therefore, it is reasonable that as soon as an anomaly has been detected at one location, anomalies are detected at other locations in the dike as well. This study assumes that in case of an anomaly detection during high water, half of the dike length l_d is likely to be reinforced. The rate of deployment D_r determines the execution speed for the flood protection measure, per work force N_w. The deployment rate will increase as the available work force N_w increases, reducing $T_{required}$. However, increasing the number of workers and trucks causes logistic problems, especially with high time pressure in such situations. Therefore, a number of N_w= 4 work forces is assumed to be available without logistic problems: the access road to the dike comes from two directions, such that a work force can begin deploying at each side. Another work force can pass at either side to start deploying the emergency measure at another required location.

6.2.4 Flood protection measure costs

Numerous flood protection measures are available for temporarily reducing the flood risk on the short-term. The choice for a measure depends on the situation, in which the critical failure mechanism, logistic limitations and time are important aspects. Of the different types of measures, the focus in this cost-benefit analysis lies on decreasing the failure probability by increasing the dike strength. The expected costs of a sensor system $E(costs)_{measure}$ depend on the purchase costs, preparing costs and deployment costs and are discounted over the period T:

$$E(\text{costs})_{\text{measure}} = C_{\text{purchase}}(t=0) + \sum_{t=0}^{T} \frac{C_{\text{preparing}}(t)}{(1+\delta)^t} + \sum_{t=0}^{T} \frac{P_H(t) \cdot P_{d1} \cdot (C_{\text{deployment}} + C_{\text{purchase}})}{(1+\delta)^t}$$

$E(\text{costs})_{\text{measure}}$	Expected costs made due to the execution of a flood protection measure	[€]
C_{purchase}	Purchase costs required for the flood protection measure	[€]
$C_{\text{preparing}}$	Yearly preparing costs	[€]
$P_H(t)$	Probability of the occurrence of a high water event per year	[1/year]
P_{d1}	Probability that an anomaly is detected, given a high water event	[-]
$C_{\text{deployment}}$	Costs for the deployment of the flood protection measure	[€]

The execution of a flood protection measure requires preparation for the flood protection measure. Therefore, the materials needed for a potential flood protection measure are purchased when the monitoring system is installed at t=0, and stored upon usage. The purchase costs C_{purchase} are assumed as:

$$C_{\text{purchase}} = C_p \cdot \frac{l_d}{2}$$

C_{purchase}	Purchase costs for the flood protection measure materials	[€]
C_p	Purchase costs of the flood protection measure per m	[€/m]
l_d	Length of the monitored dike	[m]

The costs for preparation are yearly costs assumed to be consisting of material storage, training exercises and deployment tests. The yearly preparing costs $C_{\text{preparing}}$ are assumed as a fraction of the purchase costs C_{purchase}:

$$C_{\text{preparing}}(t) = f_p \cdot C_{\text{purchase}}$$

$C_{\text{preparing}}(t)$	Yearly preparing costs (e.g. material storage, training, testing)	[€/year]
f_p	Factor for the yearly preparing costs: $f_p>0$	[-]
C_{purchase}	Purchase costs for the flood protection measure materials	[€]

The factor f_p is assumed at 0,1. After the installation of the monitoring system and the purchase of the materials required for a flood protection measure, the yearly expected costs of the flood protection measure consist of the yearly probability of applying the measure, times the associated costs of the measure. The yearly probability of applying the measure is modeled as the yearly probability of occurrence of a high water event $P_H(t)$ times the probability of detection given this event P_{d1}. The associated costs consist of $C_{\text{deployment}}$ and C_{purchase}, of which $C_{\text{deployment}}$ is defined as:

$$C_{\text{deployment}} = C_D \cdot \frac{l_d}{2}$$

$C_{\text{deployment}}$	Costs for the deployment of the flood protection measure	[€]
C_D	Costs of deployment and removal of the flood protection measure per meter	[€/m]
l_d	Length of the monitored dike	[m]

The costs for executing a flood protection consists of the deployment of the measure and the removal costs. These costs are defined as $C_{\text{deployment}}$ and depend on the length of the measure and the costs per meter C_D. Again, it is assumed that in case of an anomaly detection given high water, half of the dike length l_d needs to be reinforced (as is the case for $T_{deployment}$ in paragraph 6.2.3). Also, if a flood protection measure has been executed, the old materials are not reusable. Thus $C_{purchase}$ has to be accounted too in order to be prepared for a possible next detected threat. This approach assumes that the purchased materials have an infinite life time when stored (sand and plastic are low perishable materials after all).

6.3 Case study dike-ring 48

6.3.1 Characteristics of the early warning monitoring system

This case study considers the application of an early warning monitoring system in dike-ring 48 part Rhine and IJssel downstream. The early warning monitoring system consists of MEMS sensor modules, similar to the monitoring system S_2 in chapter 5 and is considered over a period of T=300 year. Therefore, the monitoring costs C_{sensor} per dike stretch equal the costs as derived in chapter 5. The characteristics of each dike stretch are summarized in Table 6-1 and are deduced from the database in (Deltares, 2011d).

Table 6-1: Dike stretch characteristics for dike-ring 48

Parameter	Canal of Pannerden	IJssel	Old IJssel	
l_d	6	21	12	[km]
$P(0)= P_H(0)$	0,000574	0,000605	0,000605	[1/year]
α_d	0,057	0,0635	0,0635	[1/cm]
η	0,294	0,494	0,494	[cm/year]
V(0)*	7092	7092	7092	[M€]

**Including 21 potential casualties with VOSL=6,7 M€ (Deltares, 2011c).*

Here, l_d refers to the total length of the considered dike stretch, P(0) is the probability of flooding of the considered dike stretch in year t=0, α_d is a scale parameter related to the decimation height, η is the relative water level rise and V(0) is the potential flood damage in year t.

The applied early warning monitoring system is considered to be a reliable detection system with P_{d1}=0,8. The reliability and performance of the sensor techniques is not explicitly considered in this research. Also, the monitoring system is assumed to predict failures with $P_{f,m0}$=0,8; if an anomaly has been detected given a high water event and no measure is executed, the conditional failure probability is 0,8. The sensitivity of the benefit-cost ratio for the parameters P_{d1} and $P_{f,m0}$ is considered separately for each case in paragraph 6.3.5. However, one would only rely on a monitoring system with the purpose of early warning if it is considered a reliable system, predicting dike failures with high certainty. The available warning time $T_{available}$ is derived from the current early warning potential according to the macro stability IJkdijk experiments, ranging from 1,5 to 42 hours (see Table 2-1) when monitoring deformations. The $T_{available}$ for this sensor technique referring macro instability is assumed to be normally distributed with mean value $\mu(T_{available})$=36 hours and standard deviation $\sigma(T_{available})$=8 hours. It should be emphasized that these values are not representative for the current performance of the sensor technique.

The emergency flood protection measure consists of the construction of a stability berm with big-bags. Big-bags are in fact huge sand bags (volume of approximately 1-2 m^3), which are placed at the inner slope of the dike to form an emergency stability berm. This increases the macro stability of the inner slope, by adding weight that contributes to the resisting moment. Limit states occurring during the execution of the stability berm which might contribute to the temporary instability of the dike are not concerned in this study. The purchase costs C_p are estimated at 35 €/m (Boon, 2007) and the deployment costs C_D at 100 €/m for big bags (Gilding, 2008). The yearly discount rate δ equals 5,5 %/year and the yearly economic growth γ=1,9 %/year.

Three monitoring cases are considered for this dike-ring part:

- **Case 1: Monitoring of stretch canal of Pannerden with a low preparedness**
  Early warning monitoring along 6 km dike stretch with a non-prepared flood protection measure.
- **Case 2: Monitoring of stretch canal of Pannerden with a high preparedness**
  Early warning monitoring along 6 km dike stretch with a well-prepared flood protection measure.
- **Case 3: Monitoring of stretch IJssel with a high preparedness**
  Early warning monitoring along 21 km dike stretch with a well-prepared flood protection measure.

6.3.2 Case 1: stretch canal of Pannerden with low preparedness

In this case study, 6 km dike is equipped with monitoring S_2 and the preparedness for reaction is low. This induces low costs to be made for the flood protection measure $E(costs)_{measure}$ and a low probability of successful executing the measure P_{m1}. The lower costs are achieved by accounting no purchase costs at t=0 $C_{purchase}(t=0)=0$ and no yearly preparing costs $C_{preparing}=0$. The rest of the measurement costs consists of the yearly expected costs if a measure has to be executed. The total discounted sensor costs C_{sensor} over 300 years, with δ=5,5 %/year equal 1,98 M€ (see paragraph 5.3.3).

The purchase costs $C_{purchase}$, with l_d=6 km and C_p=35 €/m, are:

$$C_{\text{purchase}} = 35 \cdot \frac{6000}{2} = 105000 \text{ €}$$

The deployment costs $C_{deployment}$, with l_d=6 km and C_d=100 €/m, are:

$$C_{\text{deployment}} = 100 \cdot \frac{6000}{2} = 300000 \text{ €}$$

The total expected flood protection measure costs $E(costs)_{measure}$ are for the considered dike stretch, with P_{d1}=0,8:

$$\text{E(costs)}_{\text{measure}} = \sum_{t=0}^{300} \frac{P_H(t) \cdot 0,8 \cdot (105000 + 300000)}{(1+0,055)^t} = 3567 \text{ €}$$

The time required to successfully execute the measure $T_{required}$ in this poorly prepared situation consists of expected values $T_{decision}$=4 hours, $T_{transportation}$=3 hours and $T_{deployment}$ which equals, with D_r=25 m/hour and N_w=4 work forces:

$$T_{\text{deployment}} = \frac{6000}{25 \cdot 4 \cdot 2} = 30 \text{ hours}$$

The average time required $T_{required}$ equals 37 hours, with an assumed standard deviation of 6 hours. The probability of successful executing the flood protection measure P_{m1} is determined at 0,46. The limit state function is visualized in Figure 6-2.

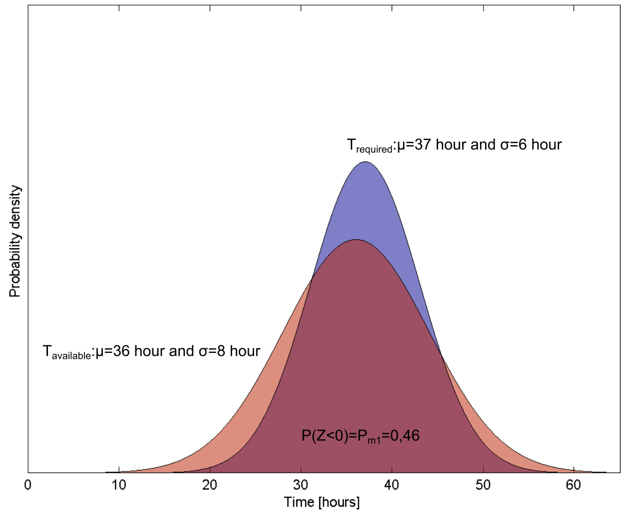

Figure 6-2: Limit state function in Case 1: stretch canal of Pannerden for P_{m1} with low preparedness

The cost-benefit analysis has been carried out over a period of 300 years, assuming that no structural dike reinforcement measures are executed in this time period (i.e. the flooding probability possibly exceeds the current safety standard). Furthermore, it is assumed that the deployment of the emergency stability berm influences the a-priori failure probability with R_m=1,05. This assumption makes the application of an early warning monitoring system always reduces the a-priori yearly flooding probability, yet the extent of the reduction depends on other model parameters. The results are presented in Table 6-2 with P_{d1}=0,8, $P_{f,m0}$=0,8 and $P_{f,d0}$=0,75.

Table 6-2: Cost-benefit analysis for Case 1: stretch canal of Pannerden with low preparedness

	Discounted E(damage) [M€]	Difference in E(damage) [M€]	C_{sensor} [M€]	$E(costs)_{measure}$ [M€]	Benefit-cost ratio ε_o [-]
A-priori (no sensor)	181,6	-	-	-	-
A-posteriori (with sensor)	178,4	3,2	1,98	0,0036	1,62

It should be emphasized that the low expected costs for the flood protection measure are caused by the low yearly probability of executing the measure (at t=0, this probability is 4,6E-4). The application of early warning sensor monitoring in Case 1 is cost-effective with a benefit-cost ratio of ε_o=1,62.

6.3.3 Case 2: stretch canal of Pannerden with high preparedness

In Case 2, the same monitoring system is used as in Case 1. Yet, the preparedness to execute the intended flood protection measure is now intensively increased. The total discounted sensor costs C_{sensor} over 300 years, with δ=5,5 %/year equal 1,98 M€ (see paragraph 5.3.3). The costs to be made for the flood protection measure $E(costs)_{measure}$ are higher, due to the purchase of the big bag materials at t=0 year:

$$C_{purchase}(t=0) = 35 \cdot \frac{6000}{2} = 105000 \text{ €}$$

Moreover, these materials have to be stored and training sessions are organized, which lead to yearly preparing costs, with f_p=0,1:

$$C_{preparing} = 0,1 \cdot 105000 = 10500 \text{ €/year}$$

The deployment costs $C_{deployment}$ are the same as in Case 1: $C_{deployment}$=300000 €. The total expected flood protection measure costs $E(costs)_{measure}$ now equal, with P_{d1}=0,8:

$$E(\text{costs})_{\text{measure}} = 105000 + \sum_{t=0}^{300} \frac{10500}{(1+0,055)^t} + \sum_{t=0}^{300} \frac{P_H(t) \cdot 0,8 \cdot (105000 + 300000)}{(1+0,055)^t} = 0,31 \text{ M€}$$

The time required to successfully execute the measure $T_{required}$ is expected to be lower in this prepared situation. The decision time is reduced to an expected value $T_{decision}$=1 hour, assuming that the crisis team can decide more efficiently due to the training exercises. Also the transportation time $T_{transportation}$ is reduced to an expected value of 1 hour, because the materials are stored in a facility nearby the monitored dike. The deployment time $T_{deployment}$ remains 30 hours. The average time required $T_{required}$ now equals 32 hours. The assumed standard deviation remains 6 hours. The probability of successful executing the flood protection measure P_{m1} is determined at 0,65. The limit state function is visualized in Figure 6-3.

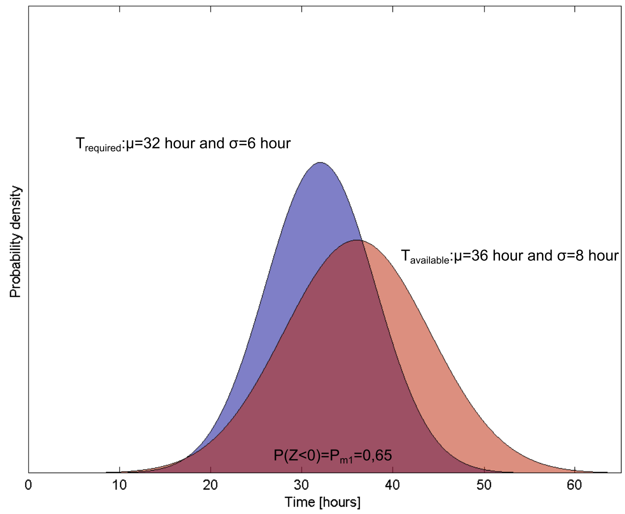

Figure 6-3: Limit state function in Case 2: stretch canal of Pannerden for P_{m1} with high preparedness

Again, the cost-benefit analysis has been carried out over a period of 300 years, assuming that no reinforcement measures are executed of this time period (i.e. the flooding probability possibly exceeds the current safety standard). The results are presented in Table 6-3, with R_m=1,05, P_{d1}=0,8, $P_{f,m0}$=0,8 and $P_{f,d0}$=0,75.

Table 6-3: Cost-benefit analysis for Case 2: stretch canal of Pannerden with high preparedness

	Discounted E(damage) [M€]	Difference in E(damage) [M€]	C_{sensor} [M€]	$E(costs)_{measure}$ [M€]	Benefit-cost ratio ε_o [-]
A-priori (no sensor)	181,6	-	-	-	-
A-posteriori (with sensor)	177,0	4,6	1,98	0,31	1,99

The expected costs for the flood protection measure $E(costs)_{measure}$ are significantly increased compared to Case 1. Yet, the a-posteriori total expected costs have been reduced due to the higher probability P_{m1}. The application of early warning sensor monitoring in Case 2 is more cost-effective than Case 1, with an benefit-cost ratio of ε_o=1,99.

6.3.4 Case 3: stretch IJssel with high preparedness

Case 3 considers an early warning monitoring system for another stretch in dike-ring 48: stretch IJssel, having a longer dike length of 21 km. The same monitoring system is used as in the previous cases. The preparedness for executing the flood protection measure is assumed to be high, because this is essential for this implementation perspective. The monitoring costs C_{sensor} have to be determined for dike stretch IJssel, since the monitoring costs have not yet been determined for this stretch (paragraph 5.2.3 does not consider monitoring of stretch IJssel alone): the total installation costs of the monitoring system are, with l_d=21 km, p=350 € per sensor module, e=200 € per CPT push-in, l_c=50 m, n=4, f_b=0,2:

$$C_{\text{installation}}(t_j) = 21 \cdot (350+200)\frac{1000}{50} \cdot 4 \cdot (1+0,2) = 1108800 \text{ €}$$

These installation costs have to be invested every t_j=10years and the yearly maintenance and operational costs sum up to:

$$C(t) = 0,1 \cdot 1108800 + 0,1 \cdot 1108800 = 221760 \text{ €/year}$$

The total discounted costs C_{sensor} over 300 years, with δ=5,5 %/year and l_d=21 km equal 6928000 €. The costs to be made for the flood protection measure $E(costs)_{measure}$ consist of the purchase of the big bag materials at t=0 year with l_d=21 km:

$$C_{\text{purchase}}(t=0) = 35 \cdot \frac{21000}{2} = 367500 \text{ €}$$

Also, these materials have to be stored and training sessions are organized, which lead to yearly preparing costs, with f_p=0,1:

$$C_{\text{preparing}} = 0,1 \cdot 367500 = 36750 \text{ €/year}$$

The deployment costs $C_{deployment}$ with l_d=21 km and C_d=100 €/m equal:

$$C_{\text{deployment}} = 100 \cdot \frac{21000}{2} = 1050000 \text{ €}$$

The total expected flood protection measure costs $E(costs)_{measure}$ are for stretch IJssel, with P_{d1}=0,8:

$$\text{E(costs)}_{\text{measure}} = 367500 + \sum_{t=0}^{300} \frac{36750}{(1+0,055)^t} + \sum_{t=0}^{300} \frac{P_H(t) \cdot 0,8 \cdot (367500+1050000)}{(1+0,055)^t} = 1,09 \text{ M€}$$

The time required to successfully execute the measure $T_{required}$ consists of expected values $T_{decision}$=1 hour and $T_{transportation}$=1 hour, defined for the high preparedness situation. However, the deployment time $T_{deployment}$ is dependent on the expected length of the stability berm and thus the total length of the dike: the longer the dike the longer the stability berm and thus the more time is needed for complete deployment. The deployment time with a number of 4 work forces for a dike of 21 km requires 105 hours to construct. The expected $T_{deployment}$ equals, with D_r=25 m/hour and N_w=4 work forces:

$$T_{\text{deployment}} = \frac{21000}{25 \cdot 4 \cdot 2} = 105 \text{ hours}$$

The average time required $T_{required}$ now equals 107 hours with assumed standard deviation 6 hours: due to the increased dike length, it is expected to take longer time to execute the emergency measure. The probability of successful executing the flood protection measure P_{m1} is determined at 5E-11, which is approximately 0: the probability that the measure is executed on time is negligible, because the total length of the flood protection measure is too long. To increase the probability P_{m1}, either another monitoring system can be applied with a higher $T_{available}$ or the deployment time $T_{deployment}$ must be reduced. The limit state function is visualized in Figure 6-4.

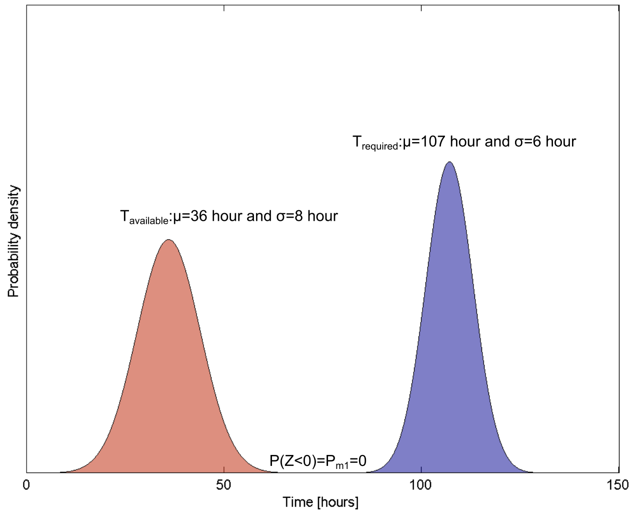

Figure 6-4: Limit state function in Case 3: stretch IJssel for P_{m1} with high preparedness

Again, the cost-benefit analysis has been carried out over a period of 300 years, assuming that no reinforcement measures are executed of this time period (i.e. the flooding probability possibly exceeds the current safety standard). The results are presented in Table 6-4, with R_m=1,05, P_{d1}=0,8, $P_{f,m0}$=0,8 and $P_{f,d0}$=0,75.

Table 6-4: Cost-benefit analysis for Case 3: stretch IJssel with high preparedness

	Discounted E(damage) [M€]	Difference in E(damage) [M€]	C_{sensor} [M€]	$E(costs)_{measure}$ [M€]	Benefit-cost ratio ε_o [-]
A-priori (no sensor)	658,4	-	-	-	-
A-posteriori (with sensor)	658,4	0	6,93	1,09	0

The expected costs for the flood protection measure $E(costs)_{measure}$ are significantly increased compared to Case 1. Yet, the a-posteriori total expected costs have been reduced due to the higher probability P_{m1}. The application of early warning sensor monitoring in Case 3 is not cost-effective because no benefit is obtained, resulting in a benefit-cost ratio of ε_o=0.

6.3.5 Sensitivity of the cost-benefit analysis for P_{d1} and $P_{f,m0}$

The reliability of the sensor system is a starting point for the application of a sensor monitoring system for early warning purposes. The cases are elaborated with a value $P_{f,m0}$=P_{d1}=0,8. However, the actual reliability and quality of the sensor techniques is highly uncertain and these monitoring system aspects are represented by the parameter P_{d1}. Also the relation of the monitored observable variable with the upcoming dike failure is subject to research: the value of parameter $P_{f,m0}$. This paragraph considers the sensitivity of the benefit-cost ratio ε_o for these parameters. The results of the cost-benefit analysis are given for varying values of P_{d1} and $P_{f,m0}$: either P_{d1} is taken constant and $P_{f,m0}$ varies or vice versa, see Figure 6-5.

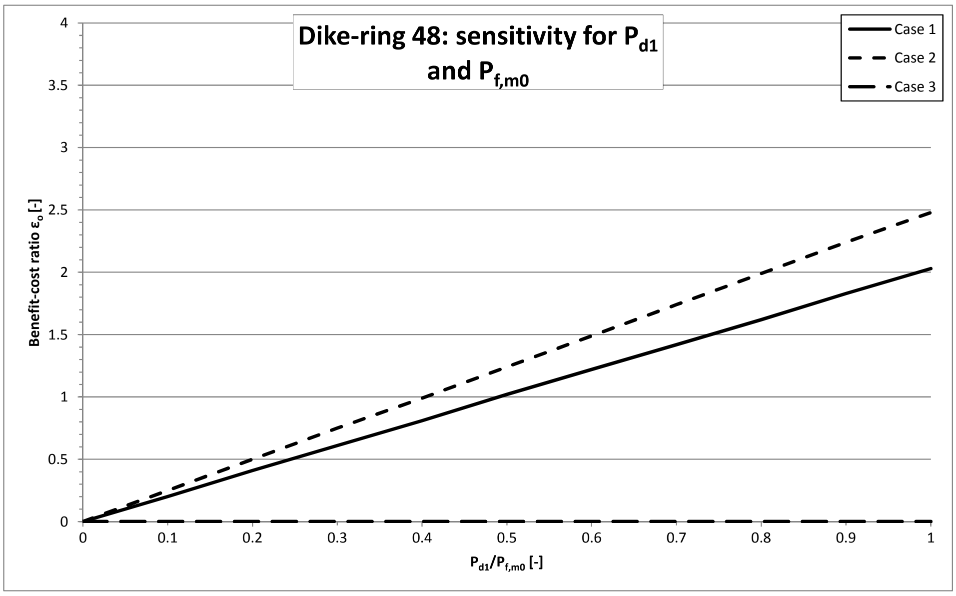

Figure 6-5: Sensitivity of the benefit-cost ratio for varying P_{d1} and $P_{f,m0}$ for all considered three cases

$P_{f,m0}$=0 represents the situation that the monitoring system has a very weak relation with the dike failure, i.e. given the detection of an anomaly during a high water event, the monitoring predicts an upcoming dike failure with a probability of 0. A value of P_{d1}=0 represents a highly unreliable monitoring system, which will never detect an upcoming dike failure during a high water event. Consequently, there is no gained benefit and the benefit-cost ratio ε_o equals 0.

Considering Case 1, the early warning monitoring is still cost-effective (i.e. ε_o>1) for $P_{f,m0}$=0,5 and P_{d1}=0,8 and vice versa. The sensitivity for Cases 2 is higher: the early warning monitoring is still cost-effective for a value of $P_{f,m0}$ larger than 0,4 and P_{d1}=0,8 and vice versa. Case 3 is not sensitive to the performance of the early warning monitoring system, as the benefit-cost ratio ε_o equals 0: no benefits have been determined.

6.4 Case study dike-ring 14

6.4.1 Characteristics of the early warning monitoring system

This case study considers the application of an early warning monitoring system in dike-ring 14 part Nieuwe Waterweg east. The same approach is followed as in paragraph 6.3, where the early warning monitoring system consists of MEMS sensor modules. The characteristics of each dike stretch are summarized in Table 6-5 and are deduced from the database in (Deltares, 2011d).

Table 6-5: Dike stretch characteristics for dike-ring 14

Parameter	Nieuwe Waterweg 1010-1019	Nieuwe Waterweg 1019-1026	New Meuse	
l_d	9	7	19	[km]
$P(0)= P_H(0)$	0,0001	0,0001	0,0001	[1/year]
α_d	0,0363	0,0588	0,1143	[1/cm]
η	0,2	0,201	0,2	[cm/year]
V(0)*	9844	9844	9844	[M€]

**Including 191 potential casualties with VOSL=6,7 M€ (Deltares, 2011c).*

Here, l_d refers to the total length of the considered dike stretch, P(0) is the probability of flooding of the considered dike stretch in year t=0, α_d is a scale parameter related to the decimation height, η is the relative water level rise and V(0) is the potential flood damage in year t.

The applied early warning monitoring system is considered to be a reliable detection system with P_{d1}=0,8 and $P_{f,m0}$=0,8. The sensitivity of the benefit-cost ratio for the parameters P_{d1} and $P_{f,m0}$ is again considered separately for each case in paragraph 6.4.5. The available warning time $T_{available}$ is derived from the current early warning potential according to the macro stability IJkdijk experiments, ranging from 1,5 to 42 hours (see Table 2-1) when monitoring deformations. The available warning time $T_{available}$ is assumed at mean value $\mu(T_{available})$=36 hours and standard deviation $\sigma(T_{available})$=8 hours. Again, it should be emphasized that these values are not representative for the current performance of the sensor technique. Yet, the $T_{available}$ is a starting point for this case study.

The emergency flood protection measure consists of the construction of a stability berm with big-bags. Limit states occurring during the execution of the stability berm that might contribute to the temporary instability of the dike are not concerned in this study. The stability berm consisting of big bags are characterized by purchase costs C_p=35 €/m (Boon, 2007) and deployment costs C_D of 100 €/m (Gilding, 2008). The yearly discount rate δ equals 5,5 %/year and the yearly economic growth γ=1,9 %/year.

Three monitoring cases are considered for this dike-ring part:

- **Case 1: Monitoring of stretch Nieuwe Waterweg 1010-1019 with a low preparedness**
  Early warning monitoring along 9 km dike stretch with a non-prepared flood protection measure.
- **Case 2: Monitoring of stretch Nieuwe Waterweg 1010-1019 with a low preparedness**
  Early warning monitoring along 9 km dike stretch with a well-prepared flood protection measure.
- **Case 3: Monitoring of stretch Nieuwe Waterweg 1019-1026 with a high preparedness**
  Early warning monitoring along 7 km dike stretch with a well-prepared flood protection measure.

6.4.2 Case 1: monitoring stretch Nieuwe Waterweg 1010-1019 with low preparedness

A total dike length of 9 km is equipped with monitoring S_2 and the preparedness for reaction is low: i.e. the purchase costs at t=0 are $C_{purchase}(t=0)=0$ and no yearly preparing costs are made, $C_{preparing}=0$. The remainder of the measurement costs consists of the yearly expected costs if a measure has to be executed. The total discounted sensor costs C_{sensor} over 300 years, with δ=5,5 %/year equal 2,97 M€ (see paragraph 5.4.2).

The purchase costs $C_{purchase}$ with l_d=9 km and C_p=35 €/m equal:

$$C_{\text{purchase}} = 35 \cdot \frac{9000}{2} = 157500 \text{ €}$$

The deployment costs $C_{deployment}$ with l_d=9 km and C_d=100 €/m equal:

$$C_{\text{deployment}} = 100 \cdot \frac{9000}{2} = 450000 \text{ €}$$

The total expected flood protection measure costs $E(costs)_{measure}$ for the considered dike stretch equal, with P_{d1}=0,8:

$$\text{E(costs)}_{\text{measure}} = \sum_{t=0}^{300} \frac{P_H(t) \cdot 0,8 \cdot (157500 + 450000)}{(1+0,055)^t} = 932 \text{ €}$$

The time required to successfully execute the measure $T_{required}$ in this poorly prepared situation consists of expected values $T_{decision}$=4 hours, $T_{transportation}$=3 hours and $T_{deployment}$ which equals, with D_r=25 m/hour and N_w=4 work forces:

$$T_{\text{deployment}} = \frac{9000}{25 \cdot 4 \cdot 2} = 45 \text{ hours}$$

The average time required $T_{required}$ now equals 52 hours, with an assumed standard deviation of 6 hours. The probability of successful executing the flood protection measure P_{m1} is determined at 0,06, see Figure 6-6.

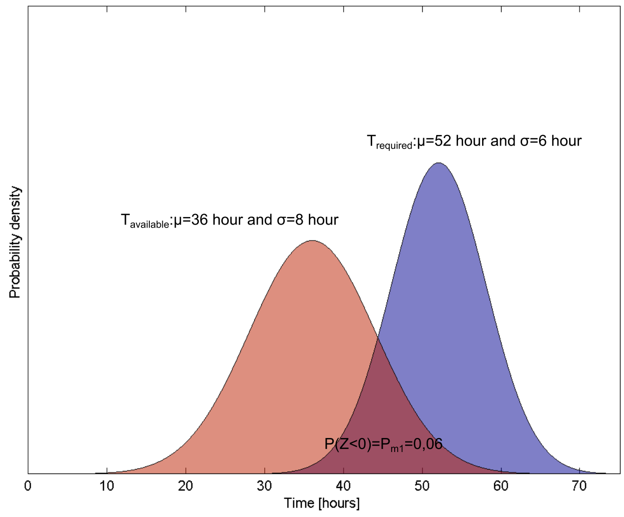

Figure 6-6: Limit state function in Case 1: stretch Nieuwe Waterweg 1010-1019 for P_{m1} with low preparedness

The cost-benefit analysis has been carried out over a period of 300 years, assuming that no reinforcement measures are executed of this time period (i.e. the flooding probability possibly exceeds the current safety standard). The results are presented in Table 6-6 with R_m=1,05, P_{d1}=0,8, $P_{f,m0}$=0,8 and $P_{f,d0}$=0,75.

Table 6-6: Cost-benefit analysis for Case 1: stretch Nieuwe Waterweg 1010-1019 with low preparedness

	Discounted E(damage) [M€]	Difference in E(damage) [M€]	C_{sensor} [M€]	$E(costs)_{measure}$ [M€]	Benefit-cost ratio ε_o [-]
A-priori (no sensor)	28,9	-	-	-	-
A-posteriori (with sensor)	28,8	0,1	2,97	0,0009	0,02

It should be emphasized that the low expected costs for the flood protection measure are caused by the low yearly probability of executing the measure (at t=0, this probability is 8E-5). The application of early warning sensor monitoring in Case 1 is not cost-effective with a benefit-cost ratio of ε_o=0,02.

6.4.3 Case 2: monitoring stretch Nieuwe Waterweg 1010-1019 with high preparedness

Case 2 considers the same situation as in Case 1, with the difference that investments are made in the preparedness for the execution of the flood protection measure. Thus, the total discounted sensor costs C_{sensor} over 300 years remain 2,97 M€. The expected costs for the measure now also consist of the purchase of materials at t=0: these purchase costs $C_{purchase}$(t=0) equal, with l_d=9 km and C_p=35 €/m:

$$C_{\text{purchase}}(t=0) = 35 \cdot \frac{9000}{2} = 157500 \text{ €}$$

These materials have to be stored over the life time of 300 years and training sessions are organized, which lead to yearly preparing costs, with f_p=0,1:

$$C_{\text{preparing}} = 0{,}1 \cdot 157500 = 15750 \text{ €/year}$$

The deployment costs $C_{deployment}$ are the same as in Case 1: $C_{deployment}$=450000 € (after all, the same stability berm has to be deployed). The total expected flood protection measure costs $E(costs)_{measure}$ now equal, with P_{d1}=0,8:

$$\text{E(costs)}_{\text{measure}} = 157500 + \sum_{t=0}^{300} \frac{15750}{(1+0{,}055)^t} + \sum_{t=0}^{300} \frac{P_H(t) \cdot 0{,}8 \cdot (157500 + 450000)}{(1+0{,}055)^t} = 0{,}46 \text{ M€}$$

The time required to successfully execute the measure $T_{required}$ is expected to be lower for this prepared situation, than in the unprepared situation in Case 1. The decision time is reduced to an expected value $T_{decision}$=1 hour and the transportation time $T_{transportation}$ is reduced to an expected value of 1 hour (see 6.3.3). The average deployment time $T_{deployment}$ remains 45 hours. The average time required $T_{required}$ now equals 47 hours with a standard deviation of 6 hours. The probability of successful executing the flood protection measure P_{m1} is equal to 0,14. The limit state function is presented in Figure 6-7.

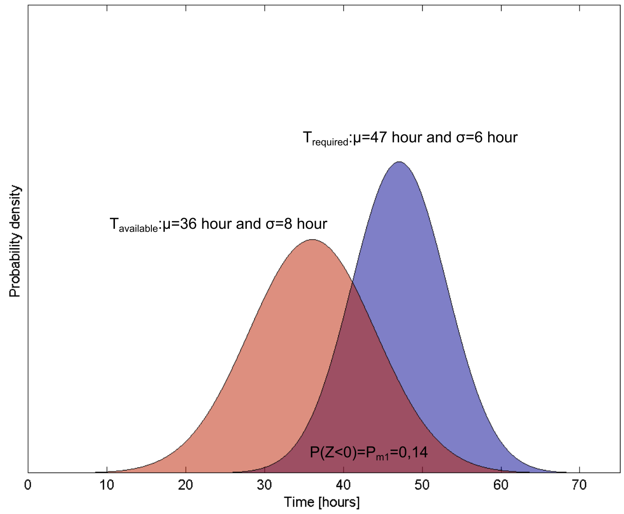

Figure 6-7: Limit state function in Case 2: stretch Nieuwe Waterweg 1010-1019 for P_{m1} with high preparedness

Elaborating the cost-benefit analysis over a period of 300 years with R_m=1,05, P_{d1}=0,8, $P_{f,m0}$=0,8 and $P_{f,d0}$=0,75 results in the values as given in Table 6-7.

Table 6-7: Cost-benefit analysis for Case 2: stretch Nieuwe Waterweg 1010-1019 with high preparedness

	Discounted E(damage) [M€]	Difference in E(damage) [M€]	C_{sensor} [M€]	$E(costs)_{measure}$ [M€]	Benefit-cost ratio ε_o [-]
A-priori (no sensor)	28,9	-	-	-	-
A-posteriori (with sensor)	28,7	0,2	2,97	0,46	0,06

The expected costs for the flood protection measure $E(costs)_{measure}$ are significantly increased compared to Case 1, but also the gained benefit is increased due to the higher probability P_{m1}. The application of early warning sensor monitoring in Case 2 is slightly more cost-effective than Case 1, with a benefit-cost ratio of ε_o=0,06. But the application of an early warning monitoring system is still not cost-effective in this case.

6.4.4 Case 3: monitoring stretch Nieuwe Waterweg 1019-1026 with high preparedness

This last case for dike-ring 14 considers the early warning monitoring of the adjacent dike stretch Nieuwe Waterweg 1019-1026 with a dike length of 7 km. Also, the preparedness for executing the flood protection measure is high. The sensor monitoring costs C_{sensor} have to be determined for dike stretch Nieuwe Waterweg 1019-1026, since the monitoring costs have not yet been determined for this stretch (paragraph 5.4.4 does not consider the monitoring of stretch Nieuwe Waterweg 1019-1026 alone). Paragraph 5.2.3 elaborates the model for the monitoring costs. Here, the total installation costs of the monitoring system are, with l_d=7 km, p=350 € per sensor module, e=200 € per CPT push-in, l_c=50 m, n=4, f_b=0,2:

$$C_{\text{installation}}(t_j) = 7 \cdot (350 + 200)\frac{1000}{50} \cdot 4 \cdot (1 + 0,2) = 369600 \text{ €}$$

These installation costs have to be invested every t_j=10years. The yearly maintenance and operational costs sum up to:

$$C(t)=0{,}1\cdot 369600+0{,}1\cdot 369600=73920 \text{ €/year}$$

The total discounted costs C_{sensor} over 300 years, with δ=5,5 %/year and l_d=21 km equal 2,309 M€. The costs to be made for the flood protection measure $E(costs)_{measure}$ consist of the purchase of the big bag materials at t=0 year with l_d=7 km:

$$C_{\text{purchase}}(t=0)=35\cdot\frac{7000}{2}=122500 \text{ €}$$

The yearly preparing costs for storage and training facilities equal, with f_p=0,1:

$$C_{\text{preparing}}=0{,}1\cdot 122500=12250 \text{ €/year}$$

The deployment costs $C_{deployment}$ with l_d=7 km and C_d=100 €/m equal:

$$C_{\text{deployment}}=100\cdot\frac{7000}{2}=350000 \text{ €}$$

The total expected flood protection measure costs $E(costs)_{measure}$ now equal for stretch Nieuwe Waterweg 1019-1026, with P_{d1}=0,8:

$$\text{E(costs)}_{\text{measure}}=122500+\sum_{t=0}^{300}\frac{12250}{(1+0{,}055)^t}+\sum_{t=0}^{300}\frac{P_H(t)\cdot 0{,}8\cdot(122500+350000)}{(1+0{,}055)^t}=0{,}36 \text{ M€}$$

The time required to successfully execute the measure $T_{required}$ consists of expected values $T_{decision}$=1 hour and $T_{transportation}$=1 hour, defined for the high preparedness situation (see paragraph 6.4.3). However, the deployment time $T_{deployment}$ is dependent on the total length of the dike. The length of stretch Nieuwe Waterweg 1019-1026 is slightly shorter than stretch Nieuwe Waterweg 1019-1026. The $T_{deployment}$ now equals with D_r=25 m/hour, N_w=4 work forces and l_d=7 km:

$$T_{\text{deployment}}=\frac{7000}{25\cdot 4\cdot 2}=35 \text{ hours}$$

The deployment time is decreased with 10 hours, compared to Case 2. The average time required $T_{required}$ now equals 37 hours with standard deviation 6 hours. The probability of successful executing the flood protection measure P_{m1} is determined at 0,46. The limit state function is visualized in Figure 6-8.

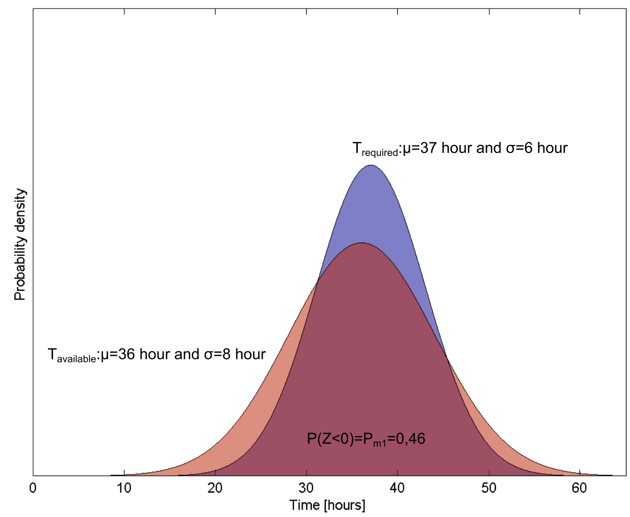

Figure 6-8: Limit state function in Case 3: stretch Nieuwe Waterweg 1019-1026 for P_{m1} with high preparedness

The cost-benefit analysis has been carried out over a period of 300 years, assuming that no reinforcement measures are executed of this time period (i.e. the flooding probability possibly exceeds the current safety standard). The results are presented in Table 6-8, with R_m=1,05, P_{d1}=0,8, $P_{f,m0}$=0,8 and $P_{f,d0}$=0,75.

Table 6-8: Cost-benefit analysis for Case 3: stretch Nieuwe Waterweg 1019-1026 with high preparedness

	Discounted E(damage) [M€]	**Difference in E(damage) [M€]**	**C_{sensor} [M€]**	**$E(costs)_{measure}$ [M€]**	**Benefit-cost ratio ε_o [-]**
A-priori (no sensor)	34,6	-	-	-	-
A-posteriori (with sensor)	34,0	0,6	2,309	0,36	0,23

The application of early warning sensor monitoring in Case 3 is more cost-effective than Case 1 and Case 2, with a benefit-cost ratio of ε_o=0,23. However, the application of an early warning sensor monitoring system is still not cost-effective in dike-ring 14.

6.4.5 Sensitivity of the cost-benefit analysis for P_{d1} and $P_{f,m0}$

The reliability of the sensor system is a starting point for the application of a sensor monitoring system for early warning purposes. The cases are elaborated with a value $P_{f,m0}$=P_{d1}=0,8. However, the actual value of P_{d1} and $P_{f,m0}$ is highly uncertain. Therefore, the sensitivity of the benefit-cost ratio ε_o for these parameters is elaborated. The results of the cost-benefit analysis are given for varying values of P_{d1} and $P_{f,m0}$: either P_{d1} is taken constant and $P_{f,m0}$ varies or vice versa, see Figure 6-9.

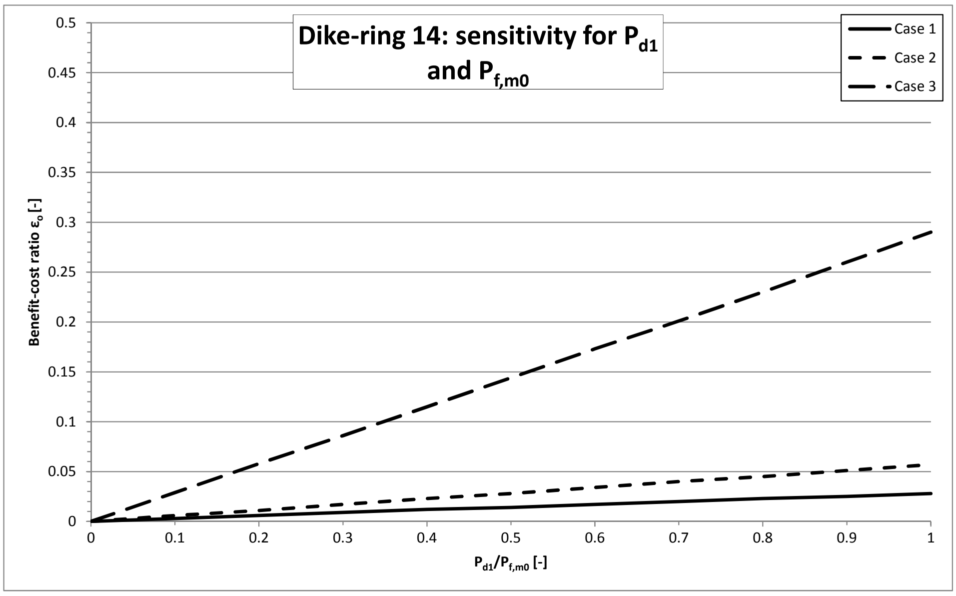

Figure 6-9: Sensitivity of the benefit-cost ratio for varying P_{d1} and $P_{f,m0}$ for all considered three cases

The early warning monitoring in all cases is not cost-effective (i.e. ε_o>1) for any variation of either $P_{f,m0}$ or P_{d1}. From all considered cases, Case 3 is most sensitive to the performance of the early warning monitoring system and Case 1 the least sensitive. Even the fictitious case with a perfectly working monitoring system with $P_{f,m0}$= P_{d1}= P_{m1}=1, Case 3 is still not cost-effective with ε_o=0,78.

6.5 Conclusions

A cost-benefit method has been set up to determine the cost-effectiveness of sensor monitoring for the application of early warning during the operational situation, in a flood risk approach. The benefit in this approach is gained by the in time execution of an emergency flood protection measure, which is triggered by the early warning monitoring system and temporary reduces the flooding probability on the short-term. The model incorporates the performance of the early warning monitoring system in terms of the reliability of the predicted dike collapse and the availability during high water events. Also the probability of successful executing the emergency flood protection measure and the effect of this measure on the flooding probability are incorporated. Constructional failure of the emergency flood protection measure is not considered.

The costs consist of the monitoring costs over the considered time period and the expected costs of the emergency flood protection measure. The expected costs of the emergency flood protection measure depend on the investments for the preparedness for applying the intended measure and the frequency of applying the measure.

Case studies are performed for dike-ring part 48 Rhine and IJssel downstream and dike-ring part 14 Nieuwe Waterweg east, in which an early warning monitoring system consisting of MEMS is considered. A monitoring time of 300 years is considered. Within the assumed boundary conditions, early warning sensor monitoring is cost-effective for dike-ring 48 cases 1 and 2. Early warning monitoring for stretch IJssel in dike-ring part Rhine and IJssel downstream with high preparedness to execute the flood protection measure is not cost-effective. No benefits are obtained, because the probability of successfully executing an emergency flood protection measure is negligible due to the long dike length. All considered cases for dike-ring 14 turn out to be not cost-effective under the taken assumptions (ε_o<1). This is due to the relatively low occurrence frequency of high water events, but this is reasonable due to the high safety standards in the Netherlands.

Due to the amount of underlying assumptions, the results of these case studies in absolute terms must be treated with care. Especially the performance of an early warning monitoring system in terms of system reliability, correctly detecting an upcoming dike failure and given prediction lead time are uncertain for the current state of the sensor techniques. Technological developments of these sensor techniques and further research are required to determine these aspects.

7 Conclusions and recommendations

7.1 Conclusions

The literature study (chapter 2) on the state of sensor techniques in flood defences concluded that the reliability of the preliminary early warning potentials is doubtful at the current state of research, because the testing circumstances are controlled and the analyses are not done independently. Therefore, sensor monitoring is primarily implemented in the periodic safety assessment and secondly in the operational situation. However, real-time monitoring during operational situations can contribute to the information supply for decision makers if the sensor performance increases. Moreover, water pressure is the only observable variable that constitutes an input for the existing dike safety assessment models used in the Netherlands.

Water pressure monitoring can be implemented in a probabilistic flood safety assessment, by updating the a-priori assessment with sensor information to the a-posteriori assessment (chapter 3). **In order to help deciding to apply sensor monitoring of water pressures for the purpose of updating the flood safety assessment, requirements are presented considering the following conditions:**

- The failure mechanism of macro instability is requires to be one of the dominant mechanisms in the total flood safety assessment.
- The water pressure schematization requires to be the dominant uncertainty aspect in the macro instability assessment.
- Sensor monitoring on itself does not affect the real flood risk, but only the assessment of the real flood risk by providing additional information during high water events. The real flood risk is only affected by physical measures.
- Water pressure monitoring reduces the epistemic uncertainty regarding water pressures caused by the translation from the hydraulic load to the water pressures. But this does not imply that the assessment of the flood risk is reduced. One must take into account the possibility that the assessed flood risk with sensor monitoring can be higher than the a-priori flood risk without sensor monitoring.
- The monitoring of significant loading events gives crucial information on the water pressure for the extrapolation to design loading conditions. One must elaborate the frequency of occurrence of valuable loading events, before installing a monitoring system.
- An additional application of sensor monitoring is to possibly identify unforeseen risks, but this is only effective if these unforeseen risks are correctly interpreted from the monitoring data and proper mitigating measures can be executed on time.
- Sensor monitoring can used for a proven strength analysis, by specifying the correlation between the historically survived and design loading condition, with the help of water pressure monitoring prior, during and after a survived high water event. However, proven strength must be considered as an additional implementation possibility for sensor monitoring.
- One must be aware that sensor monitoring might require a long monitoring time before becoming effective and requires willingness to invest in sensor monitoring.
- The implementation of water pressure monitoring for early warning purposes is to determine the short-term prediction of the water pressure development, combined with the prediction of the development of the hydraulic load. Timely execution of mitigating measures is expected to temporary reduce the flood risk on the short-term.

- The effect of sensor monitoring for early warning purposes directly depends on the practicability of the mitigating measure and the operational reliability of the sensor monitoring system.
- The quality of the sensor monitoring system (i.e. technical reliability, sensor density and measurement frequency) is required to be of a minimum quality in order to prevent unnecessary unrest and false alarms, leading to extra and unnecessary costs due to the sensor monitoring system.
- One must be aware that a different failure mechanism can be dominating during the operational situation, than was the sensor monitoring implemented for.
- A cost-benefit analysis must be evaluated for the application of sensor monitoring and other investments that might contribute to the flood safety on beforehand must be considered.

The case study for the canal of Nauerna (chapter 4) indicates that the uncertainty in soil strength and soil layer composition is dominant over the uncertainty in water pressures for the macro stability assessment. The contribution of uncertainty aspects is very case specific and every considered dike section requires an uncertainty analysis to investigate the possible impact of additional investigation. In the case of the canal of Nauerna, investments in additional soil investigation (e.g. CPT and borings) are likely to be more cost-effective than water pressure monitoring.

A cost-benefit model has been set up for the application of water pressure monitoring for the periodic safety assessment (chapter 5). The effect of sensor monitoring has been implemented in the flood risk approach by specifying the optimal strategy for dike reinforcements. Under the taken assumptions, the use of sensor monitoring for dike-ring 48 is more cost-effective than the cases for dike-ring 14.

A cost-benefit model has been set up for the application of sensor monitoring for early warning purposes during the operational situation (chapter 6). The effect of sensor monitoring relies on the prediction of a dike failure given a high water event and the timely execution of a mitigating emergency measure. Under the taken assumptions, the cases 1 and 2 for dike-ring 48 are more cost-effective than the cases for dike-ring 14. Case 3 from dike-ring 48 results in no benefits, as the successful execution of the emergency flood protection measure is negligible.

7.2 Recommendations

The recommendations following from this research are:

- The continuous technological development of the sensor techniques will provide new insights that influence the conclusions made from this research. Further research on the implementation of new developments is required.
- An analysis of the technical reliability of the monitoring systems is required to get insight into the operational reliability of monitoring system in long-term field conditions.
- During the course of this research, the lack of an unambiguous implementation of the water pressure uncertainties in the probabilistic macro instability assessment has been encountered. There is a need to elaborate a method for the implementation of water pressure uncertainty in the probabilistic macro stability assessment. The uncertainties due to water pressure monitoring need to be implemented in this method.
- Further elaboration and validation of the presented cost-benefit models for the impact of sensor monitoring is required to be able to support a balanced decision based on costs and benefits to improve the flood safety. This especially concerns the reduction rates R (chapter 5) and R_m (chapter 6), the conditional probability of anomaly detection P_{d1}, the probability

that an emergency measure has been executed successfully P_{m1} and the conditional dike failure probability without emergency measure $P_{f,m0}$.

- The monitoring costs are subject to changes due to competition and scale of fabrication. A more detailed cost analysis is required to determine the actual monitoring costs.
- The monitoring strategy of stand-by installation is worth further investigating. Stand-by installation can handle the problem of high monitoring costs for monitoring rare loading events (see the textbox in paragraph 5.2.3).
- The cost-benefit model for the operational situation is elaborated for short-term mitigating measures which temporarily affect the probability of flooding. Mitigating measures affecting the temporary impact of the flood are not elaborated and can be subject of further research.
- Research on combining both cost-benefit models for the periodic safety assessment and operational situation is required, in order to jointly consider the potential benefits. Both models interact as well: the periodic safety assessment model influences the model for the operational situation, due to training of the model with sensor monitoring information.
- This research focusses on the failure mechanism of macro instability, where further research on the implementation of sensor monitoring for other failure mechanisms is desirable.

References

Arcadis, 2011; *Toetsing Boezemkaden Nauernasche vaart.* Commissioned by HHNK. July 2011.

Boon, 2007; *Water controlling water.* Boon, M.J.J., MSc thesis, Delft University of Technology, August 2007.

Calle, 2005; *Bewezen sterkte bij dijken.* Calle, E.O.F., Geotechniek 2005, Vol. 1.

Deltacommissie, 2008; *Samen leven met water.* Results of the Delta Committee 2008 under chairman C.P. Veerman. September 2008.

Deltares, 2010: *Delft-FEWS.* Information brochure from: https://publicwiki.deltares.nl/display/FEWSDOC/Home. 2010.

Deltares, 2011a; LiveDijk Eemshaven Analyse metingen. Van der Kolk, B.J., Deltares. Delft, September 2011.

Deltares, 2011b; *D-Geo Stability version 10.1 Manual*. Deltares. Delft, 2011.

Deltares, 2011c; *Maatschappelijke kosten-baten analyse Waterveiligheid 21e eeuw*. Deltares. Delft, March 2011.

Deltares, 2011d; *OptimaliseRing version 2.3.1*. Including database file *Database_OptimaliseRing_2011_04_07.mdb*. Deltares, 2011.

Deltares, 2012; Personal conversation with Ed Calle and Ruben Jongejan, discussing the Bishop Probabilistic Random Field results regarding the $\beta=0$ model problems. July 9th 2012 at Deltares office, Delft.

EuroGEOSS, 2012; *Guidelines for assessing the Value of Information and the added value of a Geo-project.* European Global Earth Observation System of Systems. May 2012.

Feitsma, 2002; *Reliability analysis of dikes.* Feitsma, I.J., MSc thesis, Delft University of Technology, May 2002.

Flikkema, 2012; *Een hand reiken bij inzet van inspectieteam hoogwater boezemkades.* Oral presentation by Henk Flikkema at the STOWA Flood Defence Inspection Day. 29 March 2012.

Flood Control 2015, 2009; *Robust Monitoring. Added value of sensor streams in dike monitoring systems.* Deltares, TNO and IBM. December 2009.

Frieser, 2004; *Probabilistic evacuation decision model for river floods in the Netherlands.* Frieser, B.I., MSc thesis, Delft University of Technology, June 2004.

GeoDelft, 1990; *MProStab's Theoretical Background.* GeoDelft. April 1990.

GeoDelft, 2002; *MSeep User Manual.* GeoDelft. November 2002.

Gilding, 2008; *Onderzoek naar overstromingsrisico's in de veiligheidsketen*. Gilding, C.T., MSc thesis, Delft University of Technology, January 2008.

De Gooijer et al, 2007; *FLIWAS, Flood Information and Warning System.* De Gooijer, C., Wentholt, L.R., Langkamp, E.J., September 2007.

Hammitt & Shlyakhter, 1999; *The expected value of information and the probability of surprise.* Hammitt, J.K., Shlyakhter, A.I., Society for Risk Analysis, Volume 19, No. 1, 1999.

Hoss, 2010; *A comprehensive assessment of Multilayered Safety (Meerlaagsveiligheid) in flood risk management.* Hoss, F., MSc thesis, Delft University of Technology, October 2010.

Jongejan, 2004; *De observatiemethode in de geotechniek.* Jongejan, R.B., MSc thesis, Delft University of Technology, May 2004.

Kanning, 2005; *Safety format and calculation methodology slope stability of dikes.* Kanning, W., MSc thesis, Delft University of Technology, September 2005.

Kerr, 2006; *Soil moisture from space: Where are we?* Kerr, Y.H. Hydrogeology Journal 2007. September 2006.

Kok et al, 2004; *Standaardmethode2004. Schade en Slachtoffers als gevolg van overstromingen*. Kok, M., Huizinga, H.J., Vrouwenvelder, A.C.W.M., Barendregt, A., Rijkswaterstaat Dienst Weg- en Waterbouwkunde. November 2004.

Ministerie van Binnenlandse Zaken en Koninkrijkrelaties, 2012; *Oorzaak trillingen gebouw Westraven gevonden.* Press release from September 19th 2012. http://www.rgd.nl/actueel/nieuws-en-persberichten/artikel/artikel/6901/

Ministerie van Financiën, 2007; *Reële risicovrije discontovoet en risico-opslag in maatschappelijke kosten-batenanalyses.* Letter from the Minister of Finance to the House of Representatives. August 2011.

Ministerie van Verkeer en Waterstaat, 2007a; *Voorschrift Toetsen op Veiligheid Primaire Waterkeringen.* September 2007.

Ministerie van Verkeer en Waterstaat, 2007b; *Kabinetsstandpunt Rampenbeheersing Overstromingen*. Letter from the Minister of Transport, Public Works and Water Management to the House of Representatives. November 2007.

Ng & Oswalt, 2010; *Levee Monitoring System.* Ng, G., Oswalt, K. April 2010. Article viewed on 13-08-2012 at http://www.floodcontrol2015.com/news/item/11634/can-smart-levees-protect-the-sacramento-delta

NEN6740, 2006; *Geotechniek – TGB 1990 – Basiseisen en belastingen.* Nederlands Normalisatie instituut. September 2006.

Rijkswaterstaat, 2003; *Probabilistisch model hydraulische randvoorwaarden Benedenrivierengebied.* Rijkswaterstaat Rijksinstituut voor Integraal Zoetwaterbeheer en Afvalwaterbehandeling, Lelystad, December 2003.

Rijkswaterstaat, 2009a; *Technisch Rapport Actuele sterkte van dijken.* Rijkswaterstaat Waterdienst. March 2009.

Rijkswaterstaat, 2009b; *Macrostabiliteit IJkdijk, Sensor- en meettechologie.* Weijers, J., Elbersen, G.T., Koelewijn, A.R., Pals, N., September 2009.

Slijkhuis et al, 1999: *On the lack of information in hydraulic engineering models.* Slijkhuis, K.A.H., Van Gelder, P.H.A.J.M., Vrijling, J.K., Vrouwenvelder, A.C.W.M. Safety & Reliability

Stichting IJkdijk, 2010; *IJkdijk Pipingexperiment.* Koelewijn, A.R., Pals, N., Sas, M.J., Zomer, W.S., July 2010.

STOWA, 2006; *Inspectie van waterkeringen, Een overzicht van meettechnieken.* Moser, G.M., Zomer, W.S., Utrecht. July 2006.

TAW, 1990; *Probabilistic design of flood defences*. CUR. June 1990.

TAW, 1999; *Technisch rapport Zandmeevoerende wellen.* Technical Advisory Committee on water defences. March 1999.

TAW, 2001; *Technisch Rapport Waterkerende Grondconstructies.* Technical Advisory Committee on water defences. January 2001.

TAW, 2004; *Technisch Rapport Waterspanningen bij dijken.* Technical Advisory Committee on water defences. September 2004.

Ter Horst, 2005; *The safety of dikes during flood waves.* Ter Horst, W.L.A., MSc thesis, Delft University of Technology, February 2005.

TNO, 2003; *Theoriehandleiding PC-Ring Deel C.* Steenbergen, H.M.G.M., Vrouwenvelder, A.C.W.M. April 2003.

Van de Kamp, 2003: *Observatiemethode voor diepe bouwputten.* Van de Kamp, R.A.J., MSc thesis, Delft University of Technology, January 2003.

Van Marcke, 1983; Random Fields, Analysis and Synthesis. Van Marcke, E. 1983.

Van Staveren, 2006; *Uncertainty and ground conditions: A risk management approach.* Van Staveren, M. 2006.

Verruijt, 2001; *Grondmechanica.* Verruijt, A. Delft. 2001.

VNK2, 2011; *Veiligheid Nederland in kaart, De methode van VNK2 nader verklaard.* March 2011.

Vrijling et al, 2010; *Piping, Rekenfout of realiteit?* Vrijling, J.K., Kok, M., Calle, E.O.F., Epema, W.G., Van der Meer, M.T., Van den Berg, P, Scheckendiek, T. 2010.

Waterwet, 2009; *Waterwet article 2.12*. Dutch Ministry of Infrastructure and Environment. 2009.

List of figures

List of tables

Appendix A. Failure mechanisms

In the Netherlands, significant failure mechanisms are distinguished for the periodic safety assessment of flood defences. The overview is derived from (Ministerie van Verkeer en Waterstaat, 2007a). Figure A-1 gives the distinguished failure mechanisms.

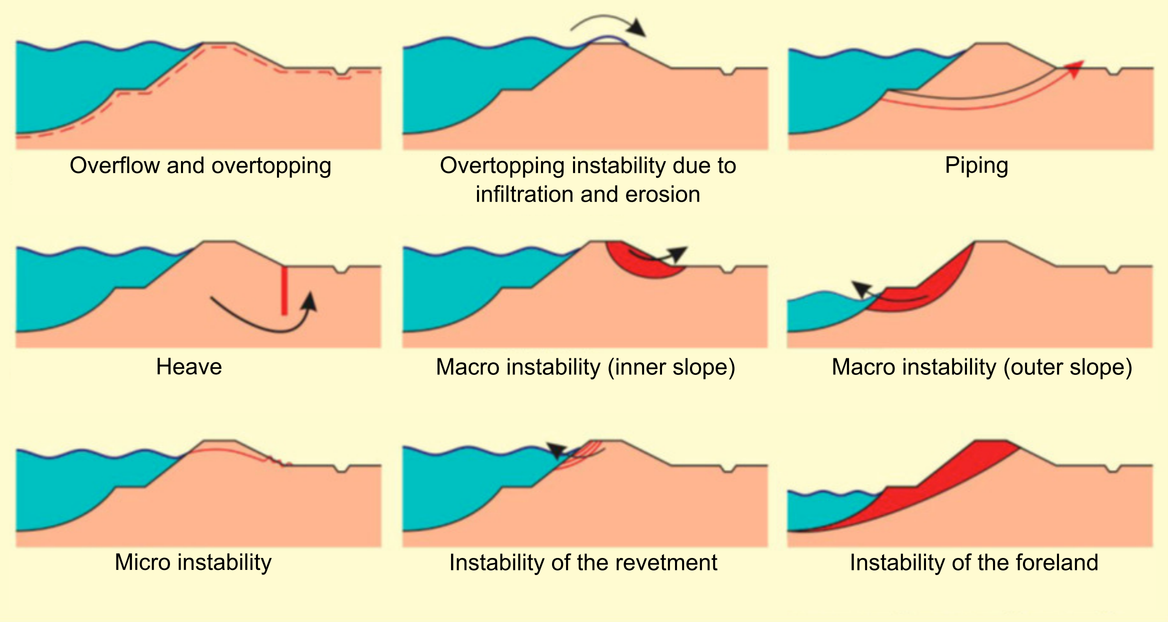

Figure A-1: Failure mechanisms for dikes (Ministerie van Verkeer en Waterstaat, 2007a)

Overflow and overtopping

The crest height turns out to be too low, with the consequence that water can flow over the dike. This overflow of water can cause inundation of the hinterland and thereby the dike has failed, without (immediate) constructional collapse of the dike. In the case of overtopping, waves cause water to enter the protected hinterland without the external water level exceeding the crest height.

Overtopping instability due to infiltration and erosion

The amount of overtopping water is usually not significant enough to lead to a dike failure. The overtopping water will flow over the crest and inner slope and then infiltrate in the soil. This water infiltration leads to decreased shear strength and increased volumetric weight of the soil. These factors both contribute to the instability of the top layer. Overtopping water can directly erode the top soil layer which leads to instabilities as well.

Macro instability (inner and outer slope)

Macro instability refers to the sliding of soil masses, either at the inner or outer slope. The sliding occurs when the resistance to sliding is smaller than the load. The balance of moments can be disturbed as the phreatic surface in the dike rises and consequently the dead weight of the soil increases.

Micro instability

Because of a water level difference between the outer and inner side of the dike, seepage of water through the dike body occurs and water leaves the dike at the inner slope. Water pressures built up due to this seepage and instability of the surface of the inner slope leads to dike collapse. Also washed out soil particles from the dike core or uplifting of an impermeable surface layer can lead to micro instability.

Piping

The same water level difference over the dike, as described at the previous mechanism, can lead to seepage underneath the dike. This is induced by soil layers with a high permeability (aquifers). When the seepage reaches a critical significance, soil particles can be carried with the groundwater flow. This results in sand boils at the inner toe of the dike and finally constructional instability of the dike. A possible low permeable top layer behind the dike (often clay) needs to crack first before a sand boil can develop. This sub mechanism is called uplift.

Heave

This mechanism holds the occurring of liquefaction of the soil caused by concentrated vertical seepage outflow at the inner dike toe. The groundwater flow induces a sudden change is soil stress and consequently the soil behaves as a liquid. The reduced strength of the liquefied soil causes instabilities. This mechanism often occurs when seepage screens are placed near the dike to reduce the risk of piping.

Instability of the revetment

Due to hydraulic loads on the dike, the dike revetment can be damaged. When a revetment is severely damaged, the inner dike body is exposed to the hydraulic loads. Erosion of the dike body leads to instabilities of the dike and a possible collapse.

Instability of the foreland

The instability of the foreland can occur when it consists out of weak soil layers (clay or peat). Due to an increase in water pressures, flow sliding (Dutch: *zettingsvloeiing*) or shear sliding of the foreland can lead to instability of the dike itself.

Instability due to non-water retaining objects

The presence of non-water retaining objects has not been mentioned in Figure A-1, but is treated separately in a flood safety assessment. Examples of these objects are trees, pipelines, stairs, houses and roads situated on the dike. This is not a stand-alone failure mechanism, but the presence of these objects often triggers one of the above mechanisms. These obstacles thereby form a threat.

Horizontal sliding

Another special failure mechanism is the horizontal sliding of the whole dike body. This mechanism has been recognized in the Netherlands due to the Wilnis dike failure in 2003. The horizontal forces induced by the external water level exceed the horizontal shear resistance of the dike body. Contrary to the other failure mechanisms, a low external water level is a governing situation. The dike body is now dry and has a low volumetric weight. This low dead weight reduces the shear strength. This is especially applicable for peat dikes, since peat has a very low dry volumetric weight.

Appendix B. Probabilistic slope failure model

The probabilistic calculations are done with D-Geo Stability: Bishop Probabilistic Random Field module, a product of Deltares. This appendix elaborates the background on the used probabilistic slope failure model. The model assumptions and schematizations are discussed to be aware of the model limitations.

Bishop's method of slices

Slope failures can be calculated with various methods, like the Bishop method of slices along a slip circle in a cross-sectional view (Verruijt, 2001). This method is commonly used in the Dutch engineering practice, but has limitations due to assumptions. Slope failure occurs when the driving moment in the dike exceeds the resisting moment. The driving moment consists of the soil weight, water pressures and external loads (e.g. traffic load) that drives the slope to slide downwards. The resisting moment consists of the shear strength of the soil along the considered slip circle. A slip circle is determined and divided into numerous slices, see Figure B-1.

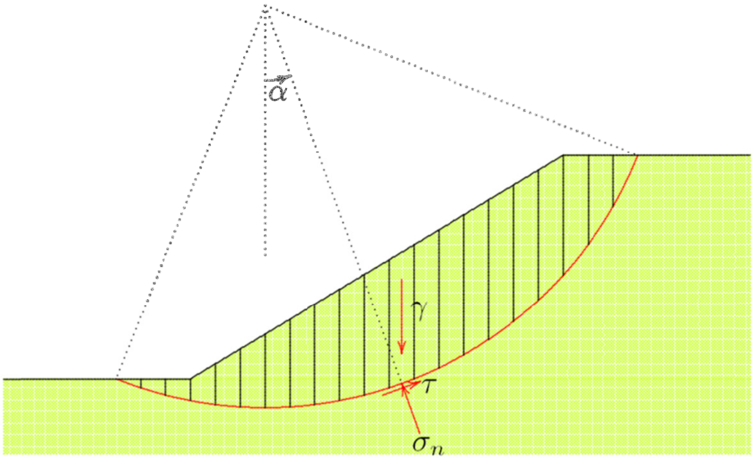

Figure B-1: Method of slices to determine slope failure (Verruijt, 2001)

The driving and resisting moments are derived for each slice. The weight of the slice forms the driving load and depends on the soil type and the water content (i.e. as the soil is saturated, the weight increases). The (drained[9]) shear strength τ along the slip surface is determined by the (drained) soil cohesion, (drained) internal friction angle and effective soil stress. The relation between these soil properties is approximated with the Mohr-Coulomb criterion (Verruijt, 2001):

$$\tau = c + \sigma' \tan \varphi$$

τ	Shear strength	[kN/m^2]
c	Cohesion (drained)	[kN/m^2]
σ'	Effective soil pressure	[kN/m^2]
φ	Internal friction angle (drained)	[°]

Shear strength increases as the soil cohesion, internal friction increases or internal friction increases. The effective soil pressure is determined by Terzaghi's law (Verruijt, 2001):

[9] Drained soil conditions are assumed for this relation, meaning that water particles in the soil can be drained off and the soil can consolidate. Undrained soil behavior implies no consolidation, such that water pressure can build up. Undrained soil behavior is induced by fast soil loading, e.g. traffic loads on a dike.

$$\sigma' = \sigma - p$$

σ'	Effective soil pressure	[kN/m^2]
σ	Normal soil pressure	[kN/m^2]
p	Water pressure	[kN/m^2]

The soil pressure increases linearly over the depth by the volumetric soil weight and gravity, and so does the effective soil stress for constant water pressure. At a certain point in the dike (e.g. along the slip circle), as the water pressure increases, the effective soil pressure decreases with the result that the shear stress decreases. In this way, increasing water pressures induces a lower safety to slope failure. The safety of a particular slip circle is derived by the ratio between driving and resisting moments:

$$F = \frac{M_r}{M_d}$$

F	Safety factor	[-]
M_r	Resisting moment; sum of all slices	[kNm/m]
M_d	Driving moment; sum of all slices	[kNm/m]

The total safety of a slope is derived by considering numerous slip circles. The slip circle with the smallest safety factor is governing for the slope safety.

Limitations of the Bishop method:
- Slope instability assumed along slip circles
- Cross-sectional approach
- Finite number of slip circle slices
- Drained soil behavior

Probabilistic computation

The probabilistic assessment of the slop failure is done with stochastic input parameters, which are lognormal distributed. The method performs a probabilistic slope stability analysis, in order to determine the probability that the safety factor is less than the required value, by solving the limit state function (Deltares, 2011b):

$$Z = F - q$$

Z	Limit state function for slope failure
F	Stochastic safety factor (computed)
q	Stochastic limit value (input model factor)

The definition of the limit state functions is based on slope failure without residual strength taken into account. The stochastic safety factor F is computed by the stochastic input parameters using Bishop's slope stability method. The limit value takes into account the uncertainties regarding the deviation between the result of the model and reality. The limit state function is solved with a first order second moment (FOSM) probabilistic analysis, by linearizing the limit state function at the design point. The design point is defined as the point at Z=0 where the probability density is maximum, i.e. the point with smallest distance to the origin. This smallest distance is denoted as the reliability index β, see Figure B-2. The variables u1 and u2 in Figure B-2 are normally distributed input variables of the limit state function. The coordinates of the design point can be expressed in terms of the reliability index β and the influence factor α of the input parameter, as calculated with the FOSM analysis. The influence factor reflects the variation sensitivity of the corresponding input parameter to the total failure probability.

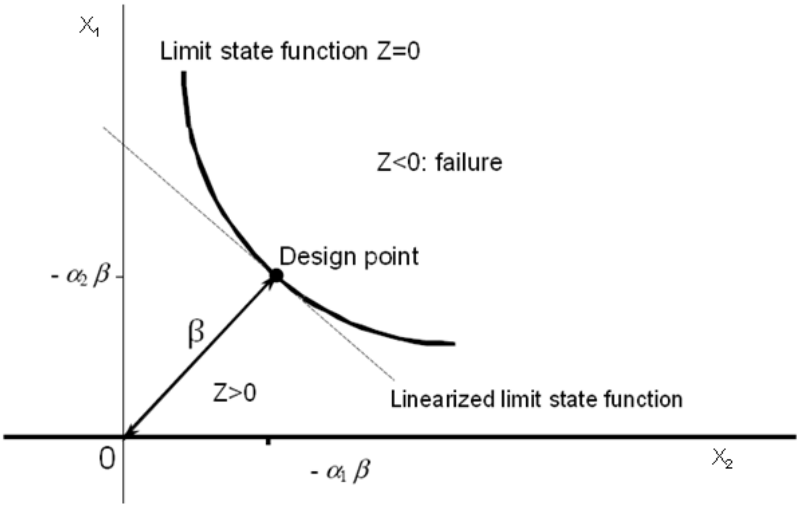

Figure B-2: Definition of the design point

The determination of the design point follows from an iterative process. The probability of failure is defined as:

$$P(Z<0)=\Phi(-\beta)$$

P(Z<0)	Probability of failure
Φ	Normal distribution
β	Reliability index

The reliability index β is the smallest distance from the origin to the design point. An increasing reliability index β results in a lower probability of failure P(Z<0). The iterative FOSM analysis is a fast and effective method. However, some disadvantages are noticeable due to the linearization of the limit state function in the design point (TNO, 2003). First, the iterative process to determine the design point does not have to converge to one point, resulting in an unstable iteration. Also, the approximation using the first order method leads to inaccurate results for strongly curved limit state functions, i.e. highly non-linear. Finally, a local minimum instead of a global minimum can be found for the minimization of the reliability index β.

Limitations of the probabilistic computation:
- Residual strength is not taken into account
- Possible unstable iteration process
- Approximation is inaccurate for highly non-linear limit state functions
- Possible local instead of global minimum is found for the reliability index β

Modeling of spatial soil variability

The variability of the soil strength properties is modeled with a random field stochastic shear strength model, computing the shear strength value in each spatial point in a soil layer based on Van Marcke's theory (Van Marcke, 1983). The geometry and soil layer composition are thereby deterministic parameters. Therefore, the choice of the geometry and soil layer composition must be done conservatively, in order to define a representative profile for the entire section. Fluctuations in the soil layer composition must be handled in a risk management approach, analyzing the possible variation based on the geotechnical length profile.

The spatial variability is described by a weak stationary function in space, with the expected value, standard deviation and the spatial correlation function. The spatial correlation function defines the correlation of shear strength between two spatial points in the soil layer as a function of the distance between the spatial points. The spatial correlation function is defined as (Deltares, 2011b):

$$\rho(\Delta x, \Delta y, \Delta z) = \left[1 - \alpha + \alpha \cdot \exp\left(-\frac{\Delta y^2}{D_v^2}\right)\right] \cdot \exp\left(-\frac{\Delta x^2 + \Delta z^2}{D_h^2}\right)$$

$\rho(\Delta x, \Delta y, \Delta z)$	Spatial correlation function	[-]
Δx	Absolute horizontal distance between two spatial points in cross-sectional direction	[m]
Δz	Absolute horizontal distance between two spatial points along dike length	[m]
Δy	Absolute vertical distance between two spatial points	[m]
α	Variance factor	[-]
D_v	Vertical correlation length	[m]
D_h	Horizontal correlation length	[m]

Here, the vertical en horizontal correlation lengths represent the damping of the correlation in vertical and horizontal direction. The horizontal correlation length ranges from 25 m to 150 m and the vertical correlation length from 0,1 m to 3 m (Rijkswaterstaat, 2009a). A small correlation length represents fast fluctuations of the soil strength in space. Analogue with the spatial correlation function: the smaller the correlation length, the faster the spatial correlation between two points decreases in space.

The variance factor α represents the ratio between local variance and the total regional variance of the soil strength for a distinct soil type, see Figure B-3. The local variance is defined as the variance of fluctuations relative to the mean value along a vertical. This value is determined by the performed borings and CPT push-ins, see σ_f in Figure B-3. The total regional variance is defined as the variance relative to the mean whole region, see σ_f in Figure B-3. The value of α varies between 0,5 and 1. A value of α=1 represents the situation that there is no statistical difference between the verticals (borings, CPT push-ins) over the whole measurement area. This situation can only be assumed for relative small measurement areas, i.e. for local investigation (TAW, 2001).

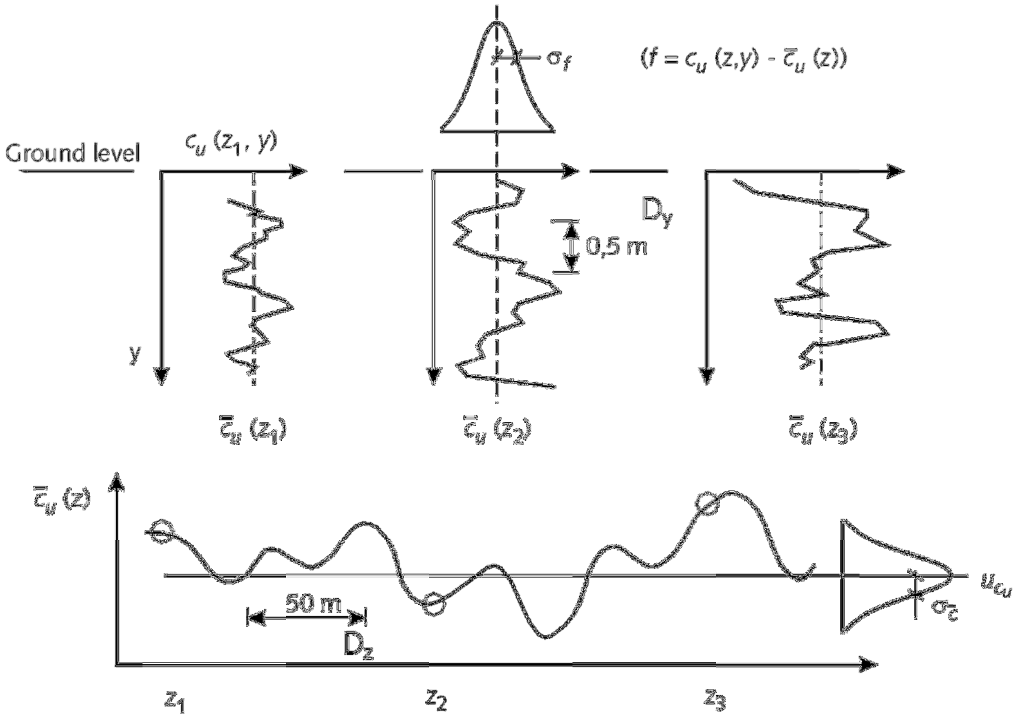

Figure B-3: Spatial variation of drained cohesion in soft soil (Kanning, 2005)

The spatial correlation ranges from 0 to 1, where a value of 0 indicates no spatial correlation between the strength in two points (e.g. relative small correlation lengths). And a correlation of 1 indicates full correlation (e.g. two spatial points close to each other). The correlation decreases as the distance between the points in space increase. The rate of decrease in space depends on the correlation length (i.e. D_h and D_v). The higher the correlation length, the lower the rate of decrease of the spatial correlation. Or, higher correlation lengths result in higher spatial correlations among two spatial points. Figure B-4 illustrates this phenomenon for the example of horizontal correlation.

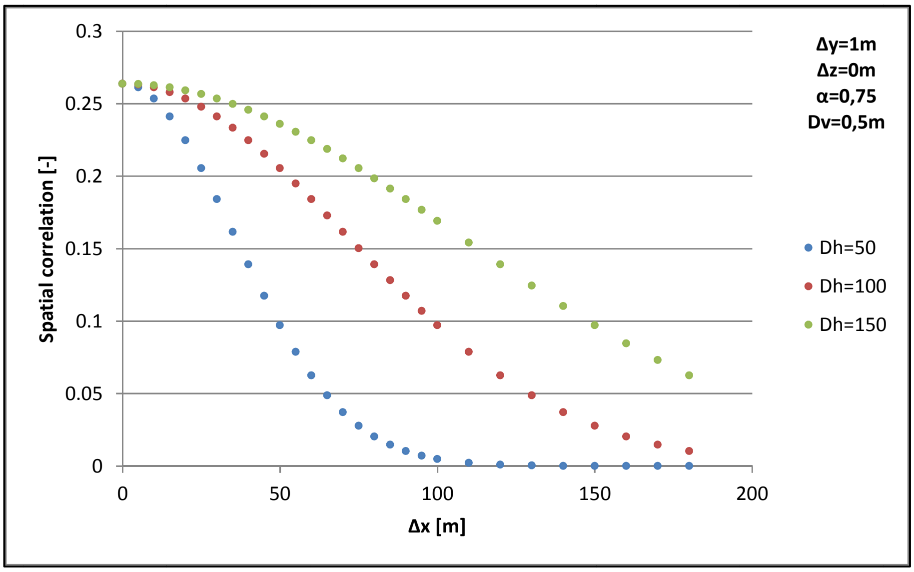

Figure B-4: Spatial correlation as a function of the horizontal distance Δx

The determination of the soil properties cohesion c and internal friction angle φ are done by laboratory tests of soil samples from the field. The number of test results to determine the parameters is limited and thereby the estimations of the expected values have a statistical variation. As the number of tests increase, the variation will decrease. The correlation of the estimation variance has been implemented in the model by modifying the spatial correlation function with the number of test samples:

$$r(\Delta x, \Delta y, \Delta z) = \frac{n}{n+1}\rho(\Delta x, \Delta y, \Delta z) + \frac{n}{n+1}$$

$r(\Delta x, \Delta y, \Delta z)$	Modified spatial correlation
$\rho(\Delta x, \Delta y, \Delta z)$	Spatial correlation function
n	Number of test samples

As the number of test samples increases, the adaptation of the original spatial correlation $\rho(\Delta x, \Delta y, \Delta z)$ decreases. Figure B-5 gives an indication of the course of the modification related to the number of test samples. Spatial correlation ranging from 0 to 1 has been plotted.

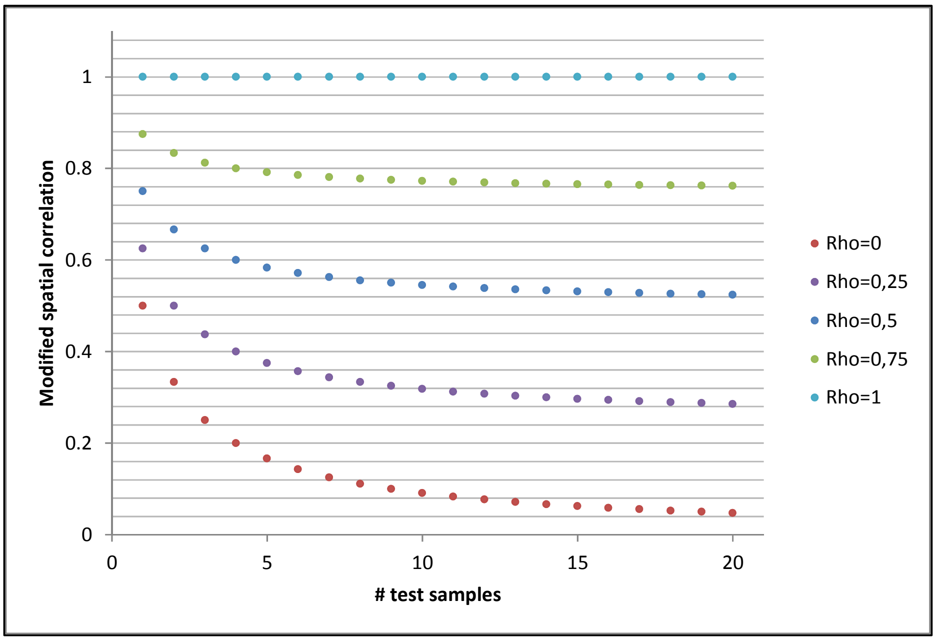

Figure B-5: Relation between the number of test samples and the modified spatial correlation

Limitations of the spatial variability modeling:

- Geometry and soil layer composition are deterministic inputs
- Spatial variability of unit weights is not taken into account

Length effect

The Bishop probabilistic random field model also takes into account the length effect. The probability of occurrence of a potential failure zone is computed for each of the failure circles according to:

$$P\left(F(Z) < F_{\text{limit value}}, Z \in [0, L]\right) = \Phi(-\beta_F) + \Phi(\beta_F)\left[1 - \exp\left(-N_F \cdot L\right)\right]$$

$P\left(F(Z) < F_{\text{limit value}}, Z \in [0, L]\right)$	Probability of occurrence of a potential failure zone
L	Section length
β_F	Reliability index of the failure circle
N_F	Frequency of intersections in section length

The probability of occurrence of a potential failure zone is computed with the cross-sectional reliability index. The frequency of intersections in the section length follows from:

$$N_F = \frac{1}{2\pi} \exp\left(-\frac{1}{2}\beta_F^2\right)\sqrt{-r_F''(0)}$$

N_F	Frequency of intersections in section length
β_F	Reliability index of the failure circle
r_F''	Second derivative at zero lag of the modified spatial correlation function

Appendix C. Water pressure schematization without measurements

The schematization of the water pressures during design loading conditions without sensor measurements is made following appendix B1 of (TAW, 2004). The procedure is summarized in this appendix. The base of the schematization however, consists of three components:

- Positioning of the phreatic surface
- Water pressure field in deeper impermeable layers (clay/peat)
- Water pressure in aquifer

The position of the phreatic surface during design loading conditions is the starting point for the water pressure schematization. The water pressures in the deeper clay and peat layers are derived from the phreatic surface by making the assumption of hydrostatic pressure. The phreatic surface is dependent on the soil material of the dike body and sub layers, as well as the geometry. Three steps are distinguished in order to make a a-priori schematization of the water pressures when no measurements are available (TAW, 2004):

- **Step 1: Description soil layer composition and geometry**
  Determine characteristic cross-sections, corresponding characteristic soil layer composition, expected irregularities and hydraulic boundary conditions.
- **Step 2: Description of relevant failure mechanisms and loading situations**
  Determine all relevant combinations of failure mechanism and loading conditions which for a water pressure schematization has to be made.
- **Step 3: Schematization based on the relevant situations as described**
  Quantitative derivation of the water pressure field for the considered situations. Model choice, groundwater flow, parameter choice and extrapolation method are elaborated to gain a safe approach.

When no measurement data is on hand (as has been determined in steps 1 and 2), the water pressure schematization in step 3 is performed following appendix B1 of (TAW, 2004). Four different dike compositions have been distinguished:

- Type 1A: Clay core with compressible subsoil
- Type 1B: Clay core with sandy subsoil
- Type 2A: Sand core (with impermeable cover layer) with compressible subsoil
- Type 2B: Sand core (with impermeable cover layer) with sandy subsoil

The schematization of the phreatic surface depends on the type of dike structure. Deviations from the four basis dike types can lead to a different behavior of the water pressures during design loading conditions.

Phreatic surface canal of Nauerna for no sensor measurements

The schematization of the position of the phreatic surface is done for an assumed clay dike body on compressible subsoil, type 1A. Figure C-1 indicates the determination aspects. The schematization consists of the points A, B, C and D.

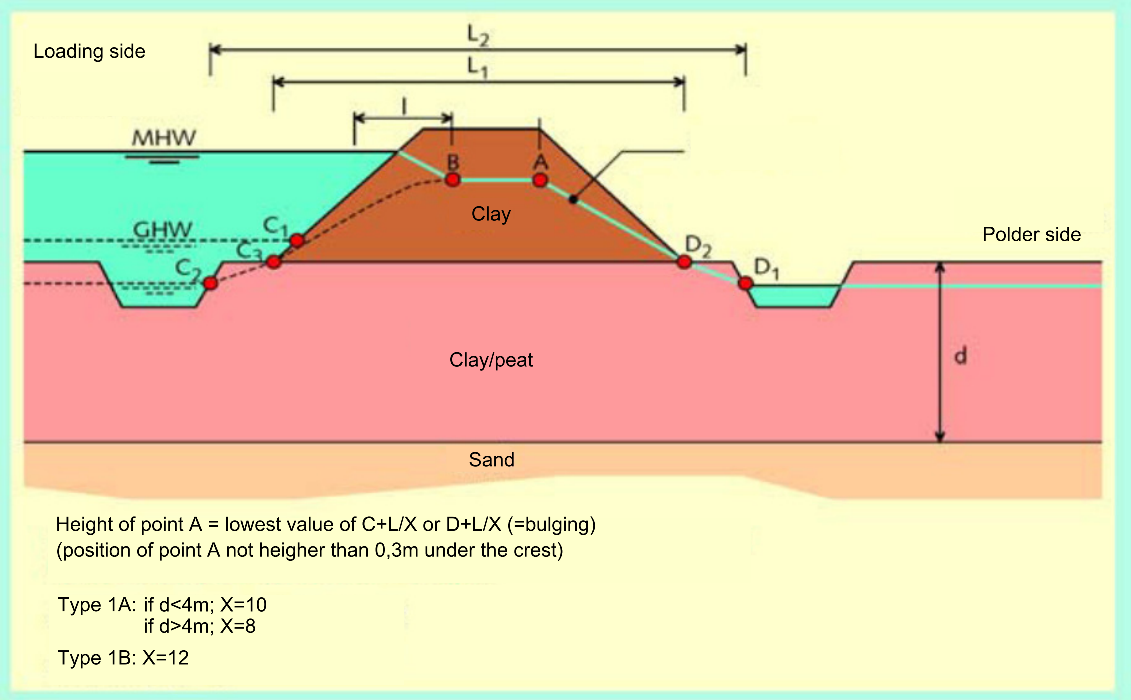

Figure C-1: Determination of the a-priori phreatic surface (TAW, 2004)

First, the position of point C is the point at the outer slope for the mean external water level: NAP -0,50 m. This holds for dikes with no foreland. Secondly, point D is the point at the inner slope at the ditch level (i.e. polder level): NAP -1,04 m. Then, point A represents the bulge of the phreatic surface and is defined as a point under the inner side of the crest. The height of point A follows from:

$$MIN\left\{C+\frac{L}{X},D+\frac{L}{X}\right\}$$

C	Vertical position of point C	[m]
D	Vertical position of point D	[m]
L	Horizontal distance between point C and D	[m]
X	Equals 10 for d<4 m and 8 for d>4 m	[m]
d	Thickness of the compressible layers	[m]

The horizontal distance between point C and D equals 8,5 m. The thickness of the compressible soil layers d equals approximately 3 m, resulting in a value X=10 m. The vertical position of point A follows from the above formula: NAP -0,20 m.

Finally, the location of point B needs to be determined. The vertical position is the same as point A: NAP -0,20 m. The horizontal position is time dependent. As the duration of the external water level increases, the penetration of the water will increase, resulting in the horizontal positioning of point B towards point A. Assuming stationary groundwater flow conditions, the horizontal position of point B is driven towards point A, whereas point A acts as a limit value.

Appendix D. Elementary case for volumetric weight

Three elementary dike cross-sections are considered, to illustrate the influence of the phreatic surface on a probabilistic slope failure analysis. The double impact of both the difference in dry and wet volumetric weight and the difference in water pressure distribution is expected to be different for each soil type. A basic dike has been schematized consisting of two soil layers. Soil type 1 consists of regular sand. Soil type 2 is either clay, peat or sand. The dike height equals 5 m, the design water level equals 4 m, an outer slope of 1:3 and an inner slope of 1:2,5. The crest has a width of 5 m. A ditch is located at the inner side. The phreatic surface is schematized in two ways: (1) as a linear function between the inner toe and the external water level (see Figure D-1) and (2) as a bilinear function with a 0,20 m higher positioning of a point in the centre of the dike (see Figure D-2). The difference in the phreatic surfaces is 0,20 m in the middle of the cross-section. The water pressures are hydrostatically distributed over the depth.

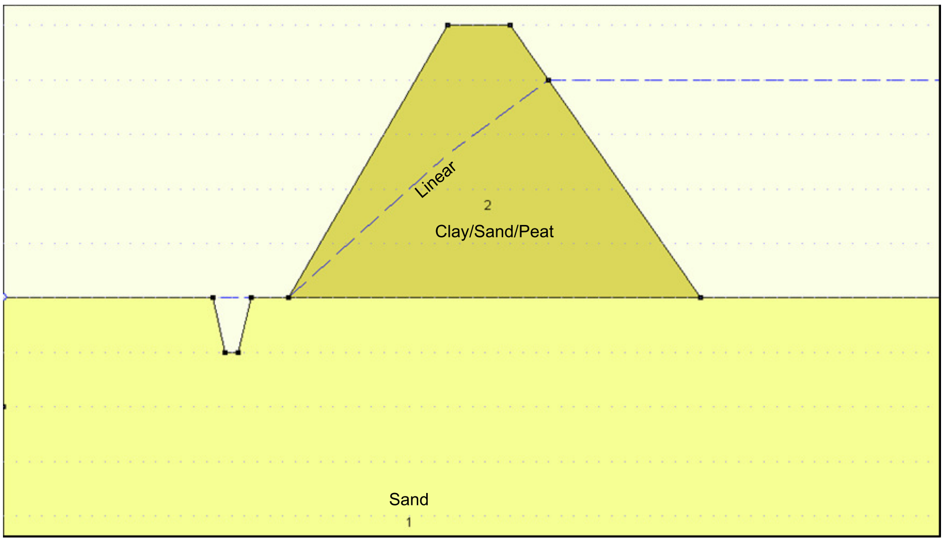

Figure D-1: Elementary dike composition consisting of two soil types and the linear phreatic surface

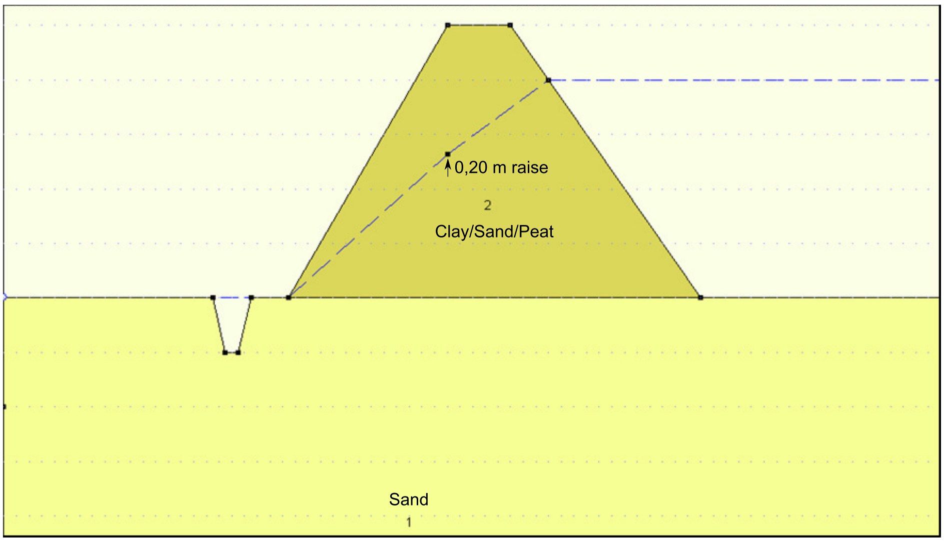

Figure D-2: Elementary dike composition consisting of two soil layers and bilinear phreatic surface

The soil characteristics are representative for the Dutch dike design and deduced from (NEN6740, 2006) and (Rijkswaterstaat, 2009a) and can be found in Table D-1.

Table D-1: Input parameters for the elementary case study for volumetric weight influence

Parameter		Sand subsoil	Clay core	Sand core	Peat core
γ_d	[kN/m^3]	18	16	17	5
γ_w	[kN/m^3]	20	16	19	12
$\mu(c)$	[kN/m^2]	0	4	0	1,5
$\mu(\varphi)$	[°]	35	25	30	20
$\sigma(c)$	[kN/m^2]	0	0,4	0	0,15
$\sigma(\varphi)$	[°]	3,5	2,5	3	2
ρ	[-]	0	0	0	0
$\sigma(p)$	[m]	Varies	Varies	Varies	Varies
$D_h(c)$	[m]	100	100	100	100
$D_v(c)$	[m]	0,5	0,5	0,5	0,5
N_c	[-]	10	10	10	10
α_c	[-]	0,75	0,75	0,75	0,75
$D_h(\varphi)$	[m]	100	100	100	100
$D_v(\varphi)$	[m]	0,5	0,5	0,5	0,5
N_φ	[-]	10	10	10	10
α_φ	[-]	0,75	0,75	0,75	0,75
$\mu(q)$	[-]	1			
$\sigma(q)$	[-]	0,075			
L	[m]	2000			

Clay core

The case of a clay dike consists of a relatively strong, impermeable soil due to the cohesion and internal friction angle. The dry and wet volumetric weight is the same, due to the tenacious characteristic water in clay. In this case, the adaption of the phreatic surface only leads to adaptations in the water pressure distribution. The weight of the active soil remains equal. The results are shown in Figure D-3.

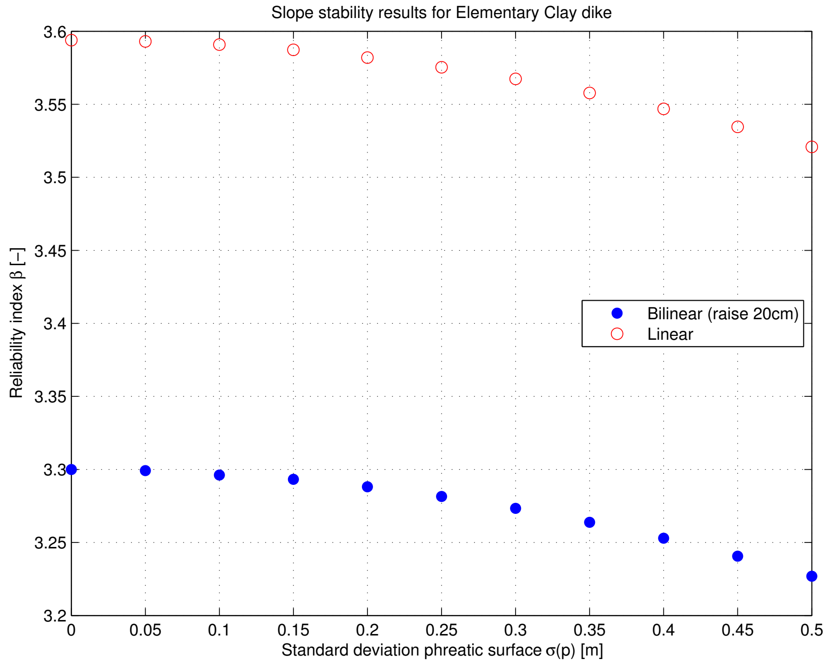

Figure D-3: Slope stability results of the clay dike for varying σ(p) and two phreatic surfaces

Sand core

The case of a sand dike consists of a strong, permeable dike body due to a high internal friction angle. The dry and wet volumetric weights vary, due to the sand pores. The permeable character of the sand makes an adaption from dry to wet soil relatively quick. In this case, the adaption of the phreatic surface mainly leads to adaptations in the water pressure distribution, but also in changes of the active soil weight. The results are shown in Figure D-3.

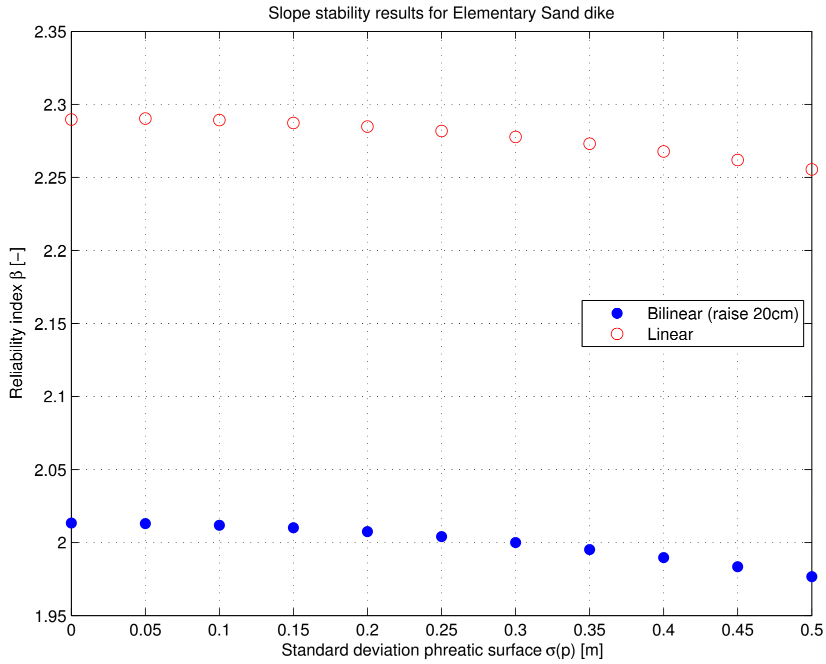

Figure D-4: Slope stability results of the sand dike for varying σ(p) and two phreatic surfaces

Peat core

The case of a peat dike consists of a weak, impermeable dike body due to the low cohesion and internal friction angle. The dry and wet volumetric weights can vary heavily, due to the organic character of peat, the water content can be significantly high. In this case, the adaption of the phreatic surface leads to adaptations in the water pressure distribution, but also in changes of the active soil weight. The results are shown in Figure D-5.

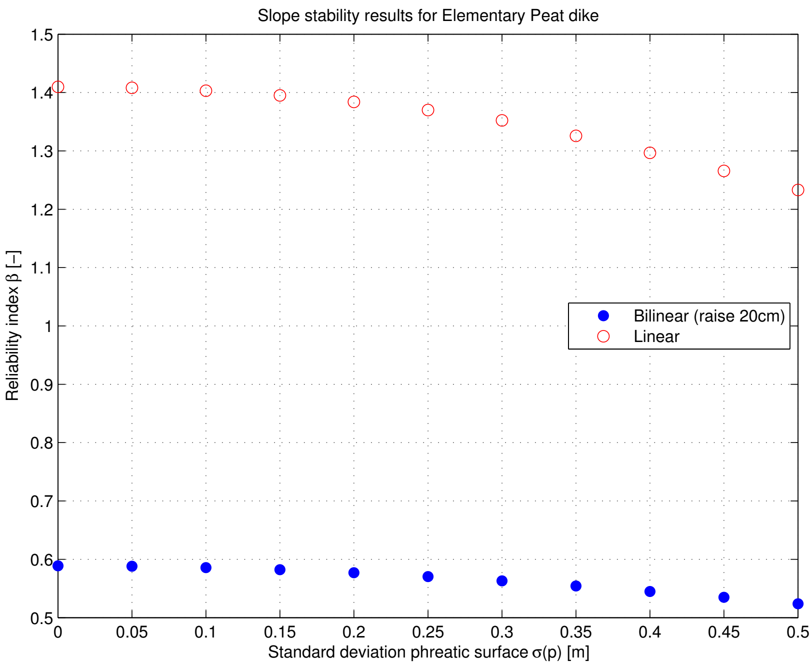

Figure D-5: Slope stability results of the peat dike for varying σ(p) and two phreatic surfaces

Concluding

In these three cases, a relation is visible between an increasing standard deviation of the phreatic surface σ(p) and decreasing reliability index (thus increasing slope failure probabilities). Also, the rise of the phreatic surface leads to a less stable dike.

The difference in slope stability due to the adapted phreatic surface Δβ is defined as:

$$\Delta\beta = \beta_{linear} - \beta_{bilinear}$$

$\Delta\beta$	Difference in slope stability	[-]
β_{linear}	Slope stability for the linear phreatic surface, per σ(p)	[-]
$\beta_{bilinear}$	Slope stability for the bilinear phreatic surface, per σ(p)	[-]

Whereas, the relative reduction $\beta_{\%}$ is defined as:

$$\beta_{\%} = \frac{\Delta\beta}{\beta_{linear}}$$

$\Delta\beta$	Difference in slope stability	[-]
β_{linear}	Slope stability for the linear phreatic surface, per σ(p)	[-]

In this case study, the mean values of Δβ are: 0,29 (clay), 0,28 (sand) and 0,71 (peat). Whereas, the mean values of $\beta_{\%}$ are: 9% (clay), 14% (sand) and 58% (peat). Hence, the difference in slope stability due to the adapted phreatic surface can be significant for large differences in the dry and wet volumetric weight. Which is the case for peaty soils.

Appendix E. Original case study

Original case study

The input parameters for the original case study with a section length L=2000 m are given in Table E-1.

Table E-1: Input parameters for the original case study

Parameter		Clay1	Clay2	Sand1	Sand2	Peat1	Peat2	Peat3
γ_d	[kN/m^3]	15,8	15,8	18	18	12,3	9,9	9,9
γ_w	[kN/m^3]	15,8	15,8	20	20	12,3	9,9	9,9
$\mu(c)$	[kN/m^2]	4,53	1,1	0	0	1,5	0,5	0,5
$\mu(\varphi)$	[°]	26,8	33,4	30	35	23,9	20,3	5,8
$\sigma(c)$	[kN/m^2]	3,55	0,16	0	0	0,5	0,1	0,1
$\sigma(\varphi)$	[°]	6,18	8,96	3	3,5	5,69	2	0,6
ρ	[-]	0	0	0	0	0	0	0
$\sigma(p)$	[m]	0,5	0,5	0,5	0,5	0,5	0,5	0,5
$D_h(c)$	[m]	50-150	50-150	50-150	50-150	50-150	50-150	50-150
$D_v(c)$	[m]	0,5	0,5	0,5	0,5	0,5	0,5	0,5
N_c	[-]	15	10	100	100	18	5	5
α_c	[-]	0,75	0,75	0,75	0,75	0,75	0,75	0,75
$D_h(\varphi)$	[m]	50-150	50-150	50-150	50-150	50-150	50-150	50-150
$D_v(\varphi)$	[m]	0,5	0,5	0,5	0,5	0,5	0,5	0,5
N_φ	[-]	15	10	100	100	18	5	5
α_φ	[-]	0,75	0,75	0,75	0,75	0,75	0,75	0,75
$\mu(q)$	[-]				1			
$\sigma(q)$	[-]				0,075			
L	[m]				2000			

The computation results for distinct horizontal correlation length D_h in the original case study are given in Table E-2, Table E-3 and Table E-4.

Table E-2: Stability results of the original case study for different σ(p) and D_h=50 m

σ(p) [m]	A-posteriori (sensor)		A-priori (no sensor)	
	P_f	β	P_f	β
0,00	4,828E-01	0,043	4,992E-01	0,002
0,05	4,834E-01	0,042	4,997E-01	0,001
0,10	4,852E-01	0,037	4,991E-01	0,002
0,15	4,881E-01	0,030	4,980E-01	0,005
0,20	4,923E-01	0,019	4,991E-01	0,002
0,25	4,977E-01	0,006	4,984E-01	0,004
0,30	4,745E-01	0,064	4,919E-01	0,020
0,35	4,804E-01	0,049	4,988E-01	0,003
0,40	4,868E-01	0,033	4,979E-01	0,005
0,45	4,935E-01	0,016	4,919E-01	0,020
0,50	4,912E-01	0,022	4,996E-01	0,001

Table E-3: Stability results of the original case study for different σ(p) and D_h=100 m

σ(p) [m]	A-posteriori (sensor)		A-priori (no sensor)	
	P_f	β	P_f	β
0,00	4,990E-01	0,003	4,868E-01	0,033
0,05	4,993E-01	0,012	4,872E-01	0,032
0,10	4,985E-01	0,004	4,882E-01	0,030
0,15	4,952E-01	0,012	4,900E-01	0,025
0,20	4,974E-01	0,007	4,925E-01	0,019
0,25	4,583E-01	0.105	4,956E-01	0,011
0,30	4,622E-01	0,095	4,994E-01	0,002
0,35	4,665E-01	0,084	4,807E-01	0,048
0,40	4,710E-01	0,073	4,853E-01	0,037
0,45	4,759E-01	0,060	4,909E-01	0,023
0,50	4,813E-01	0,047	4,964E-01	0,009

Table E-4: Stability results of the original case study for different σ(p) and D_h=150 m

σ(p) [m]	A-posteriori (sensor)		A-priori (no sensor)	
	P_f	β	P_f	β
0,00	4,775E-01	0,056	4,89E-01	0,028
0,05	4,777E-01	0,056	4,89E-01	0,028
0,10	4,784E-01	0,054	4,90E-01	0,026
0,15	4,795E-01	0,051	4,91E-01	0,023
0,20	4,810E-01	0,048	4,93E-01	0,019
0,25	4,830E-01	0,043	4,95E-01	0,014
0,30	4,853E-01	0,037	4,97E-01	0,007
0,35	4,882E-01	0,030	4,79E-01	0,052
0,40	4,916E-01	0,021	4,82E-01	0,045
0,45	4,949E-01	0,013	4,86E-01	0,036
0,50	4,983E-01	0,004	4,90E-01	0,026

The results from Table E-2, Table E-3 and Table E-4 are visualized in Figure E-1, Figure E-2 and Figure E-3.

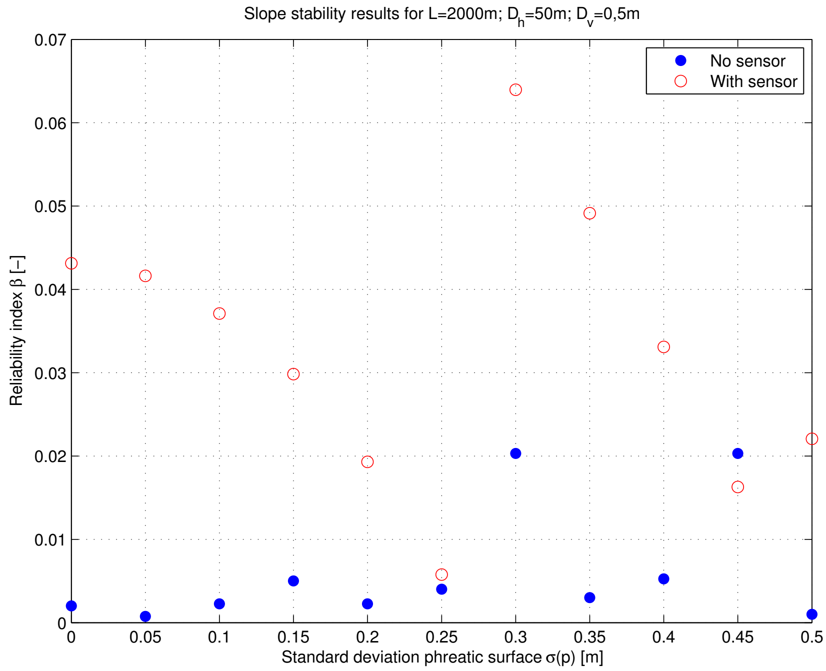

Figure E-1: Comparison of the slope stability results for D_h=50 m

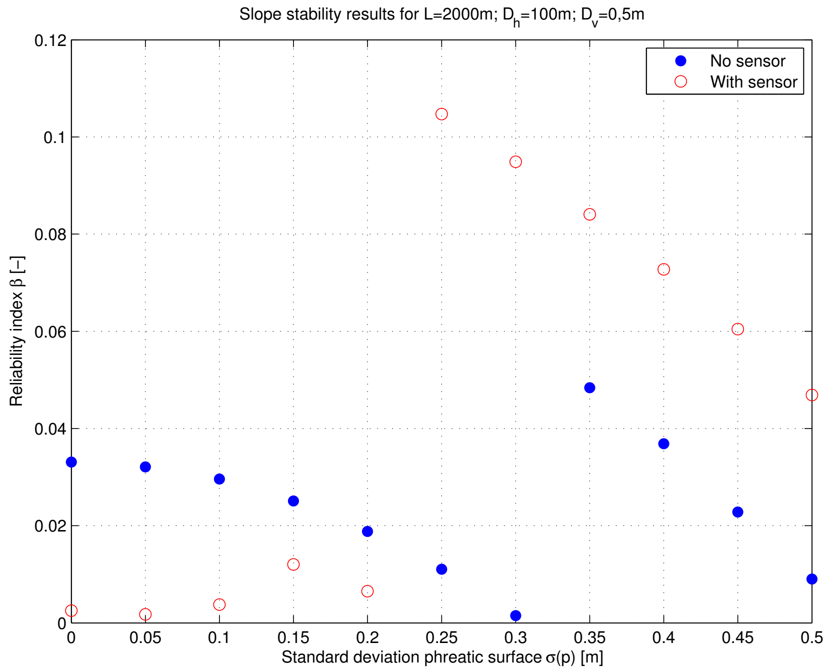

Figure E-2: Comparison of the slope stability results for D_h=100 m

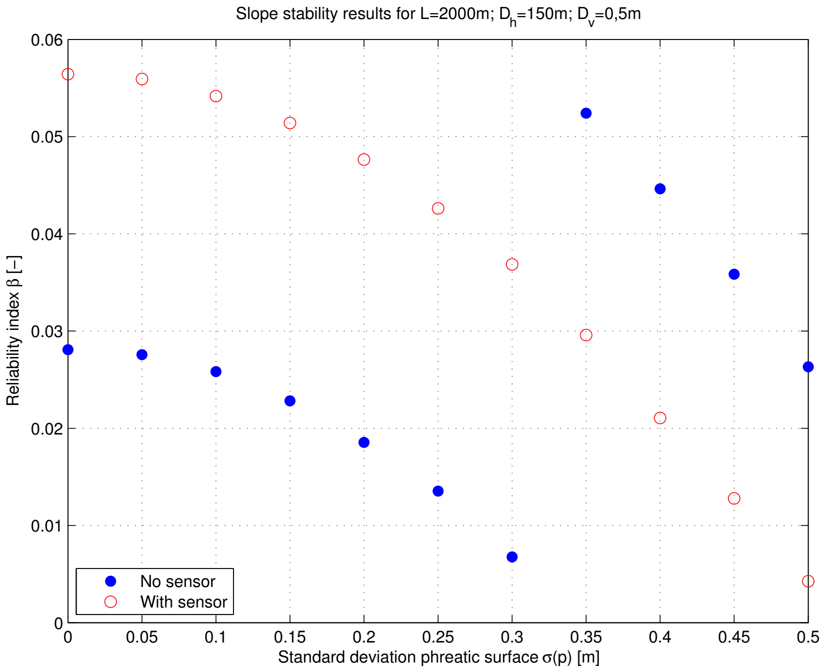

Figure E-3: Comparison of the slope stability results for D_h=150 m

The computation results for varying horizontal correlation length D_h in Case 1 are given in Table E-5.

Table E-5: Stability results of the original case study for different D_h and σ(p)=0,1 m

D_h [m]	A-posteriori (sensor)		A-priori (no sensor)	
	P_f	β	P_f	β
10	4,929E-01	0,018	4,993E-01	0,002
20	4,987E-01	0,003	4,992E-01	0,002
30	4,958E-01	0,011	4,929E-01	0,018
40	4,929E-01	0,018	4,945E-01	0,014
50	4,852E-01	0,037	4,991E-01	0,002
60	4,941E-01	0,015	4,982E-01	0,005
70	4,952E-01	0,012	4,999E-01	0,000
80	4,938E-01	0,016	4,980E-01	0,005
90	4,845E-01	0,039	4,997E-01	0,001
100	4,985E-01	0,004	4,882E-01	0,030
110	4,876E-01	0,031	4,581E-01	0,105
120	4,602E-01	0,100	4,990E-01	0,003
130	4,958E-01	0,011	4,973E-01	0,007
140	4,997E-01	0,001	4,893E-01	0,027
150	4,784E-01	0,054	4,897E-01	0,026
160	4,590E-01	0,103	4,700E-01	0,075
170	4,412E-01	0,148	4,955E-01	0,011
180	4,250E-01	0,189	4,968E-01	0,008
190	4,100E-01	0,228	4,923E-01	0,019
200	3,962E-01	0,263	4,956E-01	0,011

Appendix F. Case studies characteristics

Case 1: Variation of the horizontal correlation length D_h

The input parameters for Case 1 are given in Table F-1.

Table F-1: Input parameters for Case 1

Parameter		Clay1	Clay2	Sand1	Sand2	Peat1	Peat2	Peat3
γ_d	[kN/m^3]	15,8	15,8	18	18	12,3	9,9	9,9
γ_w	[kN/m^3]	15,8	15,8	20	20	12,3	9,9	9,9
$\mu(c)$	[kN/m^2]	4,53	1,1	0	0	1,5	0,5	0,5
$\mu(\varphi)$	[°]	26,8	33,4	30	35	23,9	20,3	5,8
$\sigma(c)$	[kN/m^2]	3,55	0,16	0	0	0,5	0,1	0,1
$\sigma(\varphi)$	[°]	6,18	8,96	3	3,5	5,69	2	0,6
ρ	[-]	0	0	0	0	0	0	0
$\sigma(p)$	[m]	0,5	0,5	0,5	0,5	0,5	0,5	0,5
$D_h(c)$	[m]	50-150	50-150	50-150	50-150	50-150	50-150	50-150
$D_v(c)$	[m]	0,5	0,5	0,5	0,5	0,5	0,5	0,5
N_c	[-]	15	10	100	100	18	5	5
α_c	[-]	0,75	0,75	0,75	0,75	0,75	0,75	0,75
$D_h(\varphi)$	[m]	50-150	50-150	50-150	50-150	50-150	50-150	50-150
$D_v(\varphi)$	[m]	0,5	0,5	0,5	0,5	0,5	0,5	0,5
N_φ	[-]	15	10	100	100	18	5	5
α_φ	[-]	0,75	0,75	0,75	0,75	0,75	0,75	0,75
$\mu(q)$	[-]				1			
$\sigma(q)$	[-]				0,075			
L	[m]				500			

The computation results for distinct horizontal correlation length D_h in Case 1 are given in Table F-2, Table F-3 and Table F-4.

Table F-2: Stability results Case 1 for different σ(p) and D_h=50 m

σ(p) [m]	A-posteriori (sensor)		A-priori (no sensor)	
	P_f	β	P_f	β
0,00	3,952E-01	0,266	4,949E-01	0,013
0,05	3,954E-01	0,265	4,950E-01	0,013
0,10	3,961E-01	0,263	4,955E-01	0,011
0,15	3,971E-01	0,261	4,963E-01	0,009
0,20	3,986E-01	0,257	4,974E-01	0,007
0,25	4,004E-01	0,252	4,988E-01	0,003
0,30	4,026E-01	0,247	4,824E-01	0,044
0,35	4,053E-01	0,240	4,847E-01	0,038
0,40	4,084E-01	0,232	4,872E-01	0,032
0,45	4,115E-01	0,224	4,896E-01	0,026
0,50	4,147E-01	0,215	4,922E-01	0,020

Table F-3: Stability results Case 1 for different σ(p) and D_h=100 m

σ(p) [m]	**A-posteriori (sensor)**		**A-priori (no sensor)**	
	P_f	β	P_f	β
0,00	2,474E-01	0,683	3,571E-01	0,366
0,05	2,476E-01	0,682	3,572E-01	0,366
0,10	2,481E-01	0,680	3,576E-01	0,365
0,15	2,489E-01	0,678	3,583E-01	0,363
0,20	2,501E-01	0,674	3,589E-01	0,361
0,25	2,515E-01	0,670	3,601E-01	0,358
0,30	2,533E-01	0,664	3,614E-01	0,355
0,35	2,554E-01	0,658	3,630E-01	0,350
0,40	2,579E-01	0,650	3,649E-01	0,345
0,45	2,605E-01	0,642	3,671E-01	0,340
0,50	2,631E-01	0,634	3,691E-01	0,334

Table F-4: Stability results Case 1 for different σ(p) and D_h=150 m

σ(p) [m]	**A-posteriori (sensor)**		**A-priori (no sensor)**	
	P_f	β	P_f	β
0,00	1,908E-01	0,875	2,831E-01	0,574
0,05	1,909E-01	0,875	2,832E-01	0,573
0,10	1,914E-01	0,873	2,836E-01	0,572
0,15	1,921E-01	0,870	2,842E-01	0,570
0,20	1,931E-01	0,867	2,850E-01	0,568
0,25	1,944E-01	0,862	2,860E-01	0,565
0,30	1,959E-01	0,856	2,874E-01	0,561
0,35	1,978E-01	0,850	2,889E-01	0,557
0,40	1,999E-01	0,842	2,908E-01	0,551
0,45	2,022E-01	0,834	2,929E-01	0,545
0,50	2,045E-01	0,826	2,949E-01	0,539

The computation results for varying horizontal correlation length D_h in Case 1 are given in Table F-5.

Table F-5: Stability results Case 1 for different D_h and $\sigma(p)$=0,1 m

D_h [m]	A-posteriori (sensor)		A-priori (no sensor)	
	P_f	β	P_f	β
10	4,970E-01	0,008	4,966E-01	0,009
20	4,926E-01	0,019	4,962E-01	0,010
30	4,595E-01	0,102	4,984E-01	0,004
40	4,587E-01	0,104	4,697E-01	0,076
50	3,961E-01	0,263	4,955E-01	0,011
60	3,503E-01	0,385	4,835E-01	0,041
70	3,155E-01	0,480	4,417E-01	0,147
80	2,882E-01	0,559	4,081E-01	0,232
90	2,662E-01	0,624	3,806E-01	0,304
100	2,481E-01	0,680	3,576E-01	0,365
110	2,330E-01	0,729	3,382E-01	0,417
120	2,202E-01	0,772	3,216E-01	0,463
130	2,093E-01	0,809	3,072E-01	0,504
140	1,997E-01	0,843	2,947E-01	0,540
150	1,914E-01	0,873	2,836E-01	0,572
160	1,840E-01	0,900	2,738E-01	0,601
170	1,774E-01	0,925	2,650E-01	0,628
180	1,715E-01	0,948	2,571E-01	0,652
190	1,662E-01	0,969	2,499E-01	0,675
200	1,614E-01	0,989	2,434E-01	0,695

Case 2: Variation of the vertical correlation length D_v

The input parameters for Case 2 are given in Table F-6.

Table F-6: Input parameters for case 2 (bold numbers are adjusted values from Case 1)

Parameter		Clay1	Clay2	Sand1	Sand2	Peat1	Peat2	Peat3
γ_d	[kN/m^3]	15,8	15,8	18	18	12,3	9,9	9,9
γ_w	[kN/m^3]	15,8	15,8	20	20	12,3	9,9	9,9
$\mu(c)$	[kN/m^2]	4,53	1,1	0	0	1,5	0,5	0,5
$\mu(\varphi)$	[°]	26,8	33,4	30	35	23,9	20,3	5,8
$\sigma(c)$	[kN/m^2]	3,55	0,16	0	0	0,5	0,1	0,1
$\sigma(\varphi)$	[°]	6,18	8,96	3	3,5	5,69	2	0,6
ρ	[-]	0	0	0	0	0	0	0
$\sigma(p)$	[m]	0,5	0,5	0,5	0,5	0,5	0,5	0,5
$D_h(c)$	[m]	**100**	**100**	**100**	**100**	**100**	**100**	**100**
$D_v(c)$	[m]	**1,5-2,5**	**1,5-2,5**	**1,5-2,5**	**1,5-2,5**	**1,5-2,5**	**1,5-2,5**	**1,5-2,5**
N_c	[-]	15	10	100	100	18	5	5
α_c	[-]	0,75	0,75	0,75	0,75	0,75	0,75	0,75
$D_h(\varphi)$	[m]	**100**	**100**	**100**	**100**	**100**	**100**	**100**
$D_v(\varphi)$	[m]	**1,5-2,5**	**1,5-2,5**	**1,5-2,5**	**1,5-2,5**	**1,5-2,5**	**1,5-2,5**	**1,5-2,5**
N_φ	[-]	15	10	100	100	18	5	5
α_φ	[-]	0,75	0,75	0,75	0,75	0,75	0,75	0,75
$\mu(q)$	[-]				1			
$\sigma(q)$	[-]				0,075			
L	[m]				500			

The computation results for distinct vertical correlation length D_v in Case 2 are given in Table F-7 and Table F-8.

Table F-7: Stability results Case 2 for different σ(p) and D_v=1,5 m

σ(p) [m]	A-posteriori (sensor)		A-priori (no sensor)	
	P_f	β	P_f	β
0,00	2,832E-01	0,573	3,914E-01	0,276
0,05	2,834E-01	0,573	3,915E-01	0,275
0,10	2,838E-01	0,572	3,918E-01	0,275
0,15	2,845E-01	0,570	3,924E-01	0,273
0,20	2,855E-01	0,567	3,931E-01	0,271
0,25	2,868E-01	0,563	3,940E-01	0,269
0,30	2,883E-01	0,558	3,951E-01	0,266
0,35	2,902E-01	0,553	3,963E-01	0,263
0,40	2,923E-01	0,547	3,979E-01	0,259
0,45	2,947E-01	0,540	3,997E-01	0,254
0,50	2,969E-01	0,533	4,015E-01	0,249

Table F-8: Stability results Case 2 for different σ(p) and D_v=2,5 m

σ(p) [m]	A-posteriori (sensor)		A-priori (no sensor)	
	P_f	β	P_f	β
0,00	2,883E-01	0,558	3,961E-01	0,263
0,05	2,885E-01	0,558	3,962E-01	0,263
0,10	2,889E-01	0,557	3,965E-01	0,262
0,15	2,896E-01	0,555	3,970E-01	0,261
0,20	2,906E-01	0,552	3,977E-01	0,259
0,25	2,918E-01	0,548	3,986E-01	0,257
0,30	2,933E-01	0,544	3,996E-01	0,254
0,35	2,951E-01	0,539	4,008E-01	0,251
0,40	2,972E-01	0,532	4,023E-01	0,247
0,45	2,995E-01	0,526	4,041E-01	0,243
0,50	3,017E-01	0,520	4,059E-01	0,238

The computation results for varying vertical correlation length D_v in Case 2 are given in Table F-9.

Table F-9: Stability results Case 2 for different D_v and σ(p)=0,1 m

D_v [m]	A-posteriori (sensor)		A-priori (no sensor)	
	P_f	β	P_f	β
0,2	1,578E-01	1,004	2,459E-01	0,687
0,4	1,830E-01	0,904	2,743E-01	0,600
0,6	1,978E-01	0,850	2,905E-01	0,552
0,8	2,071E-01	0,817	2,999E-01	0,525
1,0	2,128E-01	0,797	3,055E-01	0,509
1,2	2,163E-01	0,785	3,090E-01	0,499
1,4	2,187E-01	0,777	3,113E-01	0,492
1,6	2,203E-01	0,771	3,129E-01	0,488
1,8	2,215E-01	0,767	3,140E-01	0,485
2,0	2,224E-01	0,764	3,148E-01	0,482
2,2	2,230E-01	0,762	3,155E-01	0,480
2,4	2,235E-01	0,760	3,159E-01	0,479
2,6	2,239E-01	0,759	3,163E-01	0,478
2,8	2,242E-01	0,758	3,166E-01	0,477
3,0	2,245E-01	0,757	3,169E-01	0,476

Case 3: Reduced soil strength deviation

The input parameters for Case 3 are given in Table F-10. This case considers less variability of the soil strength variables; cohesion c and internal friction angle φ.

Table F-10: Input parameters for case 3 (bold numbers are adjusted values from Case 1)

Parameter		Clay1	Clay2	Sand1	Sand2	Peat1	Peat2	Peat3
γ_d	[kN/m^3]	15,8	15,8	18	18	12,3	9,9	9,9
γ_w	[kN/m^3]	15,8	15,8	20	20	12,3	9,9	9,9
μ(c)	[kN/m^2]	4,53	1,1	0	0	1,5	0,5	0,5
μ(φ)	[°]	26,8	33,4	30	35	23,9	20,3	5,8
σ(c)	[kN/m^2]	**1,5**	0,16	0	0	**0,2**	0,1	**0,05**
σ(φ)	[°]	**3**	8,96	3	3,5	**3**	2	**0,3**
ρ	[-]	0	0	0	0	0	0	0
σ(p)	[m]	0,5	0,5	0,5	0,5	0,5	0,5	0,5
D_h(c)	[m]	100-150	100-150	100-150	100-150	100-150	100-150	100-150
D_v(c)	[m]	0,5	0,5	0,5	0,5	0,5	0,5	0,5
N_c	[-]	15	10	100	100	18	5	5
α_c	[-]	0,75	0,75	0,75	0,75	0,75	0,75	0,75
D_h(φ)	[m]	100-150	100-150	100-150	100-150	100-150	100-150	100-150
D_v(φ)	[m]	0,5	0,5	0,5	0,5	0,5	0,5	0,5
N_φ	[-]	15	10	100	100	18	5	5
α_φ	[-]	0,75	0,75	0,75	0,75	0,75	0,75	0,75
μ(q)	[-]				1			
σ(q)	[-]				0,075			
L	[m]				500			

The computation results for distinct horizontal correlation length D_h in Case 3 are given in Table F-11 and Table F-12.

Table F-11: Stability results Case 3 for different σ(p) and D_h=100 m

σ(p) [m]	A-posteriori (sensor)		A-priori (no sensor)	
	P_f	β	P_f	β
0,00	1,322E-01	1,116	2,205E-01	0,771
0,05	1,324E-01	1,115	2,207E-01	0,770
0,10	1,330E-01	1,112	2,213E-01	0,768
0,15	1,340E-01	1,108	2,223E-01	0,764
0,20	1,354E-01	1,101	2,238E-01	0,759
0,25	1,371E-01	1,093	2,256E-01	0,753
0,30	1,393E-01	1,083	2,278E-01	0,746
0,35	1,419E-01	1,072	2,305E-01	0,737
0,40	1,447E-01	1,059	2,335E-01	0,727
0,45	1,476E-01	1,047	2,365E-01	0,718
0,50	1,509E-01	1,033	2,397E-01	0,707

Table F-12: Stability results Case 3 for different σ(p) and D_h=150 m

σ(p) [m]	A-posteriori (sensor)		A-priori (no sensor)	
	P_f	β	P_f	β
0,00	9,980E-02	1,283	1,704E-01	0,953
0,05	1,000E-01	1,282	1,706E-01	0,952
0,10	1,004E-01	1,279	1,712E-01	0,949
0,15	1,012E-01	1,275	1,720E-01	0,946
0,20	1,023E-01	1,269	1,733E-01	0,941
0,25	1,038E-01	1,260	1,749E-01	0,935
0,30	1,055E-01	1,251	1,768E-01	0,928
0,35	1,077E-01	1,239	1,791E-01	0,919
0,40	1,099E-01	1,227	1,817E-01	0,909
0,45	1,123E-01	1,214	1,843E-01	0,899
0,50	1,150E-01	1,200	1,872E-01	0,888

The computation results for varying horizontal correlation length D_h in Case 3 are given in Table F-13.

Table F-13: Stability results Case 3 for different D_h and σ(p)=0,1 m

D_h [m]	A-posteriori (sensor)		A-priori (no sensor)	
	P_f	β	P_f	β
10	4,515E-01	0,122	4,752E-01	0,062
20	4,418E-01	0,146	4,471E-01	0,133
30	3,298E-01	0,440	4,968E-01	0,008
40	2,653E-01	0,627	4,119E-01	0,223
50	2,237E-01	0,760	3,543E-01	0,374
60	1,946E-01	0,861	3,127E-01	0,488
70	1,731E-01	0,942	2,814E-01	0,579
80	1,566E-01	1,009	2,569E-01	0,653
90	1,436E-01	1,064	2,374E-01	0,715
100	1,330E-01	1,112	2,213E-01	0,768
110	1,242E-01	1,154	2,079E-01	0,814
120	1,168E-01	1,191	1,966E-01	0,854
130	1,106E-01	1,223	1,869E-01	0,889
140	1,051E-01	1,253	1,785E-01	0,921
150	1,004E-01	1,279	1,712E-01	0,949
160	9,630E-02	1,303	1,647E-01	0,975
170	9,260E-02	1,325	1,589E-01	0,999
180	8,930E-02	1,345	1,537E-01	1,021
190	8,640E-02	1,363	1,491E-01	1,040
200	8,370E-02	1,381	1,449E-01	1,059

Case 4: variation in soil layer composition

The input parameters for the Case 4 are given in Table F-14.

Table F-14: Input parameters for case 4

Parameter		Clay1	Clay2	Sand1	Sand2	Peat1	Peat2	Peat3
γ_d	[kN/m^3]	15,8	15,8	18	18	12,3	9,9	9,9
γ_w	[kN/m^3]	15,8	15,8	20	20	12,3	9,9	9,9
$\mu(c)$	[kN/m^2]	4,53	1,1	0	0	1,5	0,5	0,5
$\mu(\varphi)$	[°]	26,8	33,4	30	35	23,9	20,3	5,8
$\sigma(c)$	[kN/m^2]	3,55	0,16	0	0	0,5	0,1	0,1
$\sigma(\varphi)$	[°]	6,18	8,96	3	3,5	5,69	2	0,6
ρ	[-]	0	0	0	0	0	0	0
$\sigma(p)$	[m]	Variable	Variable	Variable	Variable	Variable	Variable	Variable
$D_h(c)$	[m]	100	100	100	100	100	100	100
$D_v(c)$	[m]	0,5	0,5	0,5	0,5	0,5	0,5	0,5
N_c	[-]	15	10	100	100	18	5	5
α_c	[-]	0,75	0,75	0,75	0,75	0,75	0,75	0,75
$D_h(\varphi)$	[m]	100	100	100	100	100	100	100
$D_v(\varphi)$	[m]	0,5	0,5	0,5	0,5	0,5	0,5	0,5
N_φ	[-]	15	10	100	100	18	5	5
α_φ	[-]	0,75	0,75	0,75	0,75	0,75	0,75	0,75
$\mu(q)$	[-]				1			
$\sigma(q)$	[-]				0,075			
L	[m]				500			

Appendix G. Background on the cost-benefit model

The background information on the cost-benefit model to determine the optimal investment strategy is based on (Deltares, 2011c).

The a-priori probability of flooding P(t), without sensor monitoring, is defined as:

$$P(t) = P(0)e^{\alpha_d \eta t}e^{-\alpha_d H(t)t}$$

P(t)	A-priori probability of flooding in year t	[1/year]
P(0)	Probability of flooding in year t=0	[1/year]
α_d	Scale parameter for exponential distribution $\alpha_d = \frac{\ln 10}{d_{10}}$	[1/cm]
d_{10}	Decimation height	[cm]
η	Relative water level rise, including subsidence	[cm/year]
H(t)	Dike heightening in year t	[cm]

The scale parameter α_d is location specific, based on the decimation height d_{10} of the water level, and determines the effect of a reinforcement on the flooding probability. The relative water level rise η depends on the assumed climate change prediction model, which is subject to discussion. Starting point for this cost-benefit analysis is a *Warm+* scenario from the KNMI. This scenario implies a sea level at the Dutch coast of 35 cm from 1990 to 2050. Also, a physical maximum for the Rhine discharge is considered. The physical maximum is implied to due lower safety standards upstream of the Rhine in Germany: floods would occur upstream in case of a high discharge, which implies a reduction of the discharge downstream in the Netherlands.

The expected damage V(t) in case of a flood is defined as:

$$V(t) = V(0)e^{\gamma t}e^{\psi \eta t}e^{\zeta H(t)t}$$

V(t)	Potential flood damage in year t	[€]
V(0)	Potential flood damage in year t=0	[€]
γ	Yearly economic growth	[%/year]
ψ	Impact parameter for additional damage due to water level rise	[1/cm]
ζ	Impact parameter for additional damage due to increased dike height	[1/cm]

The potential flood damage V(0) consist of materialistic damage (e.g. damaged structures, downfall of business) and casualties, determined with HIS-SSM (Kok et al, 2004). The casualties are expressed in monetary terms by multiplying the number of casualties with a VOSL (value of a statistical life) of 6,7 M€. The average yearly economic growth γ is assumed to be 1,9 %/year for the Dutch economy. The impact parameter ψ for water level rise represents the expected additional flood damage that would be expected, if a flood happens when the water level is higher. The flooding probability will increase as the water level rises, but the flood damage would be more severe if an actual flood occurs. The impact parameter ζ has a similar explanation, but for an increased dike height. The flooding probability decreases as the dike increases, but if a higher dike fails, this implies more severe loading conditions and thus more flood damage due to this severe loading condition.

The investment costs of dike heightening are defined as:

$$\mathrm{I(strengthening)} = (C + bu_d)e^{\lambda_d (u_d + W)}$$

I(strengthening)	Total dike strengthening costs	[€]
C	Fixed costs for dike reinforcement	[€]
b	Variable costs for dike reinforcement	[€/cm]
u_d	Dike heightening for the reinforcement	[cm]
λ_d	Scale parameter for non-linear relation between investment costs and heightening	[1/cm]
W	Total costs of earlier dike reinforcement investments	[€]

The costs for a dike strengthening are location specific and might vary over time, due to market competition. The fixed costs of a dike C are the costs required for any dike heightening, such as preparation and engineering costs. The variable costs b depends on the magnitude of the heightening and consists of additional material and labor costs. The scale parameter λ_d incorporates the non-linearity of the relation between investment costs and the amount of heightening. Later reinforcements can be more expensive, as the cheap heightening has already been executed.

Appendix H. Example calculation cost-benefit analysis for first dike heightening

The fictive location characteristics for this example are summarized in Table H-1.

Table H-1: Input characteristics for the example case study

Parameter	Value	
P(0)	0,004	[1/year]
α_d	0,04	[1/cm]
η	0,3	[cm/year]
V(0)	8201	[M€]
γ	1,9	[%/year]
ψ	0,01	[1/cm]
ζ	0	[1/cm]
C	8	[M€]
b	0,3	[M€/cm]
δ	5,5	[%/year]

The potential flood damage V(0) consists of 8000 M€ of materialistic damage and 30 expected potential casualties, with VOSL of 6,7 M€.

Monitoring system M_1

The first monitoring system (with R=0,1) are estimated at 8625 €/km for the installation costs, which need to be invested every lifetime. The lifetime of the sensors is assumed at 10 years. For a dike length of 15 km, the total installation costs equal 8625*15=129375 €. The yearly operational and maintenance costs are each assumed at 10% of the total installation costs. The total yearly costs sum up to 25875 €. Discounting these periodic investments over the life time of 50 years, results in a net present value of approximately 0,763 M€. This monitoring system can influence the dike reinforcement strategy, which leads to different developments of the yearly flood risk, see Figure H-1. Note that the flood risk in case of the direct monitoring effect leads to larger yearly flood risk during the reinforcement delay.

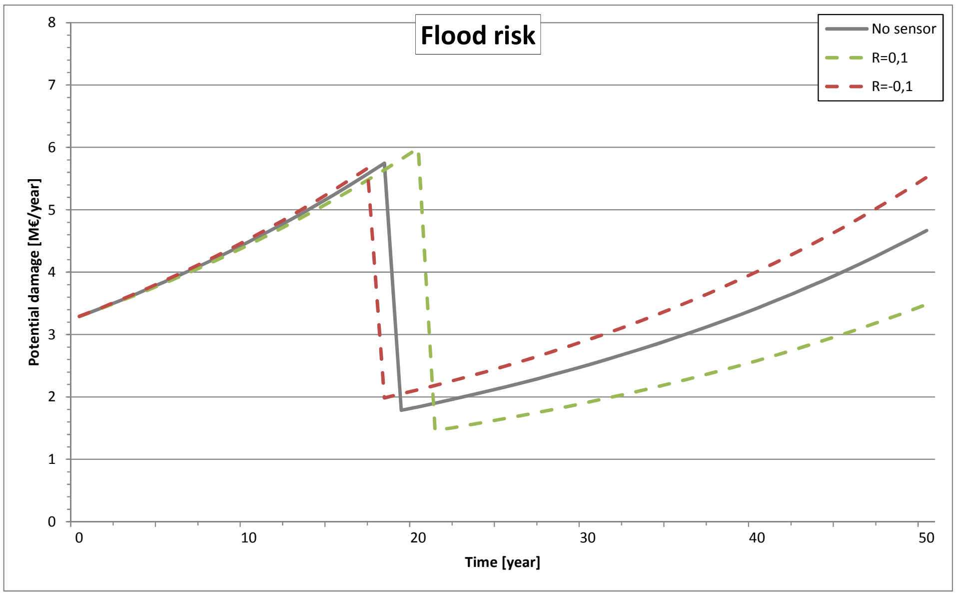

Figure H-1: Development of the yearly flood risk for monitoring system M_1

Monitoring system M_2

The first monitoring system (with R=0,1) are estimated at 23000 €/km for the installation costs, which need to be invested every lifetime. The lifetime of the sensors is assumed at 10 years. For a dike length of 15 km, the total installation costs equal 23000*15=345000 €. The yearly operational and maintenance costs are each assumed at 10% of the total installation costs. The total yearly costs sum up to 69000 €. Discounting these periodic investments over the life time of 50 years, results in a net present value of approximately 2036000 €. This monitoring system can influence the dike reinforcement strategy, which leads to different developments of the yearly flood risk, see Figure H-2. Note that the new monitoring system initiates larger deviations from the expected situation without sensors.

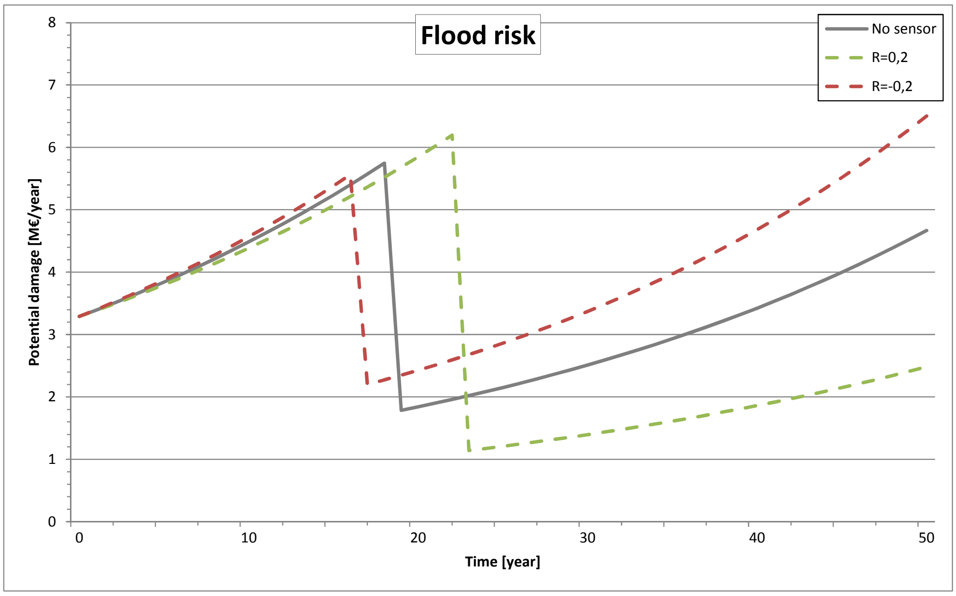

Figure H-2: Development of the yearly flood risk for monitoring system M_2

Appendix I. Mathematical derivation of the early warning event tree

The mathematical derivation for the application of sensor monitoring in operational situations, is done for the event tree as presented in Figure 6-1. The starting condition for this event tree is the occurrence of a high water event, causing flood risks on the short-term. One is interested in the event that the dike fails (i.e. when flood damage is the result), the event F=1, which can be described from Figure 6-1 using the law of total probability:

$$
\begin{gathered}
P(F=1)= \\
P(F=1 \mid M=1 \cap D=1 \cap H) \cdot P(M=1 \mid D=1 \cap H) \cdot P(D=1 \mid H) \cdot P(H)+ \\
P(F=1 \mid M=0 \cap D=1 \cap H) \cdot P(M=0 \mid D=1 \cap H) \cdot P(D=1 \mid H) \cdot P(H)+ \\
P(F=1 \mid D=0 \cap H) \cdot P(D=0 \mid H) \cdot P(H)
\end{gathered}
$$

$P(F=1)$	Probability of dike failure per year	[1/year]
$P(F=1 \mid M=1 \cap D=1 \cap H)$	Probability that the dike fails, given the measure is applied and an anomaly is detected and a high water event is present	[-]
$P(M=1 \mid D=1 \cap H)$	Probability that the measure is applied successfully, given that an anomaly is detected and a high water event is present	[-]
$P(D=1 \mid H)$	Probability that an anomaly is detected, given a high water event	[-]
$P(H)$	Probability of occurrence on a high water event per year	[1/year]
$P(F=1 \mid M=0 \cap D=1 \cap H)$	Probability that the dike fails, given the measure is not applied and an anomaly is detected and a high water event is present	[-]
$P(M=0 \mid D=1 \cap H)$	Probability that the measure is not applied successfully, given that an anomaly is detected and a high water event is present	[-]
$P(F=1 \mid D=0 \cap H)$	Probability that the dike fails, given no anomaly is detected and a high water event is present	[-]
$P(D=0 \mid H)$	Probability that no anomaly is detected, given a high water event	[-]

Each event branch in Figure 6-1 is represented by the multiplication of the conditional probabilities (i.e. serial chain of events) and the total failure probability of the dike is the sum of the three distinct event branches (i.e. either one of the branches have to occur to trigger a dike failure).

The conditional probability $P(F=1 \mid D=0 \cap H)$ represents the failure probability of the dike during a high water event, if no anomaly has been detected. The determination of this probability by expert judgment can be complicated, due to fact that a dike failure is a rare event in the Netherlands. The probability combines the actual threat of the occurring high water with the detection of an anomaly, i.e. the extent that the anomaly detection represents an actual threat. Extensive validation of the monitoring system is required, but in practice often not available. However, an upper boundary can be computed, if the following assumption is made:

$$P(F=1 \mid D=0 \cap H) < P(F=1 \mid D=1 \cap H)$$

In words, this assumption implies that the probability on a dike failure for a given high water event, is higher when an anomaly has been detected than as no anomaly would be detected. Or, the *belief* in the applied sensor monitoring system is positive, which is very reasonable to assume considering the application of sensor monitoring for flood safety (one does not apply a system without confidence in that system). Using the law of total probability, the upper boundary can be written as a function of other input variables:

$$P(F=1 \mid D=0 \cap H) =$$
$$P(F=1 \mid M=1 \cap D=1 \cap H) \cdot P(M=1 \mid D=1 \cap H) +$$
$$P(F=1 \mid M=0 \cap D=1 \cap H) \cdot P(M=0 \mid D=1 \cap H)$$

$P(F=1 \mid D=0 \cap H)$	Probability that the dike fails, given no anomaly is detected and a high water event is present	[-]
$P(F=1 \mid M=1 \cap D=1 \cap H)$	Probability that the dike fails, given the measure is applied and an anomaly is detected and a high water event is present	[-]
$P(M=1 \mid D=1 \cap H)$	Probability that the measure is applied successfully, given that an anomaly is detected and a high water event is present	[-]
$P(F=1 \mid M=0 \cap D=1 \cap H)$	Probability that the dike fails, given the measure is not applied and an anomaly is detected and a high water event is present	[-]
$P(M=0 \mid D=1 \cap H)$	Probability that the measure is not applied successfully, given that an anomaly is detected and a high water event is present	[-]

The mathematical notations previously used are rewritten in simplified notation, see Table I-1.

Table I-1: Simplified notation for the early warning cost benefit model

Mathematical notation	Simplified notation	Unit
$P(F=1)$	$P_f(t)$	[1/year]
$P(F=1 \mid M=1 \cap D=1 \cap H)$	$P_{f,a\text{-}posteriori}$	[-]
$P(M=1 \mid D=1 \cap H)$	P_{m1}	[-]
$P(D=1 \mid H)$	P_{d1}	[-]
$P(H)$	$P_H(t)$	[1/year]
$P(F=1 \mid M=0 \cap D=1 \cap H)$	$P_{f,a\text{-}priori}$	[-]
$P(M=0 \mid D=1 \cap H)$	$P_{m0}=1-P_{m1}$	[-]
$P(F=1 \mid D=0 \cap H)$	$P_{f,d0}$	[-]
$P(D=0 \mid H)$	$P_{d0}=1-P_{d1}$	[-]